UiT
THE ARCTIC UNIVERSITY OF NORWAY

Faculty of Health Sciences
Department of Pharmacy

Nanocarriers for tailored skin delivery:

More than just the carriers?

—

Selenia Ternullo

A dissertation for the degree of Philosophiae Doctor – August 2018

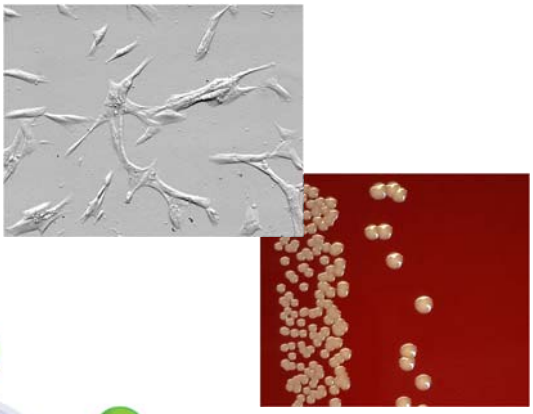

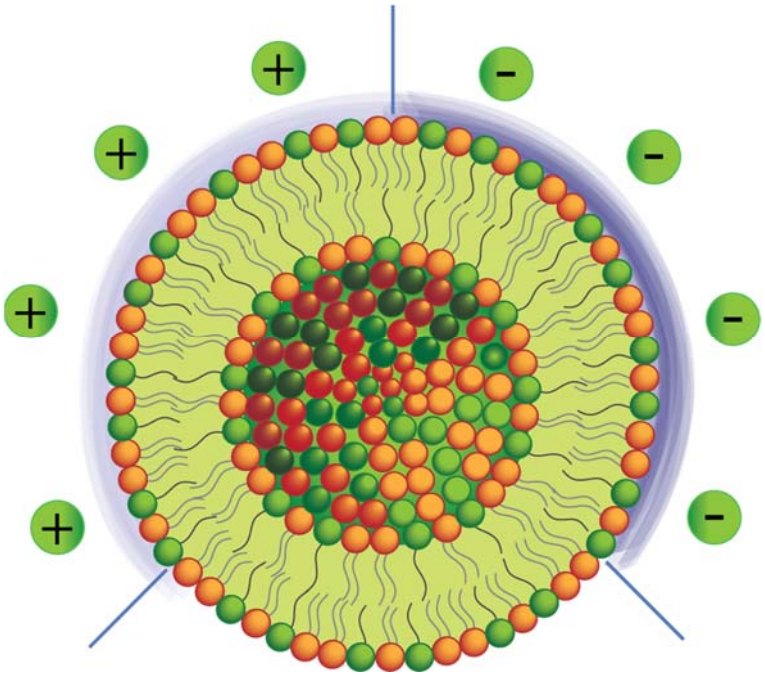

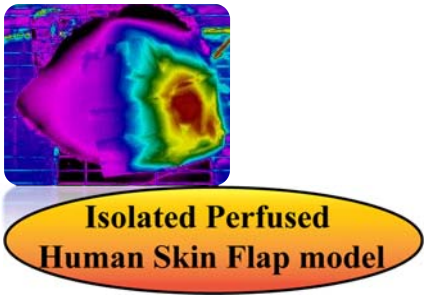

UNIVERSITY OF TROMSØ

A dissertation for the degree of Philosophiae Doctor

Nanocarriers for tailored skin delivery:

More than just the carriers?

Selenia Ternullo

Tromsø 2018

Drug Transport and Delivery Research Group
Department of Pharmacy
Faculty of Health Sciences
University of Tromsø The Arctic University of Norway
Norway

Photo content, from the bottom left to the top right:

Drawing of the Isolated Perfused Human Skin Flap model and its infrared photograph; Deformable liposome with different surface charge; Human foreskin fibroblasts (left) and *Staphylococcus aureus* (right).

To my parents

“If you remain in me and I in you, you will bear much fruit; apart from me you can do nothing.”

John 15, 5

Acknowledgements

This work was carried out at the Drug Transport and Delivery Research Group, Department of Pharmacy, University of Tromsø The Arctic University of Norway from September 2014 to August 2018. During these years in Tromsø I received help and support in different ways from so many people.

First of all I would like to express my deepest gratitude to my main supervisor Dr. Nataša Škalko-Basnet for her precious guidance and support during the past four years. Nataša, thank you for your confidence, your patience and for encouraging me, especially in the most turbulent times. Your constant and kind presence, together with precious advices for any kind of scientific and non-scientific problems has been an important support for me. Thank you also for proofreading my thesis and your valuable comments. To my co-supervisor Dr. Gøril Eide Flaten, thank you for your support and interesting inputs. I would also like to thank my other co-supervisor Dr. Ann Mari Holsæter for encouragement and help. Gøril and Ann Mari, thank you for caring about me and keeping your doors always open for me! To my co-supervisor Dr. Louis de Weerd, thank you for introducing me to your exciting medical universe, completely new for me, and for your enthusiasm especially needed when things were not so easy. Thank you for the great discussions, for your confidence and for taking time to proofread the thesis.

My sincere gratitude goes to Dr. Purusotam Basnet for supporting me with your positive attitude and sharing your extensive knowledge and valuable experience. Your guidance and contribution in the cell studies are really appreciated.

I am grateful to Dr. Mona Johannesen and Dr. Kjersti Julin for their contributions to the bacterial susceptibility testing and welcoming me in their lab. Kjersti, I enjoyed the time (short but intense) spent in the lab with you and thank you for sharing your knowledge.

My appreciation further goes to Dr. Željka Vanić for your valuable contributions in performing the liposome elasticity studies. Although I did not have the pleasure to meet you in person, thanks for the interesting discussions and always being available for me.

To my Master students, Eivind and Laura, thank you for all your intensive work in the lab thus contributing to this project and for being always positive and supportive in the intense times.

Thanks to the Department of Medical Biology at the Faculty of Health Sciences, University of Tromsø The Arctic University of Norway, for the use of their laboratory facility to run the flap experiments. I would also like to thank the engineer Knut Steinnes for his precious technical help in the lab and Dr. James Mercer for assisting me with the use of the infrared camera.

Special thanks to the engineers of our group, Skjalg Nyheim Solum and Cristiane de Albuquerque Cavalcanti Jacobsen for the technical support in the lab, for being always available for me and for useful advices in the teaching lab.

A great thanks to all my colleagues at the Department of Pharmacy and to the former and current head of department, Dr. Thrina Loennechen and Dr. Guro Forsdahl, for your support. I enjoyed being part of such a great social and working environment where I could always get a smile and any kind of support whenever I needed. A special thanks to my research group,

Drug Transport and Delivery Research Group, for the great time spent together in and out of university. It has been a pleasure working with all of you. Thanks to former and current PhD students, Andrè, Elenaz, Toril, May Wenche, Sveinung, Iren and Richard, for your support and nice time spent in the lab. A special thanks to Merete, for dedicating your time and helping me with the cells photos, you are great! My warm thanks go to my friends and officemates Margherita and Jennifer for your fundamental support especially when all got hectic. Thanks for always encouraging and taking care of me. I will never forget what you have done for me!

Thanks to Max, Paolo, Marco, Dominik, Anej, Camilla, Mette, Fabrizio, Antal, Jónína, Matteo, Jennifer and all my friends in Tromsø for the great time I had with you, for all cosy dinners, BBQ at Bukta and funny nights downtown. So many lovely memories I will bring with me! Chris, thanks for the support any time I needed. Our talks during lab breaks and dinners have been good distraction to get some "free time" in my mind. Margherita, thank you for being always present for me, for our best sushi dinners and intensive dancing classes. Margherita and Chris, what we have shared - great and bad moments - has been really important for me and even far away from each other, you will be always part of my family!

Many thanks to my family and friends back home for sharing with me this "arctic experience" and for listening at my many stories happening in Tromsø. The holidays I spent home with you all gave me great memories to bring back in Tromsø thus pushing me to move forward. A special thanks to Margaret and Salvatore, your support and prayers have guided and given me strength to complete this chapter of my life. Margaret, your "do not give up!!" worked! Federico, thank you so much for being part of this important period of my life even though thousand kilometres were separating us. Your constant support and listening at me every time I was sad or confused have meant a lot for me. Our long Skype calls and the time spent together were precious for distracting me. In the future, I wish for us for much more time we could spend together!

My deepest gratitude goes to Prof. Cristina Cavallari, the very first person believing in me. This could have never happened without you! Thanks for your support, constant presence and taking care of me as a mother does. Many thanks to Prof. Fini for his guidance, confidence in me and supporting me in starting this experience. A warm thank to Max for the support, especially in my most difficult moments, for your confidence and help for any kind of problem.

Mom, there are no words to express my gratitude to you. Even though far away from each other, you were always there for me. I never felt alone because I knew that I could always count on you with your precious advices and encouragements. You have been my source of energy and strength all these years. You and dad, divided between heaven and earth, are the best lovely and caring parents I could ever had and I dedicate my thesis to you because I could have done nothing without you. I love you!

Tromsø, August 2018

Selenia Tenuta

Table of Contents

Abstract

Skin diseases are among the top 5 most leading diseases causing non-fatal health burden worldwide and strategies to assure more effective treatments are urgently needed. Dermal therapy is very attractive due to the direct administration of the drug at the diseased skin site thus minimizing systemic side effects associated with the oral and parenteral routes. However, the great variety within the skin conditions can be a challenge in the development of effective dermal therapies. Based on the skin disease, the drug action is often required at different depths within the skin. The failure to penetrate the skin layers might result in sub-therapeutic drug levels at the targeted skin site and unsuccessful treatments. Phospholipid-based nanocarriers have great potential to overcome the current limitations in dermal therapy by assuring controlled and sustained drug delivery and promoting drug/substance transport in the deeper skin layers. The nanocarrier properties can be tailored and exploited to optimize skin drug delivery.

In the present study we optimized nanocarriers for tailored skin drug delivery. A closer-to-*in vivo* skin penetration model was developed to select nanocarriers with specific skin-targeted drug delivery potential. Deformable liposomes were found the most promising nanocarriers delivering model substances in the deeper skin layers while avoiding systemic absorption.

Further optimization of the selected nanocarrier was performed by exploring the effect of the liposomal surface charge on dermal delivery. The sustained skin penetration of drug/active substances for liposomally-associated drugs/substances was influenced by both the liposomal surface charge and physicochemical properties of the nanocarrier-associated drug/substance. The enhancement of the biological activities of both human epidermal growth factor and curcumin when incorporated in the liposomal system as compared to both active substances in solutions was found to be dependent on the liposomal surface charge.

Positively charged deformable liposomes embedded in chitosan hydrogel enabled stable bioadhesive hydrogel providing a sustained skin penetration of curcumin. The developed liposomal hydrogel formulation has a potential to be further evaluated as advanced wound dressing.

List of abbreviations

ADLs	Anionic deformable liposomes
CDLs	Cationic deformable liposomes
CLs	Conventional liposomes
CLSM	Confocal laser scanning microscopy
DIRT	Dynamic infrared thermography
DLs	Deformable liposomes
DOTAP	1,2-dioleoyl-3-trimethylammonium propane
FDA	Food and Drug Administration
FDC	Franz diffusion cells system
HaCaT	Human immortalized keratinocytes
hEGF	Human epidermal growth factor
HFF	Human foreskin fibroblasts
IPHSF	Isolated perfused human skin flap
IR	Infrared
KHb	Modified Krebs-Henseleit buffer
LPS	Lipopolysaccharide
LVP	Left ventricular pressure
MRSA	Methicillin-resistant *Staphylococcus aureus*

NDLs	Neutral deformable liposomes
NLCs	Nanostructured lipid carriers
NO	Nitric oxide
PBS	Phosphate buffer saline
PC	Phosphatidylcholine
PFR	Perfusate flow rate
PG	Propylene glycol
PIT	Perfusate inlet temperature
SA	Stearylamine
SC	*Stratum corneum*
SDC	Sodium deoxycholate
SLNs	Solid lipid nanoparticles
TCA	Trichloroacetic acid

List of publications

Paper I:

Ternullo, S., de Weerd, L., Flaten, G.E., Holsæter, A.M., Škalko-Basnet, N., 2017. The isolated perfused human skin flap model: A missing link in skin penetration studies? *Eur J Pharm Sci* 96, 334-341.

Paper II:

Ternullo, S., de Weerd, L., Holsæter, A.M., Flaten, G.E., Škalko-Basnet, N., 2017. Going skin deep: A direct comparison of penetration potential of lipid-based nanovesicles on the isolated perfused human skin flap model. *Eur J Pharm Biopharm* 121, 14-23.

Paper III:

Ternullo, S., Basnet, P., Holsæter, A.M., Flaten, G.E., de Weerd, L., Škalko-Basnet, N. Deformable liposomes for dermal delivery of human epidermal growth factor: The effect of liposomal surface charge. *Submitted manuscript*

Paper IV:

Ternullo, S., Gagnat, E., Julin, K., Johannessen, M., Basnet, P., Vanić, Ž., Škalko-Basnet, N. Nanocarriers for dermal delivery: The carrier surface charge affects biological activities of curcumin. *Manuscript*

Paper V:

Ternullo, S., Schulte-Werning, L.V., Škalko-Basnet, N. Curcumin-in-deformable liposomes-in-hydrogel: The effect of liposomal surface charge on dermal delivery of curcumin. *Manuscript*

1 Introduction

1.1 Skin diseases: current status

The Global Burden report (2010) confirmed that the skin diseases represent an important cause of health loss and their impact on patients' life and healthcare costs should not be undervalued. Skin conditions are the 4th leading cause of non-fatal disease burden (Hay et al., 2014). Moreover, all age-groups appear to be affected by skin diseases (Figure 1.1). Eczema is mainly responsible for health burden on children, acne on adolescents and several skin diseases, such as eczema, infections, non-melanoma skin cancer and ulceration, on elderly people (Hollestein and Nijsten, 2014). More recently, an estimation of the global morbidity and mortality in 2013 caused by skin diseases in all ages confirmed the previous global study (Karimkhani et al., 2017).

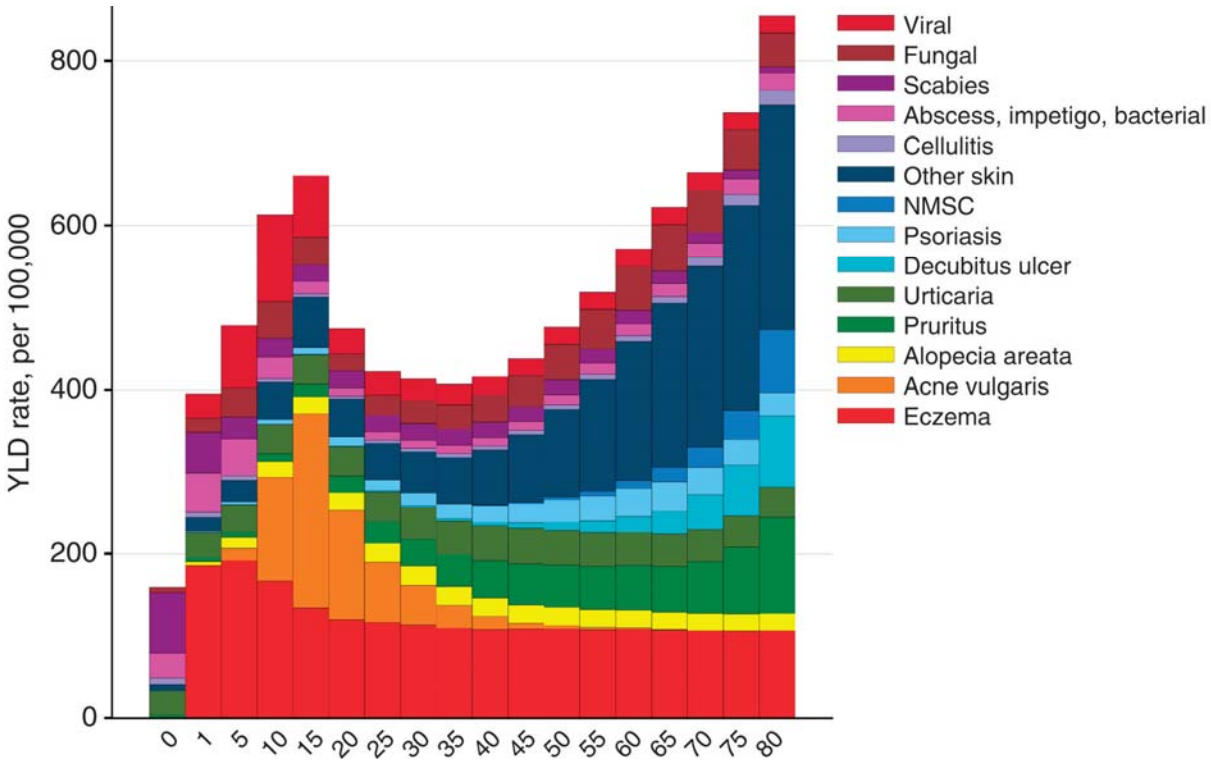

Figure 1.1: Age distribution of skin disease burden in 2010 (adapted from Hay et al., 2014 with permission from Elsevier).

Introduction

Some of the skin diseases, such as chronic wounds, are the result of other diseases' complications, i.e., foot ulcers from diabetes, pressure ulcers resulting from spinal cord injuries, and neurodegenerative processes, such as Pick's disease (Dreifke et al., 2015). Therefore, the increasing proportion of high risk-populations, e.g. diabetic, obese, smokers and elderly people, further contributes to the prevalence of skin diseases. Since the skin diseases under other medical categories were not included in the Global Burden of Disease 2010 study, i.e., melanoma reported under cancer and cutaneous leishmaniosis under infectious diseases (Hay et al., 2014), the true burden of skin diseases is substantially underestimated (Hollestein and Nijsten, 2014). Beyond these data, skin diseases have a high impact on patients' quality of life and their health status. Patients affected by skin diseases not only suffer from the pain and alteration of physical appearance, but also from psychological morbidity (Karimkhani et al., 2017). Skin diseases continue to affect patients' disability in both developed and developing countries (Mounessa et al., 2017). On top of that, it has been estimated that only in the US slightly over one quarter of the entire population was affected by at least one form of skin disease in 2013 resulting in a total healthcare cost of approximately US$ 240 per capita. These numbers exceeded the ones obtained from studies on cardiovascular diseases and diabetes (Lim et al., 2017). Moreover, nearly US$ 11 billion have been spent only in 2013 to better understand the pathophysiology of the skin diseases and for the development of new topical medications (Lim et al., 2017). This highlights that the strategies to manage and control skin diseases are a necessary use of health resources (Hay et al., 2014).

Since 1995, more than 100 dermatological drugs were approved by the Food and Drug Administration (FDA), indicating that the treatment of skin diseases is gaining more and more attention. Interestingly, more than 50% of these products are either in the form of tablets or solutions for intramuscular or intravenous injections. Therefore, part of dermatological therapies are administered systemically although the pharmacologic target resides in a specific tissue or single compartment of the body (i.e. the skin). Acne is one of the most common skin disease with high impact on adolescents. It is characterized by high sebum secretion that manifests from mild to severe inflammatory lesions in different parts of the body (de Leeuw et al., 2009). The treatment options depend on the stage and intensity of the

disease. Generally, the use of topical benzoyl peroxide, tretinoin and antibiotics represents the standard treatment today to eradicate *Corynebacterium acnes*, the causative bacteria, and to reduce the inflammation in mild to moderate acne. However, the use of topical tretinoin is limited because it often causes skin irritation, with erythema, burning sensation and photosensitivity (Goyal et al., 2016). Systemic antibiotics and antiandrogens are used either to treat severe acne manifestations or in case the previous approach was not effective. However, considering the high prevalence of microbial resistance to antibiotics when systemically administered, the effectiveness of antibiotics has become less (de Leeuw et al., 2009). The final remedy is oral isotretinoin that is very effective although moderate to serious side effects limit its use (de Leeuw et al., 2009). Treatment of psoriasis has also a great relevance worldwide. Although research has moved forward to better understand the pathogenesis and develop strategies to control the disease, the need for safe, cost- and disease-effective cures remains (Vanić, 2015). Topical treatment with anti-inflammatory agents and antibiotics is the first-line therapy of acute exacerbations of atopic dermatitis and contact dermatitis. Topical administration of prednicarbate has desired anti-inflammatory effects. However, the separation of its therapeutic effect from side effects, such as antiproliferative effect, is still a challenge (Pardeike et al., 2009). Prednicarbate has shown to induce irreversible skin atrophy in the dermis. Therefore, a targeted delivery of prednicarbate in the epidermis might be a good strategy to minimize side effects in the deeper skin layers (Schäfer-Korting et al., 2007). On the other hand, antibiotic treatments require skin biopsies of pustules and draining lesions before starting the cure to determine the pathogen type. A possible infection by methicillin-resistant *Staphylococcus aureus* (MRSA) arises challenges in the treatment with common antibiotics related to microbial resistance (Mota et al., 2017). Methotrexate administered systemically is used for controlling recalcitrant psoriasis, but several side effects, for instance hepatotoxic effects, may occur. The topical administration of methotrexate has been considered a good alternative to overcome systemic side effects. However, its hydrophilicity limits its entrance into the skin by passive diffusion (de Leeuw et al., 2009). Skin cancer is the most common form of malignancy; although melanoma accounts for a small proportion of skin cancer (approximately 74,000 US cases reported annually), it is responsible for the majority of skin cancer deaths (Goyal et al., 2016). The current standard treatment for localized skin cancers is excision of the tumour, often requiring surgeries with

deep dissections followed by soft tissue reconstruction (Goyal et al., 2016). Most of the chemotherapeutics used in the treatment are administered systemically and are toxic to healthy cells. Numerous potential drugs fail clinically because of insolubility, further increasing the need to find new approaches to overcome these limitations (DeLouise, 2012). Chronic wounds and burns are those wounds that usually fail to complete the normal wound healing cascade due to persistent inflammation and infections (Hamdan et al., 2017). Microbial infections, often followed by biofilm formation, are one of the main causes of morbidity and mortality among patients affected by chronic wounds (Byrd et al., 2018). There is no standard treatment for chronic wounds. Treatment options may include gels and occlusive dressings as moisturizing agents, surgical debridement to remove dead tissue, compression bandages, and topical drugs. Unfortunately, often the effectiveness of topical bioactive agents in the form of solutions, creams, and ointments cannot be guaranteed due to rapidly absorption of fluid thus losing their rheological characteristics (Boateng and Catanzano, 2015). The greatest challenge in post-burn recovery is cutaneous scarring causing reduced quality of life and may affect reintegration into society. Hypertrophic scarring has high prevalence and can cause neuropathic pain, surface irregularities and disabling contractures. Intralesional injections of corticosteroids are commonly used to treat hypertrophic scars, although the treatment is not fully effective (Amini-Nik et al., 2018). Steroid injections destroy collagen bundles and inhibit fibroblast growth thus resulting effective in reducing hypertrophic scarring. Promising are injections of immunomodulators (e.g. interferons) that inhibit production of fibroblast collagen. However, interferon treatment is expensive and is associated with a high risk for side effects, like the flu (Amini-Nik et al., 2018).

Currently, more than one third of the drugs under clinical evaluation are delivered either into or through the skin (Vanić, 2015) and skin therapy has been valued around US$ 9.44 billion in 2013, expecting to reach US$ 11.21 billion by 2018 (Jain et al., 2017). This highlights the need for limiting both oral and parenteral drug administration in localized skin therapy. The fate of a systemically administered drug involves hepatic first-pass metabolism, which is responsible to reduce the amount of drug that will reach the skin targeted site, thus decreasing its therapeutic effect. On the other hand, high levels of metabolite(s) produced by drug's first passage through the liver result in side effects (Wiedersberg and Guy, 2014). Many skin

diseases are also related to microbial infections, e.g. chronic wounds, burns, atopic dermatitis, impetigo, cellulitis (Gupta et al., 2012). Therefore, considering the high prevalence of microbial resistance to orally administered antibiotics, other routes of drug administration should be considered.

Topical treatment of skin diseases is therefore very attractive, enabling direct administration of drugs to the diseased skin site. This can potentially assure high drug levels at the targeted skin site and reduce the hepatic first-pass metabolism associated with the oral route. This will then allow administration of lower doses of the drug without affecting its therapeutic effect, but minimizing manifestation of side effects (Cima et al., 2014). The formation of drug reservoir in the targeted skin layer following topical application is likely to release the drug over an extended period of time. This drug depot might assure constant drug concentration at the skin site and reduce the drug concentration fluctuations, typically seen with orally administered products (Tran, 2013). A controlled and sustained drug release over long periods can assure reduction in frequencies of administration and increased patient compliance (Kristl et al., 2010). For some drugs, a continuous delivery is often required and it is difficult to be assured via oral route (Bouwstra et al., 2003). To further priorities patients' needs, dermal delivery of drugs for localized skin therapy is, in most of the cases, pain-free that could increase patient compliance as well as patients' comfort. Especially compared to the parental administration, topical skin administration additionally avoids possible infections that might arise after injections. Therefore, patients are the first who benefit from localized skin therapy.

1.1.1 Skin-targeted drug delivery

In dermatology, the choice from the vast array of topical preparations needs to be based on the potency required, site of intended use and assuring patience compliance (Schmieder et al., 2015). When selecting the adequate topical formulations, dermatologists should be aware of the basic mechanisms of dermal drug transport in order to assess whether the therapy is likely to exert the desired therapeutic effect. The term penetration denotes the entry of the drug into a specific skin layer. The first layer that a drug faces when topically administered onto skin is the *stratum corneum* (SC). The permeation refers to the drug penetration from one skin layer into another, whereas dermal absorption indicates the uptake of the drug into

the vascular system (Bolzinger et al., 2012). Drug accumulation is the amount of drug in the skin over a certain time interval. The drug can then remain either in the skin or being absorbed into the systemic circulation (Schmieder et al., 2015).

According to the skin disease, drug action at different levels within the skin is required (see Figure 1.2). Acne, for instance, requires drug action at more superficial skin levels. Chronic wounds can be differentiated according to the number of affected skin layers, thus resulting in i) superficial wounds where only the epidermal layer is affected, ii) partial-thickness wounds, involving the injury of the dermis, and iii) full-thickness wounds, where the whole skin is affected (Boateng and Catanzano, 2015). The drug needs to be delivered at the specific injured skin layer(s), according to the wound type, to exert the maximum therapeutic effect. Microbial infections either can occur in the superficial skin layers or can reach the deeper skin layers, such as the dermis (i.e. deep microbial infections).

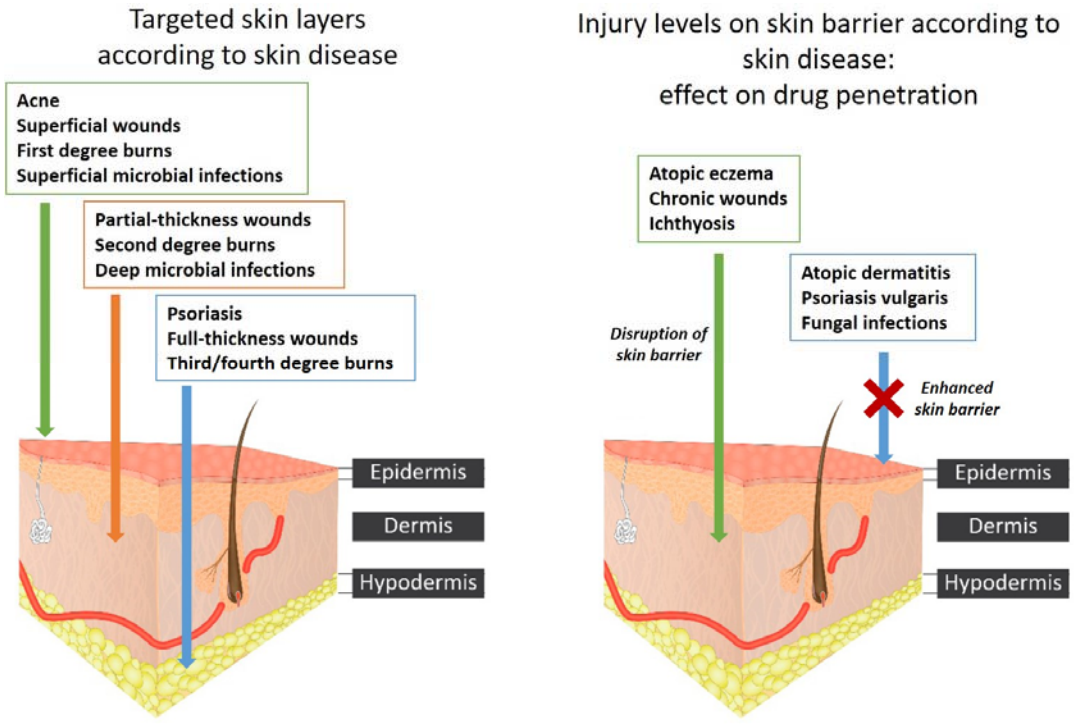

Figure 1.2: Schematic drawing on the different targeted skin layers according to the skin disease (left part) and effect on drug penetration through the skin depending on the skin disease (right part) (adapted with permission from Kotla et al., 2018. Copyright (2017) American Chemical Society).

Additionally, the level of injury of the skin barrier is not the same in all the skin diseases (Figure 1.2). Atopic eczema, chronic wounds, ichthyosis are responsible for disrupting the skin barrier, specifically the SC, thus assisting penetration of drugs deeper into the skin layers (Saraceno et al., 2013). On the contrary, in inflammatory skin diseases such as atopic dermatitis, psoriasis vulgaris and fungal infections, leucocytes invade the skin triggering keratinocytes proliferation and increasing the skin thickness (Korting and Schäfer-Korting, 2010). As a consequence, in this case, the drug delivery at the targeted skin layer might be compromised due to the enhanced barrier properties of the skin resulting in reduced therapeutic effects of a drug that could not reach the diseased skin site. Therefore, the delivery of drugs from skin formulations to the targeted skin site (skin-targeted drug delivery) can assure effectiveness of localized skin therapy.

1.2 Challenges in controllable dermal therapy

Although all these advantages of dermal drug delivery, the dermatological products reaching the market do not mirror the high number of drugs in the clinical phase of drug development. The topical drug administration for localized skin therapy is still a challenge, especially in controlling the exact amount of drug that reaches the different skin layers to assure skin-targeted drug delivery (Pardeike et al., 2009). Ideally, the drug after its release from the vehicle should penetrate the SC and permeate through the skin layers in order to reach the targeted skin site. A drug depot in the skin site might maintain therapeutic drug concentrations for a long period of time and avoid systemic absorption (Vogt et al., 2016). The main limiting step is represented by drug penetration through the SC. The skin penetration potential of the drug is dependent on its physicochemical properties, such as molecular weight, solubility, melting point, ionization and partition coefficient. Drugs with molecular weight lower than 500 Da, having low melting point and a log P of 2-3 can penetrate the SC. Due to the limited number of drugs that fulfil these criteria, the effectiveness of dermatological products is related to the type of vehicle (Roberts et al., 2017). The vehicle in which the drug is incorporated can affect some of the mentioned characteristics and therewith compensate for these limitations.

The current dermatological products for localized skin therapy are based on conventional vehicle systems including liquids (solutions), semisolid (ointments and cream), and solid systems (patches) (Planz et al., 2016). They are sufficiently effective to act as vehicle for the incorporated therapeutic agent. Once applied onto the skin, they can provide sustained release of the therapeutic agent, thus assuring prolonged local effect and minimizing its systemic absorption and side effects (Frederiksen et al., 2015). Additionally, many excipients in the traditional topical dosage forms have intrinsic beneficial properties that can act synergistically for improving and accelerating the therapeutic outcome of localized skin therapy. Physical effects, such as cooling and protective, can be assured when drug-free dermatological bases, e.g. hydrophilic emulsions, hydrogel, creams, are applied to the skin (Flaten et al., 2015). Additionally, some bases can also affect the skin barrier properties by inducing changes in its physical state and permeability. As an example, moisturizing effect on skin mediated by water-absorbing hydrogel and ointment affects the SC hydration thus increasing drug penetration (Flaten et al., 2015). Unfortunately, these conventional topical preparations often fail in assuring effective dermal drug delivery. They often cannot guarantee controlled delivery of drugs (Frederiksen et al., 2015), resulting in inadequate skin-targeted drug delivery (Figure 1.2). Moreover, they can also fail to enhance drug penetration through the SC, also limiting drug access into the deeper skin layers (Frederiksen et al., 2015). These limitations require an increase of drug concentration in these vehicles in order to make the therapy effective. This can result in toxic local reactions, such as irritation and allergy (Gupta et al., 2012). Although the current semi-solid dosage forms may mediate sustained drug release, they cannot assure a prolonged contact to the skin for long treatment intervals. This may increase the frequencies of administrations thus reducing patient compliance (Korting and Schäfer-Korting, 2010) and increase health care costs.

For these reasons, research has moved towards alternatives to conventional therapy to overcome the current limitations of dermal therapy. Several strategies have been proposed to enhance drug penetration through the SC and to control drug delivery into the skin layers to reach the targeted skin site (Goyal et al., 2016). Among them, physical methods, such as iontophoresis, sonophoresis, laser or thermal ablation, electroporation and microneedle arrays have led to FDA-approved products for dermal drug delivery (Goyal et al., 2016). The

use of chemical enhancers has also shown to assist drug penetration through the SC (Lane, 2013; Cilurzo et al., 2014). As an alternative, nanotechnology is a promising approach. Nano-sized particles have great potential as dermal delivery systems thus overcoming current limitations in controllable dermal therapy (Mota et al., 2017).

1.3 Overcoming current limitations of dermal therapy

Extensive research is focusing on advanced dermal delivery systems, such as nanocarriers, especially for improving drug penetration through the SC and enabling controlled drug delivery (Mota et al., 2017). The effectiveness of advanced delivery systems depends on several factors, which are related to their intrinsic properties but also on the interactions between them, the skin and the drug (Jain et al., 2017). For these reasons, one of the key steps in formulation development is the evaluation of the intrinsic properties of the formulation and prediction of the extent the drug will be delivered from vehicle/carrier within the skin layers (Van Gele et al., 2011).

1.3.1 Skin penetration models

The employment of skin penetration models as a tool in predicting the fate of drugs from dermatological products once applied onto the skin contributes to a more feasible development and optimization of effective localized skin therapies (Flaten et al., 2015). One of the advantages of localized skin therapy is the avoidance of drug systemic absorption. Therefore, during the development and optimization of dermatological products, it is important to confirm that no dermal absorption of the drug occurs. This concept also applies to pharmaceutical products for treatment of other diseases, due to the high interest of the topical skin route as an alternative to more traditional administration routes (Selzer et al., 2013). Finally, the demand for data predicting the rate and degree of substances across the skin is also related to the assessment of the safety aspects of compounds and xenobiotics, which can potentially be harmful in everyday use in the agrochemical, cosmetic, and pharmaceutical sectors (Schaefer et al., 2008). For all these reasons, the choice of appropriate

skin penetration models is of fundamental importance to obtain good correlation with *in vivo* situations. Moreover, considering the newly proposed classification system for topical drug products, whose aim is to simplify the development and approval of topical generic products (Shah et al., 2015), reliable and close-to-*in vivo* skin penetration models are highly urgent.

The "gold standard" skin penetration model is the *in vivo* tests in humans. However, due to ethical and costs concerns, *in vivo* human studies are generally not feasible in the early stages of formulation development (Planz et al., 2016). Additionally, they often possess high degrees of variability and low sensitivity towards detection of formulation differences, important for the screening of formulations during their early development (Ilić et al., 2017). For a long period of time, the use of *in vivo* animals has been the main alternative to the *in vivo* studies. In the last decades, the regulations finalized to restrict the use of animals have been generated and since 2009, the prohibition of animal testing for toxicological concerns on cosmetic ingredients (EU, 76/768/EEC, February 2003) has furthermore highlighted the need for other alternatives (Van Gele, et al., 2011). The use of excised animal skin has shown to be a valid approach allowing collection of a large number of data due to the higher availability of excised animal skin compared to *ex vivo* human skin. The most widely used technique to assess drug penetration through *ex vivo* human/animal skin is the Franz cell chamber, consisting of a donor and a receptor compartment separated by the human/animal skin membrane (Patel et al., 2016). Several animal species have been considered as donors, such as mouse, rat, snake and pig. The use of pig skin has been proved to be the most reliable in terms of human/animal correlation data, due to the similarities in histology, hair density and skin thickness (Sintov, 2017). Newborn pig skin has also been proposed as alternative to human skin and good flux correlation of lipophilic substances has been found between newborn pig and human skin (Cilurzo et al., 2007). However, pig SC owns lipids organized in hexagonal lattice in contrast to the orthorhombic organization of human SC, thus indicating dissimilarities in the SC lipid organization (Silva Garcia Praça et al., 2018). In general, the penetration through animal skin is higher compared to the human due to differences in the cell type, lipid composition and organization, water content, morphology and hair density (Schaefer et al., 2008). This becomes even more evident with the use of frozen/thawed animal skin. Due to the high ceramide and low cholesterol levels in pig SC, the freezing process might account for internal

ice crystalline formation that consequently disrupts the SC (Sintov, 2017). These findings have guided researchers in finding alternatives in *in vitro* models to overcome ethical and costs concerns related to *in vivo*/*ex vivo* studies involving both humans and animals. Several *in vitro* skin models have been developed for this purpose, also involving the use of phospholipids to mimic the human SC lipid composition to a higher extent (Flaten et al., 2015). Although some of the advantages in the use of *in vitro* artificial models make them useful for screening in the early stages of drug discovery or formulation development, these models still suffer from the main limitation of being not fully representative of the human skin, particularly referring to SC lipid composition and lack in the multitude of *in vivo* skin properties. The correlation between *in vitro* and *in vivo* data remains quite poor (Abd et al., 2016). Table 1.1 reports a short overview of the main skin penetration models including advantages and limitations.

Table 1.1: Advantages and limitations of different skin penetration models (adapted from Flaten et al., 2015 with permission from Elsevier and from Abd et al., 2016 with permission from Dove Medical Press).

Skin model	Advantages	Limitations
Human		
In vivo	The gold standard	Restricted use due to ethical and costs concern High inter- and intra-variability
Ex vivo skin	The most representative for in vivo humans	Different anatomical parts, e.g. abdomen, breast, back Storage
Animal		
In vivo	Reasonably easy to use compared to human Can be scaled up to humans Pig skin: similar to human skin	Ethical permission Pig skin: removal of hairs (skin damage) Other species: different barrier properties from humans
Ex vivo	Easy to obtain	Different barrier properties, variability
Reconstructed human skin	Consistence in permeability	More permeable than human skin High cost
***In vitro* lipid-based membranes**	Reproducible Storage Useful for screening	Non-biological origin Not fully representative of human skin

To overcome the mentioned limitations, research is moving towards the development of new skin penetration models, especially focusing on including the most important *in vivo* skin properties to better understand the factors determining good *in vivo* performance of newly designed dermal dosage forms. The use of human skin is highly recommended (Godin and Touitou, 2007). As already mentioned, the human skin physiology and composition differ from animal skin affecting the rate of skin drug penetration. The drug penetration rate through the skin is also the result of interactions between the vehicle/carrier and the skin, particularly referring to the SC lipids (Bouwstra et al., 2003). Therefore, dissimilarities of animal SC lipid composition and organization compared to human skin might result in poor data correlation. Another characteristic that affects the extent of skin drug penetration is the viability of the human skin tissue (Van Gele et al., 2011). When used *ex vivo*, the viability of human skin cannot be guaranteed. Moreover, the excised human skin is often frozen for practical reason. Repeated freeze-thaw cycles can alter the morphology of the SC lipids thus resulting in different penetration profiles compared to the ones obtained with fresh human skin (Barbero and Frasch, 2016). The skin active metabolism plays also a role in the drug penetration through skin, particularly influencing the efficacy and safety of dermal delivery of intensively metabolized drugs. The skin has a pool of enzymes responsible for a metabolic action towards the topically applied drug, thus affecting the effective amount of the active form of the drug that will reach the targeted site (Van Gele et al., 2011). The use of excised human skin has shown to have some good correlation with *in vivo* human studies, although the enzymatic activity is highly compromised (Van Gele et al., 2011); the skin metabolic activity is even more diminished in frozen human skin (Barbero and Frasch, 2016). Reconstructed epidermis skin models, such as SkinEthic and EpiDerm models, have shown to be suitable models for representing the contribution of skin metabolism to the penetration of corticosteroids and oestrogens (Mahmoud et al., 2005; Lombardi Borgia et al., 2008). Although promising, these *in vitro* skin models still suffer from some limitations. The medium should be serum-free; the presence of bovine serum albumin is indeed toxic to reconstructed epidermis and inhibits drug metabolism. Moreover, these models do not include the dermis or dermal fibroblast/epidermal interactions, which play a role in drug metabolism' action of the skin (Van Gele et al., 2011).

When evaluating the skin penetration of drugs, different skin models often do not possess the active dermal microcirculation, which is responsible for systemic drug absorption (Schaefer et al., 2008). To overcome this limitation, skin penetration studies using excised human/animal skin have been conducted in flow through Franz cells system. The acceptor medium, composed of a tissue culture medium, continuously flows under the skin by the aid of a pump. Under these conditions, the effect of microcirculation can be somehow investigated (Selzer et al., 2013). However, in this model the perfusion through the dermal layer cannot be assured, which is another parameter that can affect skin penetration of drugs/compounds/xenobiotics (Lane, 2013). It is worth to mention that some skin diseases, such as chronic wounds, are sensitive to perfusion, which can increase tissue oxygenation thus favouring faster healing (Desmet et al., 2018). Therefore, exploring the effect of perfusion in skin penetration studies might be useful to develop effective localized therapy. Moreover, the experimental setup in *ex vivo*/*in vitro* skin penetration studies using the Franz diffusion cells system (FDC) do not include the subcutaneous fatty tissue, which needs to be removed from the skin membrane before the start of the experiment. For testing formulations destined for localized therapy, the presence of the subcutaneous fatty tissue might not be necessary due to the fact that the drug is expected to be delivered through/into the upper skin layers and not to reach the systemic absorption. However, skin penetration models might also serve as tool to prove that no systemic absorption of drug occurred, reducing the possibility of side effects (Schäfer-Korting et al., 2007). This condition is partially affected by the presence of subcutaneous fatty tissue that also serves as a connection layer between the vascularized dermis and the muscles/nerve beneath. For all these reasons, models that minimize the number of *in vivo* human studies but, at the same time, can correlate between *in vivo* and *ex vivo* data to shorten and economize the formulation development are urgently needed.

1.3.1.1 Skin perfusion models

In the hierarchy of the most frequently used skin models categorized by their resemblance to the *in vivo* situation and proposed by Schaefer et al. (2008), the skin perfusion models are on the top position, right after the *in vivo* human studies (Figure 1.3). They represent the skin penetration models that could fulfil part of the important requirements needed when performing skin penetration studies.

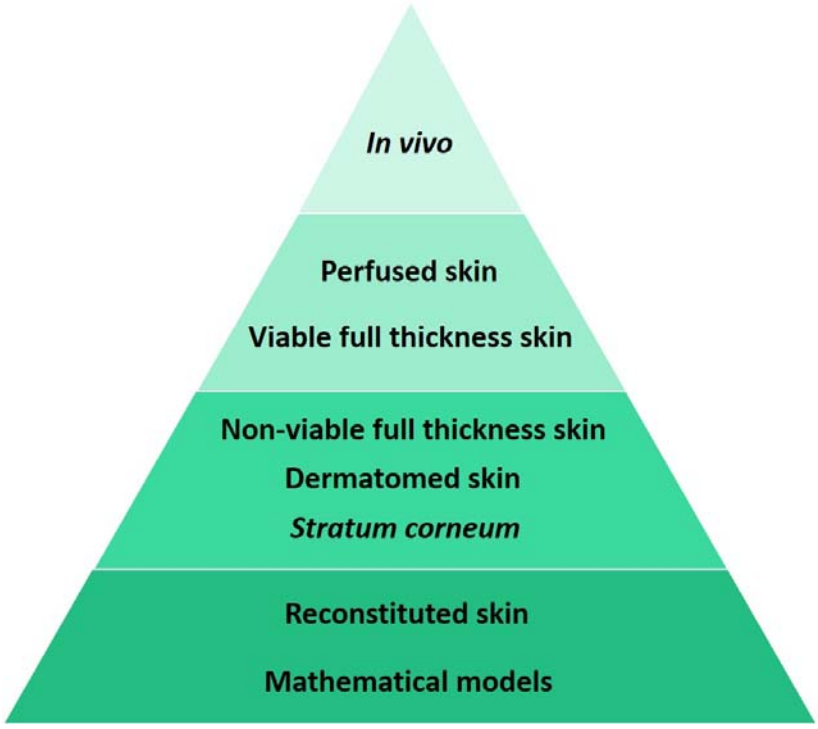

Figure 1.3: Hierarchy of the most frequently used skin models according to their resemblance to the *in vivo* situation (adapted from Schaefer et al., 2008, with permission from Springer Nature).

Skin perfusion models are composed of a surgically prepared portion of skin panni, also called flap, involving the active circulation of the dermis layer, skin metabolism and the presence of the subcutaneous fatty tissue (Patel et al., 2016). These skin models have also the advantage of being perfused with tissue-culture medium by cannulization of one of the vessels in the skin panni. To confirm and monitor flap perfusion during skin penetration experiments, dermofluorimetry is one of the mainly used technique (Kreidstein et al., 1995; Black et al., 2001). Miland and colleagues (2008) confirmed the suitability of a less invasive technique, the dynamic infrared thermography (DIRT), which was also used to differentiate between the well and less perfused areas. Additionally, methods used in *in vivo/ex vivo* investigations, e.g. mass balance, surface washings, tape stripping, can be easily transferable to the skin perfused model (Schaefer et al., 2008). Several animal specimens have been used to obtain skin perfusion models, such as pig, mouse, and rat. The first studies were performed with perfused

ear model, which showed to possess high permeability and was later used only as tool to predict penetration through premature neonate skin (Schaefer et al., 2008). Research has then moved towards other animal body parts, i.e. perfused cow udder (Kietzmann et al., 1993), pig forelimb (Wagner et al., 2003), and the isolated perfused pig skin flap (obtained from pig abdomen) (Riviere et al., 1986). Skin penetration studies performed especially using pig skin flaps have been widely demonstrated as suitable models to predict the fate of substances after their topical application onto the skin (Carver et al., 1989). Good correlation with *in vivo* studies has been obtained when testing dermal absorption of organophosphates, steroids, benzoic acid and caffeine on the isolated perfused pig skin flap (Carver et al., 1989). Wester and collaborators (1998) found also similar dermal absorption of other compounds between the pig skin perfusion model and *in vivo* studies on humans. However, the limitations of using animal skin models (Table 1.1) also applies for skin perfusion models. Skin perfusion models derived from human skin mimic the *in vivo* human studies to a greater extent, in addition to the benefit of working with metabolically active tissue and including the possibility to explore the effect of dermal vascular circulation on skin penetration of drugs (Ternullo et al., 2017).

In addition to selecting an appropriate model to study the possible penetration of active substances through the skin, it is important to select appropriate model substances to follow their penetration into/through the skin.

1.3.2 Choice of the right nanocarrier

With advances in molecular biotechnology and bioinformatics, the number of new candidate drug molecules is increasing thereof requiring newer and more effective approaches for their transport and deliver to the targeted skin site (Kristl et al., 2010). The ideal carriers for dermal drug delivery should have the ability to control dermal drug delivery. This would then assure a targeted drug delivery resulting in efficient localized skin therapy (Banerjee, 2013). As a consequence, the side effects to non-targeted tissue(s) will be minimized (Mota et al., 2017). The drug therapeutic effect would also be enhanced if the carrier can provide drug protection from enzymatic metabolism or pH and light degradation, thus increasing its stability and therapeutic effect (Vanić et al., 2015).

Colloidal systems have good potentials to be used as dermal drug delivery systems (Cevc and Vierl, 2010). When oils and amphipaths (including lipids) meet polar solvents (e.g. water) spontaneous creation of several structures occurs. Micelles, cubic phases, micro- and nano-emulsions, vesicles, dendrimers are some of their example. These structures have good potentials to overcome conventional topical treatments' limitations. Some of them can also act as the carriers, whereas others act as skin penetration enhancers thus influencing the drug transport across the skin (Cevc and Vierl, 2010). Among them, spherical micelles and microemulsions are characterized by short-life and ease to rearrange/fluctuate. Emulsions, on the other hand, can change in water and salt concentration after exposure to open skin surface (Cevc and Vierl, 2010). Nano-sized carriers represent one of the most emerging and advanced drug delivery systems, offering novel directions in the treatment of skin diseases (Vanić et al., 2015). Major classes of nanocarriers are: lipid systems (micelles, liposomes, nanoemulsions, solid lipid nanoparticles (SLNs), nanostructured lipid carriers (NLCs)), polymer systems (polymeric micelles, polymeric nanoparticles, dendrimers), nanosuspension and pro-colloidal systems (self-emulsified systems and liquid crystalline systems) (Kristl et al., 2010). Some of the lipid systems, can be further classified in two subclasses according to the lipid organization, namely vesicular lipid-based nanosystems (liposomes) and particulate lipid-based nanosystems (SLNs, NLCs). Vesicular nanosystems are soft particles composed of a lipid bilayer surrounding an aqueous compartment, whereas particulate nanosystems are composed of lipid nanoparticles having a solid lipid matrix at both room and body temperatures (Vanić et al., 2015). An overview of the major classes of nanocarriers is given in Figure 1.4.

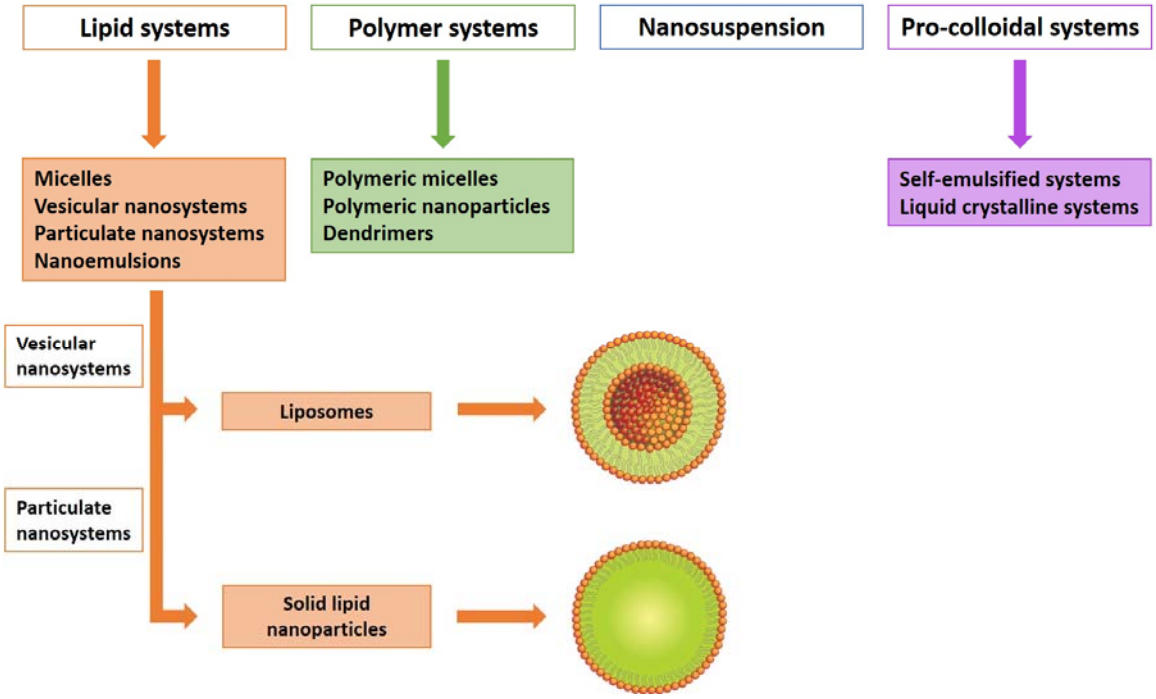

Figure 1.4: Major classes of nanocarriers.

Liposomes, SLNs and NLCs are currently very promising as nanocarriers for dermal drug delivery (Kristl et al., 2010; DeLouise, 2012). Their lipid-based composition makes them similar to the SC lipid composition thus enhancing the entry of the incorporated drug through the SC. This can subsequently promote their transport even in the deeper skin layers (Prow et al., 2011). The controlled drug delivery via nanocarriers could assure skin-targeted drug delivery. Phospholipid-based nanocarriers can also provide a sustained drug release, allowing increase of the drug retention time at the targeted skin site and enabling the drug being continuously available for its target interaction (Sala et al., 2018). In many cases, cells are the targets, and nanocarriers have shown to increase drug cellular uptake resulting in higher therapeutic effect (DeLouise, 2012). Sustained drug release can, in addition, reduce the drug doses, further reducing the risks of side effects while maintaining its therapeutic levels. Due to their peculiar structure, phospholipid-based vesicles and particles can also increase the stability and protection of the incorporated drug. By this approach, the active form of drugs can be protected via potential inhibition from enzymatic metabolism or degradation at certain pH, light exposure or oxidation (Vanić et al., 2015). Moreover, their composition makes

nanocarriers well tolerable, biocompatible and biodegradable, which are fundamental conditions to assure safety and patient compliance (Fireman et al., 2011). Their properties are a function of their size, surface characteristics and solubilisation capacity. Therefore, by changes in their physicochemical characteristics it is possible to obtain nanocarriers with different potentials in controlling dermal drug delivery (Honeywell-Nguyen and Bouwstra, 2005). The size, surface charge, rigidity and lipid organization of nanocarriers can be tailored and exploited to optimize skin drug delivery (Schmieder et al., 2015).

1.3.2.1 Carrier size control

One of the first nanocarriers largely investigated as skin drug delivery systems were the conventional liposomes (CLs). They are phospholipid-based spherical vesicles composed of one or more phospholipid bilayer(s) surrounding an inner aqueous compartment (Figure 1.4). They can incorporate hydrophilic drugs in the aqueous core, lipophilic drugs in the lipid bilayer and amphiphilic drugs will partition between these two regions (de Leeuw et al., 2009). Their phospholipid bilayer membrane mimics the structure of the SC cell membrane. This allows them to promote penetration of drugs through the main barrier of the skin, which can consequently facilitate their action as drug carriers through/into the skin, thus assuring targeted drug delivery (Banerjee, 2013). First reports on their potential to transport and deliver drugs in the epidermis and dermis were published in the early 1980s. Mezei and Gulasekharam (1980) suggested that intact liposomes could pass through the SC, allowing deposition of triamcinolone acetonide in the dermis while decreasing its percutaneous absorption when compared to a standard ointment. This theory was, a few years after, criticised by other groups stating that the liposomal size would represent an obstacle to liposome diffusion through the densely packed SC in order to reach the deeper skin layers in intact state (Ganesan et al., 1984; Ho et al., 1985). Therefore, the effect of liposome size on drug deposition in the different skin layers was one of the first properties explored in the attempt to optimize nanocarriers for topical formulations destined for localized skin therapy. In 1994, du Plessis and collaborators concluded that the location of drug deposition mediated by CLs was affected by the liposome size. Specifically, smaller liposomes (60 nm) did not allow drug deposition in the deeper skin layers. On the contrary, liposome size of 300 nm was found to be optimal for assuring high drug reservoir in the deeper skin strata (du Plessis et al., 1994).

From that time on, extensive research has been done with the aim to clarify the role of the liposome size on the transport of drugs into the skin. It is now generally believed that vesicles with a size of 600 nm or above remain mainly confined in the SC layer and as a consequence limiting drug delivery in the deeper skin layers (Verma et al., 2003). They might also form an additional lipid barrier after drying thus strengthen the SC barrier properties. Liposomes having a size of 300 nm or below are able to deliver the incorporated drug to some extent in the deeper skin layers. However, the maximum deposition of drugs in the viable dermal layers has been assured by liposomes with a size of 70 nm or below (Verma et al., 2003; Danaei, et al., 2018). Therefore, liposomes with small vesicle size might be optimal for transdermal drug delivery or for the treatment of those skin diseases requiring drug action in the deeper skin layers (Figure 1.2). On the contrary, liposomes of around 300 nm can exhibit the highest reservoir in both epidermis and dermis layers, thus showing the potential to be used for localized skin therapy. However, when investigating their mechanism of skin delivery, the most emerging conclusion is that CLs are not able to pass intact deeper into the skin (Dreier et al., 2016). It is generally reported that they remain confined to the upper layers of the SC, where they function more as a drug reservoir. They interact with the SC lipids allowing their fluidization and thus promoting skin passage of drugs. This action is however limited in the upper epidermis layers, where vesicle can break due to their larger size, compared to skin pores, and lack of elasticity (Jain et al., 2017).

The size is not the only factor that affects skin drug delivery mediated by nanocarriers. Therefore, aiming at developing optimal nanocarriers for treatment of a wider variety of skin diseases, other nanocarrier characteristics and their effects on skin penetration of nanocarriers were explored (Schmieder et al., 2015).

1.3.2.2 Carrier surface charge control

Superiority in skin penetration potential has been obtained when an additional component, i.e. surfactant, was incorporated in the phospholipid bilayers of CLs (Cevc and Blume, 1992). This new class of liposomes, called transfersomes or deformable liposomes (DLs), is similar to CLs in terms of preparation methods and structure, but the presence of single chain of surfactant in the phospholipid bilayer of the former confers to them deformable properties

(Roberts et al., 2017). This mainly occurs because the surfactant disturbs the bilayer organization and creates discontinuities thus making the bilayer less rigid. This results in vesicles able to penetrate through the SC pores smaller than their own size, reaching deeper skin layers to deliver the incorporated drug (Jain et al., 2017). This skin penetration mechanism seems to be driven by the osmotic strength, also called hydration force, which is defined as the hydration gradient between the SC (water content lower than 15%) and the other layers of the epidermis (water content of 75%) (Sala et al., 2018). The enhanced delivery of drugs into the deeper skin layers makes DLs attractive nanocarriers for transdermal delivery of numerous drugs, but also for improved dermal delivery, such as treatment of deep dermal infections (Benson, 2006; Vanić, 2015).

The possibility to incorporate a surfactant in the vesicular structure opens up to the possibility of selecting among a wide variety of surfactants, including cationic (e.g. stearylamine, SA) or anionic ones (e.g. sodium deoxycholate, SDC). Incorporation of ionic surfactants results in DLs bearing positive or negative surface charge, namely cationic (CDLs) and anionic (ADLs) deformable liposomes. The liposomal surface charge has shown to affect skin penetration of DLs (Roberts et al., 2017). The skin penetration mechanism for charged DLs is related to electrostatic interactions occurring between the nanocarrier and the negatively charged SC cells. Specifically, these interactions are more likely to be triggered when liposomes bear a positive surface charge resulting in skin penetration enhancement (Jain et al., 2017). For example, skin deposition of temoporfin was enhanced by CDLs to a higher extent compared to both ADLs and neutral deformable liposomes (NDLs) (Dragicevic-Curic et al., 2010). The ability of CDLs (SECosomes) to enhance delivery into the viable epidermis has also been shown towards macromolecules, such as siRNA (Geusens et al., 2010). On the other hand, ADLs exhibited a more sustained release and skin retention of drug/compound, such as human epidermal growth factor (hEGF), methyl nicotinate and naringin (Puglia et al., 2005; Kaminski et al., 2016; Pleguezuelos-Villa et al., 2018). However, ADLs have also shown to promote skin drug penetration (Ogiso et al., 2001; Manosroi et al., 2004). Therefore, currently, there is no clear position regarding which is the most favourable liposomal surface charge to promote skin penetration of drugs.

1.3.2.3 Role of carrier's lipid organization

As alternatives to vesicular systems, particulate lipid-based nanocarriers can be obtained by replacing the liquid lipid of an oil in water emulsion with one or more solid lipids. This leads to formation of a lipid matrix that is solid at both room and body temperatures (Fireman et al., 2011). SLNs were the first to be developed and are the most representative of this class (Pardeike et al., 2009). Their superiority compared to liposomes was observed in terms of higher drug loading of lipophilic compounds, more controlled modulation of drug release and higher enhancement in drug stability by protection from chemical/light degradation and from moisture (Jain et al., 2017). Therefore, besides particle size and surface charge, another factor that affects the extent of drug deposition into the skin layers is represented by the nanocarriers' lipid organization. Each of these factors influencing the skin penetration potential of nanocarriers cannot be considered as “single responsible”, but they are all synergistically acting to define the potentials of every nanocarrier. For example, SLNs are known to allow controlled release of the drug and improve local drug depot to a higher extent compared to DLs (Garcês et al., 2018). This is the result of small particle size and consequent higher surface area, which allows a closer contact of SLNs with the superficial junctions of corneocytes clusters of SC (Garcês et al., 2018). However, as mentioned above, because of synergistic effects, SLNs' ability of drug depot and sustained drug release are also outcomes of their lipid organization. They, indeed, possess distinct occlusive property by forming a lipid film onto the skin consequently promoting skin hydration (Garcês et al., 2018). This facilitates the entrance of drugs into the SC to be then retained locally in the skin layers (Lauterbach and Müller-Goymann, 2015). Due to these skin penetration potentials, SLNs have been investigated as nanocarrier-based topical formulations for localized skin therapy, especially for treatment of acne, psoriasis, skin mycosis and inflammations (Puglia and Bonina, 2012). In addition, the particulate SLNs' lipid organization influences other characteristics, such as stability and safety. As an example, SLNs lack the bilayer structure of the liposomes, thus being more stable in both hydrophilic and lipophilic environment. This will allow safe transport and delivery of various substances to skin (Papakostas et al., 2011). Furthermore, they exhibit good skin tolerability, and are considered to be safe and biocompatible (Doktorovová et al., 2016).

1.3.3 Basic characteristics of skin

All the factors discussed earlier that need to be explored to overcome dermal delivery's limitations cannot be effectively translated in the development of effective topical formulations for localized skin therapy, unless the most important characteristics of the skin that account for ingress and diffusion of drugs into/through the skin are considered. Therefore, this paragraph will not provide a full and detailed description of skin anatomy, physiology and functions, but only those skin barrier's properties and characteristics that are fundamental when aiming to successfully deliver drugs onto, into or through the skin.

The skin is composed of several layers (Figure 1.5), but the first barrier that a drug or drug-in-carrier has to face is represented by the SC. The “brick and mortar” model simplifies the SC macrostructure being composed of flat dead cells filled with keratin filaments and water, which are surrounded by a densely packed lipid envelope. Furthermore, corneodesmosomes are interconnecting the corneocytes providing cohesion to the entire SC (Bouwstra and Ponec, 2006). The barrier properties of the overall skin reside in the microstructure of the SC, namely the molecular architecture of the lipid structure in the extracellular space between the corneocytes (Baroli, 2010). Ceramides, cholesterol, saturated long chain fatty acids are the main lipid classes forming the SC. The lamellar organization consists of short periodicity phase with repeat units at a distance of 6 nm and a long periodicity phase with repeat distances of 13 nm. The latter has been found in all species and it has been suggested to have an important role in the skin barrier function (Bouwstra and Ponec, 2006). The lateral packing exerts also a role in skin barrier properties, especially the orthorhombic packing confers very packed lipids within the lamellae (Banerjee, 2013; van Smeden et., 2014). Iwai and collaborators (2012) further explored the SC barrier by employment of a novel methodology, the cryo-electron microscopy of vitreous skin section. The lipid organization was found to be a stacked bilayer structure of fully extended ceramides with cholesterol molecules associated with ceramide sphingoid moiety. This additionally strengthens the SC barrier properties by making it more robust and more impermeable to water, as well as to both hydrophilic and lipophilic substances. This is due to interactions occurring between the individual lipid layers that involve only hydrocarbones, making them free to form pliable matrix (Iwai et al., 2012).

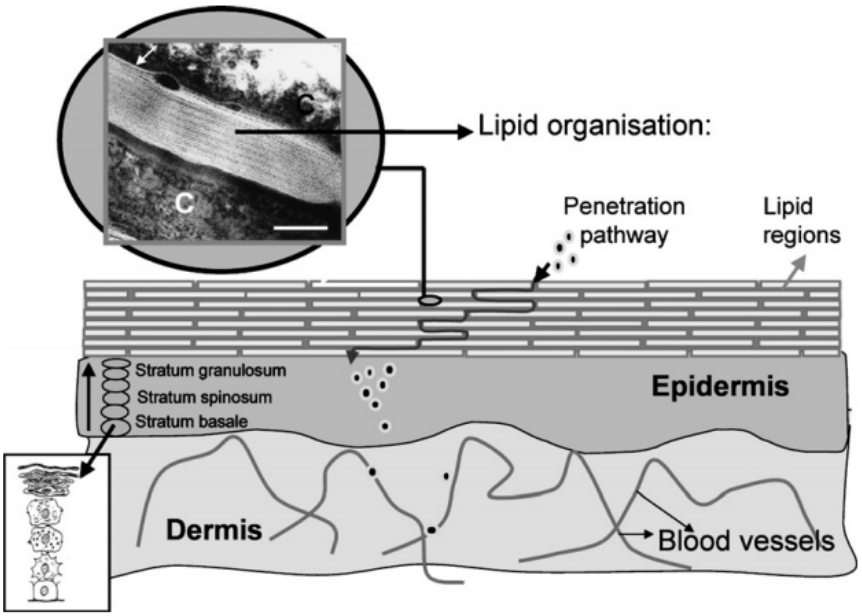

Figure 1.5: The skin layers (reprinted from Bouwstra and Ponec, 2006, with permission from Elsevier).

The "brick and mortar" model has been proposed as a representative model for the potential pathways of penetration across the SC, which occurs by passive diffusion driven by the concentration gradient of penetrant molecules (Figure 1.6) (Bolzinger et al., 2012). The intercellular pathway comprises the diffusion of molecules across the continuous path formed by the SC lipids. Lipophilic molecules will prefer this route. An alternative route is the transcellular route through the corneocytes, which involves partitioning in and out of the lipid domains (Baroli, 2010). The unique arrangement of this layer represents the basic skin penetration resistance that limits the molecules passage through the SC. This is because, for very lipophilic drugs which can overcome the SC barrier, the aqueous interface beneath the SC will obstacle the permeation from viable epidermis to dermis layer. Hydrophilic molecules, which prefer the transcellular pathway, have to cross the intercellular lipids to jump from one corneocyte to another (Bolzinger et al., 2012). Drugs can also penetrate through defects in the skin structure, such as the hair shaft and sweat glands, which create breaks in the continuity of the SC. This is called the follicular pathway. Although the appendages are only approx. 0.1% of the skin surface and are mostly important for large or ionic molecules (Lademann et al.,

2011), recently deep penetration into follicles has been reported for several nanoparticles, even followed by their uptake by the sebaceous glands (Patzelt et al., 2017).

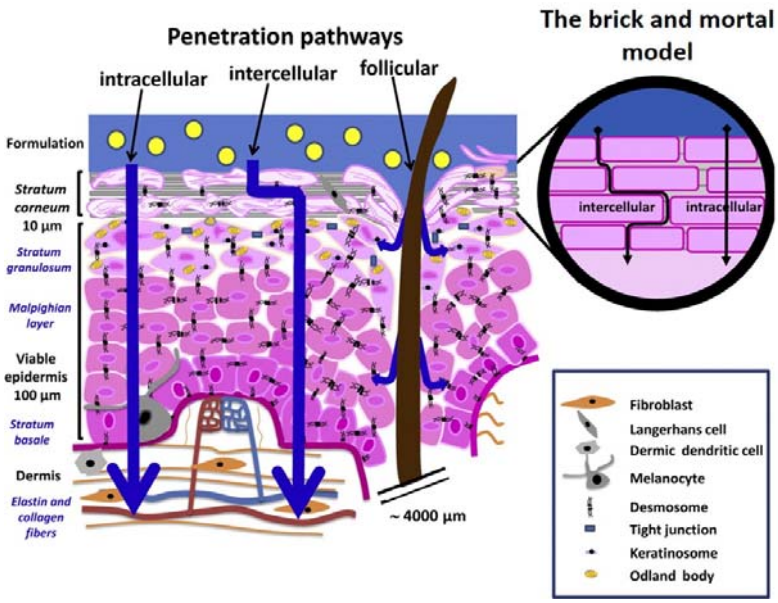

Figure 1.6: Skin penetration pathways and the brick and mortar model (adapted from Bolzinger et al., 2012, with permission from Elsevier).

The dermal drug delivery's limitations are further enhanced by the phenomenon of "healthy *vs.* diseased" skin barrier. Bouwstra and Ponec (2006) provided a detailed review on the differences in the lipid composition and organization between healthy/normal skin and diseased/damaged skin. In atopic dermatitis, a reduction in acylceramide content occurs thus altering the lamellar organization and consequently reducing the SC barrier properties. In dry skin, the same outcome is observed, but in this case, the reduced skin barrier is due to a deficiency in essential fatty acids and an increase of lipids responsible for forming a more fluid phase. In ichthyosis skin, a prominent increase in cholesterol sulphate results in a reduction of the lattice density and enhancement of SC permeability (Bouwstra and Ponec, 2006). Moreover, damage or pathological conditions cause alterations to the skin, e.g. alteration in skin thickness, modification of metabolic capacity, breakages at the skin surface, alteration of

SC microstructure. It has been widely accepted that drug penetration through/into diseased skin is highly enhanced. However, the outcome is not so obvious when considering the formulations to be applied onto diseased/damaged skin, mainly because the formulations in the development phases are usually tested on healthy skin. This aspect becomes even more fundamental when referring to nanocarriers. All the previously discussed mechanisms for skin drug penetration mediated by nanocarriers involve the direct interaction with the SC barrier, especially the SC lipids. If these are altered, changes in the skin drug penetration might occur. This is of a specific consideration in development of wound dressings.

The acidic skin surface, described as acid mantle, is another factor responsible for maintaining the SC barrier properties. Besides antimicrobial defence, the acidic pH (4.2-5.6) of the skin surface maintains the SC permeability barrier by effects on the extracellular lipid organization (Geusens et al., 2011). The acidic pH may additionally be an obstacle for nanoparticle penetration through the SC by triggering their aggregation due to reduction in electrostatic forces (Prow et al., 2011).

As mentioned earlier, when studying the skin penetration of drugs it is important to focus on the viable epidermis and dermis layers. One of the reasons is that these layers account for a metabolic barrier against drugs and nanoparticles. Enzymatic activity, for instance, on liposomes causes their fusion with the intercellular lipids thus interfering with their penetration into the deeper skin layers (Prow et al., 2011).

1.4 Vehicle for nanocarriers

The topical application of liposomal dispersions is limited due to their liquid nature (Pavelić et al., 2001). Their low viscosity may cause a short retention time of liposomal formulations at the administration site, including skin. Hydrogels, as a secondary vehicle for liposomes, have good potential to confer the appropriate rheological properties necessary for effective liposomes' application onto the skin (Pitorre et al., 2017). Hydrogels are hydrophilic polymer networks capable of absorbing large amounts of water (Gao et al., 2014; Gyles et al., 2017). Therefore, hydrogels can provide a moist environment once applied onto the skin surface

which is an important feature for promoting wounds/burns healing, together with healing of other skin pathologies characterized by dry skin (e.g. ichthyosis). Their polymeric matrix allows entrapment of drugs for prolonged release, consequently improving patient compliance due to reduction of administration frequencies (Pitorre et al., 2017). Additionally, hydrogels are biocompatible and possess good bioadhesiveness, which is one of the most important features related to trans(dermal) semisolid and solid dosage forms to assure adequate drug retention time on the skin administration site (Ribeiro et al., 2009; Cilurzo et al., 2012). Therefore, local therapeutic drug levels can be assured favouring the pharmacological response (Hurler and Škalko-Basnet, 2012). The combination of two delivery systems by incorporation of liposomes in hydrogels is a very promising strategy for improved localized skin therapy. Liposomes can be maintained at the skin site due to avoidance of rapid liposomes clearance mediated by the hydrogel and the drug release from liposomes-in-hydrogel systems is expected to be controlled and sustained (Billard et al., 2015). The hydrogel can additionally maintain liposome's structural integrity, resulting in improved stability (Gao et al., 2014).

The addition of a second vehicle creates a more complex drug delivery system. The drug needs to be initially released from liposomes into the hydrogel and then diffuse through the hydrogel to come in contact with the skin. Therefore, the drug release from liposomes-in-hydrogel systems will be affected by the physicochemical properties of the drug but also by the interaction between drug, liposome and hydrogel (Grijalvo et al., 2016). Liposomal physicochemical properties and hydrogel texture properties need to be considered during the optimization of effective liposomes-in-hydrogel systems for skin-targeted drug delivery. Considering the aqueous environment provided by the hydrogels, factors influencing the drug release from the combined delivery systems are the lipophilicity of the drug and its water solubility. Lipophilic and poorly soluble drugs would have to further partition from the lipophilic bilayer of liposomes into the aqueous phase provided by the hydrogel. Hurler et al. (2013b) performed release studies of two model compounds with different lipophilicities from liposomes-in-hydrogel systems observing an initial faster release of the more hydrophilic one, which could diffuse more easily into the hydrophilic hydrogel. Liposomal physicochemical properties have also shown to affect the drug release from the combined delivery systems.

Particularly, liposomal lipid composition can determine the extent of the interaction between liposomes and hydrogel, consequently affecting liposome integrity and drug release. As an example, hydrophobic interactions between phosphatidylcholine (PC) liposomes and poly(N-isopropylacrylamide) hydrogel are responsible for liposome stability and release of hydrophilic model compounds (Liu et al., 2012). An increase in liposome size was found to enhance sustained release of a hydrophilic compound, carboxyfluorescein, in liposomes-in-hydrogel system (Ruel-Gariepy et al., 2002). Natural polymer-based hydrogels, such as chitosan hydrogels, possess positive chains due to the presence of amino groups. Therefore, incorporation of surface charged liposomes can trigger electrostatic interactions with the charged polymer's chains of the hydrogel. When incorporated in the chitosan hydrogel, cationic liposomes have shown to enable a more sustained release of model compounds compared to both neutral and anionic ones (Hurler et al., 2013b). The hydrogel matrix's properties, such as polymer composition, porosity, mesh size and gel swelling, also regulate drug release from liposomes-in-hydrogel system (Grijalvo et al., 2016). The mesh size, as an example, affects the hydrogel mechanical strength and the drug release. Once the hydrogel swells, the mesh size increases thus enabling drug diffusion through the hydrogel matrix and its consequent release (Grijalvo et al., 2016). Last but not least, the hydrogel texture and bioadhesive properties might be affected when liposomes are incorporated in hydrogels. The liposomal surface charge can influence the hydrogel properties, such as hardness, cohesiveness and adhesiveness. Charged conventional liposomes have shown to increase the above-mentioned properties of chitosan hydrogel compared to neutral liposomes (Hurler et al., 2013b). Therefore, all these variables need to be taken into consideration when optimizing liposomes-in-hydrogel systems to assure effectiveness of the delivery systems for localized skin therapy.

During the early screening for the right choice of the nanocarrier and, later, of the hydrogel as second vehicle, the employment of model substances to be incorporated in the selected nanocarriers is necessary to shorten the optimization time frame.

1.5 Proof-of-concept on the model substances

The optimization of effective nanocarriers for skin-targeted drug delivery requires nanocarriers-associated model substances as a proof-of-concept that the selected nanocarrier can assure controlled delivery to the specific targeted skin layer(s). In this thesis, model substances are referred to as model compounds and drugs/active substances. Model compounds can be used for their specific properties, e.g. fluorescent nature, to follow their skin penetration through the skin layers once topically applied onto the skin surface in nanocarrier-based formulations. On the other hand, drugs/active substances with specific biological properties beneficial for treatment of skin diseases can be incorporated in nanocarriers as model substances. During the screening of nanocarriers with different properties (e.g. size, surface charge), the evaluation of their influence on drug/active substance's skin penetration rate and biological properties might assist in the optimization of effective nanocarriers for skin-targeted drug delivery.

1.5.1 Model compounds

During the optimization of nanocarriers as dermal delivery systems, the evaluation of their skin penetration potential and to which specific skin layer(s) they deliver the incorporated active substance can assist in the right choice of the nanocarriers for skin-targeted drug delivery, according to the skin condition and disease.

Among the techniques used to investigate the distribution of a drug mediated by the nanocarrier through the skin layers after topical administration onto the skin, confocal laser scanning microscopy (CLSM) has the advantage to avoid the cryofixing process of the skin sample (van Kuijk-Meuwissen et al., 1998). This will avoid possible changes in skin lipid organization or eventual redistribution of the marker that might occur during cryofixing the sample (van Kuijk-Meuwissen et al., 1998). Fluorescent compounds are incorporated in nanocarriers and their distribution in the skin layers can be followed by a confocal microscope. Both hydrophilic and lipophilic model fluorescent compounds are needed to predict skin distribution of both hydrophilic and lipophilic active ingredients. According to the different skin penetration pathways, the lipophilicity of the penetrant molecule is considered to be one of the most important parameters affecting the extent of active ingredients' penetration and

distribution into/through the skin (Van Gele et al., 2011). Calcein and rhodamine (Figure 1.7) are two model compounds commonly incorporated in nanocarriers to represent hydrophilic and lipophilic molecules, respectively.

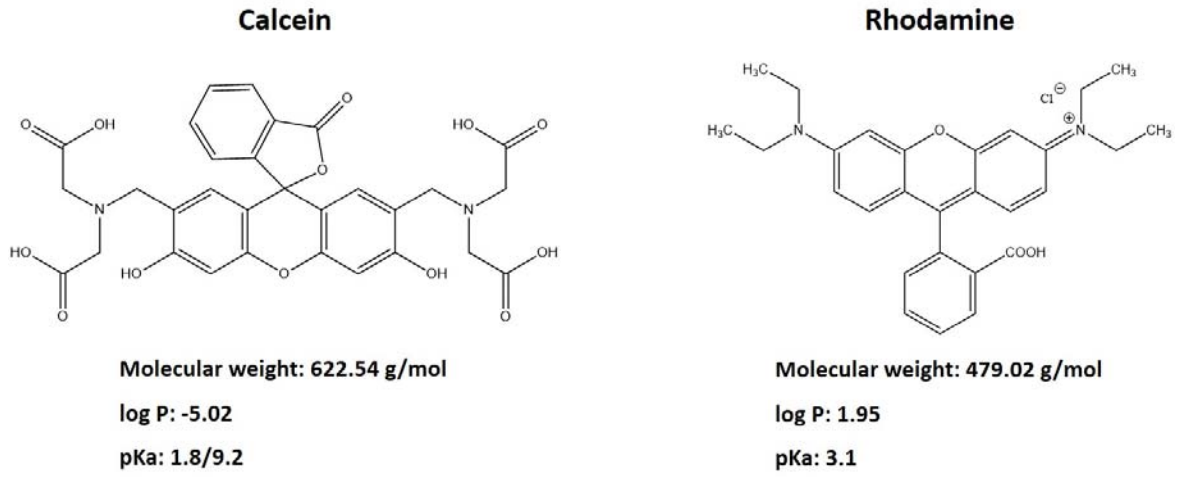

Figure 1.7: Chemical structures and basic physicochemical properties of calcein and rhodamine (log P and pKa values are from Pittman et al. (2001), Flaten et al. (2006), Gillet et al. (2011), Anissimov et al. (2012)).

Incorporation of calcein in DLs helped to clarify the controlled drug release in the skin mediated by DLs (Bahia et al., 2010). Gillet et al (2011) employed both calcein and rhodamine to compare the skin penetration potential of CLs and DLs using pig skin, concluding that both liposomes allowed calcein depot onto the skin surface, whereas rhodamine was delivered deeper into the skin layers. Rhodamine has been also incorporated in SLNs by Küchler and collaborators (2009) showing the superior ability of SLNs in enhancing skin penetration of the model compound in both viable epidermis and dermis as compared to a conventional cream.

1.5.2 Biologicals

Biologicals include any drugs produced using biotechnology, such as peptides, proteins, antigens, antibodies, nucleic acids, and cell-based therapies. Recently, the interest towards

these therapeutic agents has grown together with the number of new molecules in pipeline, formulation development and delivery technologies (Morales et al., 2017). Their attractiveness for treatment of skin diseases relies in their high selectivity, potent therapeutic efficacy and limited side effects (Škalko-Basnet, 2014). Topically administered biologicals have shown to be promising for gene and vaccine delivery, growth factors for treatment of chronic wound healing and enzymes (e.g. T4 endonuclease V) for skin cancer (de Leeuw et al., 2009; Vanić et al., 2015). Despite their high potential as skin therapeutic agents, biologicals represent a formulation challenge since they are chemically unstable and prone to aggregation, deamidation, isomerization, hydrolysis, oxidation and denaturation. Moreover, their high molecular weight and hydrophilicity limit their penetration through the SC, resulting in limited drug concentrations at the targeted site and a need for parenteral formulations (Mitragotri et al., 2014).

As a biological, hEGF is a polypeptides (6 kDa) with 53 aminoacids and 6 cystein residues (Figure 1.8) that counteract for disulphide bridges thus creating the hEGF domains important for receptor binding (Zeng and Harris, 2014).

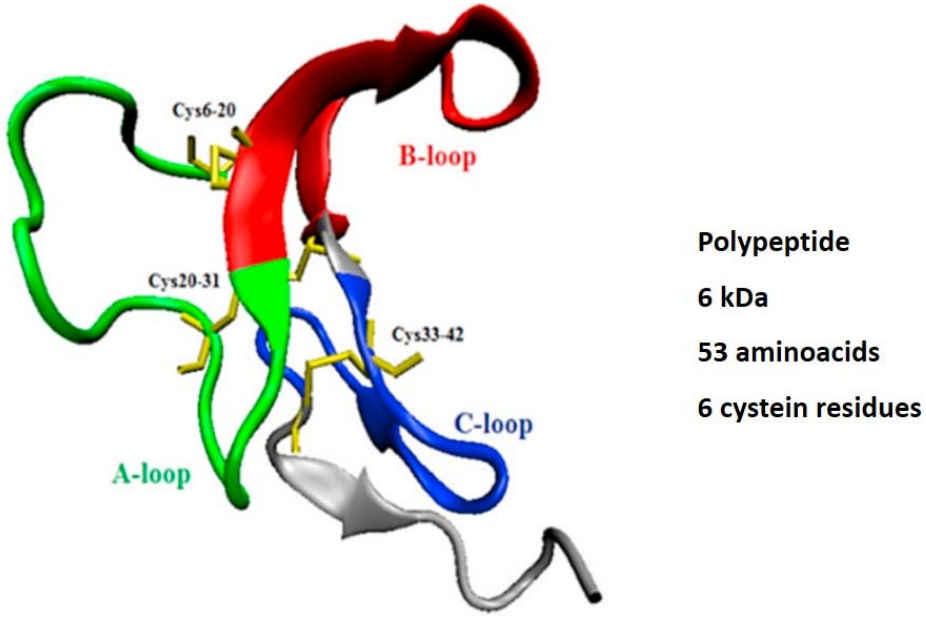

Figure 1.8: Structure of human epidermal growth factor (adapted from Mehrabi et al., 2018, with permission from Elsevier).

hEGF is one of the growth factors mainly involved in the wound healing phases by inducing cell proliferation and promoting re-epithelialisation (Xue et al., 2018). However, the endogenous hEGF is degraded by proteases in the wound bed further delaying the chronic wound healing (Saghazadeh et al., 2018). Localized therapy with hEGF might represent a good approach to assure a faster and effective wound healing (Garcia-Orue, et al., 2017). As mentioned previously, poor *in vivo* stability and enzymatic degradation limit local administration of hEGF. Additionally, its relatively high molecular weight (6 kDa) affects its SC penetration. Those limitations would require frequent hEGF administrations to achieve sufficiently high local concentrations thus exerting its therapeutic effect (Gainza et al., 2015). Subsequently, a high systemic absorption and undesired side effects can occur. Incorporation of hEGF in CLs and SLNs have shown to overcome some of its limitations related to topical administration (Alemdaroğlu et al., 2008; Gainza et al., 2014).

1.5.3 Curcumin

Often, a treatment of skin diseases requires interventions at different levels. For example, treatment of acne involves the use of both anti-inflammatory and anti-bacterial agents (de Leeuw et al., 2009); chronic wounds/burns, presenting high levels of inflammation, might also be prone to bacterial colonization with high risk of biofilm development (Byrd et al., 2018). Additionally, persistent bacterial infections are also a cause of prolonged inflammations. Therefore, topical administration of multitargeting active ingredients may result in a more effective localized skin therapies, improving a patient compliance by reducing the number of administrations.

Curcumin is a natural polyphenolic compound extracted from the rhizome of the turmeric plant *Curcuma longa L.* (Figure 1.9).

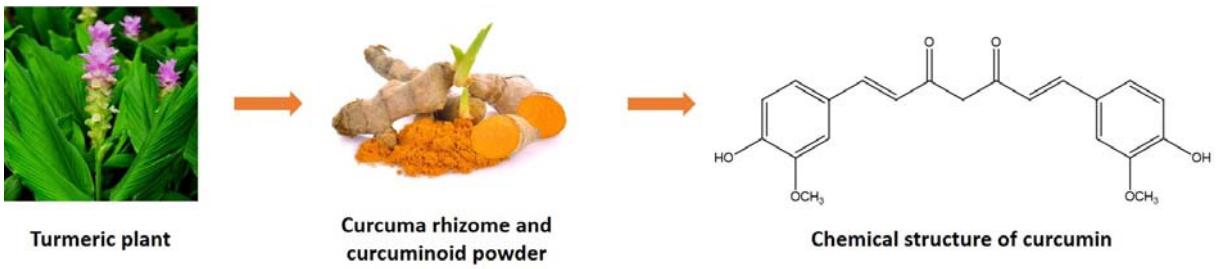

Figure 1.9: Curcumin origin and chemical structure.

In the last two decades, the numerous beneficial effects of this pleiotropic molecule, such as anti-oxidant, anti-inflammatory and anti-bacterial, have made curcumin an attractive compound for treatment of skin inflammation and infections (Krausz et al., 2015; Mehanny et al., 2016). The action of curcumin as anti-inflammatory agent is due to downregulation of different proinflammatory cytokines, such as tumour necrosis factor, interleukins and chemokines. Curcumin also inactivates the nuclear transcription factor kappa B, further reducing the degree of inflammation. Additionally, curcumin has shown to act at molecular levels in different phases of the wound healing process, further increasing its potential for chronic wound therapy. Curcumin is promising for managing scar formation and treatment of post burn hypertrophic scarring (Amini-Nik et al., 2018). More recently, the revealed anti-bacterial effect of curcumin makes it a good alternative to the overuse of antibiotics, often object of microbial resistance (Krausz et al., 2015). Curcumin, as multitargeting active ingredient, might therefore be a good candidate for local treatment of skin diseases that require interventions at different levels. However, its hydrophobic nature (log P = 3.29, Araiza-Calahorra et al., 2018) makes its incorporation in conventional topical dosage forms challenging (Basnet et al., 2012). Moreover, it is chemically unstable, especially at the physiological pH, and photosensitive. When applied locally on skin, side effects, such as erythema, peeling and hot phenomenon, might occur (Zhao et al., 2013). Incorporation of curcumin in nanocarriers, such as CLs, SLNs, propylene glycol (PG) liposomes, has shown to overcome these limitations by increasing its stability and enhancing therapeutic effects (Mehanny et al., 2016).

1.5.4 Chitosan

Chitosan-based hydrogels are one of the most studied advanced drug delivery systems due to the numerous intrinsic biological properties of this biopolymer (Billard et al., 2015). Chitosan is a linear polysaccharide composed of N-acetyl-glucosamine and glucosamine units linked by β-(1-4) bonds and it can be easily obtained from deacetylation of the natural polymer chitin (Gyles et al., 2017). The ratio between the two monomeric units, expressed as the degree of deacetylation, together with the molecular weight affect its physical and biological properties (Verlee et al., 2017). Solubility, anti-microbial effect and bioadhesiveness are examples of chitosan properties affected by its degree of deacetylation. The structure is shown in Figure 1.10.

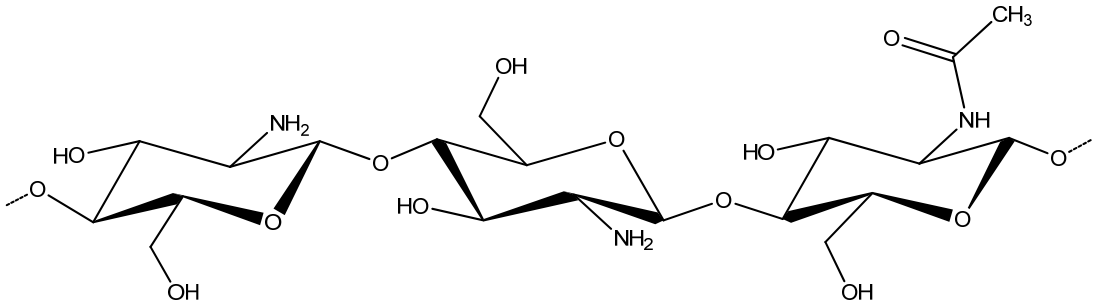

Figure 1.10: Chemical structure of chitosan.

Besides its non-toxicity, chitosan is attractive because of its biodegradability, bioadhesiveness, bacteriostatic action and improvement of drug transport across biological barriers (Billard et al., 2015). Most of these properties can be ascribed to the presence of amino groups on the polysaccharide's backbone that confer positive charge to chitosan chains at acidic pH (Perinelli et al., 2018). Good bioadhesion of chitosan to skin can be assured due to electrostatic interactions between the positively charged polymer with the negative SC cells (Ribeiro et al., 2009). This leads to increased retention time at the administration site resulting in improved therapy and patient compliance. The positive chains of chitosan can crosslink the negative bacterial cells thus modifying the bacteria cell membrane permeability (Perinelli et al., 2018). This leads to an efflux of ions and proteins from the cytoplasm to the extracellular space

exerting a toxic effect on bacteria. The anti-bacterial activity is more pronounced when chitosan has a high degree of deacetylation (Perinelli et al., 2018). Chitosan-based hydrogel has therefore beneficial properties for improving chronic wounds and burn healing, due to the fact that it can protect the wound from bacterial infection, offers a moist environment, and is biocompatible, all properties that an ideal wound dressing should have (Hamedi et al., 2018). Chitosan has also shown to accelerate the repair of different tissues and facilitate contraction of wounds thus further contributing to improve wound healing. Chitosan might also synergistically act with the beneficial effects of the incorporated active ingredient thus increasing the efficacy of wound dressings. Additionally, the combination of nanocarriers and chitosan hydrogel as advanced delivery systems has shown to be promising for improved chronic wound healing (Hurler et al., 2013a). Tigecycline nanoparticles-in-chitosan hydrogels exhibited strong anti-bacterial activity against *S. aureus* in both *in vitro* and *in vivo* studies, additionally assuring *in vitro* wound closure within 48 hrs (Nimal et al., 2016). Niosomes-in-chitosan hydrogel showed to enhance the anti-bacterial properties of the incorporated moxifloxacin when tested *in vitro* against both *Pseudomonas aeruginosa* and *S. aureus* by Sohrabi et al. (2016), exhibiting good potential to treat burn infections.

2 Aims of the thesis

The general aim of this thesis was the development and optimization of nanocarriers for tailored skin delivery. The possibility to develop nanocarriers that can carry/transport the incorporated drug/substance into the specific targeted skin layers, according to the skin condition and disease state, can contribute to the development of effective localized skin therapy.

The specific aims were the following:

- Validation and optimization of a newly developed close-to-*in vivo* skin penetration model.
- Selection of a nanocarrier with specific skin-targeted drug delivery potential by direct comparison of three nanocarriers on the developed skin penetration model.
- Assessment of the influence of the surfactants used to prepare nanocarrier on the physicochemical properties of the selected nanocarrier.
- Evaluation of the effect of the selected nanocarrier's surface charge on the skin penetration behaviour of hydrophilic and lipophilic active substance.
- Evaluation of the biological activities of two active substances when incorporated in the selected nanocarriers with different surface charges.
- Evaluation of the influences of nanocarrier's surface charge on the hydrogel texture and bioadhesiveness and skin penetration of curcumin from curcumin-in-liposomes-in-hydrogel formulation.

3 Summary of papers

3.1 Paper I

In the first paper we validated the isolated perfused human skin flap (IPHSF) as a new close-to-*in vivo* skin penetration model to be used as a tool in optimization of dermal delivery systems for skin therapy.

The IPHSF was validated in terms of its ability to discriminate the skin penetration of two model compounds with different lipophilicities. Two fluorescent markers, a hydrophilic (calcein) and a lipophilic (rhodamine), were used.

A preliminary perfusion experiment was performed to monitor the physiological parameters of the flaps during the whole experiment. It also assisted in identifying the best perfused areas of the flap (skin surface temperature of ca. 32 °C), which were used to establish the skin flap surface area suitable to apply the solutions of the fluorescent markers for the skin penetration studies. The human skin flaps were perfused with modified Krebs-Henseleit buffer (KHb) (pH 7.4, 290 mOsm/kg). The skin surface temperature and therewith indirectly skin perfusion was monitored with an infrared (IR) camera.

For the IPHSF skin penetration studies, the solutions (7 mL) of the fluorescent markers were applied onto the best perfused (32 °C) skin area (49 cm^2) of the IPHSF, as identified by the IR camera. The skin penetration studies were performed for 6 hrs and markers in the perfusate quantified spectrofluorometrically. CLSM technique was employed to provide information about the localization of the fluorescent markers in the human skin flaps. For comparison, *in vitro* and *ex vivo* skin penetration studies were carried out in the Franz diffusion cells system (FDC) using cellophane membrane and human/pig skin, respectively.

In both the preliminary perfusion experiments and skin penetration studies the physiological parameters of the flaps were maintained constant and the human skin flaps well perfused (skin surface temperature of 32 °C) for the whole period of the experiments. A low percentage of penetrated calcein through the IPHSF was found, while no rhodamine was detected in the perfusate. This was confirmed by CLSM images of a cross-section of the human skin flaps.

Calcein was uniformly distributed through the skin flap, while rhodamine mainly accumulated in the SC. *Ex vivo* skin penetration studies in the FDC using full human skin revealed a lower percentage of penetrated calcein compared to the IPHSF. The same penetration profiles of rhodamine were observed both in the IPHSF and in *ex vivo* human skin. A higher penetration of both markers was observed through both *in vitro* cellophane membrane and *ex vivo* pig skin, compared to the IPHSF.

We showed that the model could be used in skin penetration studies assuring constant experimental conditions and reproducible results. Moreover, the model appeared to be able to show the different penetration potential of the two markers. The role of skin perfusion on the skin penetration of the model compounds was also revealed. This model could be a promising tool for optimization of skin formulations in conditions resembling the human studies.

3.2 Paper II

The aim of the second paper was to compare the skin penetration potential of three commonly used phospholipid-based nanocarriers, namely CLs, DLs and SLNs, on the IPHSF model developed in Paper I.

CLs and DLs were prepared by the film hydration method, whereas SLNs were made by the solvent injection method. Two fluorescent markers, calcein (hydrophilic) or rhodamine (lipophilic), were incorporated in CLs, DLs and SLNs, respectively. *In vitro* and *ex vivo* skin penetration studies in the Franz diffusion cells system (FDC) using the cellophane membrane and pig/human full thickness skin, respectively, were performed for comparison with the skin penetration studies on IPHSF.

All nanocarriers ranged in size between 200-300 nm. The surface charge and the entrapment efficiency for both markers mirrored the lipid composition and type of surfactant used in the three nanocarriers. No penetration of both nanocarrier-associated markers was observed through the full IPHSF confirming the suitability of all tested nanocarriers for dermal drug delivery. The delivery of both markers into/through the skin layers was dependent on the type of nanocarriers, as observed by CLSM technique. CLs formed a depot on the skin surface retaining both markers to a higher extent in the superficial skin layers. DLs and SLNs enabled higher penetration of both markers into the deeper skin layers compared to CLs. No nanocarrier-associated markers permeated the *ex vivo* human skin in the FDC, in agreement with findings from the IPHSF model. The penetration profiles through both *in vitro* cellophane and *ex vivo* pig skin differed from the findings obtained with the IPHSF model.

The skin penetration studies on IPHSF model highlighted the differences in the skin penetration potential of the three phospholipid-based nanocarriers that were found dependent on their lipid composition and surface charge. This study might assist in the choice of the optimal nanocarrier for targeted drug delivery into the specific skin layers, depending on the skin condition and disease.

3.3 Paper III

In Paper III we aimed at developing hEGF-containing DLs to improve hEGF dermal delivery for localized chronic wound therapy. We explored the effect of the liposomal surface charge on hEGF skin penetration, as well as on its *in vitro* mitogenic activity.

hEGF-containing NDLs, CDLs and ADLs were reduced to the desired size by extrusion through polycarbonate membrane. All hEGF-containing DLs were characterized in terms of size, zeta potential and drug load capacity. Polyamide membrane and full thickness human skin in the Franz diffusion cells system were used to evaluate the *in vitro* release and *ex vivo* skin penetration of hEGF, respectively.

Finally, the mitogenic activity of hEGF in all DLs was explored by *in vitro* cell proliferation studies using human foreskin fibroblasts (HFF) and human immortalized keratinocytes (HaCaT). Both HFF and HaCaT were treated with the hEGF liposomal formulations for 24 and 48 hrs, respectively.

All DLs were within the vesicle size range of 300-350 nm. The hEGF entrapment efficiency was not affected by the liposomal surface charge and was found to be high for all DLs (~ 80%). No significant differences were observed in the *in vitro* hEGF release from the different DLs through polyamide membrane, although ADLs exhibited the most sustained release of hEGF. All DLs assured dermal delivery of hEGF because no penetration of hEGF through the full thickness human skin was detected. Comparing the liposomal surface charge, ADLs exhibited the highest retention onto the human skin surface thus providing a hEGF depot. Moreover, ADLs exhibited the best enhancement of hEGF mitogenic activity, even compared to the positive control (hEGF in solution). This effect was highly evident in both HFF and in HaCaT treated for 48 and 24 hrs, respectively.

We showed that the liposomal surface charge plays a role in both nanocarriers' skin penetration potential towards hEGF and in the enhancement of its mitogenic activity. ADLs exhibited the best enhancement effect on hEGF activity showing a potential to be used in skin formulations for improved chronic wound therapy.

3.4 Paper IV

In the fourth paper, we focused on DLs as nanocarriers for dermal delivery of a multitargeting active compound curcumin, for treatment of skin inflammation and infections.

NDLs, CDLs and ADLs containing curcumin were prepared and the influence of the liposomal surface charge on the skin penetration potential of curcumin-DLs was explored in *ex vivo* skin penetration studies using the full thickness human skin. The anti-bacterial activity of curcumin-DLs was evaluated *in vitro* against two clinical strains of Gram-positive bacteria, namely *S. aureus* and *Streptococcus pyogenes*. Curcumin-DLs were also evaluated for anti-inflammatory activity by exploring their effect on nitric oxide (NO) production in lipopolysaccharide (LPS)-induced macrophages. The biological activities of curcumin-DLs were compared to free curcumin (curcumin in solution) and empty NDLs, CDLs and ADLs, respectively. Finally, the liposomal formulations were tested in *in vitro* cell proliferation studies to assess their safety in healthy human foreskin fibroblasts (HFF).

The vesicle size of all DLs was within the targeted range (200-300 nm) and the entrapment efficiency of curcumin in DLs mirrored the type of surfactants used to prepare the different DLs. ADLs entrapped the highest amount of curcumin, whereas CDLs exhibited the lowest entrapment efficiency. *Ex vivo* skin penetration studies revealed that CDLs assured the most sustained penetration of curcumin through the full thickness human skin. All curcumin-DLs inhibited both *S. aureus* and *S. pyogenes* growth; curcumin-CDLs exhibited the strongest anti-bacterial activity compared to the other liposomal formulations and curcumin in solution. All DLs enhanced curcumin's anti-inflammatory activity compared to curcumin in solution, while CDLs assured the strongest effect. No toxicity of DLs in HFF was observed at both 12 and 24 hrs exposure. All curcumin-DLs exhibited a proliferation effect in HFF.

The findings confirmed an effect of the liposomal surface charge on DLs as nanocarriers. Curcumin-CDLs are therefore promising for improved localized skin therapy for treatment of skin diseases involving inflammation and infection.

3.5 Paper V

In Paper V we introduced curcumin-containing deformable liposomes-in-hydrogel system as a final formulation, in a form of wound dressing, for previously developed curcumin-DLs.

We explored the effect of the liposomal surface charge on the chitosan hydrogel's texture and bioadhesive properties, as well as on curcumin *ex vivo* penetration through the full thickness human skin.

The charged liposomes exhibited a positive effect on the hydrogels' hardness, whereas negatively affected both the hydrogels' cohesiveness and adhesiveness. The incorporation of all DLs in chitosan hydrogel did not affect its bioadhesion to human skin. NDLs-in-hydrogel showed superior bioadhesion as compared to both plain chitosan hydrogel and curcumin-in-hydrogel. All DLs-in-hydrogel systems assured a sustained skin penetration of curcumin compared to curcumin in solution. CDLs-in-hydrogel system exhibited the most sustained skin penetration of curcumin.

The DLs-in-hydrogel systems were also evaluated in terms of stability. The hydrogel texture properties slightly decreased after a storage for one month at room temperature (23-24 °C). NDLs-in-hydrogel system preserved the same original hydrogel properties to a higher extent than both CDLs- and ADLs-in-hydrogel system. On the other hand, the presence of CDLs in hydrogel caused no changes in gel's bioadhesiveness as compared to NDLs and ADLs.

The incorporation of curcumin in deformable liposomes-in-hydrogel system showed to be a suitable method to obtain curcumin-based formulations for topical treatment of skin diseases. CDLs-in-hydrogel system has a good potential to be further evaluated in terms of anti-bacterial, anti-inflammatory and anti-biofilm properties for improved localized skin therapy, particularly targeting chronic wounds/burns and scars.

4 Experimental section

Materials and methods employed in this thesis are described in Paper I-V. This section aims to provide a more detailed description of the human skin flap and methodology used to develop and validate the IPHSF as skin penetration model. Additionally, the methodology not included in the papers is described in more details.

4.1 The IPHSF model

4.1.1 Human skin flap

The human skin flaps are surgically-derived portion of skin, including the subcutaneous fatty tissue, excised from the abdomen of female patients during abdominoplasty. The human skin flaps are normally discarded after surgery, therefore no ethical approval was required from the Norwegian Ethical Committee. The experiments were performed in accordance with the Declaration of Helsinki Principles.

The human skin flap comprises the vascular system of both the dermis and the subcutaneous fat layer. This allows selection of one of the vessels to be cannulated thus perfusing the human skin flap with a physiological medium, which will be referred as perfusate throughout the thesis. Kreidstein et al. (1991) performed perfusion studies on the isolated human skin flap showing that it remains metabolically active for up to 5 hrs when *in vitro* perfused. Miland et al. (2008) using DIRT showed that the skin of the IPHSF is not uniformly perfused. There are areas with a higher perfusion, so-called hot spots, and areas that are less perfused. These areas are easily identified using an IR camera, which provides real-time information on skin perfusion. The perfusion pattern is related to the vascular anatomy of the flap (de Weerd et al., 2009). Therefore, to perform skin penetration studies on the IPHSF we based our experimental setup of the human skin flap perfusion using the established method by Miland et al. (2008) with some modifications.

4.1.2 Preliminary human skin flap perfusion experiment

A preliminary experiment on human skin flap perfusion was performed to confirm that the physiological parameters of the IPHSF were maintained constant during the entire duration of the experiment (6 hrs). The human skin flap, after excision, was placed on a metal grid at room temperature and one vessel was selected and cannulated with an arteriotomy cannula. The cannula, with a diameter of 1 mm, was then connected to a perfusion apparatus thus providing the entrance of perfusate in the human skin flap's vascular system. The perfusate was KHb with the following composition (in mM): 110 NaCl, 3.8 KCl, 1.4 KH_2PO_4, 1.2 $MgSO_4$, 31 $NaHCO_3$, 2.5 $CaCl_2$, 11 glucose and 10 sucrose. Human serum albumin was added to the perfusate in the concentration of 30 mg/mL. The pH of KHb was adjusted to 7.4, whereas the osmolarity was 290 mOsm/kg. The human skin flap perfusion design is shown in Figure 4.1.

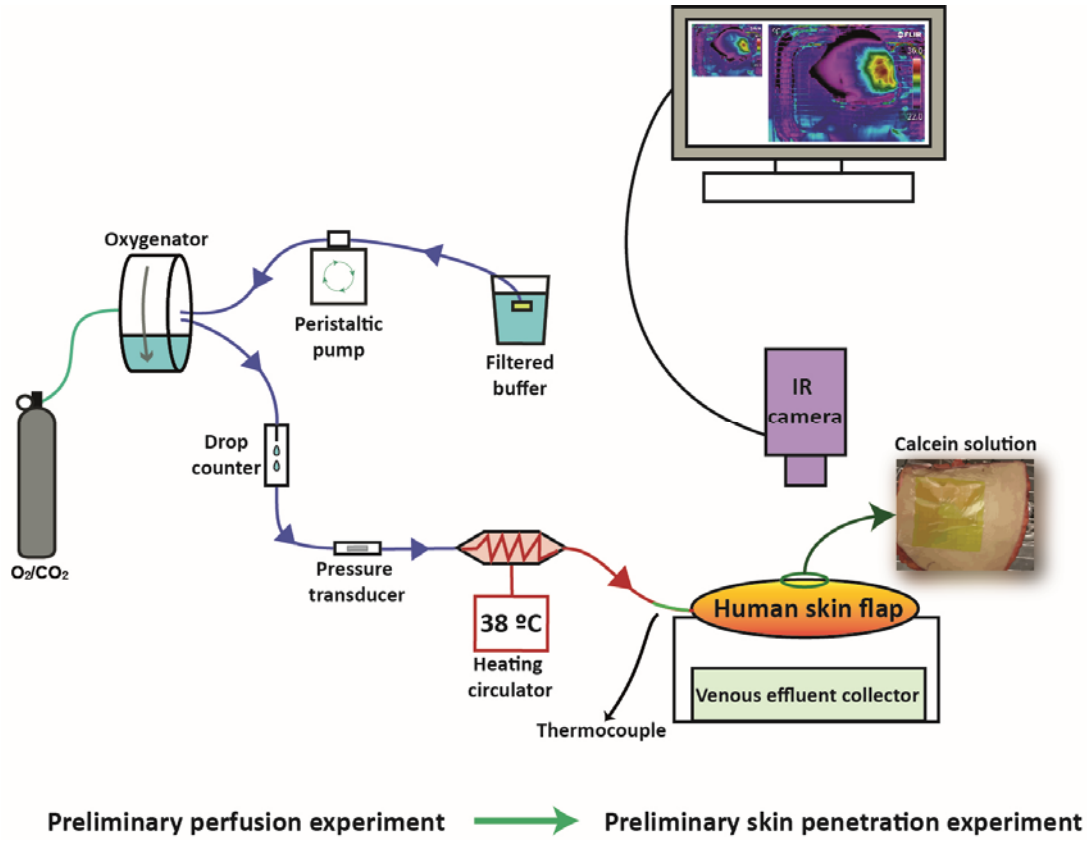

Figure 4.1: Design of human skin flap perfusion (left part) and skin penetration study (right part) in preliminary experiments.

Adapted from Ternullo et al., 2017 (Paper I) with permission from Elsevier.

Before entering the human skin flap, the perfusate was allowed to pass by an oxygenator with the aid of a peristaltic pump in order to be filtered and gassed with 95% O_2/5% CO_2. The perfusate additionally passed by a heating circulator set at 38 °C to assure an inlet temperature in the flap of 32 °C. The temperature of the perfusate entering the flap was monitored by a thermocouple, whereas a drop counter was used to monitor the perfusate flow rate (PFR) (6-8 mL/min). The perfusion inlet pressure, expressed as left ventricular pressure (LVP) was monitored by a pressure transducer, whereas the skin surface temperature was monitored by an IR camera used to monitor skin flap perfusion by DIRT technique (FLIR ThermaCAM S65 HS, FLIR Systems). DIRT images were taken at the start of skin flap perfusion and during the minutes after to assure that the perfusion occurred. The experiment of 6 hrs was started when a suitable flap area was well-perfused (skin surface temperature of 32 °C). DIRT images were then taken every 1 hr for a period of 6 hrs. The physiological parameters of IPHSF, namely PFR (mL/min), LVP (mmHg) and perfusate inlet temperature (°C) were measured on-line using PhysAcq software. The human skin flap perfusion was performed within 90 min after the flap excision.

4.1.3 Preliminary skin penetration experiment on IPHSF

To validate the experimental setups and analytical method to quantify the penetrated marker in the perfusate, calcein was used as a model substance to be tested on IPHSF. Calcein (10 mM) was applied as a solution in KHb and the marker penetration through the IPHSF explored for 6 hrs. IR camera was used to select the best perfused skin flap area (49 cm^2) where calcein solution (7 mL) was applied by the aid of a syringe. An adhesive patch was used as donor chamber. The experiment was carried out for 6 hrs only when no leakage was observed. DIRT images were taken before the start of the perfusion, at the time of the marker application (time 0) and every 1 hr for a period of 6 hrs. All physiological parameters of the IPHSF were monitored and recorded during the experiment. Additionally, to exclude any oedema formation, the human skin flap was weighed before and after the experiment. The perfusate was collected every 1 hr for a period of 6 hrs to quantify the amount of penetrated calcein. An aliquot of perfusate was also collected at time 0 to assure that no intrinsic fluorescent skin

constituents were detected. The analytical method of calcein quantification is discussed in the next subparagraph. The design of the skin penetration study is presented in Figure 4.1.

4.1.3.1 Quantification of the marker in the perfusate

The amount of penetrated marker in the perfusate was quantified using the analytical method previously described by Bahia et al. (2010), with some modifications. Figure 4.2 shows a schematic drawing of the employed analytical method.

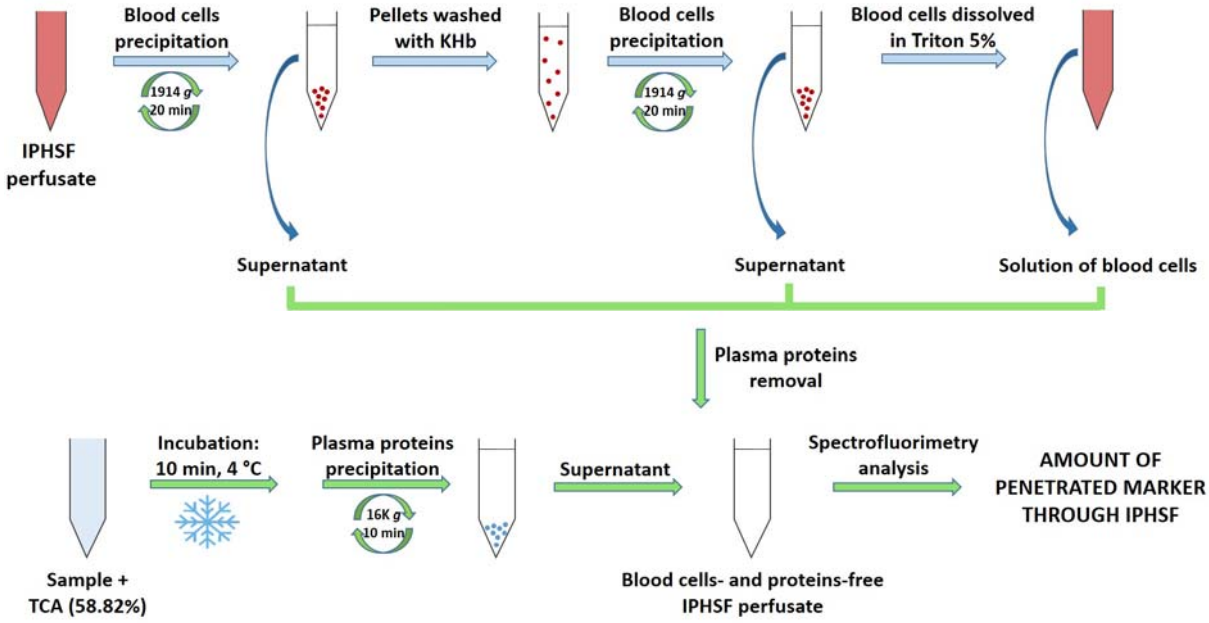

Figure 4.2: Schematic drawing of the analytical method used to quantify the fluorescent marker in IPHSF perfusate.

To remove blood cells, the perfusate (10 mL) was centrifuged at 1914 *g* for 20 min. The supernatant was separated from the pellets. To assure that no calcein precipitated together with the blood cells, the pellets were firstly washed with 10 mL of KHb, then centrifuged again (1914 *g*, 20 min). The supernatant was separated from the pellets, which were finally dissolved in 10 mL of Triton solution (5% w/v). The supernatant from the first and second cycle of centrifugation and the dissolved pellets in Triton solution were then treated with

trichloroacetic acid (TCA) (58.82%, w/v) to precipitate plasma proteins, using the following protocol. An aliquot of sample was added to TCA (volume ratio of 4:1) and incubated for 10 min at +4 °C. After incubation, the sample was centrifuged at 16000 *g* for 10 min. The supernatant (blood cells- and plasma proteins-free) was separated from the pellets and the marker concentration was determined spectrofluorometrically (Polarstar fluorimeter, Fluostar, BMG Technologies, Offenburg, Germany) using a multiplate reader (COSTAR 96). The excitation and emission wavelengths for calcein were at 485 and 520 nm, respectively.

4.1.3.2 Penetration profiles and permeability equation

The penetration profile of calcein through the IPHSF after the preliminary skin penetration experiment was obtained by plotting the cumulative amount of penetrated calcein against time (Figure 4.3). The linear part of the curve was used to calculate the flux rate (j, µg/cm^2·s), representing the steady-state condition (Figure 4.3). The first part of the curve represented in Figure 4.3 was considered as a lag time, representing the time required for calcein to saturate the skin before reaching the steady-state condition with constant flux rate.

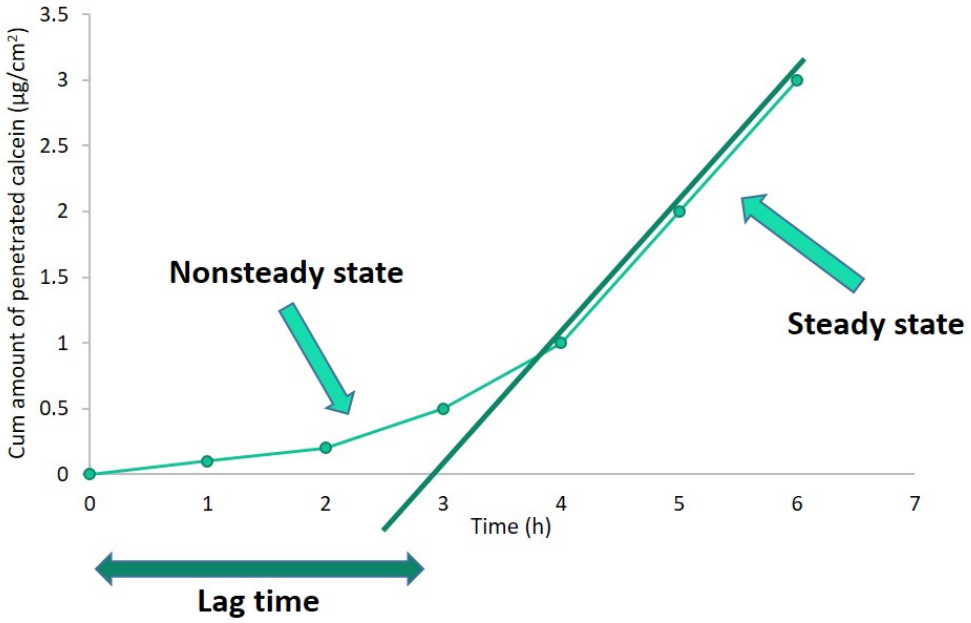

Figure 4.3: Penetration profile of calcein through the IPHSF.

The apparent permeability coefficient (P_{app}) was calculated from Equation 1:

$$P_{app} = j/C_d \qquad \text{(Equation 1)}$$

The equation is a simplification of the Fick's first law, where C_d (µg/mL) is the concentration of calcein solution in the donor compartment (adhesive patch) at time 0, assuming to be almost constant over the time frame of the experiment.

4.1.4 Skin penetration experiments on IPHSF model

The experimental setup illustrated above was used to perform the skin penetration studies on the IPHSF. In Paper I, we validated the IPHSF in its ability to distinguish the skin penetration of two model compounds with different lipophilicities, namely calcein (hydrophilic) and rhodamine (lipophilic) (Figure 4.4). In Paper II we performed the skin penetration experiments on IPHSF model exploring the skin penetration enhancement of three different phospholipid-based nanocarriers, namely CLs, DLs and SLNs, on calcein and rhodamine individually incorporated in the nanocarriers (Figure 4.4). In addition to the weight of the human skin flaps, the flap thickness was measured before and after the skin penetration experiments. Both parameters were used to exclude oedema formation. The IPHSF perfusate, withdrawn every 1 hr, was treated as described above (Figure 4.2) to quantify the penetrated markers. The non-penetrated amounts of the fluorescent markers (retained onto the skin surface) were quantified at the end of the experiment by fluorescence measurements.

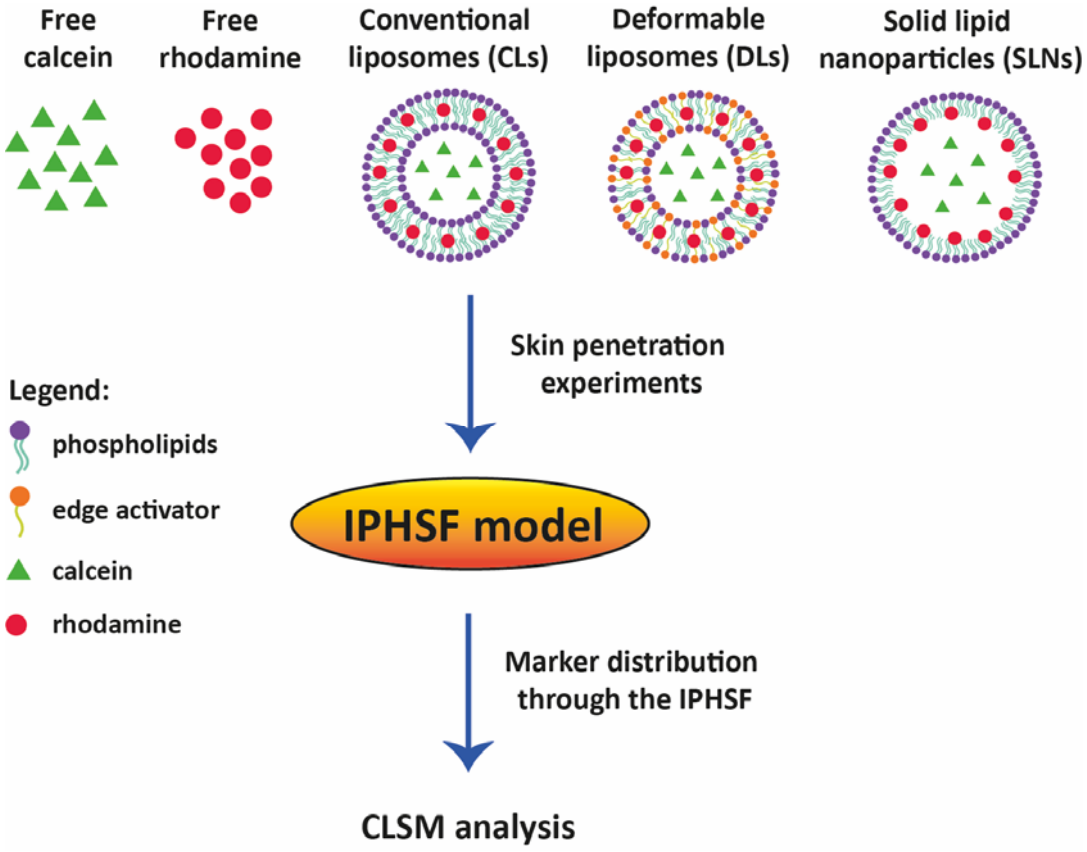

Figure 4.4: Skin penetration experiments on the IPHSF model. Calcein and rhodamine were individually incorporated in the three different phospholipid-based nanocarriers.

4.1.4.1 CLSM analysis

CLSM technique was employed to localize the penetrated markers within the human skin flap at the end of the skin penetration experiments (Figure 4.4). The sample preparation was performed using the imprint method (Brommeland et al., 2003). At the end of the experiment, the treated area was cross-sectionally cut by the use of a scalpel and the slices attached onto the microscope slides. The remaining cells were sprayed with formalin to be fixed before CLSM analysis. In Paper I, cross-sectioned slices from the untreated area of the human skin flap were analysed to explore possible effects of the perfusion on the skin penetration of the two markers. In Paper I-II, a human skin flap slices taken before starting the perfusion were used as a control. All the prepared samples were analysed using a Leica TCS SP5 microscope equipped with an Argon laser. Laser lines of 488 and 568 nm were used to excite calcein and

rhodamine, respectively. The spectral range for fluorescence detection was 500-550 nm for calcein and 570-610 nm for rhodamine, respectively. The images were acquired with a 10x0.4 objective and in *z*-sections of 1 to 100 µm thickness. The gain, off-set and zoom were kept as constant as possible thus maintaining the same setup for all images. The images were superimposed using Volocity® v.6.3 software (PerkinElmer, MA, USA).

4.2 Assessment of liposome elasticity

To confirm the membrane elasticity of the DLs bearing different surface charge, the bilayer elasticity of empty NDLs, CDLs and ADLs was determined with a home-made device as described earlier (Palac et al., 2014). Liposomal dispersions were extruded through a membrane with a pore size of 100 nm using a constant external pressure of 2.5 bar. The amount of liposomal dispersion extruded in 5 min was determined (J). The mean diameter and polydispersity index of the different liposomal dispersions were monitored by photon correlation spectroscopy measurements before and after extrusion, respectively. Empty CDLs were thermostated at 50-60 °C prior the measurements.

The degree of membrane elasticity of the liposomes (E) was calculated using the Equation 2:

$$E = J \cdot \left(r_v / r_p\right)^2 \qquad \text{(Equation 2)}$$

where J is the amount of dispersion (g) extruded in 5 min, r_v is the liposome mean diameter (nm) after extrusion and r_p is the membrane pore size (nm).

5 Results and discussion

The aim of this work was to develop and optimize nanocarriers for tailored/controllable skin delivery of active substances. Their ability of nanocarriers to deliver the incorporated drug/active substance through the skin layers in a controlled manner makes them good candidates in development of effective topical formulations for skin-targeted drug delivery tailored to the skin disease (Kristl et al., 2010; Banerjee, 2013). Nanocarriers' skin penetration behaviour is determined by their physicochemical properties, such as the size, surface charge and lipid organization. By modification of those properties, controlled drug delivery can be achieved (Honeywell-Nguyen and Bouwstra, 2005). A new skin penetration model was firstly developed with features mimicking the human studies to provide closer-to-*in vivo* predictions of the fate of the nanocarrier-associated drug/active substance once it is topically administered onto the skin. Once validated, the model was used to compare nanocarriers with different physicochemical properties in terms of their skin penetration potential. This assisted us in the selection of one of the nanocarrier with tailored skin penetration behaviour targeting dermal drug delivery. By modification of the nanocarrier surface charge, we then explored its ability as a dermal carrier and possible enhanced therapeutic effect of two substances individually incorporated in the nanocarrier. Effective skin formulations should also assure adequate retention time of the nanocarrier-associated drug/substance at the skin site. Chitosan hydrogel was therefore used as a second vehicle for active substance-containing nanocarriers and the effect of nanocarrier surface charge on both hydrogel properties and skin penetration of the active substance from liposomes-in-hydrogel formulation was evaluated.

5.1 Validation of IPHSF model

The development and optimization of effective formulations for skin-targeted drug delivery requires reliable skin penetration models to understand the drug penetration into/through the skin (Godin and Touitou, 2007). The high interest towards nanocarriers as dermal delivery systems is still growing. Considering the possibility to modify nanocarriers' physicochemical properties to obtain targeted skin penetration rate of the nanocarrier-associated

drug/substance, the skin models that can provide predictions of skin drug penetration kinetics closer to the human studies are in high demand (Prow et al., 2011). This may assist in the development of nanocarrier-based formulations with tailored properties for skin-targeted drug delivery.

Skin perfusion models offer the advantage of working with metabolically active skin tissue also including the dermal vascular system with active microcirculation. Therefore, the opportunity to evaluate the effect of dermal circulation on the skin penetration of drugs is considered a step closer to *in vivo* evaluation (Patel et al., 2016). Human-based skin perfusion model has not been reported and validated as skin penetration model prior to our work. The fact that it is derived from human skin makes it a promising model resembling the human studies to a greater extent. Its metabolic activity has been explored by Kreidstein et al. (1991), confirming that the human skin flap can stay metabolically active for at least 5 hrs when *in vitro* perfused with a medium mimicking the physiological fluid in the *in vivo* dermal layer. The human skin flap perfusion has been monitored by several techniques, such as dermofluorimetry (Kreidstein et al., 1995; Black et al., 2001). Miland et al (2008) employed DIRT technique as a less invasive method. The authors found a good correlation between skin surface temperature, measured by an IR camera, and human skin flap perfusion. DIRT technique additionally allowed the distinction between well and less perfused skin flap areas. We therefore based our experimental setups regarding human skin flap perfusion on the method established by Miland et al (2008) with some modifications. In this section, the validation of the IPHSF as skin penetration model will be presented and discussed.

5.1.1 Human skin flap perfusion and design of skin penetration studies on IPHSF

The optimization of the experimental setups to perform skin penetration studies on IPHSF involved:

- Confirming that the physiological parameters of the IPHSF could be maintained constant during the experiment;
- Monitoring the human skin flap perfusion by DIRT to assure constant perfusion of the human skin flap area destined for topical application of fluorescent markers;

- Establishing a constant best perfused skin area of IPHSF suitable for the topical application of fluorescent markers;
- Optimizing the volume of the marker solutions to be applied onto the selected best perfused skin area of the IPHSF.

A preliminary flap perfusion experiment was therefore performed to optimize the above listed experimental parameters. The flap perfusion was not performed for 6 hrs as for the skin penetration studies, but 80 min were considered a suitable period of time to establish the best perfused skin flap area. To further prove the suitability of DIRT in monitoring the IPHSF perfusion, cycles of perfusion with warm and cool perfusate, respectively, were performed (Figure 5.1). This would result in higher skin surface temperature detected by the IR camera when the perfusate entering the flap is warm and lower skin surface temperature of the flap when perfused with cool perfusate. The physiological parameters of the human skin flap, namely PFR and LVP, were maintained constant during the timeframe of the perfusion experiment (Figure 5.1). DIRT technique allowed the detection of a hot spot indicating where the cycles of warm perfusion (perfusate inlet temperature (PIT) of approx. 37 °C) started. This area was even more evident after 5 min of warm perfusion showing a distinct well perfused skin flap area (skin surface temperature of approx. 32 °C) (Figure 5.1 b, d). On the contrary, perfusion with cool perfusate (PIT of approx. 24 °C) showed a lower skin surface temperature of the skin flap area (Figure 5.1 c) similar to the DIRT image recorded at the start of perfusion (Figure 5.1 a). The warm cycles of perfusion allowed us to establish the IPHSF area (49 cm^2) with best perfusion (skin surface temperature of approx. 32 °C) (Figure 5.1 d) to be used as skin application area for the markers solution in the skin penetration studies. One human skin flap was consequently used to optimize the volume of marker solution to be applied. As donor chamber, an adhesive patch was used and different volumes of water were injected under the patch with a help of syringe. A volume of 7 mL was found to be the most suitable avoiding both the formation of air bubbles and leakage of solution.

We could confirm the ability of the DIRT technique to distinguish between the well and less perfused skin flap areas. The IPHSF physiological parameters and perfusion dynamic were in accordance with findings by Miland et al. (2008).

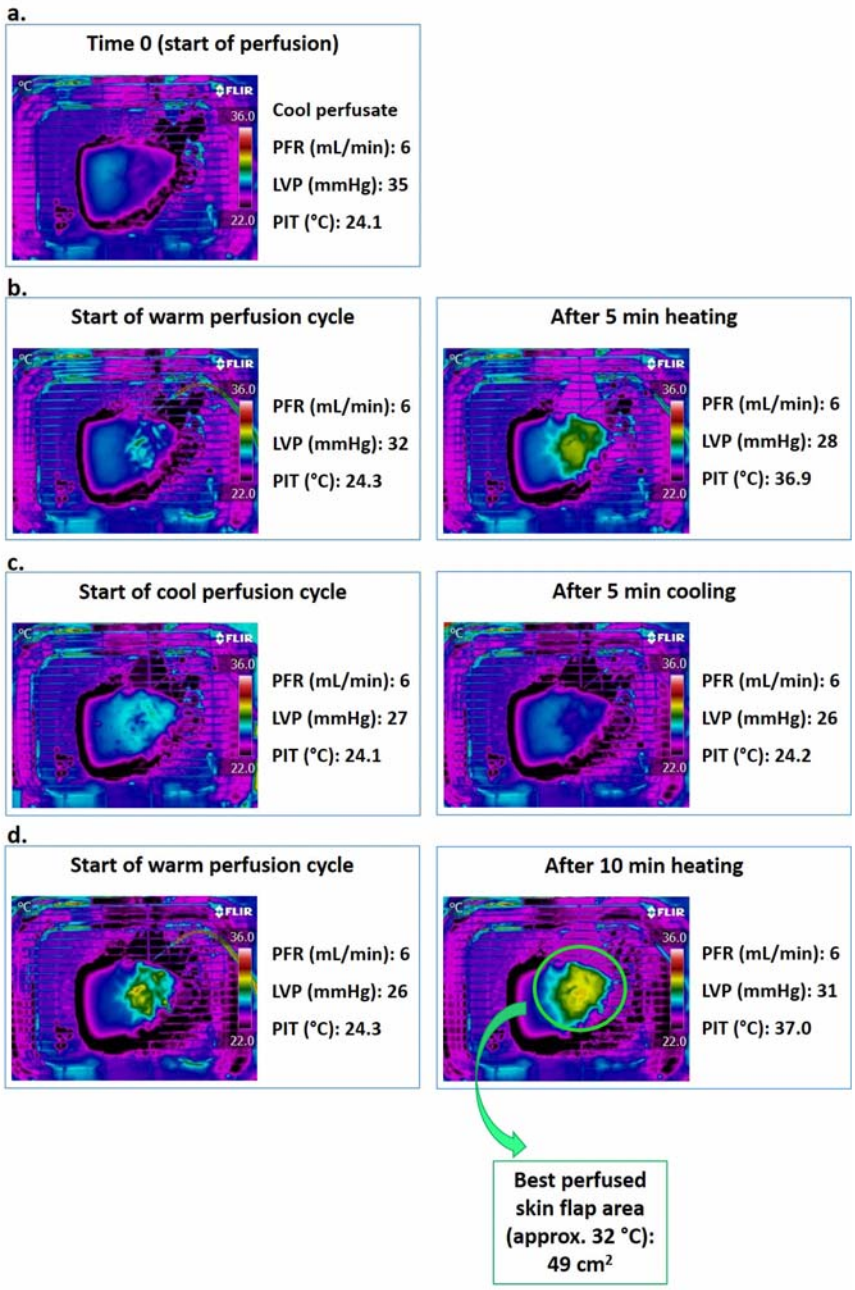

Figure 5.1: Physiological parameters and DIRT images of IPHSF in the preliminary perfusion experiment. The IPHSF physiological parameters, namely PFR (mL/min), LVP (mmHg) and PIT (°C), were recorded at the same time intervals of DIRT images acquisition. The skin flap perfusion was performed starting with cool perfusate (a) and alternating cycles of perfusion with warm (b, d) and cool perfusate (c). DIRT images were recorded at the start of each perfusion cycle (left column) and after 5 min (right column).

PFR: perfusate flow rate; LVP: left ventricular pressure; PIT: perfusate inlet temperature.

The established experimental setups were then applied in a preliminary skin penetration experiment where calcein penetration through the IPHSF was evaluated. As shown in Figure 5.2 a, no leakage of calcein solution was observed. Although calcein solution spread through the patch, approx. 95% of the applied volume was recovered at the end of the experiment. To protect calcein from UV degradation, aluminium foil was placed on top of the adhesive patch throughout the experiment. The DIRT image of IPHSF, taken 1 min after the start of perfusion (Figure 5.2 b), showed the presence of a hot spot, corresponding to the area where the perfusion started to occur. DIRT images were then continuously recorded to select the best perfused skin flap area (49 cm^2) where calcein solution was applied (Figure 5.2 c). The best perfused skin flap area was constantly perfused throughout the experiment. Representative DIRT images taken 3 and 6 hrs (Figure 5.2 d and e, respectively) after the application of calcein solution indicated and confirmed a constant good perfusion of the treated area. IPHSF physiological parameters were also maintained constant throughout the experiment. The perfusion inlet pressure, expressed as LVP, differed from the recorded values during the preliminary perfusion experiment (Figure 5.1). The higher pressure observed in the skin penetration experiment was attributed to a smaller diameter (1 mm) cannula used to cannulate one of the vessels for flap perfusion. The higher inlet pressure might be responsible for oedema formation, however the flap weight variation (before and after the experiment) was below 10% and therefore found acceptable (Kreidstein et al., 1991).

A low percentage of calcein (1.23%) was detected in the perfusate. The minute amount of penetrated calcein through the IPHSF was expected due to its hydrophilic nature (log P = -5.02) thus limiting the entry of calcein into the SC (Gillett et al., 2011; Bolzinger et al., 2012). As described in Section 4.1.3.1, we also performed fluorescence measurements of washed pellets after blood cells precipitation and cells disintegration in Triton solution. No fluorescence was detected in both samples, allowing us to exclude any possible precipitation of calcein with blood cells. Moreover, no fluorescence was measured in the IPHSF perfusate withdrawn before the application of calcein solution thus indicating no interference of skin constituents in the fluorescence measurements.

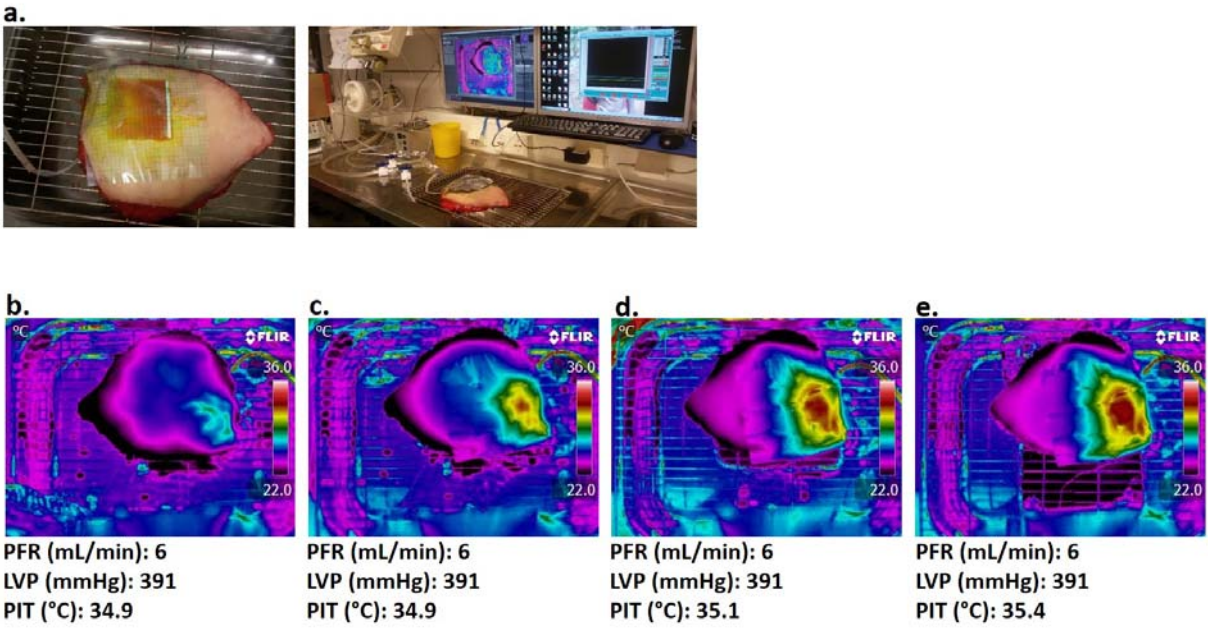

Figure 5.2: Photographs and DIRT images of the preliminary skin penetration study. (a) is the photograph of calcein solution applied onto the IPHSF (left) and the design of the skin penetration experiment (right). DIRT images were recorded 1 min after the start of perfusion (b), at the time of application of calcein solution (c) and 3 and 6 hrs after the application of calcein (d and e, respectively). Below each DIRT image are the IPHSF physiological parameters, namely PFR, LVP and PIT, recorded at the same time as the acquisition of DIRT images.

The preliminary experiments on IPHSF were considered satisfactory in terms of optimization of all parameters required for performing the skin penetration studies using IPHSF. Further validation of IPHSF as skin penetration model was performed.

5.1.2 Skin penetration studies using IPHSF model (Paper I)

Lipophilicity is one of the physicochemical properties of a drug that determines its skin penetration potential (Baroli, 2010). Lipophilic drugs are expected to penetrate the lipophilic SC to a higher extent than the hydrophilic ones. On the contrary, hydrophilic drugs are more able to diffuse through the aqueous viable epidermis and dermis, once they penetrate the SC (Bolzinger et al., 2012). To optimize the IPHSF as a skin penetration model we therefore

evaluated its ability to detect different skin penetration potential of two fluorescent markers with different lipophilicities, namely calcein (hydrophilic) and rhodamine (lipophilic).

During the skin penetration experiment, the best perfused skin flap areas where the two markers were applied exhibited constant perfusion (skin surface temperature of approx. 32 °C) throughout the skin penetration study (data presented in Paper I). Moreover, the same dynamic of perfusion was observed as for both the preliminary perfusion and skin penetration experiment. The IPHSF physiological parameters were also kept constant throughout the skin penetration experiments (data presented in Paper I), further indicating the suitability of IPHSF to be used as a skin penetration model in constant experimental conditions. In all skin penetration experiments the perfusion inlet pressure, expressed as LVP, was similar to the one recorded in the preliminary skin penetration experiment due to the employment of the same cannula diameter (1 mm). This further confirmed the reproducibility of the experimental design. Both weight and thickness variation were below 10% in all tested IPHSFs thus excluding oedema formation (data presented in Paper I).

Low amount of calcein penetrated through the full IPHSF (Figure 5.3 a), whereas no rhodamine was detected in the perfusate after 6 hrs (Figure 5.3 b). Considering their lipophilicity, calcein as hydrophilic marker was not expected to penetrate the SC due to the lipid-rich composition of SC extracellular space (Iwai et al., 2012). However, permeation of calcein through the layers below the SC might be enhanced because of the presence of desmosomes in the viable epidermis that provides a hydrophilic environment (Baroli, 2010). This might explain the presence of calcein in the perfusate indicating its dermal absorption and resulting in a higher P_{app} value compared to rhodamine (Figure 5.3). On the contrary, the higher lipophilicity of rhodamine (log P = 1.95) might assist its penetration and consequent retention in the lipophilic SC while limiting its entrance into the dermal circulation. This supports the lack of rhodamine in the perfusate. Due to its poor water solubility, rhodamine was applied in solution containing 0.5% (v/v) of PG, employed as solubilizing agent. The presence of PG might affect drug/compound penetration through the skin because of its action as penetration enhancer (Lane, 2013). No rhodamine penetrated the full IPHSF thus indicating limited, if any, influence of PG on the marker penetration (Figure 5.3b). However, we used PG in a lower concentration compared to the ones reported in literature that suggest its role as penetration enhancer

(Watkinson et al., 2009). The amount of rhodamine retained onto the skin flap surface was lower than for calcein, indicating the higher ability of lipophilic compounds in penetrating the SC (Bolzinger et al., 2012).

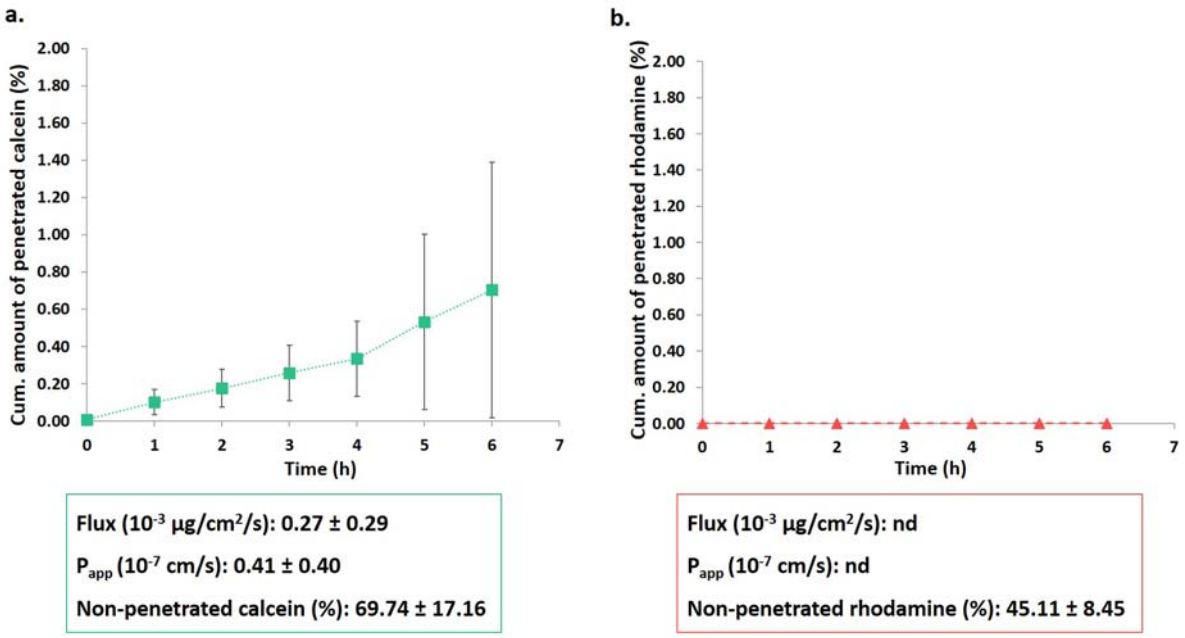

Figure 5.3: Penetration of calcein (a) and rhodamine (b) through the IPHSF over 6 hrs.

nd: non-determined because rhodamine was below detectable level in the perfusate. Results are expressed as mean (n = 3) ± SD.

Adapted from Ternullo et al., 2017 (Paper I) with permission from Elsevier.

The IPHSF was able to confirm the different penetration potentials of the two markers ($p < 0.05$). Moreover, the penetration profile of calcein was found similar to the data obtained from the preliminary skin penetration experiment. Taking into consideration that the inter-variability related to the use of human skin flaps obtained from different donors might have led to discrepancies when performing replicates, we could show that IPHSF can be used as a skin penetration model assuring reproducible results.

The visual distribution of the two markers through the IPHSF by CLSM analysis of the cross-section of the treated flap area (Figure 5.4 c) confirmed the markers penetration profiles. Calcein was uniformly distributed throughout the IPHSF, also reaching the deeper skin layers to be available for dermal absorption. This explains the presence of calcein in the perfusate. Rhodamine was mainly located in the SC and exhibited a weaker fluorescence in the deeper skin layers, mirroring its skin penetration profile. Wester et al. (1998) reported similar findings when testing compounds with different log P values on the isolated perfused pig skin flap model. The higher the log P, the lower was the amount of compound detected in the perfusate (Wester et al., 1998). To explore any possible effect of perfusion on the two markers' penetration, CLSM analysis were also performed on untreated IPHSF area (Figure 5.4 a) but still perfused, as confirmed by DIRT. Although exhibiting a weaker fluorescence compared to the treated area, both markers were detected through the skin layers indicating an effect of the perfusion on their penetration (Figure 5.4 d). Moreover, the same penetration trend was observed as for the treated area: calcein exhibited fluorescence through all the cross-section IPHSF, while rhodamine was mainly located in the SC and superficial skin layers. When performing the skin penetration experiments of rhodamine on the IPHSF, we were able to visualize a non-perfused area (Figure 5.4 a). This was analysed by CLSM to further explore the effect of the perfusion on rhodamine penetration through IPHSF. No fluorescence was detected (Figure 5.4 e) indicating that the absence of perfusion limited rhodamine penetration in the untreated area.

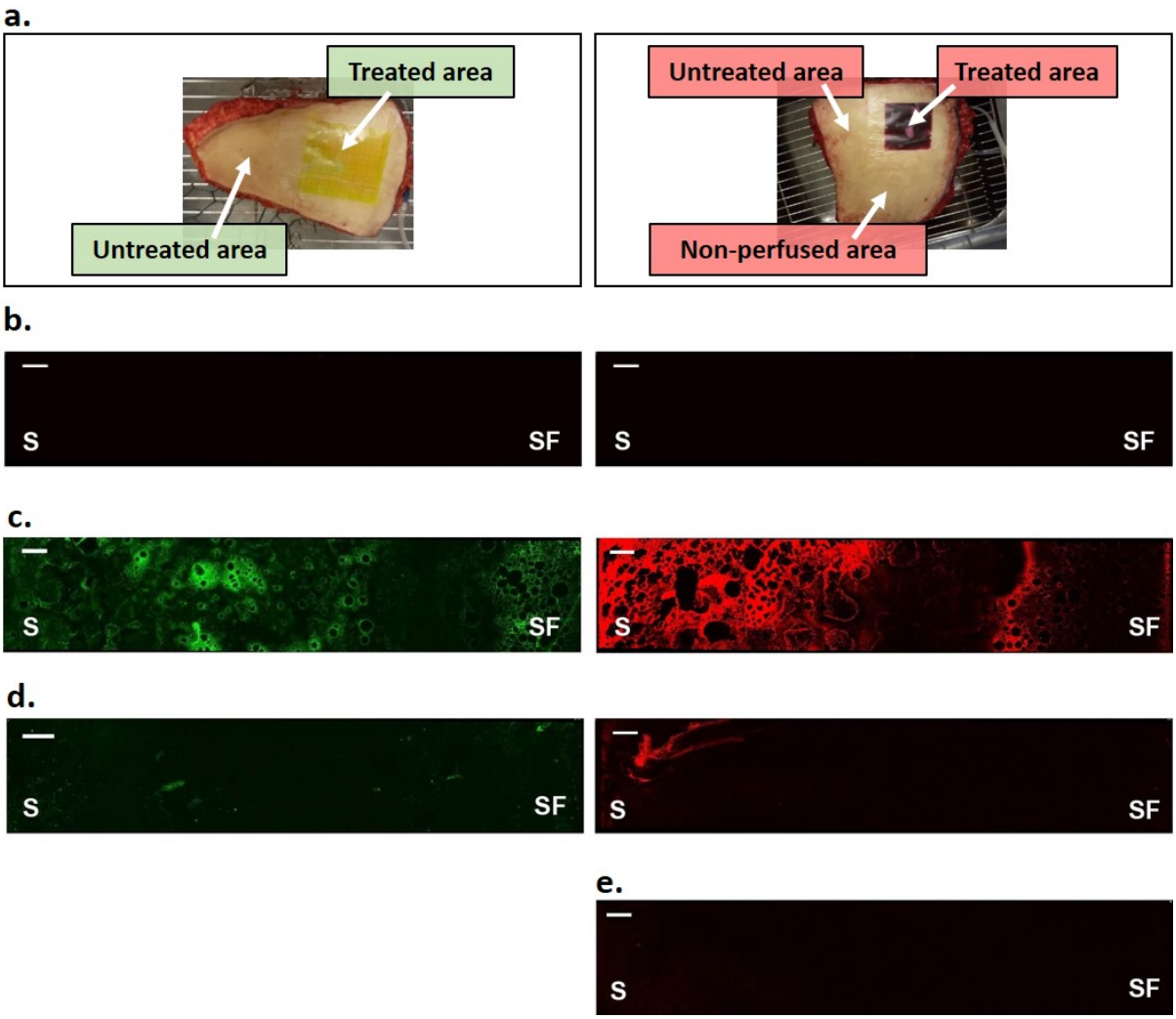

Figure 5.4: Calcein (left column) and rhodamine (right column) localization into the IPHSF. (a) is the IPHSF areas analysed by CLSM. The negative control (b) is cross-section of flap before the start of perfusion, (c) is the treated area, (d) is untreated area and (e) is non-perfused area detected in flaps where rhodamine was applied. The slices were cross-sectionally cut starting from the skin surface (S) to the subcutaneous fat (SF). Scale bar of 500 µm.
Adapted from Ternullo et al., 2017 (Paper I) with permission from Elsevier.

The findings suggest that the IPHSF is a promising skin penetration model able to assure constant experimental conditions and reproducible results. Moreover, it clearly indicated the importance of the perfusion in the skin penetration of the two fluorescent markers.

5.1.3 IPHSF *vs*. *ex vivo*/*in vitro* skin models (Paper I)

To further validate the IPHSF model, a comparison with established skin models, namely different *ex vivo*/*in vitro* membranes in the FDC, was performed. As skin model membranes, we selected *ex vivo* full thickness human skin that is one of the most appropriate skin models resembling closer-to-*in vivo* conditions (Planz et al., 2016). *Ex vivo* full thickness pig skin was employed as the animal skin model for comparison of data obtained from human-based skin models, in our case IPHSF. The choice of pig skin relies on its greater resemblance of human skin compared to other animal species, especially referring to skin thickness and histology (Sintov, 2017). Skin penetration studies were additionally performed using an *in vitro* membrane, namely cellophane, to investigate IPHSF/*in vitro* data correlation.

Lower amount of calcein penetrated through the full thickness human skin in FDC compared to IPHSF, whereas rhodamine penetration through *ex vivo* human skin in FDC was similar to the penetration profile obtained from IPHSF (data presented in Paper I). This might indicate that the presence of perfusion in IPHSF exerted a positive effect on the penetration of the hydrophilic marker, highlighting the role of perfusion and dermal active microcirculation in skin penetration of substances (Patel et al., 2016). Both the pig skin and cellophane membrane exhibited higher permeability compared to IPHSF thus resulting in poor correlation between animal skin/artificial membrane and human skin, in agreement with literature (Schaefer et al., 2008; Abd et al., 2016). In contrast to the findings on calcein, rhodamine exhibited more similar penetration profile when tested on both IPHSF and pig skin. Earlier work by Dick and Scott (1992) addressed this behaviour by stating that pig SC lipid composition better mimics the human SC considering the penetration of lipophilic substances.

The poor correlation between the IPHSF and animal/artificial membranes suggests the need for using the skin penetration models that resemble the *in vivo* conditions to a greater extent. Although higher similarities were observed between the IPHSF and *ex vivo* human skin, the perfusion of IPHSF clearly had a strong influence on the penetration of model compounds. The IPHSF model might be therefore considered as the missing link model between *in vivo* and *in vitro* skin penetration studies. The developed IPHSF model could be a promising tool in optimization of formulations destined for skin administration.

5.2 Penetration potential of nanocarriers in the IPHSF model (Paper II)

Phospholipid-based nanocarriers as dermal delivery systems represent a promising approach to overcome the current dermal therapy's limitations (Mota et al., 2017). They can enhance skin penetration of the associated drugs/substances and most importantly, assure controlled drug penetration into/through the skin layers. By tailoring their physicochemical properties, nanocarriers with different skin penetration potentials can be developed and modulation of the depth within the skin to which the drug/substance will be delivered can be achieved (Schmieder et al., 2015). This translates in a good potential to develop nanocarrier-based formulations with skin-targeted drug delivery according to the skin conditions and disease state. In this study, we selected three phospholipid-based nanocarriers, namely CLs, DLs and SLNs, commonly used as dermal delivery systems. The choice was based on the fact that they possess different lipid organization. CLs and DLs have the phospholipids arranged into vesicular structures that surround an aqueous core, whereas SLNs are particulate nanosystems where the phospholipids are organized in a homogeneous solid matrix (Jain et al., 2017).

Aiming at developing nanosystems for dermal drug delivery, we decided to develop nanocarriers with a targeted particle size between 200 and 300 nm. The selected size range has shown to be optimal in assuring nanocarrier deposition into the skin providing adequate drug reservoir (du Plessis et al., 1994). Considering other physicochemical properties, the surface of both CLs and SLNs was neutral due to the presence of the neutral PC. DLs were found negatively charged and this can be attributed to the presence of anionic surfactant, SDC, in accordance with published data (Palac et al., 2014). The characteristics of the phospholipid-based nanocarriers are presented in Paper II.

As discussed earlier, to achieve good *in vivo* prediction of drug penetration into/through the skin it is important to use skin penetration models that can provide experimental conditions similar to the human studies. This also applies for screening of nanocarriers with different physicochemical properties. The IPHSF model showed a good potential in providing closer-to-*in vivo* predictions of skin diffusion kinetics. We therefore used the developed skin penetration model as a tool to follow the skin penetration of calcein and rhodamine, individually

incorporated in the three nanocarriers. The physiological parameters of the IPHSF model were maintained constant and the skin flap areas, treated with the different formulations, stayed well-perfused throughout the skin penetration experiments (data presented in Paper II). These findings further confirmed the use of the IPHSF model in constant and reproducible experimental conditions. The penetrated amount of both nanocarrier-associated markers in the perfusate was below the detectable level, indicating no markers penetration through the full IPHSF. This confirmed the suitability of all nanocarriers as dermal delivery systems. As discussed earlier, this might be explained considering the nanocarrier size, which was targeted to be optimal for dermal delivery of drugs. Considering calcein penetration through the IPHSF when applied in solution (Paper I), the lack in calcein dermal absorption when applied in nanocarrier-based formulations might be also explained by the nanocarriers' ability in controlling and sustaining its penetration within the skin layers (Chen et al., 2011). To get a better insight into the skin penetration potential of the different nanocarriers, we quantified the amount of markers retained onto the IPHSF surface (non-penetrated markers) after 6 hrs of the skin penetration study (Figure 5.5).

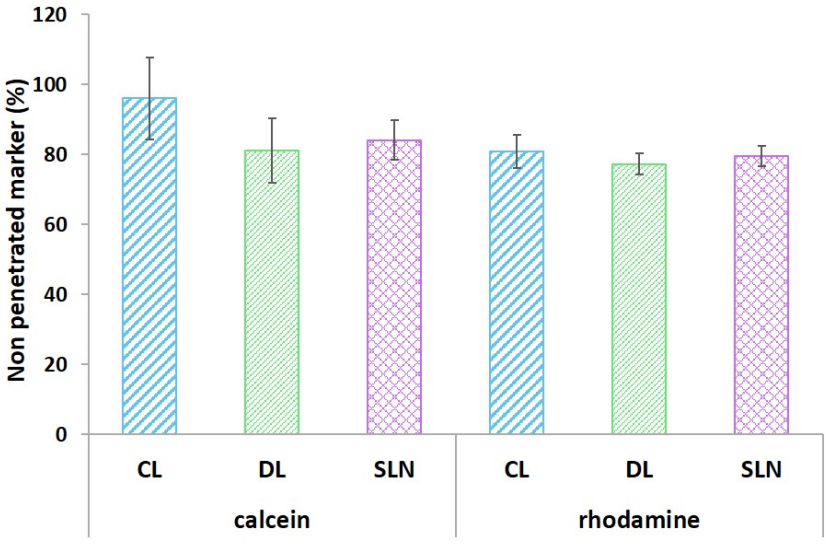

Figure 5.5: Calcein and rhodamine retained onto the IPHSF surface after 6 hrs of skin penetration study. Results are shown as mean (n = 3) ± SD. (from Ternullo et al., 2017 (Paper II) with permission from Elsevier).

CLs retained the highest amount of both markers onto the IPHSF surface, indicating a drug depot onto the skin surface and a weaker skin penetration enhancing effect compared to both DLs and SLNs. The superior ability of both DLs and SLNs in enhancing skin penetration of the associated drug compared to CLs was in accordance with published data (Uchino et al., 2014; Clares et al., 2014). This might be contributed to their different skin penetration mechanisms according to the lipid organization. CLs have demonstrated that their skin penetration enhancing effect on drugs is limited to the SC and eventually to the more superficial skin layers (Dreier et al., 2016). DLs have shown superior ability, compared to CLs, in enhancing drug/substance transport into the deeper skin layers due to their deformability provided by the presence of surfactant in the liposomal phospholipid bilayer (Jain et al., 2017). On the other hand, SLNs possess occlusive properties thus promoting skin hydration and consequently skin penetration of the SLNs-associated drugs (Papakostas et al., 2011).

When comparing the two markers, calcein from all nanocarriers was retained onto the IPHSF surface to a higher extent than rhodamine, as observed for markers applied in solution (Figure 5.3). This indicates that the skin penetration rate of any compound is the result of its physicochemical properties, affected by the nanocarriers' characteristics and their interactions with the skin.

5.2.1 Skin-targeted delivery of markers by nanocarriers on the IPHSF model

The skin penetration studies using the three nanocarriers allowed us to prove that all nanocarriers were able to assure dermal delivery of both markers when tested on the IPHSF model. The evaluation of the amount of markers retained onto the IPHSF surface was an indication of the different skin penetration behaviour of the tested nanocarriers. However, no information on the skin depth to which the markers were delivered by the different nanocarriers was acquired at this stage. We therefore employed CLSM technique to visualize the differences in the skin-targeted drug delivery potential of the three nanocarriers for both calcein and rhodamine (Figure 5.6).

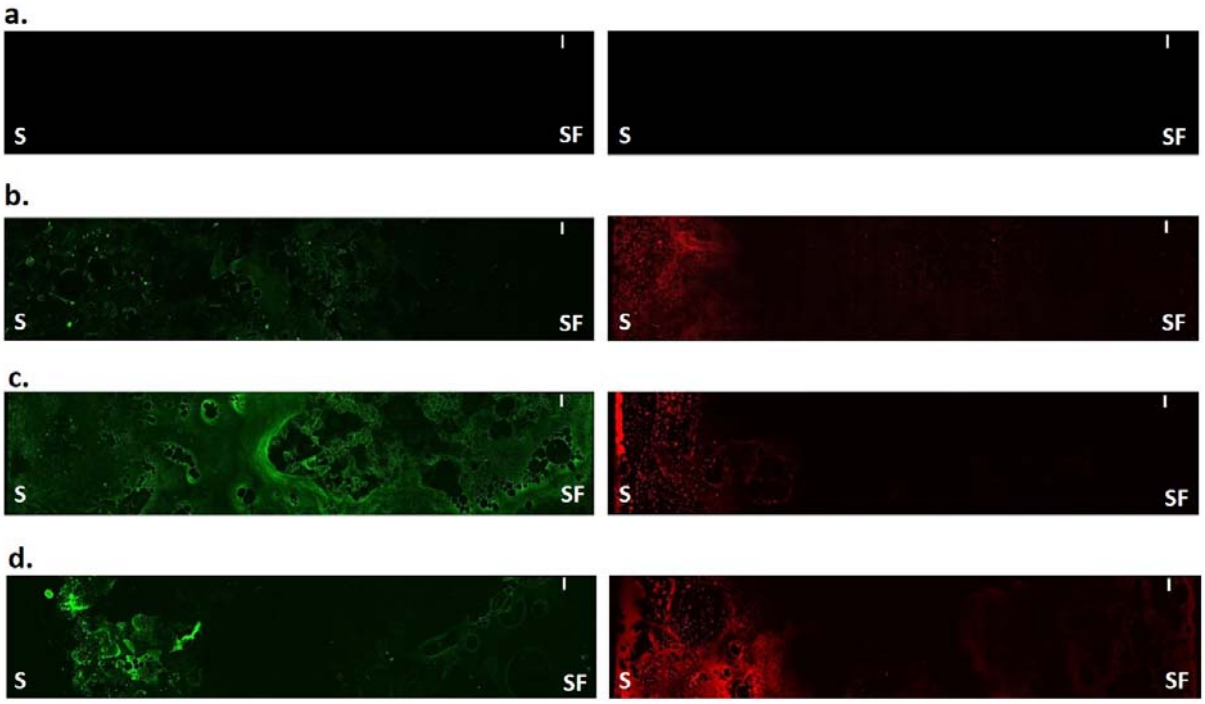

Figure 5.6: Distribution of calcein (green fluorescence, left side) and rhodamine (red fluorescence, right side) through IPHSF from CLs (b), DLs (c) and SLNs (d), respectively. As control, untreated IPHSF before perfusion was used (a). Each CLSM image shows the cross sections of IPHSF cut starting from the skin surface (S) to the subcutaneous fat (SF).
Adapted from Ternullo et al., 2017 (Paper II) with permission from Elsevier.

As earlier observed for the markers in solution (Paper I) and independently of the type of nanocarrier, calcein was found more uniformly distributed through the IPHSF as compared to rhodamine, which was mainly located in the upper skin layers close to SC. Therefore, the different lipophilicities of the two markers affected their distribution through the IPHSF, even when applied associated with nanocarriers. Calcein penetration into the dermal layer might be favoured by continuous dermal perfusion that assures a hydrophilic environment thus enabling diffusion of the hydrophilic marker. However, differences in the depth to which the markers were delivered were detected according to the type of nanocarrier. Both DLs (Figure 5.6 c) and SLNs (Figure 5.6 d) enabled delivery of the two markers into the deeper skin layers as compared to CLs (Figure 5.6 b), in agreement with the findings from the skin penetration profiles (Figure 5.5). DLs exhibited the best penetration enhancing effect on calcein, even

compared to SLNs. Regarding rhodamine, DLs enabled higher deposition of the lipophilic marker into the SC than CLs and SLNs, whereas both DLs and SLNs delivered rhodamine into the deeper skin layers compared to CLs. CLSM analysis confirmed that the skin penetration depth of the two markers was dependent on the type of nanocarrier. The enhanced skin penetration mediated by both DLs and SLNs was more evident for calcein, which was localized into the deeper skin layers compared to rhodamine. This can be related to the different partitioning of the two markers depending on their lipophilicity. Rhodamine, a lipophilic marker, has intrinsic capacity to diffuse into the SC thus making the nanocarriers' contribution as penetration enhancers less evident. On the other hand, the nanocarrier action will be more evident for associated compounds with lower log P, as calcein. Our results were in agreement with reported findings (Chen et al., 2011).

This comparison allowed us to gain a better insight on the different skin penetration potential of the tested nanocarriers. DLs exhibited satisfactory dermal delivery for both model compounds, with potential ability to enhance skin drug penetration and assure controlled and sustained drug penetration into/through the skin. Therefore, we selected DLs to further proceed with the optimization of effective nanocarriers for controllable skin delivery.

When comparing the three nanocarriers, DLs' ability as dermal delivery systems might be also explained by their negative surface charge, which has shown to promote the skin penetration of the nanocarrier-associated drug (Mota et al., 2017). Therefore, once we selected DLs, we decided to further explore the effect of the liposomal surface charge on their potential as dermal delivery systems.

5.3 Effect of surfactants on the physicochemical properties of nanocarriers (Paper III and IV)

To further explore the effect of liposomal surface charge on the nanocarriers' potential as dermal delivery systems, different surfactants were selected and employed to prepare NDLs, CDLs and ADLs, respectively, with adequate liposome membrane elasticity. Therefore, the lipid:surfactant ratio (85:15, w/w) in all DLs was selected based on the literature reporting

development of DLs with satisfactory membrane elasticity (Dragicevic-Curic et al., 2010; Palac et al., 2014). The amount of surfactant was kept low considering the cytotoxicity concerns related to administration of surfactants in higher concentrations, especially referring to polysorbate 20 and stearylamine (Eskandani et al., 2013; Dhawan and Nagarsenker, 2017). Two model drug/active substances, namely hEGF and curcumin, were selected and individually incorporated in the DLs bearing different surface charge to evaluate the nanocarrier's influence on their skin penetration rate and biological activities of carrier-associated substances. The choice of the two active substances was based on their biological activities beneficial for treatment of several skin diseases. hEGF, a biological, improves wound healing by promoting cell proliferation and differentiation (Xue et al., 2018), whereas the anti-oxidant, anti-inflammatory and anti-bacterial effects of curcumin make this pleiotropic molecule promising for treatment of skin inflammation and infections, including impaired wound healing (Mehanny et al., 2016). Moreover, both hEGF and curcumin possess limitations for the development of pharmaceutical products for localized skin therapy. The low *in vivo* stability of hEGF together with its high susceptibility towards enzymatic degradation makes topical application of hEGF a challenge (Gainza et al., 2015). On the other hand, curcumin's lipophilicity and chemical instability limit its incorporation in hydrophilic wound dressings, such as hydrogel (Zhao et al., 2013). Therefore, the incorporation of hEGF and curcumin, individually, in DLs might overcome these limitations by improving their dermal delivery and enhancing their efficacy in the treatment of skin diseases.

The optimization of the effective nanocarriers requires the screening of their physicochemical characteristics, which determine their ability as dermal delivery systems. The vesicle size can affect the drug deposition in the different skin layers (Verma et al., 2003). Our focus was on the liposomal surface charge, therefore we prepared DLs with similar vesicle size in order to exclude the possible effect of the vesicle size on their skin penetration potential. Considering that hEGF is a rather big molecule (6 kDa), hEGF-containing DLs were prepared within a vesicle size range of 300-350 nm (data presented in Paper III) in order to enable sufficient drug load. Curcumin-containing DLs were within the vesicle size range of 200-300 nm (data presented in Paper IV), which was the same size range selected for the comparison of the different nanocarriers (Paper II).

The zeta potential of all DLs was found to be dependent on the type of surfactant. NDLs exhibited a neutral surface due to the presence of both neutral lipid, PC, and non-ionic surfactant, polysorbate 20. CDLs and ADLs bear strong positive and negative surface charges because of the presence of stearylamine and sodium deoxycholate, respectively. These findings were confirmed for both hEGF- and curcumin-containing DLs (data presented in Paper III and IV, respectively).

The surface potential of hEGF can vary according to the pH of the medium in which the protein is dissolved (Miklavžin et al., 2018). To evaluate any possible influence of hEGF surface potential on the DLs surface, we determined the zeta potential of hEGF in the medium used to prepare DLs, namely phosphate buffer saline (PBS) at pH 7.4. hEGF in PBS exhibited a zeta potential of - 11.4 mV. Considering the hEGF isoelectric point (pH = 4.43) (Kim et al., 2015), the protein in PBS (pH 7.4) is mainly exhibiting ionized groups, therefore its negative surface charge. This also indicates that hEGF possesses higher hydrophilicity suggesting its accommodation in the aqueous core of the DLs. Therefore minimal interaction between hEGF and the liposomal bilayers is expected to occur. This might explain the rather weak effect of hEGF on the zeta potential of all DLs, indicating limited adsorption of the protein on liposomal surface.

The membrane elasticity is the distinctive characteristic of DLs enabling the nanocarriers to deliver the incorporated drug in the deeper skin layers by squeezing through the skin pores much smaller than their actual size (Jain et al., 2017). The liposomal component mainly responsible for the membrane elasticity is the surfactant, which influences the interfacial tension of the liposomal membrane. Therefore, the degree of membrane elasticity may vary according to the type of employed surfactant (El Zaafarany et al., 2010). The degree of membrane elasticity of empty DLs is shown in Figure 5.7. Empty ADLs exhibited the highest degree of membrane elasticity, followed by NDLs. Empty CDLs showed the lowest elasticity value typical for liposomes with rigid membranes (Palac et al., 2014). The presence of SA can trigger repulsions in the CDLs membrane resulting in an alteration of the bilayer packing (El Zaafarany et al., 2010). This might negatively affect the CDLs membrane elasticity.

We did not test the membrane elasticity of hEGF-DLs due to the fact that hEGF is expected to accommodate itself in the aqueous core of DLs. We also proved that hEGF minimally interacts

with the liposomal membrane. Therefore, the influence of hEGF on the surfactant arrangement in the liposomal bilayer might be marginal thus resulting in a minimal effect on the liposomal membrane elasticity.

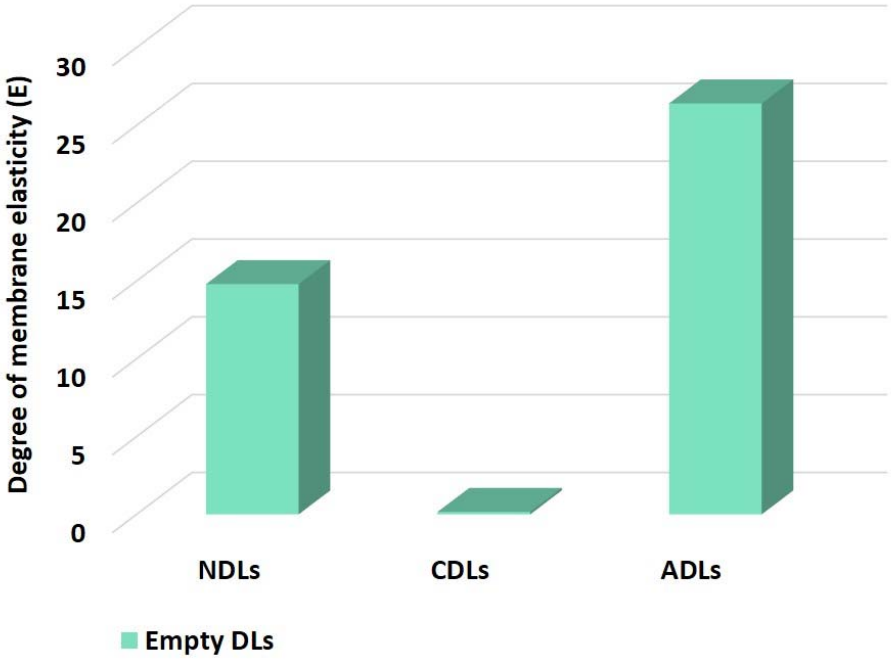

Figure 5.7: The degree of membrane elasticity of empty DLs bearing different surface charge.

However, the incorporation of curcumin in all DLs affected their membrane elasticity (data presented in Paper IV). The presence of curcumin in both NDLs and ADLs reduced their membrane elasticity by more than five- and three-fold, respectively. Despite this finding, the degree of membrane elasticity of both curcumin-NDLs and curcumin-ADLs was found acceptable for elastic liposomal membranes and in agreement with literature (Palac et al., 2014). On the contrary, curcumin in CDLs contributed to an increased membrane elasticity by more than 45-fold in comparison to empty CDLs. Both curcumin and SA accommodate themselves in the liposomal bilayers, therefore the presence of curcumin might reduce the packing alteration caused by SA thus resulting in a higher liposome membrane elasticity. All

curcumin-DLs exhibited similar membrane elasticity enabling comparison of the different DLs by only exploring the effect of their surface charge.

To assure the effectiveness of nanocarrier-based skin formulations, a sufficient drug/substance load in the nanocarrier should be achieved. Adequate entrapment efficiency can assure that the nanocarrier can achieve the drug/substance concentration at the level required to exert the activity in the targeted skin layer(s). All DLs entrapped similar hEGF content (data presented in Paper III). hEGF is expected to accommodate itself in the aqueous core due to its hydrophilic nature. Therefore, the presence of the different surfactants in the liposomal phospholipid bilayers should not affect the drug entrapment. The hEGF content was found to be rather high for all DLs; this might be partially explained by the employment of surfactants with high hydrophilic/lipophilic balance values, namely polysorbate 20 and sodium deoxycholate, which provide better incorporation of hydrophilic drugs (Bnyan et al., 2018), as well as the vesicle size.

The entrapment efficiency of curcumin was found to be affected by the presence of surfactants in the DLs phospholipid bilayer, as expected. The lipophilic nature of curcumin enables its accommodation in the phospholipid bilayer, therefore a competition might occur between curcumin and the surfactant thus affecting the entrapment of this lipophilic compound (Bnyan et al., 2018). ADLs enabled the highest incorporation of curcumin, whereas the lowest was observed for CDLs (data presented in Paper IV). As discussed earlier, SA can induce repulsions in the liposomal bilayer thus altering the lipid packing. This might limit the amount of lipophilic compounds able to accommodate within the lipid bilayer of CDLs, as reported for the drug celecoxib bearing similar lipophilicity as curcumin (Bragagni et al., 2012). Despite the lower entrapment efficiency observed for CDLs, we decided that the curcumin content was sufficient to further proceed with the developed liposomal system.

The screening of the physicochemical properties of the nanocarriers was considered satisfactory in terms of liposomal size, surface charge, membrane elasticity and active substance loading capacity to proceed with the optimization of the nanocarriers, focusing on their ability to enhance the activities of associated substances.

5.4 Effect of the liposomal surface charge on DL's skin penetration potential (Paper III and IV)

To evaluate the skin penetration of both hEGF and curcumin from NDLs, CDLs and ADLs, respectively, *ex vivo* full human skin in FDC was employed as a skin penetration model. At this stage, due to time and access limitations, we could not test the liposomal formulations on the IPHSF model. Moreover, the non-fluorescent nature of hEGF would require the use and validation of other methods such as fluorescence labelling, to visualize the drug distribution through the IPHSF. Therefore, both hEGF- and curcumin-containing DLs were tested using *ex vivo* full human skin in FDC; this skin model was the one for which we obtained the most similar penetration profiles when compared to the IPHSF model (Paper I and II). Moreover, *ex vivo* human skin in FDC still represents one of the most reliable skin models closer to the *in vivo* human studies (Planz et al., 2016). The IPHSF model may instead be used in the later stage of formulation development, when the optimized nanocarrier-based formulation needs to be tested in the conditions closer to the *in vivo* ones. This would additionally limit the *in vivo* animal studies. The use of full thickness human skin might lead to skin penetration profiles that differ from damaged/diseased skin, which often has a compromised SC barrier resulting in enhanced drug penetration (Bouwstra and Ponec, 2006). However, healthy skin with intact SC can assist in pilot studies to screen nanocarriers with different characteristics thus helping in the selection of the appropriate nanocarrier.

Independently of the liposomal surface charge, all DLs assured dermal delivery of hEGF; no hEGF was detected in the receptor medium indicating absence of protein dermal absorption over 6 hrs of skin penetration study. The hEGF hydrophilic nature together with its relatively high molecular weight (6 kDa) might also have contributed to limiting its skin penetration especially through the SC (Bolzinger et al., 2012). The quantification of hEGF retained onto the skin surface at the end of the experiment, expressed as non-penetrated hEGF, helped in the discrimination of the different DLs' potential in enhancing hEGF skin penetration (Figure 5.8).

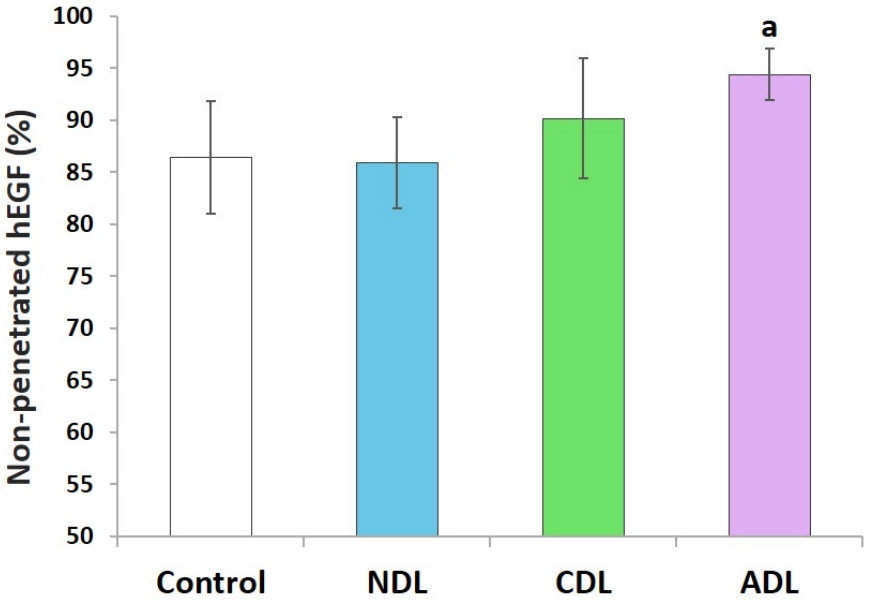

Figure 5.8: hEGF retention onto the human skin surface from the different DLs after 6 hrs of skin penetration studies. hEGF solution in PBS was used as control. Results are expressed as mean (n = 3) ± SD. [a]*p* = 0.04 vs. NDL.

The charged DLs enabled higher retention of hEGF onto the skin surface compared to NDLs, which exhibited a minimal improvement in hEGF skin penetration compared to hEGF in PBS solution (control). Comparing the liposomal surface charge, ADLs assured the most sustained hEGF skin penetration, whereas CDLs enhanced skin penetration of hEGF to a slightly higher extent. Considering the lower degree of membrane elasticity, CDLs were not expected to be superior in enhancing skin penetration of hEGF compared to ADLs, which exhibited higher elastic membrane. Therefore, in this case, it seems that the liposomal surface charge is the main contributor responsible for the skin penetration potential. The positive surface charge of CDLs might trigger electrostatic interaction with the negative SC keratinocytes thus improving skin penetration of hEGF. Choi et al. (2017) reported recently the enhanced skin penetration of hEGF via CDLs made of PC, cholesterol and 1,2-dioleoyl-3-trimethylammonium propane (DOTAP), in agreement with our findings although the composition of our CDLs was different. On the other hand, the hEGF depot via ADLs might assure a sustained hEGF release over prolonged time thus reducing the frequencies of administration and increasing patient

compliance. High retention onto the skin surface of naringin, a hydrophilic and high molecular weight compound similar to hEGF, mediated by ADLs, has been recently reported by Pleguezuelos-Villa et al. (2018).

The most sustained skin penetration of hEGF mediated by ADLs differed from the earlier findings obtained with calcein, although both compounds are hydrophilic. The differences might be explained considering the different molecular weight, which affects their skin penetration. The higher molecular weight of hEGF compared to calcein limits the SC penetration of the protein to a higher extent (Baroli, 2010).

Unlike for hEGF, DLs with different surface charge assisted in curcumin penetration through the full human skin over 24 hrs (Figure 5.9). The presence of curcumin in the receptor medium provided an indication of the DLs' potential in delivering the incorporated active substance into the deeper skin layers reaching the dermal vascular system. The membrane elasticity of all curcumin-DLs might have played a role in the skin penetration enhancement of curcumin via DLs (Jain et al., 2017). Another possible explanation might be related to the presence of albumin (10 g/L) in the receptor medium, which was added to improve curcumin partitioning from the skin into the aqueous receptor medium. Additionally, it has been shown that *in vitro* studies tend to underestimate the *in vivo* skin penetration of lipophilic compounds (Agrawal et al., 2015). Therefore, the presence of albumin in the receptor fluid might have enhanced curcumin penetration through the full human skin. Since the two active substances differ in lipophilicity, their penetration profiles are not expected to be similar (Bolzinger et al., 2012). On the other hand, the amount of penetrated curcumin through the full human skin was low for all DLs. This indicated that all DLs were suitable as dermal delivery systems assuring minimal systemic absorption of curcumin.

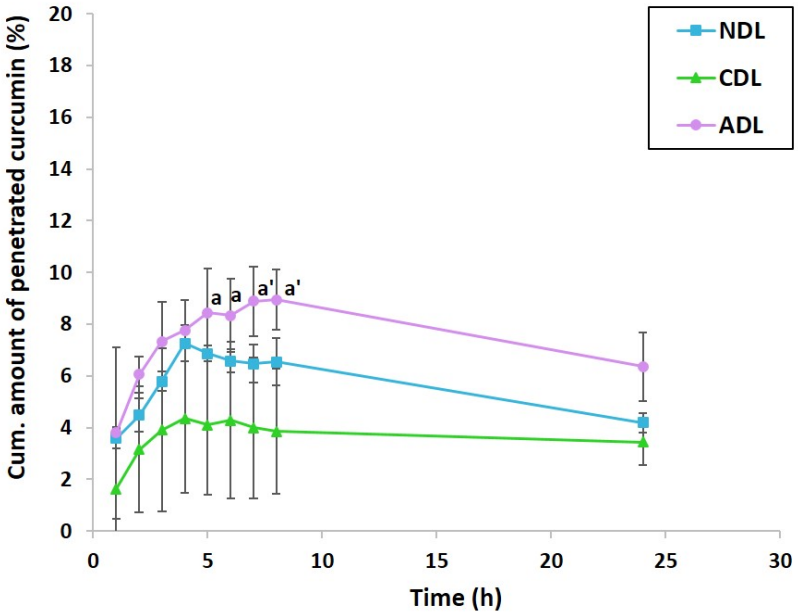

Figure 5.9: Curcumin penetration from different DLs through the full thickness human skin over 24 hrs. Results are expressed as mean (n = 3) ± SD. [a]Significantly higher ([a]$p < 0.05$, [a']$p < 0.005$) than CDL.

Our main focus was to explore the effect of the liposomal surface charge on the curcumin skin penetration and a different potential of the DLs was indeed observed. ADLs showed the most skin penetration enhancing effect on curcumin, as previously reported for other lipophilic compounds incorporated in ADLs (Paolino et al., 2012). On the contrary, CDLs enabled the most sustained skin penetration of curcumin. Curcumin-containing cationic deformable liposomes have been recently developed by Jose et al. (2017); although their liposomes differed in composition being composed of DOTAP and sodium cholate, a sustained curcumin penetration through pig skin has been observed, in agreement with our findings. The charged DLs exhibited similar degree of membrane elasticity, therefore the liposomal surface charge seemed to be the main factor determining the different nanocarriers' skin penetration potential, as observed for hEGF.

The longer duration of the skin penetration studies on curcumin (24 hours) compared to hEGF allowed us to also assess the curcumin stability in the physiological pH (7.4) of the receptor medium. This information might assist when developing curcumin-containing wound

dressings to optimize the frequency of dressing changes. Wound dressings are normally applied on open wounds, with compromised SC barrier properties. This might result in enhanced curcumin penetration through the skin and possible permeation in the dermis, where curcumin might be degraded by its close-to-neutral pH (Mehanny et al., 2016). This might cause a decrease in curcumin's therapeutic efficacy. For all DLs, curcumin showed to be stable up to 8 hrs because after 24 hrs the amount of penetrated curcumin was lower possibly indicating curcumin pH-degradation. This finding will be later used when developing hydrogel-based wound dressings with curcumin (Paper V).

As discussed in this chapter, the liposomal surface charge showed to play a role in the nanocarrier's ability as dermal delivery systems. Moreover, the effectiveness of liposomal systems in assuring sustained delivery was also dependent on the physicochemical properties of the active substances.

5.5 Effect of the liposomal surface charge on the biological activities of associated active substances

The liposomal surface charge may also enhance the targeted cellular delivery of the liposome-associated drug (Meng et al., 2018). The interaction of the nanocarrier with the targeted cell membrane and subsequent cellular uptake of the associated drug/substance might be better promoted via charged liposomes, thus assuring adequate concentration level at the targeted site and therewith enhance biological activities (Meng et al., 2018). By modification of the liposomal surface, the interaction nanocarrier/cell membrane can be optimized and the cellular uptake of the liposome-associated drug/substance enhanced.

Both hEGF and curcumin have shown to exert their therapeutic effects at cellular level. We therefore evaluated the effect of the liposomal surface charge on the biological activities of the two active substances, individually incorporated in DLs.

5.5.1 Mitogenic activity of hEGF-containing DLs (Paper III)

Although topical hEGF is promising for improved chronic wound therapy, its short half-life and high sensitivity to enzymatic degradation limit its efficacy once topically administered onto the skin. DLs have potential to assure hEGF protection from enzymatic degradation and its sustained release at the skin site, thus resulting in enhanced biological activity (Gainza et al., 2014). We therefore evaluated the mitogenic activity of hEGF when incorporated in DLs, aiming at exploring any effect of the liposomal surface charge on hEGF activity. The *in vitro* mitogenic activity of hEGF liposomal formulations was tested in two cell lines, namely HFF and HaCaT, because their proliferation at the wounded skin area has shown to be beneficial for improving wound healing (Werner et al., 2007). All DLs were reduced in vesicle size to approx. 150 nm to avoid possible liposome precipitation during the experiment. The drug load was determined prior to the cell experiments.

The mitogenic effect of hEGF-containing DLs in HFF is presented in Figure 5.10. At the highest lipid concentration (50 μg/mL), both hEGF-NDLs and hEGF-ADLs exhibited higher HFF proliferation compared to control (untreated cells). This effect was more evident after 48 hrs treatment, where the mitogenic activity of hEGF incorporated in both NDLs and ADLs was also superior to the activity of hEGF in solution (free hEGF). The most potent effect was observed for hEGF-ADLs. After 48 hrs treatment, hEGF-ADLs (lipid concentration of 50 μg/mL) assured 77 and 45% more proliferation than control and free hEGF, respectively. A different response was observed when HFF were treated with hEGF-CDLs. After 24 hrs treatment, hEGF-CDLs at the lowest lipid concentrations (1 and 10 μg/mL) improved cell proliferation compared to control, whereas a lower HFF proliferation was observed at the highest lipid concentration of hEGF-CDLs. This cytotoxic effect might be due to both high concentration of hEGF and SA. The positive charge of SA in the CDLs bilayer might promote the interaction of surfactant with the cell membrane thus compromising the integrity of HFF (Tahara et al., 2018). After 48 hrs treatment, hEGF-CDLs at 10 μg/mL increased HFF proliferation by 40% compared to control. The different effect of hEGF-CDLs observed between the 24 and 48 hrs treatment might be due to a cell response dependent on the incubation time, as previously observed for hEGF-containing nanofibers (Bertoncelj et al., 2014).

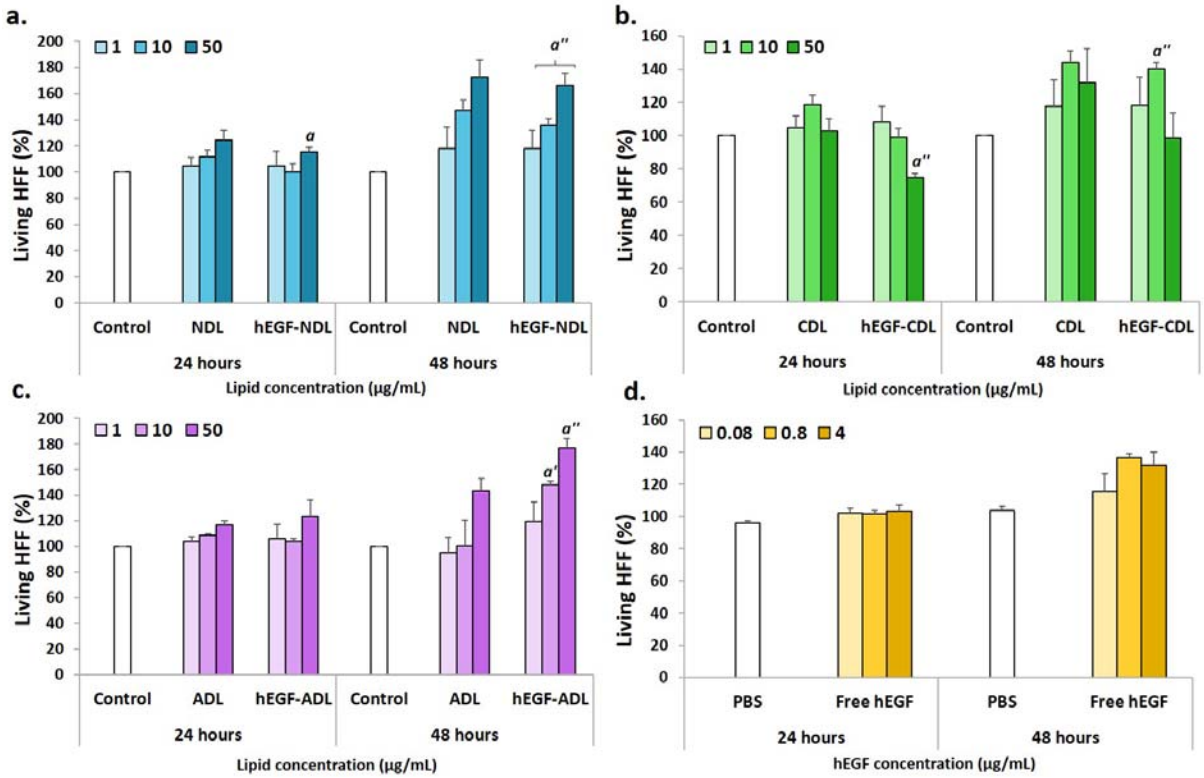

Figure 5.10: Effect of hEGF-NDLs (a), hEGF-CDLs (b) and hEGF-ADLs (c) on HFF proliferation after 24 and 48 hrs treatment. (d) is hEGF in PBS at same hEGF concentrations as in DLs. Results are expressed as mean (n = 3) ± SD. [a]Significantly different than control (untreated HFF): [a]$p < 0.03$, [a']$p < 0.002$, [a'']$p < 0.0001$.

The mitogenic effect of hEGF-containing DLs in HaCaT is presented in Figure 5.11. After 24 hrs treatment, both hEGF-NDLs and hEGF-ADLs, at the highest lipid concentration, exhibited superior mitogenic effect in HaCaT cells as compared to both control and free hEGF. As observed for HFF, ADLs exhibited the best enhancement of hEGF mitogenic activity and increased HaCaT proliferation by 36 and 41% more compared to control and free hEGF, respectively. Regarding hEGF-CDLs, the same effect was observed as in the HFF cells. Treatment of HaCaT for 48 hrs with all hEGF-DLs resulted in a lower cell proliferation compared to control, differing from HFF proliferation profiles (Figure 5.10). This indicated that the proliferation rate is additionally dependent on the cell lines (Gainza et al. 2014).

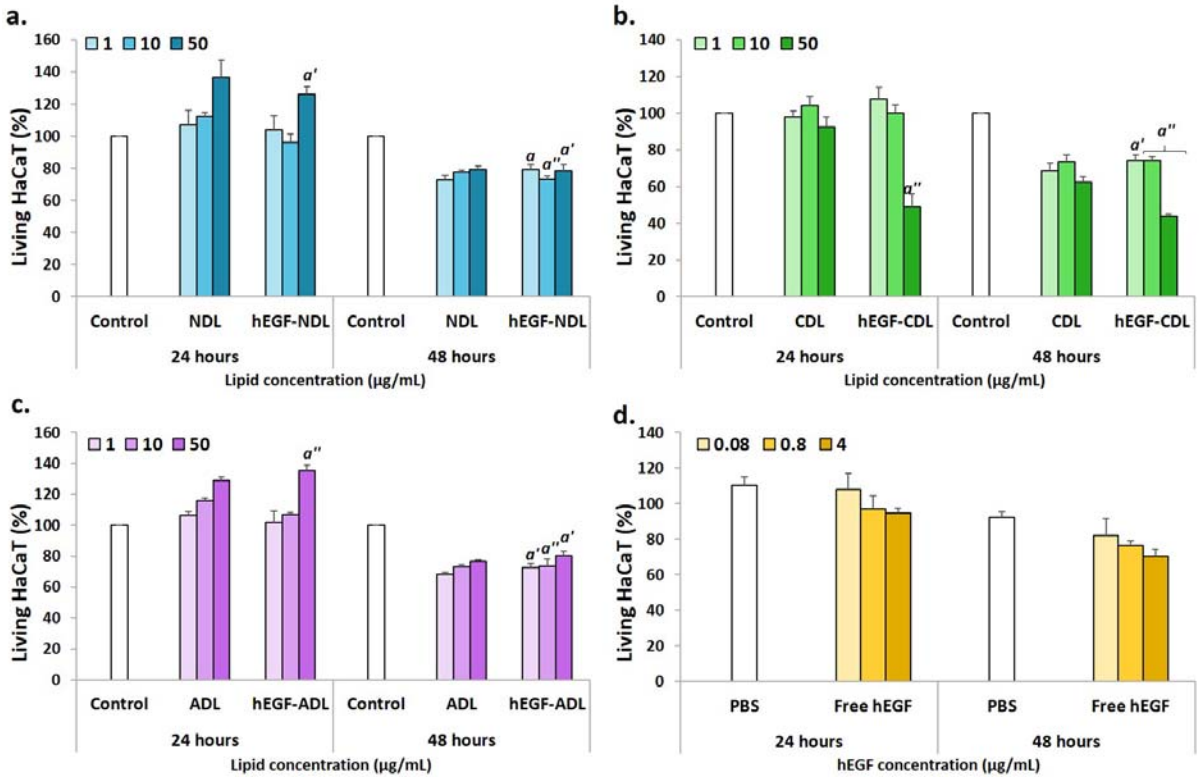

Figure 5.11: Effect of hEGF-NDLs (a), hEGF-CDLs (b) and hEGF-ADLs (c) on HaCaT proliferation after 24 and 48 hrs treatment. (d) is hEGF in PBS at same hEGF concentrations as in DLs. Results are presented as mean (n = 3) ± SD. [a]Significantly different than control (untreated HaCaT): [a]$p < 0.03$, [a']$p < 0.002$, [a'']$p < 0.0001$.

The significant enhancement of hEGF mitogenic activity in both cell lines mediated by ADLs might be explained by the depot effect revealed in the *ex vivo* skin penetration studies (Figure 5.8). ADLs enabled hEGF sustained skin penetration thus assuring continuous presence of hEGF therapeutic levels at the administration site.

5.5.2 Biological activities of curcumin-containing DLs (Paper IV)

The attractiveness of curcumin for improved localized skin therapy is particularly based on the fact that this molecule has numerous beneficial activities, such as anti-oxidant, anti-inflammatory and anti-microbial, allowing curcumin action at different pathology levels (Hussain et al., 2017). This might result in more effective skin therapies accompanied by

reduction of the number of treatments and thus increasing patient compliance. Curcumin's anti-oxidant activity has been fully established (Mohanty and Sahoo, 2017), therefore we mainly focused on both *in vitro* anti-inflammatory and anti-bacterial activity of curcumin-containing DLs targeting treatment of skin inflammation and bacterial infections, particularly chronic wounds and burns.

5.5.2.1 Anti-bacterial activity

Chronic wounds and burns are characterized by a high incidence of bacterial infections, which cause morbidity and even mortality among patients (Siddiqui and Bernstein, 2010). The treatment with oral antibiotics often fails due to the increasing incidence of bacterial resistance to antibiotics (Zhou et al., 2018). The administration of topical curcumin formulations might represent a promising approach to limit the overuse of antibiotics and their related microbial resistance. We evaluated the possible *in vitro* anti-bacterial activity of curcumin-containing DLs against two clinical strains of Gram-positive bacteria, namely *S. aureus* and *S. pyogenes*, which are commonly colonizing the wounded area at both the initial and later stages of chronic wound formation (Byrd et al., 2018).

All curcumin-containing DLs exhibited growth inhibition of both bacteria compared to control (untreated bacteria) (Figure 5.12). The anti-bacterial effect of curcumin-containing DLs was not dose-dependent, indicating that lower curcumin concentration exhibited satisfactory anti-bacterial effect. Considering the liposomal surface charge, CDLs showed the best enhancement of curcumin's anti-bacterial activity against both bacteria also compared to free curcumin (CUR-PG). The superior activity of curcumin when incorporated in CDLs as compared to both NDLs and ADLs might be related to an enhanced interaction with the negative bacterial cell membrane resulting in an increased curcumin availability at the site of action to exert its anti-bacterial effect. This would also explain the superior anti-bacterial activity of curcumin-CDLs compared to free curcumin, which would initially require to interact with the bacterial membrane to exert the therapeutic effect (Simões et al., 2018).

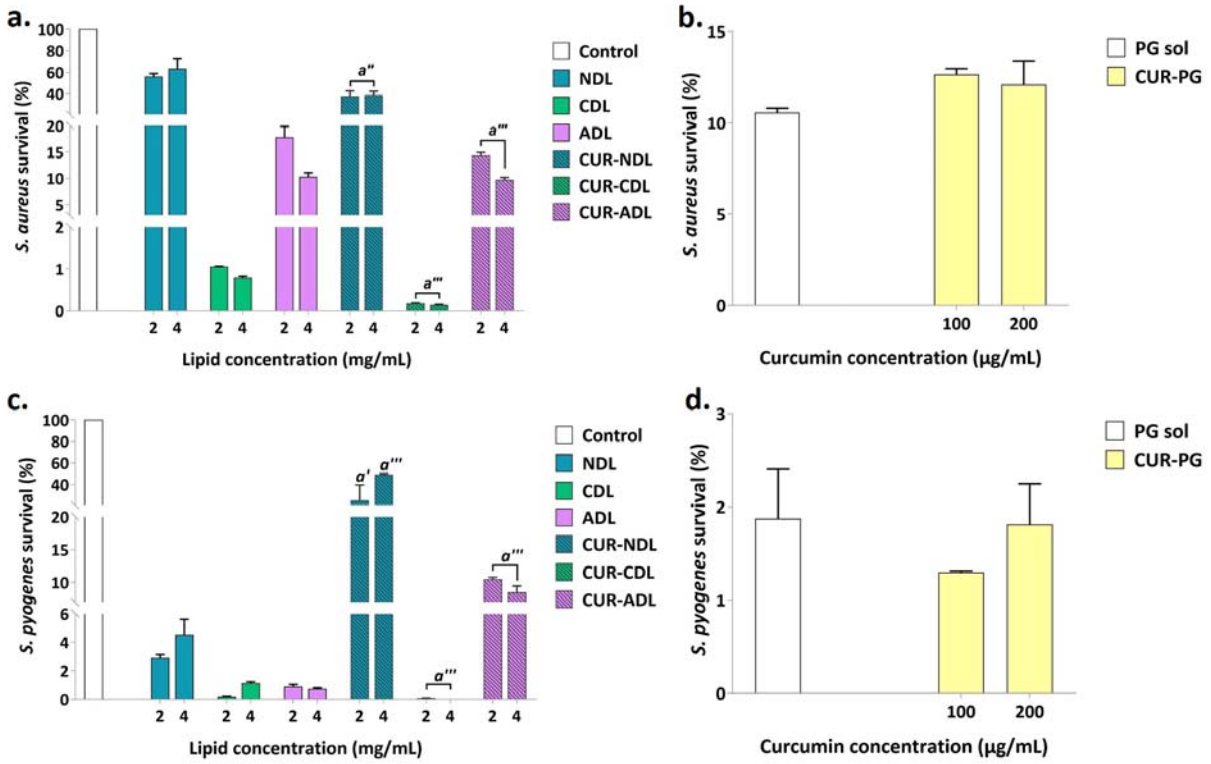

Figure 5.12: Effect of different curcumin-containing DLs on *S. aureus* (a) and *S. pyogenes* (c) growth after 4 hrs treatment. Effect of curcumin in PG solution (CUR-PG) on *S. aureus* and *S. pyogenes* is showed in (b) and (d), respectively, where PG sol is PG (20%, w/v) solution in PBS. Results are expressed as mean (n = 2) ± SD. [a]Significantly lower than control (untreated bacteria): [a]$p < 0.03$, [a']$p < 0.002$, [a'']$p < 0.0002$, [a''']$p < 0.0001$.

Curcumin-containing DLs were also tested in terms of *in vitro* anti-bacterial activity against a Gram-negative bacteria, *P. aeruginosa*, commonly colonizing the wounded area and often able to form biofilms. All DLs did not show any enhanced anti-bacterial activity of curcumin when compared to free curcumin (data not shown). Considering the interaction between DLs and bacterial cell membrane, a possible explanation might be in the differences between Gram-positive and Gram-negative bacterial membranes. The different membrane composition of Gram-negative bacteria might not favour an interaction with DLs. The less susceptibility of Gram-negative bacteria towards curcumin incorporated in nanoparticles has also been observed by Krausz et al. (2015).

5.5.2.2 Anti-inflammatory activity

Skin inflammation, especially in chronic wounds, is characterized by an excessive NO production by LPS-induced macrophages. Large quantities of NO might result in the cell death caused by a formation of an extremely reactive radical (Deldar et al., 2018). Moreover, regarding the chronic wounds, NO can induce impaired collagen synthesis further delaying wound healing (Park et al., 2013).

Curcumin-containing DLs were evaluated in terms of *in vitro* anti-inflammatory activity by exploring any possible NO inhibition in LPS-induced macrophages (Figure 5.13). A dose-dependent effect was observed for all curcumin-containing DLs. Independently of the liposomal surface charge, all curcumin-containing DLs (10 and 50 µg/mL as lipid concentration) were superior in inhibiting NO production compared to free curcumin. Therefore, DLs showed satisfactory enhancing effect on curcumin's anti-inflammatory activity. This might be explained by a possible increase of curcumin uptake in macrophages mediated by DLs, in agreement with recent findings on enhanced glucocorticoids uptake in macrophages when the drugs were incorporated in phosphatidylserine liposomes (Gauthier et al., 2018). As observed for the anti-bacterial activity, curcumin-containing CDLs were the most potent. This might be explained by the positive surface charge of CDLs that can allow stronger interaction of CDLs with the negative membrane of macrophages compared to both NDLs and ADLs. Considering the *ex vivo* skin penetration profiles (Figure 5.9), the most sustained skin penetration of curcumin by CDLs might assure constant therapeutic levels of curcumin at the targeted cellular level thus enhancing curcumin's interaction with macrophages and consequently increasing its anti-inflammatory activity. Zhao et al. (2013) observed this correlation between sustained curcumin release and enhanced anti-inflammatory activity when curcumin was incorporated in PG liposomes.

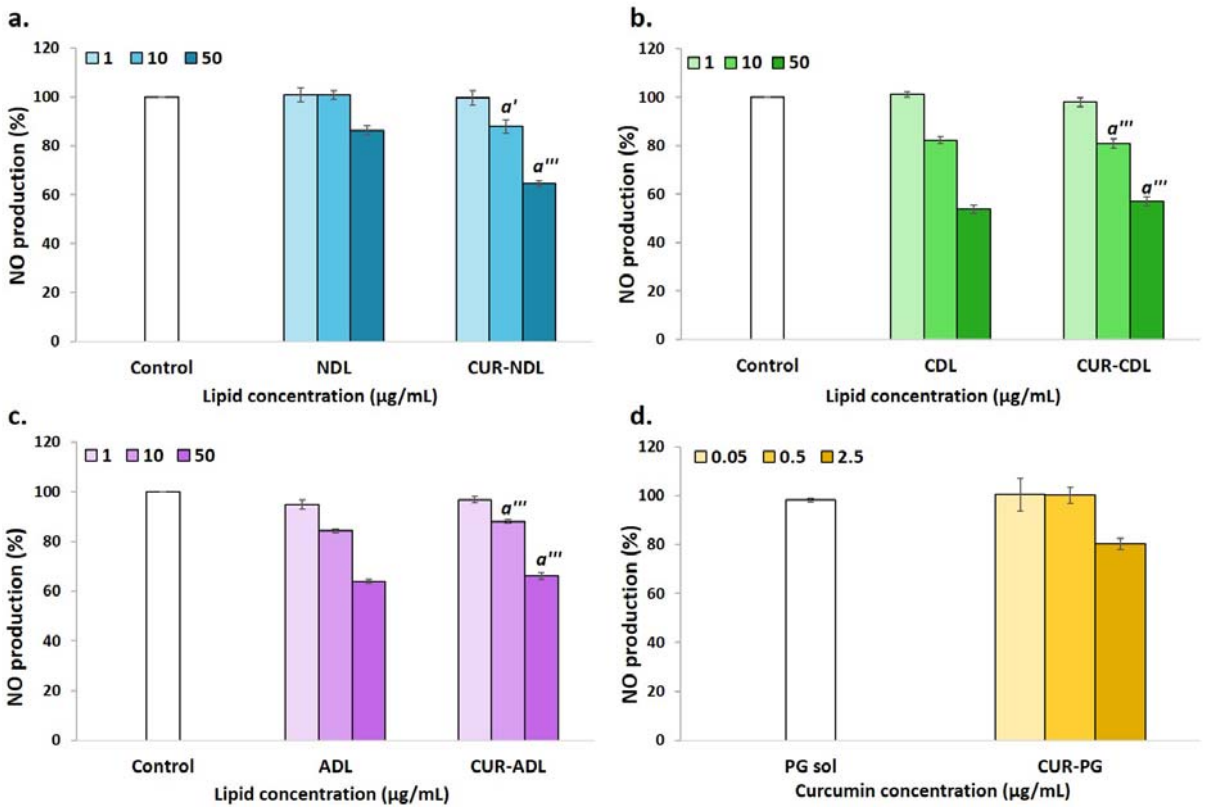

Figure 5.13: Effect of curcumin-containing NDLs (a), CDLs (b) and ADLs (c) on NO production in LPS-induced macrophages. (d) shows the effect of free curcumin (curcumin in PG (20%, w/v) solution, CUR-PG), tested at the same curcumin concentrations as in DLs. Results are presented as mean (n = 3 ± SD). [a]Significantly lower than control (untreated LPS-induced macrophages): $^{a}p < 0.03$, $^{a'}p < 0.002$, $^{a''}p < 0.0002$, $^{a'''}p < 0.0001$.

It can be argued that the enhanced anti-inflammatory activity of curcumin-containing DLs, especially CDLs, might be only a consequence of the possible cytotoxic effect exerted by the presence of surfactants, particularly ionic, in the DLs phospholipid bilayer (Dhawan and Nagarsenker, 2017). The strong NO inhibition might be then the result of apoptosis/necrosis of macrophages rather than an effect mediated by the intrinsic anti-inflammatory effect of curcumin enhanced by its incorporation in DLs. We therefore evaluated the *in vitro* viability of healthy HFF after the treatment with the different curcumin-containing DLs. All DLs exhibited no cytotoxic effect in HFF and they additionally enabled cell proliferation after both 12 and 24 hrs exposure (data presented in Paper IV). CDLs at the highest tested lipid concentration (50

μg/mL) did not exhibit HFF proliferation, however they enabled viable HFF comparable to control (untreated HFF). This lack of CDLs cytotoxicity further supported the hypothesis that DLs, particularly CDLs, enhanced curcumin's anti-inflammatory activity.

The screening of the DLs bearing different surface charge revealed the development of delivery systems able to enhance the biological activities of the nanocarrier-associated active substance thus showing good potential for improved localized skin therapy.

5.6 Effect of the liposomal surface charge on the DLs-in-hydrogel systems (Paper V)

The developed curcumin-DLs formulations, particularly curcumin-CDLs, are promising to be used for treatment of skin inflammation and bacterial infections. As an example, the several beneficial effects of curcumin might improve the healing of chronic wounds and burns; their healing is typically delayed due to persistent inflammation and consequent infections (Hussain et al., 2017). Curcumin has also shown to control scar formation and curcumin-based skin formulations are promising for treatment of hypertrophic post burn scarring (Amini-Nik et al., 2018). We have additionally shown that when incorporated in DLs, particularly CDLs, curcumin exhibited more potent effects than when applied in solution. To enable topical application of curcumin-containing DLs onto the skin we decided to incorporate the liposomal formulations into a second vehicle and develop potential curcumin-based wound dressings. As second vehicle, we selected chitosan hydrogel that has shown to possess adequate rheological properties that can guarantee efficacy of the wound dressings for treatment of chronic wounds/burns (Hamedi et al., 2018). Chitosan can offer a moist environment and protect the wounded area from bacterial infections, also because of its intrinsic anti-bacterial as well as wound helaing effect (Perinelli et al., 2018; Hurler et al., 2013a). The latter effect might synergistically act with curcumin assisting in effective localized chronic wound therapy, especially preventing microbial colonization and biofilm development. The incorporation of liposomes in hydrogel introduces more parameters affecting both hydrogel's texture properties and drug/substance penetration from liposomes-in-hydrogel systems through/into

skin (Hurler et al., 2013b). To develop a suitable combination of the two delivery systems, all these factors need to be explored. We therefore evaluated the effect of the liposomal surface charge on hydrogel's texture and bioadhesive properties, as well as on curcumin penetration from the DLs-in-hydrogel systems through the *ex vivo* human skin.

5.6.1 Texture properties

Hydrogel's texture properties, such as the hardness, cohesiveness and adhesiveness, can determine the efficacy of the hydrogel formulation. Hydrogel's hardness can affect the ease of hydrogel application onto the skin, thus influencing patient compliance. The adhesiveness, on the other hand, affects the contact time of the hydrogel with the skin that might be related to the retention time of the drug on the skin administration site.

Chitosan hydrogel is often used in therapy comprising drug, polymer and humectants and addition of active substances and excipients can change its texture properties (Hurler et al., 2013b). The incorporation of liposomes in chitosan hydrogel has shown to modify chitosan hydrogel's texture properties, including the changes after incorporation of liposomes bearing different surface charges (Hurler et al., 2013b). Based on these findings, we also added glycerol (10%, w/w) in the liposomal hydrogel formulations. The addition of glycerol showed to improve the texture properties of liposomal hydrogel formulations (Hurler et al., 2012), due to its influence on the hydrogen bonds between water and chitosan. We incorporated 15% (w/w) of liposomal dispersions in chitosan hydrogel based on previous findings from Hurler et al. (2012) stating that the addition of up to 15% (w/w) of liposomal dispersions did not cause significant changes in the texture properties of chitosan hydrogel.

In Figure 5.14 the texture properties of chitosan hydrogel after the incorporation of the different curcumin-containing DLs are presented.

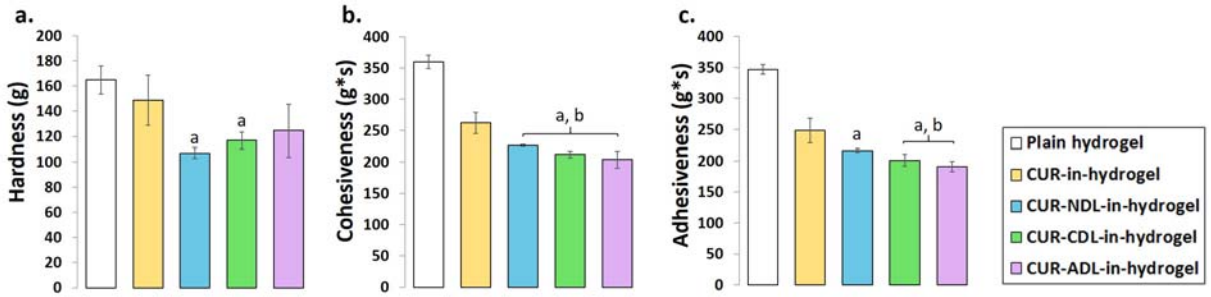

Figure 5.14: Effect of the liposomal surface charge on the texture of DLs-in-hydrogel.
CUR-in-hydrogel is curcumin in PG solution incorporated in chitosan hydrogel at the same concentration as curcumin in DLs. Results are expressed as mean (n = 3) ± SD. [a]Significant *vs*. plain hydrogel ($p < 0.05$), [b]significant *vs*. CUR-in-hydrogel ($p < 0.05$).

Compared to plain chitosan hydrogel, the incorporation of all DLs weakened the texture properties, regardless of the liposomal surface charge and the presence of glycerol as stabilizing agent. Similar results were also observed when incorporating deformable propylene glycol liposomes in Carbopol hydrogel, although the effect of the liposomal surface charge was not investigated (Vanić et al., 2014). Hurler et al. (2013b) observed a reduction of chitosan hydrogel' texture properties after incorporation of CLs bearing different surface charge, in agreement with our findings. The negative effect observed for all DLs was even more evident compared to the incorporation of free curcumin (curcumin in PG solution). PG has been shown to enhance the viscoelasticity of hydrogels by triggering hydrogen bonds between the polymer and water (Islam et al., 2004). This might explain the more positive effect of free curcumin compared to DLs. Comparing the liposomal surface charge, the charged DLs increased the hydrogel hardness, whereas negatively affected both the cohesiveness and adhesiveness. Possible interactions between the charged DLs and the positively charged chitosan chains might result in an increased hydrogel hardness. On the other hand, the electrostatic interactions between charged DLs and chitosan chains might destabilize the chitosan network compared to the neutral DLs. NDLs are not expected to interact with the polymer and this might explain their positive effect on both the cohesiveness and adhesiveness compared to the charged DLs.

Despite the influence of the charged DLs on the texture properties of chitosan hydrogel, we further proceeded in exploring the effect of the liposomal surface charge on the hydrogel's bioadhesion to human skin.

5.6.2 Bioadhesiveness

Texture properties can tailor the therapy outcomes of the hydrogel formulations. However, when considering topical application of hydrogel formulations onto the skin, the interaction between hydrogel and the skin needs to be considered. Good bioadhesiveness of hydrogel formulations is indeed responsible for an adequate retention time of the incorporated drug/substance at the skin administration site (Ribeiro et al., 2009). This can result in more effective localized skin therapy. Bioadhesive wound dressings for chronic wounds and burns might assure adequate protection of the wound bed from microbial infections in the dressings exhibit strong bioadhesion (Boateng and Catanzano, 2015). For these reasons, we further investigated the DLs-in-hydrogel formulations in terms of hydrogel bioadhesiveness. We based our bioadhesiveness study on a method previously developed in our group by Hurler and Škalko-Basnet (2012). Briefly, the DLs-in-hydrogel formulations were placed onto a die, which was pushed onto the slice of human skin for a constant period of time (10 s). The bioadhesiveness was expressed as the detachment force needed to redraw the die from the human skin, representing the force needed to break the bonds between hydrogel and skin (Figure 5.15 a). The amount of retained formulation onto the skin surface after the removal of the die was also determined (Figure 5.15 b). The bioadhesiveness of chitosan hydrogel was not affected by incorporation of DLs. Regarding the detachment force, no significant differences were observed between the different DLs-in-hydrogel formulations and plain chitosan hydrogel. NDLs-in-hydrogel exhibited superior bioadhesion compared to the other formulations. The neutral surface of NDLs might account for negligible interactions with the chitosan chains thus leaving the intrinsic bioadhesive properties of chitosan unaltered. The amount of formulations retained on the skin after the bioadhesion tests was found similar for all tested formulations and the absolute values (approx. 65%) were in agreement with previous findings on conventional liposomes-containing chitosan hydrogel (Hurler and Škalko-Basnet, 2012). The fact that almost 70% of all DLs-in-hydrogel formulations remained onto the

skin surface is promising to overcome the challenge of short retention time of wound dressings on the exudate-rich wounded areas, which limit the wound dressings' bioadhesion due to their high water content.

In the used experimental setup for the bioadhesiveness studies, the determined force might be the result of the force needed to detach the hydrogel from the skin (bioadhesiveness) and the force necessary to detach the die from the part of hydrogel left onto the skin (adhesiveness). We are aware that the obtained values might not be the absolute values of bioadhesiveness. We were mainly interested in using the constant experimental conditions aiming at detecting any differences among the DLs with different surface charge. To investigate the matter, we performed a bioadhesion study using another experimental setup, where the human skin was fixed on the die and the formulation placed at the bottom (Figure 5.15 c). The die carrying the human skin, with the SC facing the formulation, was pressed onto the formulation for the same period of time (10 s) as in the previous bioadhesion study.

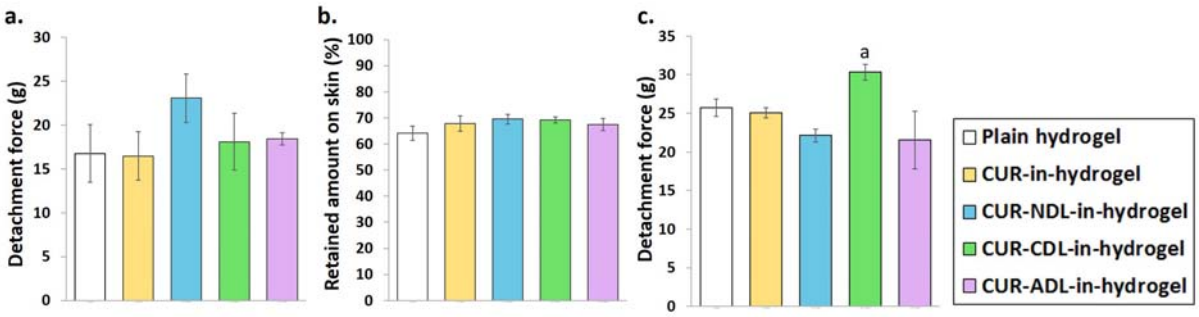

Figure 5.15: Effect of the liposomal surface charge on bioadhesiveness of chitosan hydrogel (n = 3 ± SD). Bioadhesiveness expressed as detachment force (a) and amount of formulation retained on the skin surface (b). (c) is the detachment force determined with the second experimental setup (the skin on the die and the formulation placed at the bottom). [a]Significantly greater than both CUR-NDL-in-hydrogel and CUR-ADL-in-hydrogel.

Although the absolute values determined in the second experimental set up were found slightly higher compared to the first setup (Figure 5.15 a), we confirmed that the original

chitosan bioadhesiveness (plain hydrogel) was not significantly weakened by DLs incorporation into the hydrogel. In this case, NDLs exhibited slightly lower bioadhesion compared to plain chitosan hydrogel and curcumin-in-hydrogel, whereas CDLs-in-hydrogel exhibited the highest detachment force. To explain these discrepancies between the two experimental setups, it is also important to mention that the second experimental setup was performed with DLs-in-hydrogel formulations which were non-freshly prepared (approx.3 weeks old). Therefore, the lower detachment force observed for NDLs-in-hydrogel might be explained by lower stability of NDLs, whose neutral surface might cause faster liposome aggregation compared to the charged DLs thus resulting in lower bioadhesiveness. In agreement with this hypothesis are the findings from the stability studies of DLs-in-hydrogel formulations, whose bioadhesiveness was determined using the first experimental setup. Stability studies were performed after one month of storage of the formulations at room temperature (23-24 °C) (Figure 5.16).

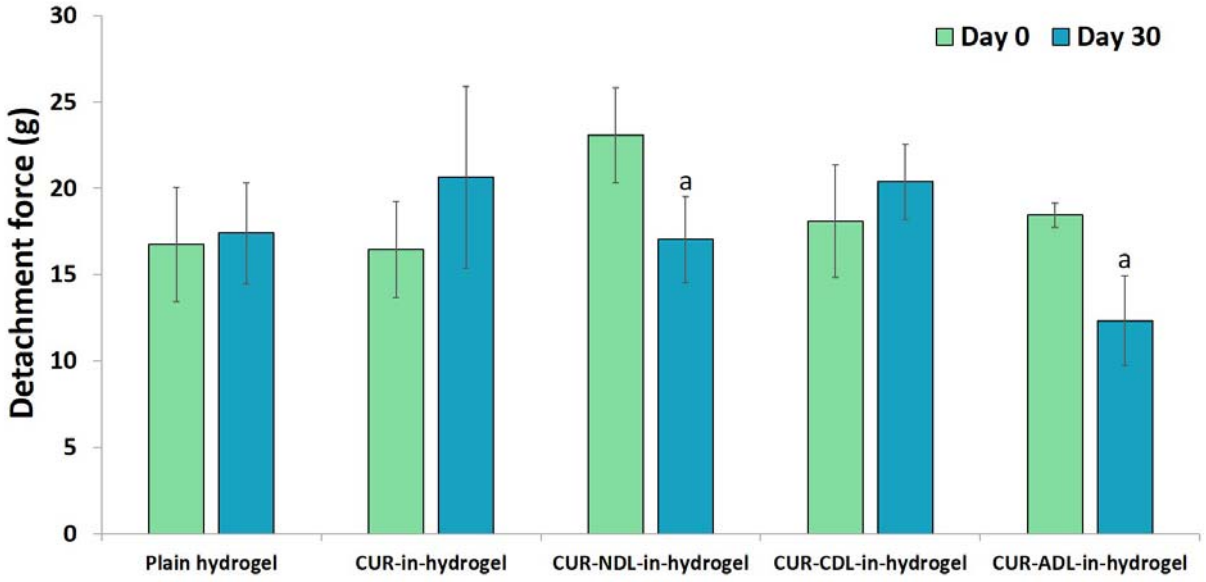

Figure 5.16: Effect of the liposomal surface charge on bioadhesiveness of chitosan hydrogel: stability testing. The bioadhesiveness, expressed as detachment force, was measured on original formulations (day 0) and after storage for one month at 23-24 °C (day 30) (n = 3 ± SD) [a]$p < 0.05$ vs. day 0.

Both NDLs- and ADLs-in-hydrogel exhibited loss of bioadhesiveness upon storage, whereas the positive charge of CDLs preserved the original bioadhesiveness of chitosan hydrogel, as observed with bioadhesiveness study using the second experimental setup (Figure 5.15 c). Therefore, a correlation could be found between the two experimental setups, supported by the findings from the stability studies (Figure 5.16).

The repulsion between CDLs and the positive chitosan chains might stabilize the liposomes embedded in the chitosan matrix to a greater extent thus preserving the hydrogel bioadhesiveness. Therefore, although the original texture properties were weakened after the storage of formulations for one month (data presented in Paper V), CDLs combined with chitosan hydrogel exhibited satisfactory bioadhesion to human skin, even upon the storage period.

5.6.3 *Ex vivo* skin penetration of curcumin from DLs-in-hydrogel

Wound dressings that can assure sustained skin penetration of the incorporated drug might provide sufficient drug/substance concentration at the skin site over prolonged period of time and enhanced drug/substance efficacy (Billard et al., 2015). Considering the combination of two delivery systems, in our case DLs and chitosan hydrogel, the drug penetration though/into the skin is the result of more complex penetration dynamics. We additionally included the liposomal surface charge as another parameter that can play a role in curcumin penetration from DLs-in-hydrogel through skin. The evaluation of any effect of the liposomal surface charge on the skin penetration of curcumin from DLs-in-hydrogel systems may assist in the development of liposomal hydrogel formulations with tailored curcumin skin penetration profiles. The possibility to obtain wound dressings with controlled skin penetration of the incorporated drug/substance can directly improve localized skin therapy according to the targeted skin condition/disease.

Curcumin penetration from DLs-in-hydrogel systems through the *ex vivo* human skin is presented in Figure 5.17. The previous findings from *ex vivo* skin penetration studies on curcumin-containing DLs (Figure 5.9, paper IV) highlighted a possible pH degradation of curcumin due to lower amount of penetrated curcumin detected in the receptor medium after

8 hrs of skin penetration study. We therefore decided to conduct the *ex vivo* skin penetration studies of liposomal hydrogel formulations for 8 hrs.

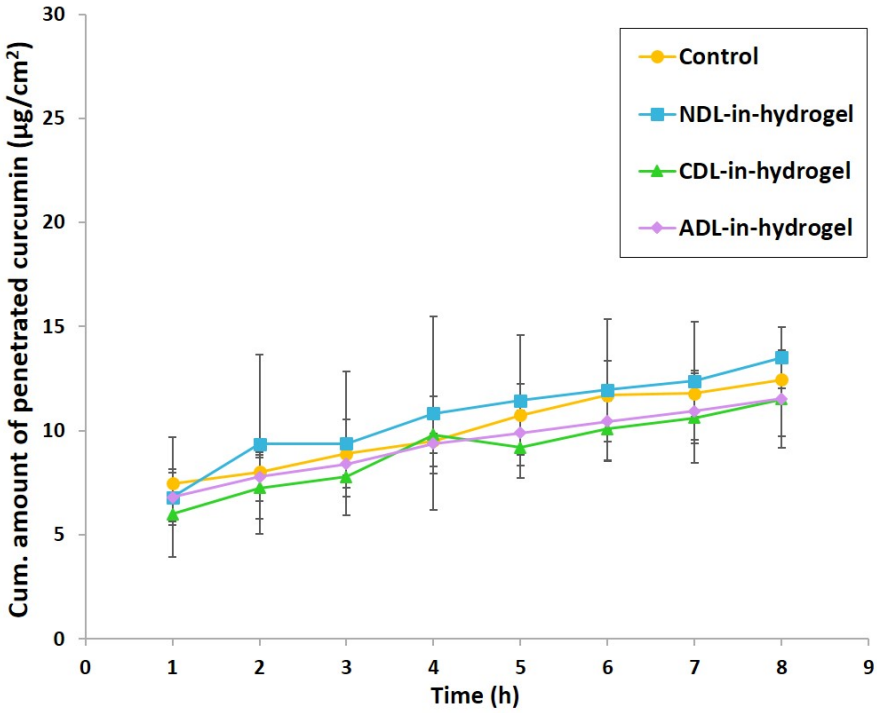

Figure 5.17: Curcumin penetration from different DLs-in-hydrogel through the full thickness human skin over 8 hrs. Curcumin in PG-in-hydrogel was used as control. Results are expressed as mean (n = 3) ± SD.

Low amount of curcumin penetrated the full thickness human skin, regardless of the liposomal surface charge. The DLs-in-hydrogel formulations enabled dermal delivery of curcumin assuring minimal systemic absorption. Considering the lipophilicity of curcumin, its partitioning from the liposome bilayer into the hydrogel matrix and the consequent diffusion into the hydrogel might be slower due to its low affinity with the hydrophilic chitosan (Hurler et al., 2013b). This might explain the sustained skin penetration of curcumin observed for all DLs-in-hydrogel formulations. Slow *in vitro* release of curcumin from lipospheres embedded in hydroxyl propyl methyl cellulose-based gel was recently reported by Jain and collaborators (2016), in agreement with our findings. CDLs enabled the most sustained skin penetration on

curcumin, followed by ADLs. The repulsion between CDLs and chitosan chains, having the same positive charge, might minimally affect CDLs membrane integrity thus slowing curcumin partitioning from CDLs into the hydrogel. Sustained *in vitro* release of a lipophilic fluorescent dye via positively charged CLs-in-chitosan hydrogel has been reported by Hurler et al. (2013b), and was in agreement with our findings. On the other hand, low mobility of liposomes embedded in hydrogel bearing opposite charge has been recently reported by El Kechai and collaborators (2017), who observed that positive liposomes were highly immobilized in a negative hyaluronic acid hydrogel. Therefore, the electrostatic interactions between our negative ADLs and positive chitosan chains can cause immobilization of ADLs within the hydrogel matrix thus limiting curcumin diffusion. This might explain the sustained curcumin penetration from ADLs-in-hydrogel. NDLs-in-hydrogel exhibited the highest amount of penetrated curcumin, also compared to control (curcumin in PG). The minimal interaction between NDLs and chitosan chains might affect liposome's integrity thus resulting in faster curcumin release from NDLs and consequent diffusion through the hydrogel to reach the skin. Considering the liposomes' mobility within the chitosan matrix, the neutral surface of NDLs minimally interacts with the polymer chains thus marginally interfering with NDLs mobility allowing faster curcumin delivery into/through the skin.

The liposomal surface charge has shown to influence curcumin penetration from liposomal hydrogel formulations through the *ex vivo* human skin. The evaluation of the effect of the liposomal surface charge on the skin penetration of curcumin assisted in the selection of the optimal DLs to be combined with chitosan hydrogel to obtain desired skin penetration profile of curcumin. These findings, together with the longer-term bioadhesiveness of CDLs-in-hydrogel, confirmed that the two delivery systems, namely CDLs and chitosan hydrogel, should be further evaluated as advanced wound dressings.

6 Conclusions

The optimization of nanocarriers with tailored properties for controllable skin delivery of both hydrophilic and lipophilic active substances was achieved.

A close-to-*in vivo* skin penetration model was developed able to discriminate the different penetration potentials of two model compounds with different lipophilicities and prove the influence of dermal perfusion on the drug skin penetration. The screening of three different nanocarriers using the IPHSF model showed that the lipid organization of the nanocarriers affected their skin penetration potential of the two model compounds, which were delivered at different skin depth according to the type of employed nanocarrier. Deformable liposomes exhibited satisfactory dermal delivery of both hydrophilic and lipophilic marker by delivering them in the deeper skin layers while avoiding their systemic absorption.

The selected nanocarrier could be optimized to entrap active substances with different physicochemical properties. Nanocarriers with tailored characteristics and satisfactory drug load could be developed by manipulating the type of incorporated surfactant. Further nanocarrier optimization showed that the liposomal surface charge affected the skin penetration potential of deformable liposomes for both hydrophilic and lipophilic active substances. The sustained skin penetration of liposomally-associated active substance could be achieved by tailoring both the liposomal surface charge and the physicochemical properties of active substance. The charged nanocarriers were able to enhance the therapeutic effects of the nanocarrier-associated active substance, possibly by promoting cellular uptake of the active substance and making it available at the targeted site of action. Therefore, the optimization of deformable liposomes, in terms of liposomal surface charge, permitted the development of promising skin formulations for improved localized skin therapy.

The nanocarriers bearing different surface charge incorporated in the chitosan hydrogel affected both the stability of hydrogel and its bioadhesiveness, as well as the skin penetration of nanocarrier-associated active substance. The combination of cationic deformable liposomes and chitosan hydrogel resulted in a wound dressing with good bioadhesiveness, able to sustain the skin penetration of curcumin.

7 Perspectives

Further validation of the IPHSF model as a skin penetration model mimicking damaged/diseased skin could provide a promising tool for exploring drug penetration and optimizing the nanocarrier-based skin formulations when applied onto damaged/diseased skin.

The liposomal formulations with hEGF and curcumin could be tested on the IPHSF model to further examine the effect of the liposomal surface charge on the dermal delivery of both hEGF and curcumin into/through the specific skin layer(s).

Both hEGF- and curcumin-containing deformable liposomes could be tested on the damaged/diseased skin to further prove the effectiveness of the developed liposomal formulations in terms of sustained penetration of the nanocarrier-associated active substances.

To confirm the anti-inflammatory activities of curcumin-containing deformable liposomes, their effect on proinflammatory cytokines could be explored.

To evaluate the anti-biofilm effect of curcumin-containing deformable liposomes, the anti-bacterial effect might be also evaluated against other Gram-negative bacteria and biofilm models.

The liposomal hydrogel formulations with curcumin should be tested in terms of both anti-inflammatory and anti-bacterial activity to confirm their potential in treatment in chronic wounds.

The selected formulations with the most promising properties in terms of both dermal delivery and enhancement of therapeutic properties of the associated active substance could be tested *in vivo* to further prove their efficacy and potential for improved localized skin therapy.

8 References

Abd, E., Yousef, S.A., Pastore, M.N., Telaprolu, K., Mohammed, Y.H., Namjoshi, S., Grice, J.E., Roberts, M.S., **2016**. Skin models for the testing of transdermal drugs. *Clin Pharmacol* 8, 163-176.

Agrawal, R., Sandhu, S.K., Sharma, I., Kaur, I.P., **2015**. Development and evaluation of curcumin-loaded elastic vesicles as an effective topical anti-inflammatory formulation. *AAPS PharmSciTech* 16, 364-374.

Alemdaroğlu, C., Degim, Z., Celebi, N., Şengezer, M., Alömeroglu, M., Nacar, A., **2008**. Investigation of epidermal growth factor containing liposome formulation effects on burn wound healing. *J Biomed Mater Res A* 85, 271-283.

Amini-Nik, S., Yousuf, Y., Jeschke, M.G., **2018**. Scar management in burn injuries using drug delivery and molecular signalling: Current treatments and future directions. *Adv Drug Deliv Rev* 123, 135-154.

Anissimov, Y.G., Zhao, X., Roberts, M.S., Zvyagin A.V., **2012**. Fluorescence recovery after photo-bleaching as a method to determine local diffusion coefficient in the *stratum corneum*. *Int J Pharm* 435, 93-97.

Araiza-Calahorra, A., Akhtar, M., Sarkar, A., **2018**. Recent advances in emulsion-based delivery approaches for curcumin: From encapsulation to bioaccessibility. *Trends Food Sci Technol* 71, 155-169.

Bahia, A.P.C.O., Azevedo, E.G., Ferreira, L.A.M., Frézard, F., **2010**. New insights into the mode of action of ultradeformable vesicles using calcein as hydrophilic fluorescent marker. *Eur J Pharm Sci* 39, 90–96.

Banerjee, R., **2013**. Overcoming the *stratum corneum* barrier: a nano approach. *Drug Deliv Transl Res* 3, 205-208.

Barbero, A.M., Frasch, H.F., **2016**. Effect of frozen human epidermis storage duration and cryoprotectant on barrier function using two model compounds. *Skin Pharmacol Physiol* 29, 31-40.

Baroli, B., **2010**. Penetration of nanoparticles and nanomaterials in the skin: fiction or reality? *J Pharm Sci* 99, 21-50.

Basnet, P., Hussain, H., Tho, I., Škalko-Basnet, N., **2012**. Liposomal delivery system enhances anti-inflammatory properties of curcumin. *J Pharm Sci* 101, 598-609.

Benson, H.A.E., **2006**. Transfersomes for transdermal drug delivery. *Exp Opin Drug Deliv* 3, 727-737.

Bertoncelj, V., Pelipenko, J., Kristl, J., Jeras, M., Cukjati, M., Kocbek, P., **2014**. Development and bioevaluation of nanofibers with blood-derived growth factors for dermal wound healing. *Eur J Pharm Biopharm* 88, 64-74.

Billard, A., Pourchet, L., Malaise, S., Alcouffe, P., Montembault, A., Ladavière, C., **2015**. Liposome-loaded chitosan physical hydrogel: toward a promising delayed-release biosystem. *Carbohydr Polym* 115, 651-657.

Black, C.E., Huang, N., Neligan, P.C., Levine, R.H., Lipa, J.E., Lintlop, S., Forrest, C.R., Pang, C.Y., **2001**. Effect of nicotine on vasoconstrictor and vasodilator responses in human skin vasculature. *Am J Physiol Regul Integr Comp Physiol* 281, 1097-1104.

Bnyan, R., Khan, I., Ehtezazi, T., Saleem, I., Gordon, S., O'Neill, F., Roberts, M., **2018**. Surfactant effects on lipid-based vesicles properties. *J Pharm Sci* 107, 1237-1246.

Boateng, J., Catanzano, O., **2015**. Advanced therapeutic dressings for effective wound healing - A review. *J Pharm Sci* 104, 3653-3680.

Bolzinger, M.A., Briançon, S., Pelletier, J., Chevalier, Y., **2012**. Penetration of drugs through skin, a complex rate-controlling membrane. *Curr Opin Colloid Interface Sci* 17, 156-165.

Bouwstra, J.A., Honeywell-Nguyen, P.L., Gooris, G.S., Ponec, M., **2003**. Structure of the skin barrier and its modulation by vesicular formulations. *Prog Lipid Res* 42, 1-36.

Bouwstra, L.A., Ponec, M., **2006**. The skin barrier in healthy and diseased state. *Biochim Biophys Acta* 1758, 2080-2095.

Bragagni, M., Mennini, N., Maestrelli, F., Cirri, M., Mura, P., **2012**. Comparative study of liposomes, transfersomes and ethosomes as carriers for improving topical delivery of celecoxib. *Drug Deliv* 19, 354-361.

Brommeland, T., Lindal, S., Straume, B., Dahl, I.L., Hennig, R., **2003**. Does imprint cytology of brain tumours improve intraoperative diagnoses? *Acta Neurol Scand* 108,153-156.

Byrd, A.L., Belkaid, Y., Segre, J.A., **2018**. The human skin microbiome. *Nat Rev Microbiol* 16, 143-155.

Carver, M.P., Williams, P.L., Riviere, J.E., **1989**. The isolated perfused porcine skin flap III. Percutaneous absorption pharmacokinetics of organophosphates, steroids, benzoic acid, and caffeine. *Toxicol Appl Pharmacol* 97, 324-337.

Cevc, G., Blume, G., **1992**. Lipid vesicles penetrate into intact skin owing to the transdermal osmotic gradients and hydration force. *Biochim Biophys Acta* 1104, 226-232.

Cevc, G., Vierl, U., **2010**. Nanotechnology and the transdermal route: A state of the art review and critical appraisal. *J Control Release* 141, 277-299.

Chen, M., Liu, X., Fahr, A., **2011**. Skin penetration and deposition of carboxyfluorescein and temoporfin from different lipid vesicular systems: *In vitro* study with finite and infinite dosage application. *Int J Pharm* 408, 223-234.

Choi, J.U., Lee, S.W., Pangeni, R., Byun, Y., Yoon, I-S., Park, J.W., **2017**. Preparation and *in vivo* evaluation of cationic elastic liposomes comprising highly skin-permeable growth factors combined with hyaluronic acid for enhanced diabetic wound-healing therapy. *Acta Biomater* 57, 197-215.

Cilurzo, F., Gennari, C.G.M., Minghetti, P., **2012**. Adhesive properties: a critical issue in transdermal patch development. *Expert Opin Drug Deliv* 9, 33-45.

Cilurzo, F., Minghetti, P., Sinico, C., **2007**. Newborn pig skin as model membrane in *in vitro* drug permeation studies: A technical note. *AAPS PharmSciTech* 8, A94.

Cilurzo, F., Vistoli, G., Selmin, F., Gennari, C.G.M., Musazzi, U.M., Franze, S., Lo Monte, M., Minghetti, P., **2014**. An insight into the skin penetration enhancement mechanism of N-methylpyrrolidone. *Mol Pharmaceutics* 11, 1014−1021.

Cima, M.J., Lee, H., Daniel, K., Tanenbaum, L.M., Mantzavinou, A., Spencer, K.C., Ong, Q., Sy, J.C., Santini Jr, J., Schoellhammer, C.M., Blankschtein, D., Langer, R.S., **2014**. Single compartment drug delivery. *J Control Release* 190, 157-171.

Clares, B., Calpena, A.C., Parra, A., Abrego, G., Alvarado, H., Fangueiro, J.F., Souto, E.B., **2014**. Nanoemulsions (NEs), liposomes (LPs) and solid lipid nanoparticles (SLNs) for retinyl palmitate: effect on skin permeation. *Int J Pharm* 473, 591-598.

Danaei, M., Dehghankhold, M., Ataei, S., Hasanzadeh Davarani, F., Javanmard, R., Dokhani, A., Khorasani, S., Mozafari, M.R., **2018**. Impact of particle size and polydispersity index on the clinical applications of lipidic nanocarrier systems. *Pharmaceutics* 10, 57.

de Leeuw, J., de Vijlder, H.C., Bjerring, P., Neumann, H.A.M.., **2009**. Liposomes in dermatology today. *J Eur Acad Dermatol Venereol* 23, 505-516.

de Weerd, L., Miland, A.O., Mercer, J.B., **2009**. Perfusion dynamics of free DIEP and SIEA flaps during the first postoperative week monitored with dynamic infrared thermography. *Ann Plast Surg* 62, 42-47.

Deldar, Y., Pilehvar-Soltanahmadi, Y., Dadashpour, M., Montazer Saheb, S., Rahmati-Yamchi, M., Zarghami, N., **2018**. An *in vitro* examination of the antioxidant, cytoprotective and anti-inflammatory properties of chrysin-loaded nanofibrous mats for potential wound healing applications. *Artif Cells Nanomed Biotechnol* 46, 706-716.

DeLouise, L.A., **2012**. Applications of nanotechnology in dermatology. *J Invest Dermatol* 132, 964-975.

Desmet, C.M., Préat, V., Gallez, B., **2018**. Nanomedicines and gene therapy for the delivery of growth factors to improve perfusion and oxygenation in wound healing. *Adv Drug Deliv Rev* 129, 262-284.

Dhawan, V.V., Nagarsenker, M.S., **2017**. Catanionic systems in nanotherapeutics – Biophysical aspects and novel trends in drug delivery applications. *J Control Release* 266, 331-345.

Dick, I.P., Scott, R.C., **1992**. Pig ear skin as an *in-vitro* model for human skin permeability. *J Pharm Pharmacol* 44, 640-645.

Doktorovová, S., Kovačević, A.B., Garcia, M.L., Souto, E.B., **2016**. Preclinical safety of solid lipid nanoparticles and nanostructured lipid carriers: Current evidence from *in vitro* and *in vivo* evaluation. *Eur J Pharm Biopharm* 108, 235-252.

Dragicevic-Curic, N., Gräfe, S., Gitter, B., Winter, S., Fahr, A., **2010**. Surface charged temoporfin-loaded flexible vesicles: *In vitro* skin penetration studies and stability. *Int J Pharm* 384, 100-108.

Dreier, J., Sørensen, J.A., Brewer, J.R., **2016**. Superresolution and fluorescence dynamics evidence reveal that intact liposomes do not cross the human skin barrier. *PLoS ONE* 11, e0146514.

Dreifke, M.B., Jayasuriya, A.A., Jayasuriya, A.C., **2015**. Current wound healing procedures and potential care. *Mater Sci Eng C* 48, 651-662.

du Plessis, J., Ramachandran, C., Weiner, N., Müller, D.G., **1994**. The influence of particle size of liposomes on the deposition of drug into the skin. *Int J Pharm* 103, 277-282.

El Kechai, N., Geiger, S., Fallacara, A., Cañero Infante, I., Nicolas, V., Ferrary, E., Huang, N., Bochot, A., Agnely, F., **2017**. Mixtures of hyaluronic acid and liposomes for drug delivery: Phase behavior, microstructure and mobility of liposomes. *Int J Pharm* 523, 246-259.

El Zaafarany, G.M., Awad, G.A.S., Holayel, S.M., Mortada, N.D., **2010**. Role of edge activators and surface charge in developing ultradeformable vesicles with enhanced skin delivery. *Int J Pharm* 397, 164-172.

Eskandani, M., Hamishehkar, H., Ezzati Nazhad Dolatabadi, J., **2013**. Cyto/Genotoxicity study of polyoxyethylene (20) sorbitan monolaurate (tween 20). *DNA Cell Biol* 32, 498-503.

Fireman, S., Toledano, O., Neinmann, K., Loboda, N., Dayan, N., **2011**. A look at emerging delivery systems for topical drug products. *Dermatol Ther* 24, 477-488.

Flaten, G.E., Dhanikula, A. B., Luthman, K., Brandl, M., **2006**. Drug permeability across a phospholipid vesicle based barrier: A novel approach for studying passive diffusion. *Eur J Pharm Sci* 27, 80-90.

Flaten, G.E., Palac, Z., Engesland, A., Filipović-Grčić, J., Vanić, Ž., Škalko-Basnet, N., **2015**. *In vitro* skin models as a tool in optimization of drug formulation. *Eur J Pharm Sci* 75, 10–24.

Frederiksen, K., Guy, R.H., Petersson, K., **2015**. Formulation considerations in the design of topical, polymeric film-forming systems for sustained drug delivery to the skin. *Eur J Pharm Biopharm* 91, 9-15.

Gainza, G., Pastor, M., Aguirre, J.J., Villullas, S., Pedraz, J.L., Hernandez, R.M., Igartua, M., **2014**. A novel strategy for the treatment of chronic wounds based on the topical administration of rhEGF-loaded lipid nanoparticles: *In vitro* bioactivity and *in vivo* effectiveness in healing-impaired db/db mice. *J Control Release* 185, 51-61.

Gainza, G., Villullas, S., Pedraz, J.L., Hernandez, R.M., Igartua, M., **2015**. Advances in drug delivery systems (DDSs) to release growth factors for wound healing and skin regeneration. *Nanomedicine: NBM* 11, 1551-1573.

Ganesan, M.G., Weiner, N.D., Flynn, G.L. and Ho, N.F.H., **1984**. Influence of liposomal drug entrapment on percutaneous absorption. *Int J Pharm* 20, 139-154.

Gao, W., Vecchio, D., Li, J., Zhu, J., Zhang, Q., Fu, V., Li, J., Thamphiwatana, S., Lu, D., Zhang, L., **2014**. Hydrogel containing nanoparticle-stabilized liposomes for topical antimicrobial delivery. *ACS Nano* 8, 2900-2907.

Garcês, A., Amaral, M.H., Sousa Lobo, J.M., Silva, A.C., **2018**. Formulations based on solid lipid nanoparticles (SLN) and nanostructured lipid carriers (NLC) for cutaneous use: A review. *Eur J Pharm Sci* 112, 159-167.

Garcia-Orue, I., Pedraz, J.L., Hernandez, R.M., Igartua, M., **2017**. Nanotechnology-based delivery systems to release growth factors and other endogenous molecules for chronic wound healing. *J Drug Deliv Sci Technol* 42, 2-17.

Gauthier, A., Fisch, A., Seuwen, K., Baumgarten, B., Ruffner, H., Aebi, A., Rausch, M., Kiessling, F., Bartneck, M., Weiskirchen, R., Tacke, F., Storm, G., Lammers, T., Ludwig, M-G., **2018**.

Glucocorticoid-loaded liposomes induce a pro-resolution phenotype in human primary macrophages to support chronic wound healing. *Biomaterials* 178, 481-495.

Geusens, B., Strobbe, T., Bracke, S., Dynoodt, P., Sanders, N., Van Gele, M., Lambert, J., **2011**. Lipid-mediated gene delivery to the skin. *Eur J Pharm Sci* 43, 199-211.

Geusens, B., Van Gele, M., Braat, S., De Smedt, S.C., Stuart, M.C., Prow, T.W., Sanchez, W., Roberts, M.S., Sanders, N., Lambert, J., **2010**. Flexible nanosomes (SECosomes) enable efficient siRNA delivery in cultured primary skin cells and in the viable epidermis of *ex vivo* human skin. *Adv Funct Mater* 20, 4077-4090.

Gillet, A., Lecomte, F., Hubert, P., Ducat, E., Evrard, B., Piel, G., **2011**. Skin penetration behaviour of liposomes as a function of their composition. *Eur J Pharm Biopharm* 79 (2011) 43–53.

Godin, B., Touitou, E., **2007**. Transdermal skin delivery: predictions for humans from *in vivo*, *ex vivo* and animal models. *Adv Drug Deliv Rev* 59, 1152-1161.

González-Rodríguez, M.L., Rabasco, A.M., **2011**. Charged liposomes as carrier to enhance the permeation through the skin. *Expert Opin Drug Deliv* 8, 857-871.

Goyal, R., Macri, L.K., Kaplan, H.M., Kohn, J., **2016**. Nanoparticles and nanofibers for topical drug delivery. *J Control Release* 240, 77-92.

Grijalvo, S., Mayr, J., Eritja, R., Díaz Díaz, D., **2016**. Biodegradable liposome-encapsulated hydrogels for biomedical applications: a marriage of convenience. *Biomater Sci* 4, 555-574.

Gupta, M., Agrawal, U., Vyas, S.P., **2012**. Nanocarrier-based topical drug delivery for the treatment of skin diseases. *Expert Opin Drug Deliv* 9, 783-804.

Gyles, D.A., Diniz Castro, L., Carréra Silva Jr, J.O., Ribeiro-Costa, R.M., **2017**. A review of the designs and prominent biomedical advances of natural and synthetic hydrogel formulations. *Eur Polym J* 88, 373-392.

Hamdan, S., Pastar, I., Drakulich, S., Dikici, E., Tomic-Canic, M., Deo, S., Daunert, S., **2017**. Nanotechnology-driven therapeutic interventions in wound healing: potential uses and applications. *ACS Cent Sci* 3, 163-175.

Hamedi, H., Moradi, S., Hudson, S.M., Tonelli, A.E., **2018**. Chitosan based hydrogels and their applications for drug delivery in wound dressings: A review. *Carbohydr Polym* 199, 445-460.

Hay, R.J., Johns, N.E., Williams, H.C., Bolliger, I.W., Dellavalle, R.P., Margolis, D.J., Marks, R., Naldi, L., Weinstock, M.A., Wulf, S.K., Michaud, C., Murray, C.J.L., Naghavi, M., **2014**. The

global burden of skin disease in 2010: An analysis of the prevalence and impact of skin conditions. *J Invest Dermatol* 134, 1527–1534.

Ho, N.F.H., Ganesan, M.G., Weiner, N.D. and Flynn, G.L., **1985**. Mechanism of topical delivery of liposomally entrapped drugs. *J Control Release* 2, 61-65.

Hollestein, L.M., Nijsten, T., **2014**. An insight into the Global Burden of Skin Diseases. *J Invest Dermatol* 134, 1499-1501.

Honeywell-Nguyen, P.L., Bouwstra, J.A., **2005**. Vesicles as a tool for transdermal and dermal delivery. *Drug Discov Today Technol* 2, 67-74.

Hurler, J., Engesland, A., Poorahmary Kermany, B., Škalko-Basnet, N., **2012**. Improved texture analysis for hydrogel characterization: Gel cohesiveness, adhesiveness, and hardness. *J Appl Polym Sci* 125, 180-188.

Hurler, J., Škalko-Basnet, N., **2012**. Potentials of chitosan-based delivery systems in wound theapy: bioadhesion study. *J Funct Biomater* 3, 37-48.

Hurler, J., Sørensen, K.K., Fallarero, A., Vuorela, P., Škalko-Basnet, N., **2013a**. Liposomes-in-hydrogel delivery system with mupirocin: *In vitro* antibiofilm studies and *in vivo* evaluation in mice burn model. *Biomed Res Int* 498485.

Hurler, J., Žakelj, S., Mravljak, J., Pajk, S., Kristl, A., Schubert, R., Škalko-Basnet, N., **2013b**. The effect of lipid composition and liposome size on the release properties of liposomes-in-hydrogel. *Int J Pharm* 456, 49-57.

Hussain, Z., Thu, H.E., Amjad, M.W., Hussain, F., Ahmed, T.A., Khan, S., **2017**. Exploring recent developments to improve antioxidant, anti-inflammatory and antimicrobial efficacy of curcumin: A review of new trends and future perspectives. *Mat Sci Eng C* 77, 1316-1326.

Ilić, T., Pantelić, I., Lunter, D., Đorđević, S., Marković, B., Ranković, D., Daniels, R., Savić, S., **2017**. Critical quality attributes, *in vitro* release and correlated *in vitro* skin permeation-*in vivo* tape stripping collective data for demonstrating therapeutic (non)equivalence of topical semisolids: A case study of “ready-to-use” vehicles. *Int J Pharm* 528, 253-267.

Islam, M.T., Rodríguez-Hornedo, N., Ciotti, S., Ackermann, C., **2004**. Rheological characterization of topical carbomer gels neutralized to different pH. *Pharm Res* 21, 1192-1199.

Iwai, I., Han, H.M., den Hollander, L., Svensson, S., Öfverstedt, L.G., Anwar, J., Brewer J., Bloksgaard, M., Laloeuf, A., Nosek, D., Masich, S., Bagatolli, L.A., Skoglund, U., Norlén, L., **2012**. The human skin barrier is organized as stacked bilayers of fully extended ceramides with

cholesterol molecules associated with the ceramide sphingoid moiety. *J Invest Dermatol* 132, 2215-2225.

Jain, A., Doppalapudi, S., Domb, A.J., Khan, W., **2016**. Tacrolimus and curcumin co-loaded liposphere gel: Synergistic combination towards management of psoriasis. *J Control Release* 243, 132-145.

Jain, S., Patel, N., Shah, M.K., Khatri, P., Vora, N., **2017**. Recent advances in lipid-based vesicles and particulate carriers for topical and transdermal application. *J Pharm Sci* 106, 423-445.

Jose, A., Labala, S., Venuganti, V.V.K., **2017**. Co-delivery of curcumin and STAT3 siRNA using deformable cationic liposomes to treat skin cancer. *J Drug Target* 25, 330-341.

Kaminski, G.A.T., Sierakowski, M.R., Pontarolo, R., dos Santos, L.A., de Freitas, R.A., **2016**. Layer-by-layer polysaccharide-coated liposomes for sustained delivery of epidermal growth factor. *Carbohydr Polym* 140, 129–135.

Karimkhani, C., Dellavalle, R.P., Coffeng, L.E., Flohr, C., Hay, R.J., Langan, S.M., Nsoesie, E.O., Ferrari, A.J., Erskine, H.E., Silverberg, J.I., Vos, T., Naghavi, M., **2017**. Global skin disease morbidity and mortality: An update from the Global Burden of Disease Study 2013. *JAMA Dermatol* 153, 406-412.

Kietzmann, M., Löscher, W., Arens, D., Maaβ, P., Lubach, D., **1993**. The isolated perfused bovine udder as an *in vitro* model of percutaneous drug absorption skin viability and percutaneous absorption of dexamethasone, benzoyl peroxide, and etofenamate. *J Pharmacol Toxicol Methods* 30, 75-84.

Kim, N.A., Lim, D.G., Lim, J.Y., Kim, K.H., Jeong, S.H., **2015**. Fundamental analysis of recombinant human epidermal growth factor in solution with biophysical methods. *Drug Dev Ind Pharm* 41, 300-306.

Korting, H.C., Schäfer-Korting, M., **2010**. Carriers in the topical treatment of skin disease, in: Schäfer-Korting M. (Ed.), *Drug Delivery, Handbook of Experimental Pharmacology*. Springer-Verlag, 435–468.

Kotla, N.G., Chandrasekar,B., Rooney, P., Sivaraman,G., Larrañaga,A., Krishna, K.V., Pandit, A., Rochev, Y., **2017**. Biomimetic lipid-based nanosystems for enhanced dermal delivery of drugs and bioactive agents. *ACS Biomater Sci Eng* 3, 1262−1272.

Krausz, A.E., Adler, B.L., Cabral, V., Navati, M., Doerner, J., Charafeddine, R.A., Chandra, D., Liang, H., Gunther, L., Clendaniel, A., Harper, S., Friedman, J.M., Nosanchuk, J.D., Friedman, A.J., **2015**. Curcumin-encapsulated nanoparticles as innovative antimicrobial and wound healing agent. *Nanomedicine: NBM* 11, 195-206.

Kreidstein, M.L., Levine, R.H., Knowlton, R.J., Pang, C.Y., **1995**. Serial fluorimetric assessments of skin perfusion in isolated perfused human skin flaps. *Br J Plast Surg* 48, 288-293.

Kreidstein, M.L., Pang, C.Y., Levine, R.H., Knowlton, R.J., **1991**. The isolated perfused human skin flap: design, perfusion technique, metabolism, and vascular reactivity. *Plast Reconstr Surg* 87, 741-749.

Kristl, J., Teskač, K., Ahlin Grabnar, P., **2010**. Current view on nanosized solid lipid carriers for drug delivery to the skin. *J Biomed Nanotechnol* 6, 529-542.

Küchler, S., Abdel-Mottaleb, M., Lamprecht, A., Radowski, M.R., Haag, R., Schäfer-Korting, M., **2009**. Influence of nanocarrier type and size on skin delivery of hydrophilic agents. *Int J Pharm* 377, 169-172.

Lademann, J., Richter, H., Schanzer, S., Knorr, F., Meinke, M., Sterry, W., Patzelt, A., **2011**. Penetration and storage of particles in human skin: perspectives and safety aspects. *Eur J Pharm Biopharm* 77, 465-468.

Lane, M.E., **2013**. Skin penetration enhancers. *Int J Pharm* 447, 12–21.

Lauterbach, A., Müller-Goymann, C.C., **2015**. Applications and limitations of lipid nanoparticles in dermal and transdermal drug delivery via the follicular route. *Eur J Pharm Biopharm* 97, 152-163.

Lim, H.W., Collins, S.A.B., Resneck, J.S., Bolognia, J.L., Hodge, J.A., Rohrer, T.A., Van Beek, M.J., Margolis, D.J., Sober, A.J., Weinstock, M.A., Nerenz, D.R., Smith Begolka, W., Moyano, J.V., **2017**. The burden of skin disease in the United States. *J Am Acad Dermatol* 76, 958-972.

Liu, Y., Li, Z.C., Liang, D.H., **2012**. Behaviors of liposomes in a thermo-responsive poly(N-isopropylacrylamide) hydrogel. *Soft Matter* 8, 4517–4523.

Lombardi Borgia S., Schlupp, P., Mehnert, W., Schäfer-Korting, M., **2008**. *In vitro* skin absorption and drug release – A comparison of six commercial prednicarbate preparations for topical use. *Eur J Pharm Biopharm* 68, 380-389.

Mahmoud, A., Haberland, A., Dürrfeld, M., Heydeck, D., Wagner, S., Schäfer-Korting, M., **2005**. Cutaneous estradiol permeation, penetration and metabolism in pig and man. *Skin Pharmacol Physiol* 18, 27-35.

Manosroi, A., Kongkaneramit, L., Manosroi, J., **2004**. Stability and transdermal absorption of topical amphotericin B liposome formulations. *Int J Pharm* 270, 279-286.

Mehanny, M., Hathout, R.M., Geneidi, A.S., Mansour, S., **2016**. Exploring the use of nanocarrier systems to deliver the magical molecule; Curcumin and its derivatives. *J Control Release* 225, 1-30.

Mehrabi, M., Mansouri, K., Soleymani, B., Hoseinkhani, Z., Shahlaie, M., Khodarahmi, R., **2017**. Development of a human epidermal growth factor derivative with EGFR-blocking and depleted biological activities: A comparative *in vitro* study using EGFR-positive breast cancer cells. *Int J Biol Macromol* 103, 275-285.

Meng, H., Leong, W., Leong, K.W., Chen, C., Zhao, Y., **2018**. Walking the line: The fate of nanomaterials at biological barriers. *Biomaterials* 174, 41-53.

Mezei, M., Gulasekharam, V., **1980**. Liposomes – a selective drug delivery system for the topical route of administration. Lotion dosage form. *Life Sci* 26, 1473-1477.

Miklavžin, A., Cegnar, M., Kerč, J., Kristl, J., **2018**. Effect of surface hydrophobicity of therapeutic protein loaded in polyelectrolyte nanoparticles on transepithelial permeability. *Acta Pharm* 68, 275-293.

Miland, Å.O., de Weerd, L., Weum, S., Mercer, J.B., **2008**. Visualising skin perfusion in isolated human abdominal skin flaps using dynamic infrared thermography and indocyanine green fluorescence video angiography. *Eur J Plast Surg* 31, 235-242.

Mitragotri, S., Burke, P.A., Langer, R., **2014**. Overcoming the challenge in administering biopharmaceuticals: formulation and delivery strategies. *Nat Rev Drug Discov* 13, 655-672.

Mohanty, C., Sahoo, S.K., **2017**. Curcumin and its topical formulations for wound healing applications. *Drug Discov Today* 22, 1582-1592.

Morales, J.O., Fathe, K.R., Brunaugh, A., Ferrati, S., Li, S., Monetnegro-Nicolini, M., Mousavikhamene, Z., McConville, J.T., Prausnitz, Smyth, H.D.C., **2017**. Challenges and future prospects for the delivery of biologics: Oral mucosal, pulmonary and transdermal routes. *AAPS Journal* 19, 652-668.

Mota, A.H., Rijo, P., Molpeceres, J., Pinto Reis, C., **2017**. Broad overview of engineering of functional nanosystems for skin delivery. *Int J Pharm* 532, 710-728.

Mounessa, J., Braunberer, T., Dunnick, C.A., Dellavalle, R.P., **2017**. Minimal improvements in the global burden of skin disease from 1990 to 2013. *J Am Acad Dermatol* 76, 148-149.

Nimal, T. R., Baranwal, G., Bavya, M. C., Biswas, R., Jayakumar, R., **2016**. Anti-staphylococcal activity of injectable nano tigecycline/chitosanPRP composite hydrogel using *Drosophila melanogaster* model for infectious wounds. *ACS Appl Mater Interfaces* 8, 22074−22083.

Ogiso, T., Yamaguchi, T., Iwaki, M., Tanino, T., Miyake, Y., **2001**. Effect of positively and negatively charged liposomes on skin permeation of drugs. *J Drug Target* 9, 49-59.

Palac, Z., Engesland, A., Flaten, G.E., Škalko-Basnet, N., Filipović-Grčić, J., Vanić, Ž., **2014**. Liposomes for (trans)dermal drug delivery: the skin-PVPA as a novel *in vitro stratum corneum* model in formulation development. *J Liposome Res* 24, 313–322.

Paolino, D., Cosco, D., Cilurzo, F., Trapasso, E., Morittu, V.M., Celia, C., Fresta, M., **2012**. Improved *in vitro* and *in vivo* collagen biosynthesis by asiaticoside-loaded ultradeformable vesicles. *J Control Release* 162, 143-151.

Papakostas, D., Rancan, F., Sterry, W., Blume-Peytavi, U., Vogt, A., **2011**. Nanoparticles in dermatology. *Arch Dermatol Res* 303, 533-550.

Pardeike, J., Hommoss, A., Müller, R.H., **2009**. Lipid nanoparticles (SLN, NLC) in cosmetics and pharmaceutical dermal products. *Int J Pharm* 366, 170-184.

Park, J.E., Abrams, M.J., Efron, P.A., Barbul, A., **2013**. Excessive nitric oxide impairs wound collagen accumulation. *J Surg Res* 183, 487–492.

Patel, P., Schmieder, S., Krishnamurthy, K., **2016**. Research techniques made simple: drug delivery techniques, part 2: commonly used techniques to assess topical drug bioavailability. *J Invest Dermatol* 136, 43-49.

Patzelt, A., Cheung Mak, W., Jung, S., Knorr, F., Meinke, M.C., Richter, H., Rühl, E., Yee Cheung, K., Tran, N.B.N.N., Lademann, J., **2017**. Do nanoparticles have a future in dermal drug delivery? *J Control Release* 246, 174-182.

Pavelić, Ž., Škalko-Basnet, N., Schubert, R., **2001**. Liposomal gels for vaginal drug delivery. *Int J Pharm* 219, 139-149.

Perinelli, D.R., Fagioli, L., Campana, R., Lam, J.K.W., Baffone, W., Palmieri, G.F., Casettari, L., Bonacucina, G., **2018**. Chitosan-based nanosystems and their exploited antimicrobial activity. *Eur J Pharm Sci* 117, 8-20.

Pitorre, M., Gondé, H., Haury, C., Messous, M., Poilane, J., Boudaud, D., Kanber, E., Rossemond Ndombina, G.A., Benoit, J-P., Bastiat, G., **2017**. Recent advances in nanocarrier-loaded gels: Which drug delivery technologies against which diseases? *J Control Release* 266, 140-155.

Pittman, J.L., Schrum, K.F., Gilman, S.D., **2001**. On-line monitoring of electroosmotic flow for capillary electrophoretic separations. *Analyst* 126, 1240-1247.

Planz, V., Lehr, C-M., Windbergs, M., **2016**. *In vitro* models for evaluating safety and efficacy of novel technologies for skin drug delivery. *J Control Release* 242, 89-104.

Pleguezuelos-Villa, M., Mir-Palomo, S., Díez-Sales, O., Vila Buso, M.A.O., Ruiz Sauri, A., Nácher, A., **2018**. A novel ultradeformable liposomes of Naringin for anti-inflammatory therapy. *Colloids Surf B Biointerfaces* 162, 265-270.

Prow, T.W., Grice, J.E., Lin, L.L., Faye, R., Butler, M., Becker, W., Wurm, E.M.T., Yoong, C., Robertson, T.A., Soyer, H.P., Roberts, M.S., **2011**. Nanoparticles and microparticles for skin drug delivery. *Adv Drug Deliv Rev* 63, 470-491.

Puglia, C., Bonina, F., **2012**. Lipid nanoparticles as novel delivery systems for cosmetics and dermal pharmaceuticals. *Exp Opin Dru Deliv* 9, 429-441.

Puglia, C., Esposito, E., Menegatti, E., Nastruzzi, C., Rizza, L., Cortesi, R., Bonina, F., **2005**. Effect of charge and lipid concentration on *in-vivo* percutaneous absorption of methyl nicotinate from liposomal vesicles. *J Pharm Pharmacol* 57, 1169-1176.

Ribeiro, M.P., Espiga, A., Silva, D., Baptista, P., Henriques, J., Ferreira, C., Silva, J.C., Borges, J.P., Pires, E., Chaves, P., Correia, I.J., **2009**. Development of a new chitosan hydrogel for wound dressing. *Wound Repair Regen* 17, 817-824.

Riviere, J.E., Bowman, K.F., Monteiro-Riviere, N.A., Dix, L.P., Carver, M.P., **1986**. The isolated perfused porcine skin flap (IPPSF). I. A novel *in vitro* model for percutaneous absorption and cutaneous toxicology studies. *Fund Appl Toxicol* 7, 444-453.

Roberts, M.S., Mohammed, Y., Pastore, M.N., Namjoshi, S., Yousef, S., Alinaghi, A., Haridass, I.N., Abd, E., Leite-Silva, V.R., Benson, H.A.E., Grice, J.E., **2017**. Topical and cutaneous delivery using nanosystems. *J Control Release* 247, 86-105.

Ruel-Gariepy, E., Leclair, G., Hildgen, P., Gupta, A., Leroux, J.C., **2002**. Thermosensitive chitosan-based hydrogel containing liposomes for the delivery of hydrophilic molecules. *J Control Release* 82, 373–383.

Saghazadeh, S., Rinoldi, C., Schot, M., Kashaf, S.S., Sharifi, F., Jalilian, E., Nuutila, K., Giatsidis, G., Mostafalu, P., Derakhshandeh, H., Yue, K., Swieszkowski, W., Memic, A., Tamayol, A., Khademhosseini, A., **2018**. Drug delivery systems and materials for wound healing applications. *Adv Drug Deliv Rev* 127, 138-166.

Sala, M., Diab, R., Elaissari, A., Fessi, H., **2018**. Lipid nanocarriers as skin drug delivery systems: Properties, mechanisms of skin interactions and medical applications. *Int J Pharm* 535, 1-17.

Saraceno, R., Chiricozzi, A., Gabellini, M., Chimenti, S., **2013**. Emerging applications of nanomedicine in dermatology. *Skin Res Technol* 19, 13-19.

Schaefer, U.F., Hansen, S., Schneider, M., Luengo Contreras, J., Lehr, C.M., **2008**. Models for skin absorption and skin toxicity testing, in: Kim, K., Ehrhardt, K.J. (Eds.), *Drug Absorption Studies: In Situ, in Vitro and in Silico Models*. Springer, New York, 3–33.

Schäfer-Korting, M., Mehnert, W., Korting, H-C., **2007**. Lipid nanoparticles for improved topical application of drugs for skin diseases. *Adv Drug Deliv Rev* 59, 427-443.

Schmieder, S., Patel, P., Krishnamurthy, K., **2015**. Research techniques made simple: drug delivery techniques, part 1: concepts in transepidermal penetration and absorption. *J Invest Dermatol* 135, 1-5.

Selzer, D., Abdel-Mottaleb, M.M.A., Hahn, T., Schaefer, U.F., Neumann, D., **2013**. Finite and infinite dosing: Difficulties in measurements, evaluations and predictions. *Adv Drug Deliv Rev* 65, 278-294.

Shah, V.P., Yacobi, A., Rădulescu, F.Ş., Miron, D.S., Lane, M.E., **2015**. A science based approach to topical drug classification system (TCS). *Int J Pharm* 491, 21-25.

Siddiqui, A.R., Bernstein, J.M., **2010**. Chronic wound infection: facts and controversies, *Clin Dermatol* 28, 519-526.

Silva Garcia Praça, F., Silva Garcia Medina, W., Eloy, J.O., Petrilli, R., Mazureki Camposa, P., Ascenso, A., Bentley, M.V.L.B., **2018**. Evaluation of critical parameters for *in vitro* skin permeation and penetration studies using animal skin models. *Eur J Pharm Sci* 111, 121-132.

Simões, D., Miguel, S.P., Ribeiro, M.P., Coutinho, P., Mendonça, A.G., Correia, I.J., **2018**. Recent advances on antimicrobial wound dressing: a review. *Eur J Pharm Biopharm* 127, 130-141.

Sintov, A.C., **2017**. Cumulative evidence of the low reliability of frozen/thawed pig skin as a model for *in vitro* percutaneous permeation testing. *Eur J Pharm Sci* 102, 261-263.

Škalko-Basnet, N., **2014**. Biologics: the role of delivery systems in improved therapy. *Biologics: Targets and Therapy* 8, 107-114.

Sohrabi, S., Haeri, A., Mahboubi, A., Mortazavi, A., Dadashzadeh, S., **2016**. Chitosan gel-embedded moxifloxacin niosomes: An efficient antimicrobial hybrid system for burn infection. *Int J Biol Macromol* 85, 625-633.

Tahara, K., Kobayashi, M., Yoshida, S., Onodera, R., Inoue, N., Takeuchi, H., **2018**. Effects of cationic liposomes with stearylamine against virus infection. *Int J Pharm* 543, 311-317.

Ternullo, S., de Weerd, L., Flaten, G.E., Holsæter, A.M., Škalko-Basnet, N., **2017**. The isolated perfused human skin flap model: A missing link in skin penetration studies? *Eur J Pharm Sci* 96, 334-341.

Tran, T-N.T., **2013**. Cutaneous drug delivery: An update. *J Investig Dermatol Symp Proc* 16, 67-69.

Uchino, T., Lefeber, F., Gooris, G., Bouwstra, J., **2014**. Characterization and skin permeation of ketoprofen-loaded vesicular systems. *Eur J Pharm Biopharm* 86, 156-166.

Van Gele, M., Geusens, B., Brochez, L., Speeckaert, R., Lambert, J., **2011**. Three-dimensional skin models as tools for transdermal drug delivery: challenges and limitations. *Exp Opin Drug Deliv* 8, 705-720.

van Kuijk-Meuwissen, M.E., Junginger, H.E., Bouwstra J.A., **1998**. Interactions between liposomes and human skin *in vitro*, a confocal laser scanning microscopy study. *Biochim Biophys Acta* 1371, 31-39.

van Smeden, J., Janssens, M., Gooris, G.S., Bouwstra, J.A., **2014**. The important role of s*tratum corneum* lipids for the cutaneous barrier function. *Biochim Biophys Acta* 1841, 295-313.

Vanić, Ž., **2015**. Phospholipid vesicles for enhanced drug delivery in dermatology. *J Drug Discov Develop and Deliv* 2, 1010.

Vanić, Ž., Holsæter, A.M., Škalko-Basnet, N., **2015**. (Phospho)lipid-based nanosystems for skin administration. *Curr Pharm Des* 21, 4174-4192.

Vanić, Ž., Hurler, J., Ferderber, K., Golja Gašparović, P., Škalko-Basnet, N., Filipović-Grčić, J., **2014**. Novel vaginal drug delivery system: deformable propylene glycol liposomes-in-hydrogel. *J Liposome Res* 24, 27-36.

Verlee, A., Mincke, S., Stevens, C.V., **2017**. Recent developments in antibacterial and antifungal chitosan and its derivates. *Carbohydr Polym* 164, 268-283.

Verma, D.D., Verma, S., Blume, G., Fahr, A., **2003**. Particle size of liposomes influences dermal delivery of substances into skin. *Int J Pharm* 258, 141-151.

Vogt, A., Wischke, C., Neffe, A.T., Ma, N., Alexiev, U., Lendlein, A., **2016**. Nanocarriers for drug delivery into and through the skin – Do existing technologies match clinical challenges? *J Control Release* 242, 3-15.

Wagner, S.M., Nogueira, A.C., Paul, M., Heydeck, D., Klug, S., Christ, B., **2003**. The isolated normothermic hemoperfused porcine forelimb as a test system for transdermal absorption studies. *J Artif Organs* 6, 183-191.

Watkinson, R.M., Guy, R.H., Hadgraft, J., Lane, M.E., **2009**. Optimisation of cosolvent concentration for topical drug delivery – II: influence of propylene glycol on ibuprofen permeation. *Skin Pharmacol Physiol* 22, 225-230.

Werner, S., Krieg, T., Smola, H., **2007**. Keratinocyte–fibroblast interactions in wound healing. *J Investig Dermatol* 127, 998-1008.

Wester, R.C., Melendres, J., Sedik, L., Maibach, H., Riviere, J.E., **1998**. Percutaneous absorption of salicylic acid, theophylline, 2, 4-dimethylamine, diethyl hexyl phthalic acid, and *p*-aminobenzoic acid in the isolated perfused porcine skin flap compared to man *in vivo*. *Toxicol Appl Pharmacol* 151, 159-165.

Wiedersberg, S., Guy, R.H., **2014**. Transdermal drug delivery: 30+ years of war and still fighting! *J Control Release* 190, 150-156.

Xue, M., Zhao, R., Lin, H., Jackson, C., **2018**. Delivery systems of current biologicals for the treatment of chronic cutaneous wounds and severe burns. *Adv Drug Deliv Rev* 129, 219-241.

Zeng, F., Harris, R.C., **2014**. Epidermal growth factor, from gene organization to bedside. *Semin Cell Dev Biol* 28, 2-11.

Zhao, Y-Z., Lu, C-T., Zhang, Y., Xiao, J., Zhao, Y-P., Tian, J-L., Xu, Y-Y., Feng, Z-G., Xu, C-Y., **2013**. Selection of high efficient transdermal lipid vesicle for curcumin skin delivery. *Int J Pharm* 454, 302-309.

Zhou, J., Yao, D., Qian, Z., Hou, S., Li, L., Jenkins, A.T.A., Fan, Y., **2018**. Bacteria-responsive intelligent wound dressing: Simultaneous *In situ* detection and inhibition of bacterial infection for accelerated wound healing. *Biomaterials* 161, 11-23.

Paper I

European Journal of Pharmaceutical Sciences 96 (2017) 334–341

Contents lists available at ScienceDirect

European Journal of Pharmaceutical Sciences

journal homepage: www.elsevier.com/locate/ejps

The isolated perfused human skin flap model: A missing link in skin penetration studies?

Selenia Ternullo [a], Louis de Weerd [b,c], Gøril Eide Flaten [a], Ann Mari Holsæter [a], Nataša Škalko-Basnet [a,*]

[a] Drug Transport and Delivery Research Group, Department of Pharmacy, University of Tromsø The Arctic University of Norway, Universitetsveien 57, 9037 Tromsø, Norway
[b] Department of Plastic and Reconstructive Surgery, University Hospital of North Norway, Sykehusvegen 38, 9019 Tromsø., Norway
[c] Department of Clinical Medicine, University of Tromsø The Arctic University of Norway, Universitetsveien 57, 9037 Tromsø, Norway

ARTICLE INFO

Article history:
Received 9 June 2016
Received in revised form 3 September 2016
Accepted 3 October 2016
Available online 05 October 2016

Keywords:
Human skin
Skin therapy
Skin models
Skin penetration
Isolated perfused human flap

ABSTRACT

Development of effective (trans)dermal drug delivery systems requires reliable skin models to evaluate skin drug penetration. The isolated perfused human skin flap remains metabolically active tissue for up to 6 h during *in vitro* perfusion. We introduce the isolated perfused human skin flap as a close-to-*in vivo* skin penetration model. To validate the model's ability to evaluate skin drug penetration the solutions of a hydrophilic (calcein) and a lipophilic (rhodamine) fluorescence marker were applied. The skin flaps were perfused with modified Krebs-Henseleit buffer (pH 7.4). Infrared technology was used to monitor perfusion and to select a well-perfused skin area for administration of the markers. Flap perfusion and physiological parameters were maintained constant during the 6 h experiments and the amount of markers in the perfusate was determined. Calcein was detected in the perfusate, whereas rhodamine was not detectable. Confocal images of skin cross-sections shoved that calcein was uniformly distributed through the skin, whereas rhodamine accumulated in the *stratum corneum*. For comparison, the penetration of both markers was evaluated on *ex vivo* human skin, pig skin and cellophane membrane. The proposed perfused flap model enabled us to distinguish between the penetrations of the two markers and could be a promising close-to-*in vivo* tool in skin penetration studies and optimization of formulations destined for skin administration.

1. Introduction

(Trans)dermal delivery of drugs and cosmeceuticals has gained increasing interest in pharmaceutical and cosmetic fields. The skin represents an attractive route of drug delivery for both local and systemic effects. In this context, investigating the drug penetration into/through the skin is of fundamental importance regarding both the desired drug's therapeutic efficacy and its potential toxicity (DeLouise, 2012; Prow et al., 2011). Skin, especially the *stratum corneum* (SC) layer, exhibits very efficient barrier properties which limit drug penetration into/through the skin and needs to be overcome for successful trans(dermal) delivery (Bouwstra et al., 2003; Lane, 2013).

Therefore, reliable skin models able to predict and evaluate the (desired or undesired) penetration of molecules/nanosystems *in vivo* and serve as a tool in optimization of topical formulations are required (Flaten et al., 2015). *In vivo* studies, especially in humans, are the golden standard tool in skin penetration studies. However, in the early stages of drug development, *in vivo* studies are restricted due to ethical and economical concerns (Parra et al., 2016). Moreover, new regulations limit the use of animals for *in vivo* studies in the initial stages of product development (Flaten et al., 2015). Therefore, *in vitro* and *ex vivo* techniques are gaining more interest as tools to study skin penetration (Patel et al., 2016).

The skin perfusion models comprise a surgically prepared portion of skin (flap) including subcutaneous fatty tissue with assured continuous vascular circulation. These models offer the benefits of living metabolically-active tissue and are considered the missing link between *in vitro* and *in vivo* methods (Schaefer et al., 2008). These models overcome some of the limitations of the *in vitro* studies using human or animal skin, such as the use of only epidermis and the upper part of the dermis and the lack of a dermal vascular system (de Lange et al., 1992; Patel et al., 2016). Several animal specimens have been used for the skin perfusion model, such as the isolated perfused pig skin flap (Riviere et al., 1986), the isolated blood-perfused pig ear (de Lange et al., 1992), the isolated perfused bovine udder (Kietzmann et al., 1993) and the pig

Abbreviations: CM, Cellophane membrane; CLSM, confocal laser scanning microscopy; DIRT, dynamic infrared thermography; FDC, Franz diffusion cells; HS, human skin; IR, infra red; IPHSF, isolated perfused human skin flap; KHb, modified Krebs-Henseleit buffer; PS, pig skin; PG, propylene glycol; SC, *stratum corneum*.

* Corresponding author at: Nataša Škalko-Basnet, Drug Transport and Delivery Research Group, Department of Pharmacy, University of Tromsø The Arctic University of Norway, Universitetsveien 57, 9037 Tromsø, Norway.
E-mail addresses: selenia.ternullo@uit.no (S. Ternullo), Louis.De.Weerd@unn.no (L. de Weerd), goril.flaten@uit.no (G.E. Flaten), ann-mari.holsater@uit.no (A.M. Holsæter), natasa.skalko-basnet@uit.no (N. Škalko-Basnet).

http://dx.doi.org/10.1016/j.ejps.2016.10.003
0928-0987/

forelimb (Wagner et al., 2003). Pig skin is considered the most suitable animal model to mimic human skin. Therefore, pig skin flap has been widely studied as skin perfusion model and skin penetration of different substances has been investigated using the isolated perfused pig skin flap model (Carver et al., 1989, 1990; Williams et al., 1990; Wester et al., 1998; Inman et al., 2003).

However, use of animal skin retains the limitations of correlations between animal and human skin. Kreidstein et al. (1991) designed the isolated perfused human skin flap model using transverse paraumbilical skin flap. This tissue is normally discarded in abdominal dermolipectomy (Kreidstein et al., 1991). Several techniques have confirmed the perfusion of the flap (Black et al., 2001; Kreidstein et al., 1995; Lipa et al., 1999; Miland et al., 2008). Miland et al. (2008) confirmed the suitability of the dynamic infrared thermography (DIRT) to monitor skin flap perfusion and to differentiate between well and less perfused areas.

To the best of our knowledge, the isolated perfused human skin flap (IPHSF) has not been used to study (trans)dermal penetration. Such a model could be a valuable tool in skin penetration studies and in optimization of dosage forms/delivery systems for skin therapy.

This study evaluated the feasibility of the IPHSF as a skin penetration model. To validate the IPHSF model, two fluorescent markers, a hydrophilic (calcein) and a lipophilic (rhodamine), were used and their penetration investigated over a 6 h period. Confocal laser scanner microscopy (CLSM) technique was used to follow the fluorescent markers penetration through the IPHSF. These data were compared with the *ex vivo* (human and pig skin) and *in vitro* (cellophane membrane) penetration studies in Franz diffusion cells (FDC).

2. Material and methods

2.1. Material

Calcein, rhodamine B, sodium chloride, potassium chloride, magnesium sulfate, sodium bicarbonate, trichloroacetic acid (≥99.0%), ethanol (96%, *v*/v) and Triton™ X-100 were from Sigma-Aldrich Chemie (Steinheim, Germany); human serum albumin (30 mg/mL) from Octapharma AG (Lachen, Switzerland); propylene glycol (PG) from NMD – Norwegian Medical Depot AS (Oslo, Norway) and glucose, calcium chloride and potassium dihydrogen phosphate from Merck KGaA (Darmstadt, Germany). Sucrose was product of VWR International bvba/sprl (Leuven, Belgium). Pig ears were purchased from Nurtura AS (Bardufoss, Norway).

2.2. Human skin flap

Eight human skin flaps were used in this study and were obtained from the abdomen of female patients (mean age 49.5 years, range 40–66 years) who underwent abdominoplasty (Table 1). All patients gave their written consent prior to the surgery and the experiments were performed according to the Declaration of Helsinki Principles. Since these skin panni are normally disposed of by incineration, no ethical approval for their use was required according to Norwegian Ethical Committee. The procurement and disposal of human skin flaps were in accordance with the policy of the University Hospital of North Norway, Tromsø.

2.3. Preliminary perfusion experiment

A modification of the perfusion design of the model described by Miland et al. (2008) was used. The human skin flap, after its excision, was wrapped in gauze soaked with physiological solution and placed in a sealed plastic box to maintain it at room temperature until it was transferred in the laboratory where the flap experiments were performed. To perfuse the human skin flap, it was placed on a metal grid and one vessel was selected and cannulated with an arteriotomy cannula (diameter 1 mm; DLP® Metronic Inc., Minneapolis, USA), which was then connected to the perfusion apparatus (Fig. 1). The cannulation was performed at room temperature. The perfusate was modified Krebs-Henseleit buffer (KHb) comprising (in mM): 110 NaCl, 3.8 KCl, 1.4 KH2PO4, 1.2 MgSO4, 31 NaHCO3, 2.5 CaCl2, 11 glucose and 10 sucrose. Human serum albumin (30 mg/mL) was added to the perfusate. The perfusate had a pH of 7.4 and an osmolarity of 290 mOsm mimicking the physiological conditions.

The perfusion flow rate (6–8 mL/min) was monitored using a drop counter and the pressure by inline pressure transducer (Transpac® IV; Abbott Laboratories, North Chicago, IL, USA).

All perfusions were initiated within 90 min after the excision of skin panni (Miland et al., 2008).

2.4. Validation of the IPHSF model

Preliminary calcein skin penetration experiments through the IPHSF were performed to validate the experimental setups and the analytical method of the quantification of penetrated marker in the perfusate. Calcein solution (10 mM) in KHb was applied onto the perfused skin flap (Fig. 1). The skin diffusion area (49 cm^2) exhibiting best perfusion (skin temperature of *ca.* 32 °C) was measured with an IR camera (FLIR ThermaCAM S65 HS, FLIR Systems). An adhesive patch constituted the donor chamber and calcein solution (7 mL) was applied onto the selected well-perfused skin area using a syringe. The experiment was carried out for 6 h when no leakage of the solution was observed. The weight of the flap was determined before and after the perfusion period. The penetrated calcein was assessed spectrofluorometrically in the perfusate collected after 6 h from a metal container placed under the flap. To assure that no inherent fluorescent skin constituents were detected, the perfusate was also collected when calcein solution was applied (time 0). Moreover, the non-penetrated calcein (retained on the flap surface) was swept and quantified at the end of experiment.

Table 1
Characteristics of human skin flaps.

Flap number	Age (years)	Weight (g)	Thickness (cm)	Type of experiment
0a	51	–[a]	–[a]	Preliminary perfusion test
0b	42	1110	–[a]	Preliminary skin penetration experiment (calcein)
1	47	443	1.90	Skin penetration experiment (calcein)
2	41	526	1.63	Skin penetration experiment (calcein)
3	54	603	1.26	Skin penetration experiment (calcein)
4	40	1187	0.90	Skin penetration experiment (rhodamine)
5	57	1570	1.68	Skin penetration experiment (rhodamine)
6	66	525	0.93	Skin penetration experiment (rhodamine)
7	42	–	0.23[b]	*Ex vivo* skin penetration experiment in FDC (calcein)
8	42	–	0.17[b]	*Ex vivo* skin penetration experiment in FDC (rhodamine)

[a] Weight and thickness of the flaps were not determined in the preliminary study used to validate the experimental design of the perfusion technique and experimental set up.
[b] Thickness (cm) refers to the full skin obtained from the human skin flap. Weight was not determined since not relevant for *ex vivo* study.

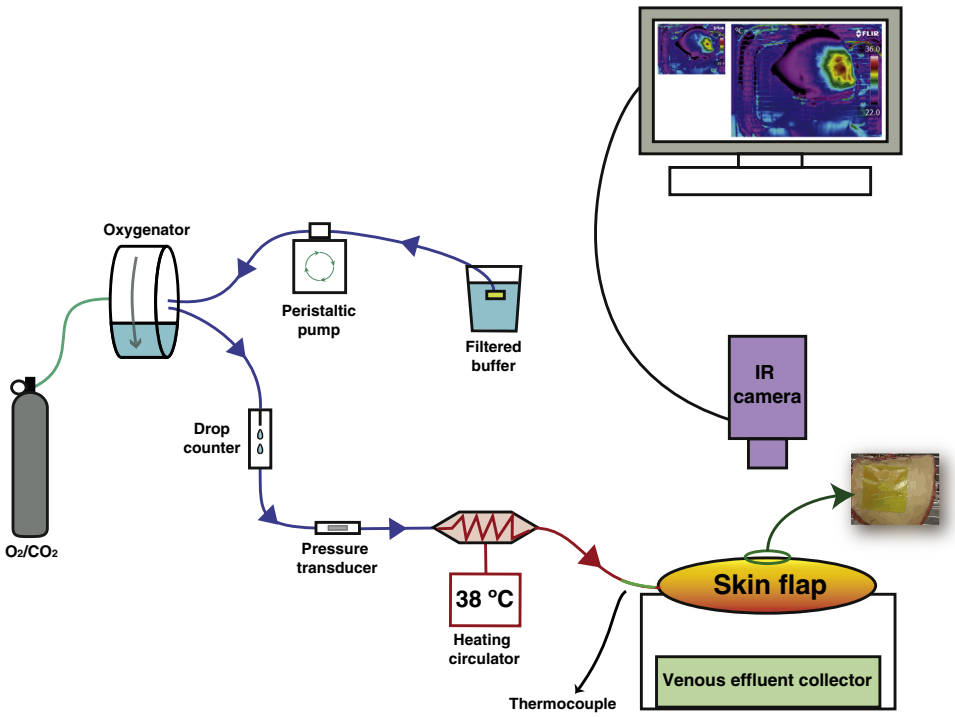

Fig. 1. Flap perfusion design. The perfusate was filtered and gassed with 95% O_2/5% CO_2 using a rotating surface oxygenator. The perfusion flow rate (6–8 mL/min) was monitored using a drop counter and the perfusion pressure measured with an inline pressure transducer. A heating circulator was set at 38 °C and a thermocouple inserted in the cannula to monitor the temperature of the perfusate entering the flap. The IR camera monitored the skin surface temperature throughout the perfusion period. The flow, pressure and temperature of the perfusate were monitored on-line using PhysAcq software. The perfusate from IPHSF was collected using a metal container.

2.4.1. Quantification of calcein in the perfusate

The analytical method used to detect and quantify calcein in the perfusate was based on Bahia et al. (2010) with modifications. The collected perfusate was centrifuged to remove blood cells (1914 *g*, 20 min). To assure that no calcein precipitated with the blood cells the pellets were firstly washed with KHb (10 mL) and secondly dissolved in Triton solution 5% (*w*/*v*; 10 mL). Trichloroacetic acid (58.82%, *w*/*v*) was used to precipitate plasma protein. Calcein concentrations in the supernatants, pellets washed after blood cells precipitation and pellets dissolved in Triton solution were determined spectrofluorometrically (excitation and emission wavelengths at 485 and 520 nm, respectively) on a Polarstar fluorimeter (Fluostar; BMG Technologies, Offenburg, Germany) using a multiplate reader (COSTAR 96). Three parallels were determined for each sample. Eq. (1) (derived from the Fick's first law) was used to calculate the apparent permeability coefficient (P_{app}) where J is the observed flux rate (μg/cm^2/s) and C_d is the concentration of calcein solution in the patch (μg/mL). The flux was calculated from the linear part of the curve, representing the steady-state condition.

$$P_{app}\ (cm/s) = J/C_d \quad (1)$$

2.5. Skin penetration experiments on IPHSF model

Calcein (10 mM) in KHb and rhodamine (10 mM) in KHb/PG (0.5%, *v*/*v*) were applied onto the skin flaps perfused with KHb (Fig. 1). The weight and thickness of each flap were determined before and at the end of the experiment. The perfusate was collected at time 0 and every hour for a period of 6 h and sink conditions were maintained. The penetrated and non-penetrated markers were quantified as described in the methods for validation of the IPHSF model.

2.6. Confocal laser scanning microscopy (CLSM)

CLSM analysis was performed on a Leica TCS SP5 microscope (Leica Microsystems CMS GmbH, Mannheim, Germany) equipped with an Argon laser. The samples were prepared using the imprint method (Brommeland et al., 2003). A cross-sectioned slide of the flap was cut by a scalpel and attached onto a microscope slide. The cells remaining on the slide were fixed in formalin (SPRAYFIX®, Histolab Products AB, Gothenburg, Sweden). The flap areas used in CLSM are shown in Fig. 2a. Calcein and rhodamine were excited using 488 and 568 nm laser lines, respectively. Fluorescence was detected using the following spectral range: 500–550 nm for calcein, 570–610 nm for rhodamine. When required, images were acquired in *Z*-sections of 1 to 100 μm thickness and were superimposed.

2.7. Ex vivo and in vitro skin penetration experiments

Ex vivo and *in vitro* skin penetration experiments were carried out on Franz diffusion cells (FDC; PermeGear, Bethlehem, USA) of 1.77 cm^2 diffusion area and with 12 mL receiver volume (Hurler et al., 2012). *Ex vivo* skin penetration experiments were performed using human skin (HS) and pig ear skin (PS). Human skin (HS) was obtained from human skin flaps, which were not the same as the flaps used in skin penetration experiments on IPHSF model (Table 1). Cellophane membrane (CM; Max Bringmann KG, Wendelstein, Germany) was employed in *in vitro* experiments. The same solutions of the fluorescent markers tested in the IPHSF were added into the donor chamber (600 μL). The receiver chamber was filled with KHb. Samples (500 μL) were collected at 1, 2, 4 and 6 h and replaced by fresh acceptor medium to maintain sink conditions. All experiments were carried out at 32 °C. Calcein and rhodamine concentrations were determined spectrofluorometrically. Eq. (1) was used to calculate the P_{app}.

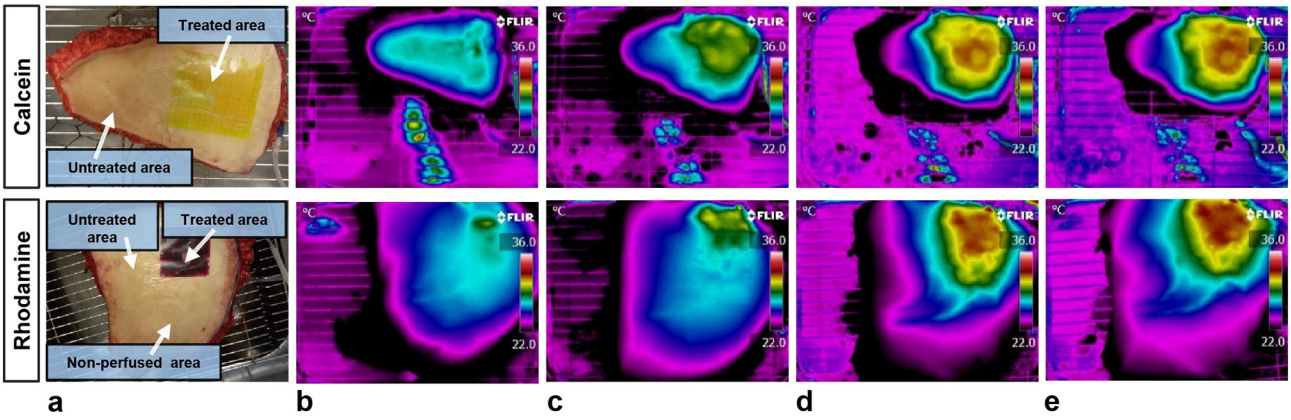

Fig. 2. Photographs and DIRT images of representative flaps in skin penetration experiments. The a represents the photographs of flaps. The b are DIRT images recorded 1 min after the start of the perfusion (skin temperature below 32 °C). The c, d and e are DIRT images recorded at time 0, 3 and 6 h after the application of the markers, respectively (skin temperature at *ca.* 32 °C).

2.8. Statistical evaluation

The Student's *t*-test was used for the comparison of two means. A significance level of $p < 0.05$ was considered significant.

3. Results

Any model destined for application in the development and optimization of skin formulations needs to be validated to confirm its robustness and wider applicability.

3.1. Validation of IPHSF model

Table 1 provides an overview of the characteristics of the flaps used in experiments. The perfusion experimental set up of Miland et al. (2008) was modified to identify the areas of the flap with skin temperature of at least 32 °C corresponding to adequate perfusion (Fig. 1). This enabled us to establish the area (49 cm^2) of well-perfused skin surface suitable to apply fluorescent markers. Once the area was selected, we focused on optimizing the volume (mL) of the marker solution to be applied. Calcein solution (7 mL) was injected into an adhesive patch (donor chamber) attached to the selected well-perfused skin area and penetration studies performed to further validate the model and confirmed its applicability.

The IPHSF was further validated in respect to possible oedema formation and the weight changes. Variation of <10% in the weight observed during 6 h of perfusion was found acceptable (data not shown).

Calcein was detected in the perfusate. Moreover, in the perfusate collected at time 0 no fluorescence was detected, indicating that no inherent fluorescent skin constituents were present in the perfusate and could be detected spectrofluorometrically.

3.2. Assuring perfusion during the skin penetration studies

Physiological parameters were monitored throughout the experiment. The flow, perfusion pressure and inlet temperature were kept constant during 6 h (Table 2).

All areas where the markers were applied were well perfused throughout the experiment and no leakage of markers from the donor chambers were observed (Fig. 2a). DIRT images, taken 1 min after the start of the perfusion, showed a hot spot indicating where the skin perfusion started (Fig. 2b). A distinct area of rewarming appeared corresponding to the perfusion area of the cannulated vessel. DIRT images were also taken before and after the application of markers (Fig. 2c) and confirmed well-perfused skin in areas where the markers were applied throughout the experiment (Fig. 2d, e).

3.3. Penetration of fluorescent markers in IPHSF model

DIRT images of flap areas where markers were applied showed that the area was still perfused after 6 h. Interestingly, DIRT images of flap areas next to where rhodamine was applied showed also the less well-perfused area (skin surface temperature lower than 32 °C) (Fig. 2e). To further investigate this area, a cross-section of the area was analyzed by CLSM. CLSM images of the marker-free skin area showed no presence of both markers, as expected (Fig. 3a). CLSM images of calcein (green) in the perfused-treated area indicated a uniformly distributed fluorescence through the skin flap, while rhodamine (red) exhibited a bright fluorescence in the SC but decreasing fluorescence in the viable epidermis and subcutaneous fat tissue (Fig. 3b). CLSM images of both markers in the well-perfused-untreated area indicated a weaker fluorescence as compared to the treated area (Fig. 3c). In the less well-perfused areas we could only detect a weak fluorescence of rhodamine (Fig. 3d).

CLSM images confirmed the skin penetration profiles of the two markers in the IPHSF model.

Table 2
Characteristics and physiological parameters of IPHSF recorded during 6 h of experiment (mean ± SD).

Flap	Flow (mL/min)	Perfusion inlet pressure (mm Hg)	Inlet temperature (°C)	Weight variation (%)[a]	Thickness variation (%)[a]
1	5.96 ± 0.02	311.95 ± 46.37	35.69 ± 0.18	+ 8.58	− 13.16
2	6.06 ± 0.18	305.88 ± 50.29	35.43 ± 0.19	+ 5.70	− 1.23
3	6.59 ± 0.06	307.84 ± 63.70	35.93 ± 0.18	+ 8.79	+ 2.38
4	7.00 ± 0.05	393.23 ± 36.60	36.90 ± 0.06	+ 6.40	+ 4.44
5	5.61 ± 1.12	325.90 ± 12.75	36.04 ± 0.13	+ 2.58	+ 2.38
6	6.46 ± 0.55	295.72 ± 11.82	36.33 ± 0.14	+ 7.81	+ 6.45

[a] Variation (%) calculated from weight and thickness measured before and after perfusion of flaps.

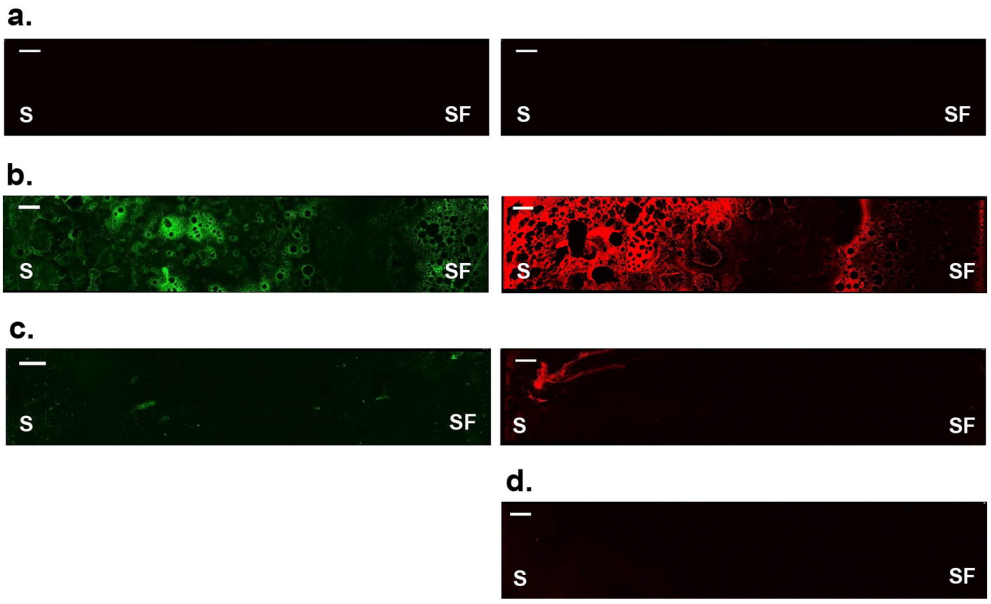

Fig. 3. Representative CLSM images of cross-sections of IPHSF at the end of skin penetration experiments. CLSM images of calcein (green fluorescence) in IPHSF are shown in the left column, while CLSM images of rhodamine (red fluorescence) are shown in the right column. The a represents the intact flap cut before the perfusion (control). The b is treated area; c untreated area. The d is a non-perfused area observed by DIRT in flap where rhodamine was applied. Cross-sectioned slides of IPHSF were cut starting from the skin surface (S; left side) to the subcutaneous fat (SF; right side). Scale bar represents 500 μm.

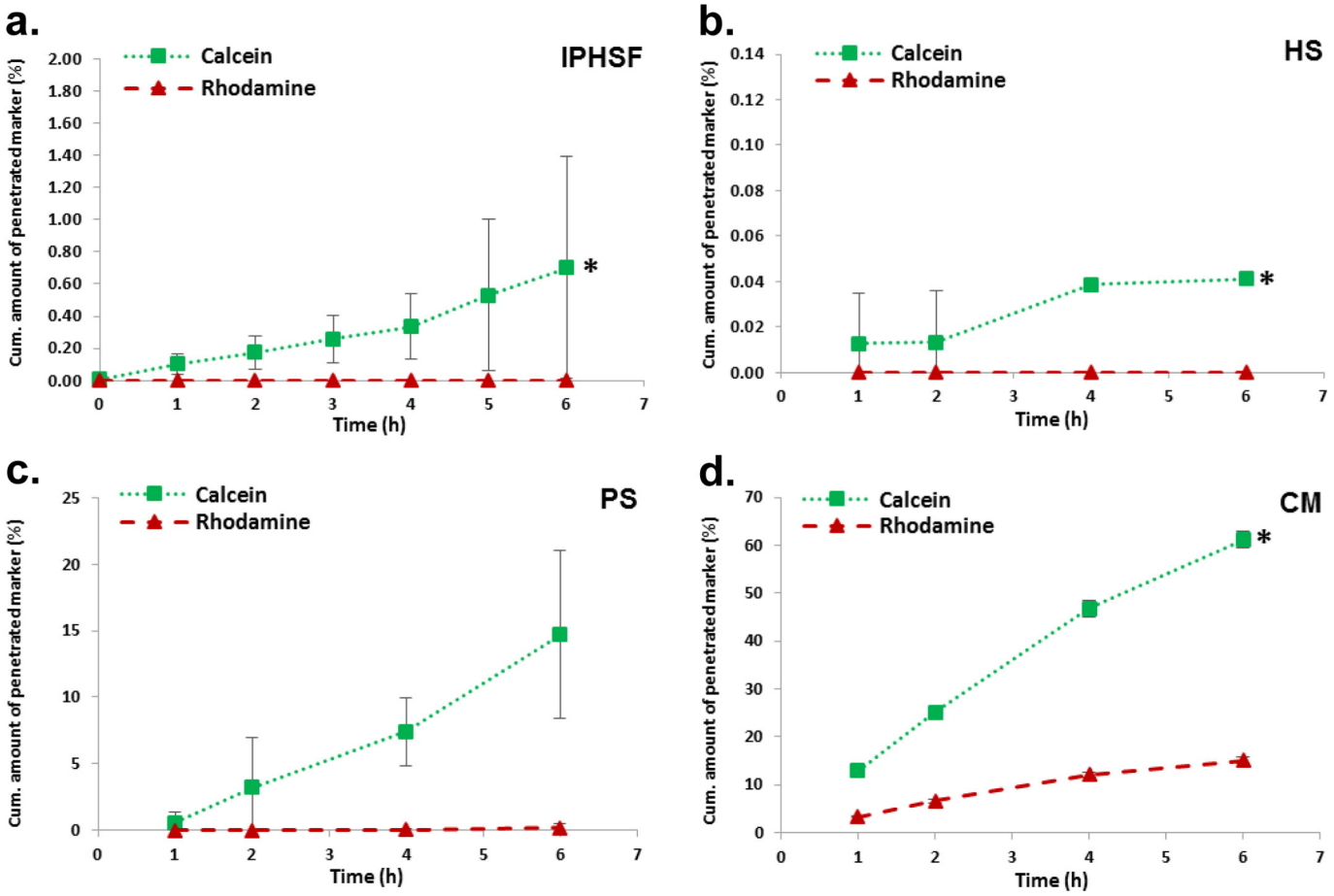

Fig. 4. Penetration profiles of calcein and rhodamine through IPHSF (a), HS (b), PS (c) and CM (d). The concentration of calcein in KHb and rhodamine in KHb/PG (0.5%, *v*/v) solutions was 10 mM. The penetration of both markers was investigated for a period of 6 h. All experiments were conducted in triplicates and the results are presented as mean ± SD. $^{*}p < 0.05$.

3.4. Correlation between the skin penetration in the IPHSF model and ex vivo and in vitro studies

Penetration of two markers through IPHSF model is presented in Fig. 4a. No fluorescence was detected in the perfusate at time 0, assuring that no inherent skin constituents were detected with our analytical method employed to quantify the penetrated markers in the perfusate. Calcein was detected in the perfusate, whereas rhodamine was not detectable. *Ex vivo* skin penetration studies using human skin revealed lower calcein penetration as compared to IPHSF ($p < 0.05$) (Fig. 4b). The same penetration profiles of rhodamine were observed both in the IPHSF and in *ex vivo* studies on human skin (Fig. 4a, b). More calcein and rhodamine penetrated through the pig skin and cellophane membrane compared to the *ex vivo* human skin and the IPHSF (Fig. 4c, d). Calcein exhibited higher flux and P_{app} than rhodamine; whereas the non-penetrated rhodamine was recovered to higher extent (Table 3).

4. Discussion

The organization of the lipid domains in the SC is considered the main contributor to the barrier property of the skin (Bouwstra et al., 2003; Schmieder et al., 2015). This barrier property of the skin can be seen as a synergy between the cooperation and interactions between SC macro- and micro-structure, bi- and three-dimensional supramolecular organization of the lipid matrix and composition of the SC (Baroli, 2010). However, dermal circulation is responsible for the clearance of the drug from the skin and should not be neglected (Lane, 2013). The introduction of nanocarriers has opened a means to improve penetration of drug into/through the skin. Nanoparticles are expected to enhance or limit the ingress and diffusion of drugs into/through the skin depending on their physicochemical properties, particularly size (Vanić et al., 2015).

Consequently, there is an increasing need to understand the penetration into/through the skin and the interaction between the carrier, drug and the skin not only to optimize the therapeutic applications, but also to minimize potential side effects (Bolzinger et al., 2012; DeLouise, 2012). However, reliable skin models able to predict and investigate desired or undesired penetration through the skin remain challenging. Human skin perfusion models offer the benefits of living tissue with active microcirculation, mimicking the application in human to a greater extent (Schaefer et al., 2008; Patel et al., 2016). Moreover, they provide a mean to study the effects of dermal vasculature on the systemic absorption. However, no human skin perfusion model has been used to assess the penetration of drugs/markers into the skin and as a tool in dermatological product development. Kreidstein et al. (1991) have shown that the human skin flap is metabolically and physiologically stable for at least 5 h of *in vitro* perfusion. We used DIRT to measure skin perfusion. A number of studies have shown a good correlation between skin temperature and skin perfusion. As such DIRT can provide us indirectly with information on skin perfusion and its dynamics (de Weerd et al., 2006, 2009).

The perfusion of IPHSF was performed using the established method by Miland et al. (2008) with modifications. To validate the model, preliminary skin penetration studies were performed on perfused skin flaps in order to establish the experimental design of skin penetration studies on IPHSF. In both preliminary and skin penetration studies, we observed the same dynamics of perfusion. This confirmed that experimental conditions remained constant throughout the experiments. Moreover, little variation (<10%) in the weight and thickness of all flaps during 6 h perfusion excluded oedema formation and assured a good tissue perfusion as reported earlier (Black et al., 2001; de Lange et al., 1992; Lipa et al., 1999). Similar to Miland et al. (2008) a perfusion flow rate between 6 and 8 ml/min was maintained during the experiments. The perfusion pressure was higher than 50 mmHg, which we attribute to the smaller cannula diameter and the different software used to monitor the baseline perfusion in our experiments as compared to Miland et al. (2008).

The IPHSF model was able to distinguish between the penetrations of two markers (0.7% calcein and 0% rhodamine). Calcein penetrated to a lower extent, as expected, since it is a hydrophilic marker with low log*P* (−5.02) (Gillet et al., 2011) with limited skin penetration potential (Bolzinger et al., 2012). Interestingly, calcein was detected in the perfusate, which would suggest that the circulation enabled its penetration. Rhodamine has a higher log*P* (1.95) (Anissimov et al., 2012) and due to its lipophilicity was prepared in solution containing PG (0.5%; *v*/v) as a solubilizing agent. Therefore, we expected that PG would act as a penetration enhancer (Lane, 2013). However, the concentration of PG used in our study was relatively low compared to the PG concentration used in other studies suggesting its role as penetration enhancer (Trottet et al., 2004; Watkinson et al., 2009). Similar penetration results were reported by Wester et al. (1998) and their studies on the isolated perfused pig skin flap model. Tested compounds with lower log*P* were detected in higher percentage in the perfusate compared to compounds with higher log*P*. Although we could not detect rhodamine in the perfusate, the amount of rhodamine retained at the administration site on the flap was less than calcein. This suggests that rhodamine remained within SC rather than penetrating deeper into epidermis, as expected (Bolzinger et al., 2012). The extracellular space in SC and stratum granulosum exhibits hydrophobic properties due to its lipid-rich composition, whereas the layers below the stratum granulosum represent hydrophilic environment due to desmosome-rich composition (Iwai et al., 2012; Schmieder et al., 2015). The IPHSF results were supported by the CLSM images of the cross-section of skin flaps. While calcein was found uniformly distributed throughout the flap, rhodamine exhibited a bright fluorescence in the SC but weaker fluorescence in the viable epidermis and subcutaneous fat tissue. Gillet et al. (2011) reported similar accumulation of rhodamine in the SC and negligent amount within the epidermis. The same penetration profile of rhodamine observed in the IPHSF model was seen in full human skin in FDC. Water present on the surface of skin might cause swelling of the polar head-group regions in the lipid bilayers, and hence disruption of the lipid domains, which could explain the higher fluxes of hydrophilic molecules such as calcein (Bolzinger et al., 2012). However, the percentage of penetrated calcein through full human skin in FDC was significantly lower ($p < 0.05$) than through the IPHSF model indicating that the perfusion might play an important role in the penetration of compounds through the skin, as recently suggested by Patel et al. (2016). For the hydrophilic marker calcein we observed a positive effect of perfusion on its

Table 3
In vitro and *ex vivo* penetration of calcein and rhodamine (mean ± SD).

	Calcein			Rhodamine		
Barrier type	Flux (10^{-3} μg/cm^2/s)	P_{app} (10^{-7} cm/s)	Non-penetrated amount[a] (%)	Flux (10^{-3} μg/cm^2/s)	P_{app} (10^{-7} cm/s)	Non-penetrated amount[a] (%)
IPHSF	0.27 ± 0.29	0.41 ± 0.40	69.74 ± 17.16	nd[b]	nd	45.11 ± 8.45
HS	0.06 ± 0.01	0.09 ± 0.02	86.60 ± 12.28	nd	nd	39.28 ± 9.16
PS	20.47 ± 6.53	25.92 ± 8.27	43.15 ± 16.41	0.15 ± 0.22	0.19 ± 0.27	4.12 ± 2.49
CM	67.67 ± 1.85	91.22 ± 2.49	28.49 ± 2.23	10.87 ± 0.40	22.11 ± 0.82	2.40 ± 0.38

[a] The amount retained at skin surface.
[b] nd, flux and P_{app} were not determined because no penetrated rhodamine was detected.

skin penetration, whereas for the lipophilic marker rhodamine the penetration profile was not influenced by the perfusion to a greater extent.

These results support considerations that *ex vivo* skin studies do not resemble the *in vivo* situations to a satisfactory extent. This is a clear advantage of the skin perfusion models, since these models investigate the drug penetration considering also the dermal perfusion (Schaefer et al., 2008). Wagner et al. (2002) also reported that hydrophobic flufenamic acid penetrated less through the human skin in FDC system than in *in vivo* studies. We confirmed that the perfusion played a role in the penetration of both markers by analyzing cross-section of perfused skin flap areas where the markers were not applied (as visible by DIRT images). CLSM images of these untreated perfused areas showed the presence of both markers in the skin and subcutaneous tissue of untreated areas confirming that perfusion affected the penetration. Such findings stress the importance of perfusion in a skin penetration model.

The results obtained with the IPHSF model were compared with the results obtained on the established skin models. Both penetration studies through the pig skin and cellophane membrane showed a higher penetration of the markers compared to their penetration through the IPHSF model and human skin in FDC system, strongly indicating the importance of having a model that contains human skin. Interestingly, calcein penetrated through pig skin more than rhodamine. Observed P_{app} of calcein across pig skin was similar as in an established *in vitro* model mimicking human SC lipid composition (Engesland et al., 2013). Rhodamine penetration through the pig skin, IPHSF model and human skin on FDC system was similar and as expected since it is known that pig skin mimics human skin better for the lipophilic penetrants (Dick and Scott, 1992). Penetration of both markers through cellophane membrane was significantly higher than in other models used in this study ($p < 0.05$); calcein penetrated more than rhodamine in agreement with Ansari et al. (2006) who tested the penetration of three drugs with different lipophilicity through human skin, cellophane and natural membranes. They found that penetration of water soluble diclofenac sodium through cellophane was higher than through all other membranes, while penetration of lipophilic erythromycin through cellophane was lower (Ansari et al., 2006).

Although different *in vitro* and *ex vivo* animal skin models help us to simplify the drug penetration, the results obtained from those models differ from the results obtained with IPHSF model suggesting the importance of this missing link in reaching the close-to-*in vivo* situation.

The limitation of this study is the relatively small number of experiments; therefore, the results should be interpreted within the context of this limitation. Moreover, the IPHSF model is metabolically active for 6 h and skin drug penetration studies on IPHSF model have to be performed within this time limit. Specific equipment, such as infrared camera, is needed to perform skin flap experiments as well as the help of selected professionals to cannulate the skin flap. Therefore, we are aware that the IPHSF model cannot be used as skin perfusion model in the early stages of drug development. However, the model might be used, after the fully validated methodologies have been employed, to study skin drug penetration in conditions closer to the *in vivo* human ones since the importance of perfusion and the use of human skin in skin penetration studies is clear.

The next step in full utilization of the proposed model is to evaluate the penetration of nanoparticles and nanoparticle-associated drugs.

5. Conclusions

We demonstrated that the isolated perfused human skin flap model can be used in the skin penetration studies since it provides constant experimental conditions and perfusion, assuring reproducible results. Moreover, the model proves the benefits of working with living tissue using a byproduct of surgery, and avoiding animal use. The model was able to distinguish between the penetrations of two markers and is a promising tool in optimization of formulations destined for skin administration.

Conflict of interest

The authors declare no conflicts of interest.

Acknowledgements

The authors acknowledge Dr. James Mercer for providing the laboratory space where the flap experiments were performed and useful advices. We are grateful to Randi Olsen for the professional technical support in confocal microscopy. This research did not receive any specific grant from funding agencies in the public, commercial or not-for-profit sectors.

References

Anissimov, Y.G., Zhao, X., Roberts, M.S., Zvyagin, A.V., 2012. Fluorescence recovery after photo-bleaching as a method to determine local diffusion coefficient in the stratum corneum. Int. J. Pharm. 435, 93–97.
Ansari, M., Kazemipour, M., Aklamli, M., 2006. The study of drug permeation through natural membranes. Int. J. Pharm. 327, 6–11.
Bahia, A.P.C.O., Azevedo, E.G., Ferreira, L.A.M., Frézard, F., 2010. New insights into the mode of action of ultradeformable vesicles using calcein as hydrophilic fluorescent marker. Eur. J. Pharm. Sci. 39, 90–96.
Baroli, B., 2010. Penetration of nanoparticles and nanomaterials in the skin: fiction or reality? J. Pharm. Sci. 99, 21–50.
Black, C.E., Huang, N., Neligan, P.C., Levine, R.H., Lipa, J.E., Lintlop, S., Forrest, C.R., Pang, C.Y., 2001. Effect of nicotine on vasoconstrictor and vasodilator responses in human skin vasculature. Am. J. Physiol. Regul. Integr. Comp. Physiol. 281, 1097–1104.
Bolzinger, M.A., Briançon, S., Pelletier, J., Chevalier, Y., 2012. Penetration of drugs through skin, a complex rate-controlling membrane. Curr. Opin. Colloid Interface Sci. 17, 156–165.
Bouwstra, J.A., Honeywell-Nguyen, P.L., Gooris, G.S., Ponec, M., 2003. Structure of the skin barrier and its modulation by vesicular formulations. Prog. Lipid Res. 42, 1–36.
Brommeland, T., Lindal, S., Straume, B., Dahl, I.L., Hennig, R., 2003. Does imprint cytology of brain tumours improve intraoperative diagnoses? Acta Neurol. Scand. 108, 153–156.
Carver, M.P., Williams, P.L., Riviere, J.E., 1989. The isolated perfused porcine skin flap. III. Percutaneous absorption pharmacokinetics of organophosphates, steroids, benzoic acid, and caffeine. Toxicol. Appl. Pharmacol. 97, 324–337.
Carver, M.P., Levi, P.E., Riviere, J.E., 1990. Parathion metabolism during percutaneous absorption in perfused porcine skin. Pestic. Biochem. Physiol. 38, 245–254.
de Lange, J., van Eck, P., Elliott, G.R., de Kort, W.L.A.M., Wolthuis, O.L., 1992. The isolated blood-perfused pig ear: an inexpensive and animal-saving model for skin penetration studies. J. Pharmacol. Toxicol. Methods 27, 71–77.
de Weerd, L., Mercer, J.B., Setså, L.B., 2006. Intraoperative dynamic infrared thermography and free-flap surgery. Ann. Plast. Surg. 57, 279–284.
de Weerd, L., Miland, Å.O., Mercer, J.B., 2009. Perfusion dynamics of free DIEP and SIEA flaps during the first postoperative week monitored with dynamic infrared thermography. Ann. Plast. Surg. 62, 42–47.
DeLouise, L.A., 2012. Applications of nanotechnology in dermatology. J. Invest. Dermatol. 132, 964–975.
Dick, I.P., Scott, R.C., 1992. Pig ear skin as an in-vitro model for human skin permeability. J. Pharm. Pharmacol. 44, 640–645.
Engesland, A., Skar, M., Hansen, T., Škalko-Basnet, N., Flaten, G.E., 2013. New applications of phospholipid vesicle-based permeation assay: permeation model mimicking skin barrier. J. Pharm. Sci. 102, 1588–1600.
Flaten, G.E., Palac, Z., Engesland, A., Filipović-Grčić, J., Vanić, Ž., Škalko-Basnet, N., 2015. In vitro skin models as a tool in optimization of drug formulation. Eur. J. Pharm. Sci. 75, 10–24.
Gillet, A., Lecomte, F., Hubert, P., Ducat, E., Evrard, B., Piel, G., 2011. Skin penetration behaviour of liposomes as a function of their composition. Eur. J. Pharm. Biopharm. 79, 43–53.
Hurler, J., Berg, O.A., Skar, M., Conradi, A.H., Johnsen, P.J., Škalko-Basnet, N., 2012. Improved burns therapy: liposomes-in-hydrogel delivery system for mupirocin. J. Pharm. Sci. 101, 3906–3915.
Inman, A.O., Still, K.R., Jederberg, W.W., Carpenter, R.L., Riviere, J.E., Brooks, J.D., Monteiro-Riviere, N.A., 2003. Percutaneous absorption of 2,6-di-*tert*-butyl-4-nitrophenol (DBNP) in isolated perfused porcine skin. Toxicol. in Vitro 17, 289–292.
Iwai, I., Han, H.M., den Hollander, L., Svensson, S., Öfverstedt, L.G., Anwar, J., Brewer, J., Bloksgaard, M., Laloeuf, A., Nosek, D., Masich, S., Bagatolli, L.A., Skoglund, U., Norlén, L., 2012. The human skin barrier is organized as stacked bilayers of fully extended ceramides with cholesterol molecules associated with the ceramide sphingoid moiety. J. Investig. Dermatol. 132, 2215–2225.
Kietzmann, M., Löscher, W., Arens, D., Maaβ, P., Lubach, D., 1993. The isolated perfused bovine udder as an in vitro model of percutaneous drug absorption skin viability and percutaneous absorption of dexamethasone, benzoyl peroxide, and etofenamate. J. Pharmacol. Toxicol. Methods 30, 75–84.
Kreidstein, M.L., Pang, C.Y., Levine, R.H., Knowlton, R.J., 1991. The isolated perfused human skin flap: design, perfusion technique, metabolism, and vascular reactivity. Plast. Reconstr. Surg. 87, 741–749.

Kreidstein, M.L., Levine, R.H., Knowlton, R.J., Pang, C.Y., 1995. Serial fluorimetric assessments of skin perfusion in isolated perfused human skin flaps. Br. J. Plast. Surg. 48, 288–293.
Lane, M.E., 2013. Skin penetration enhancers. Int. J. Pharm. 447, 12–21.
Lipa, J.E., Neligan, P.C., Perreault, T.M., Baribeau, J., Levine, R.H., Knowlton, R.J., Pang, C.Y., 1999. Vasoconstrictor effect of endothelin-1 in human skin: role of ETA and ETB receptors. Am. J. Physiol. Heart Circ. Physiol. 276, 359–367.
Miland, Å.O., de Weerd, L., Weum, S., Mercer, J.B., 2008. Visualising skin perfusion in isolated human abdominal skin flaps using dynamic infrared thermography and indocyanine green fluorescence video angiography. Eur. J. Plast. Surg. 31, 235–242.
Parra, A., Clares, B., Rosselló, A., Garduño-Ramírez, M.L., Abrego, G., García, M.L., Calpena, A.C., 2016. Ex vivo permeation of carprofen from nanoparticles: a comprehensive study through human, porcine and bovine skin as anti-inflammatory agent. Int. J. Pharm. 501, 10–17.
Patel, P., Schmieder, S., Krishnamurthy, K., 2016. Research techniques made simple: drug delivery techniques, part 2: commonly used techniques to assess topical drug bioavailability. J. Investig. Dermatol. 136, 43–49.
Prow, T.W., Grice, J.E., Lin, L.L., Faye, R., Butler, M., Becker, W., Wurm, E.M.T., Yoong, C., Robertson, T.A., Soyer, H.P., Roberts, M.S., 2011. Nanoparticles and microparticles for skin drug delivery. Adv. Drug Deliv. Rev. 63, 470–491.
Riviere, J.E., Bowman, K.F., Monteiro-Riviere, N.A., Dix, L.P., Carver, M.P., 1986. The isolated perfused porcine skin flap (IPPSF). I. A novel in vitro model for percutaneous absorption and cutaneous toxicology studies. Fundam. Appl. Toxicol. 7, 444–453.
Schaefer, U.F., Hansen, S., Schneider, M., Luengo Contreras, J., Lehr, C.M., 2008. Models for Skin Absorption and Skin Toxicity Testing. In: Kim, K., Ehrhardt, K.J. (Eds.), Drug Absorption Studies: In Situ, in Vitro and in Silico Models. Springer, New York, pp. 3–33.
Schmieder, S., Patel, P., Krishnamurthy, K., 2015. Research techniques made simple: drug delivery techniques, part 1: concepts in transepidermal penetration and absorption. J. Invest. Dermatol. 135, 1–5.
Trottet, L., Merly, C., Mirza, M., Hadgraft, J., Davis, A.F., 2004. Effect of finite doses of propylene glycol on enhancement of in vitro percutaneous permeation of loperamide hydrochloride. Int. J. Pharm. 274, 213–219.
Vanić, Ž., Holsæter, A.-M., Škalko-Basnet, N., 2015. (Phospho)lipid-based nanosystems for skin administration. Curr. Pharm. Des. 21, 4174–4192.
Wagner, H., Kostka, K.H., Lehr, C.M., Schaefer, U.F., 2002. Human skin penetration of flufenamic acid: in vivo/in vitro correlation (deeper skin layers) for skin samples from the same subject. J. Invest. Dermatol. 118, 540–544.
Wagner, S.M., Nogueira, A.C., Paul, M., Heydeck, D., Klug, S., Christ, B., 2003. The isolated normothermic hemoperfused porcine forelimb as a test system for transdermal absorption studies. J. Artif. Organs 6, 183–191.
Watkinson, R.M., Guy, R.H., Hadgraft, J., Lane, M.E., 2009. Optimisation of cosolvent concentration for topical drug delivery — II: influence of propylene glycol on ibuprofen permeation. Skin Pharmacol. Physiol. 22, 225–230.
Wester, R.C., Melendres, J., Sedik, L., Maibach, H., Riviere, J.E., 1998. Percutaneous absorption of salicylic acid, theophylline, 2,4-dimethylamine, diethyl hexyl phthalic acid, and *p*-aminobenzoic acid in the isolated perfused porcine skin flap compared to man *in vivo*. Toxicol. Appl. Pharmacol. 151, 159–165.
Williams, P.L., Carver, M.P., Riviere, J.E., 1990. A physiologically relevant pharmacokinetic model of xenobiotic percutaneous absorption utilizing the isolated perfused porcine skin flap. J. Pharm. Sci. 79 (4), 305–311.

Paper II

European Journal of Pharmaceutics and Biopharmaceutics 121 (2017) 14–23

Contents lists available at ScienceDirect

European Journal of Pharmaceutics and Biopharmaceutics

journal homepage: www.elsevier.com/locate/ejpb

Research paper

Going skin deep: A direct comparison of penetration potential of lipid-based nanovesicles on the isolated perfused human skin flap model

Selenia Ternullo[a], Louis de Weerd[b], Ann Mari Holsæter[a], Gøril Eide Flaten[a], Nataša Škalko-Basnet[a,*]

[a] Drug Transport and Delivery Research Group, Department of Pharmacy, University of Tromsø The Arctic University of Norway, Universitetsveien 57, 9037 Tromsø, Norway

[b] Department of Plastic and Reconstructive Surgery, University Hospital of North Norway, Sykehusvegen 38, 9019 Tromsø and Department of Clinical Medicine, University of Tromsø The Arctic University of Norway, Universitetsveien 57, 9037 Tromsø, Norway

ARTICLE INFO

Keywords:
Local skin therapy
Phospholipid-based nanosystems
Skin penetration
Human skin
Liposomes
Isolated perfused human flap

ABSTRACT

Phospholipid-based nanocarriers are attractive drug carriers for improved local skin therapy. In the present study, the recently developed isolated perfused human skin flap (IPHSF) model was used to directly compare the skin penetration enhancing potential of the three commonly used nanocarriers, namely conventional liposomes (CLs), deformable liposomes (DLs) and solid lipid nanoparticles (SLNs). Two fluorescent markers, calcein (hydrophilic) or rhodamine (lipophilic), were incorporated individually in the three nanosystems. The nanocarrier size ranged between 200 and 300 nm; the surface charge and entrapment efficiency for both markers were dependent on the lipid composition and the employed surfactant. Both carrier-associated markers could not penetrate the full thickness human skin, confirming their suitability for dermal drug delivery. CLs exhibited higher retention of both markers on the skin surface compared to DLs and SLNs, indicating a depo formation. DLs and SLNs enabled the deeper penetration of the two markers into the skin layers. *In vitro* and *ex vivo* skin penetration studies performed on the cellophane membrane and full thickness pig/human skin, respectively, confirmed the findings. In conclusion, efficient dermal drug delivery can be achieved by optimization of a lipid nanocarrier on the suitable skin-mimicking model to assure system's accumulation in the targeted skin layer.

1. Introduction

According to the Global Burden of Disease Study 2010, the skin diseases are the fourth leading cause of disease burden at global level. The skin-related illnesses are cause of the disability affecting between 30 and 70% of individuals [1]. Despite progress achieved in the local skin therapy, the treatment of skin diseases remains challenging [2]. Topical drug delivery for localized skin therapy bears some advantages compared to the traditional administration routes, such as the avoidance of systemic administration, the lower dose of drug required to reach the desired level at the targeted site and the reduction of systemic side effects [3]. In addition, an increase in the antimicrobial resistance among the drugs used to treat skin infections systemically, is emphasising the need for an efficient localized antimicrobial skin therapy [4]. However, the penetration of drugs into the deeper skin layers, especially through the *stratum corneum* (SC), remains an important challenge in the development of effective topical formulations destined to exert localized effect in the skin [5]. For example, in the inflammatory skin diseases (e.g. dermatitis, psoriasis) and fungal skin infections, leucocytes invade the skin leading to an increase in the proliferation and differentiation of keratinocytes and consequent increase in the skin thickness and further enhancement of the skin barrier properties exerted mainly by the SC [6]. The formulations that fail to achieve the optimal therapeutic drug levels within the deeper skin layers, or to assure the depot at the skin surface, are considered suboptimal. Among the emerging approaches employed to improve the dermal delivery of drugs, nanodermatology represents one of the most promising [7,8]. Nanocarriers have shown to improve the solubility of highly hydrophobic drugs, increase drug chemical and physical stability, deliver higher concentration of drugs to the targeted site and provide sustained and controlled release of the associated drugs [9]. Phospholipid-based nanosystems are of a particular interest and have

Abbreviations: CLs, conventional liposomes; CLSM, confocal laser scanner microscopy; DLs, deformable liposomes; IPHSF, isolated perfused human skin flap; IR, infrared; KHb, modified Krebs-Henseleit buffer; PC, phosphatidylcholine; PG, propylene glycol; PI, polydispersity index; SC, *stratum corneum*; SDCh, sodium deoxycholate; SLNs, solid lipid nanoparticles

* Corresponding author.
E-mail addresses: selenia.ternullo@uit.no (S. Ternullo), Louis.De.Weerd@unn.no (L. de Weerd), ann-mari.holsater@uit.no (A.M. Holsæter), goril.flaten@uit.no (G.E. Flaten), natasa.skalko-basnet@uit.no (N. Škalko-Basnet).

http://dx.doi.org/10.1016/j.ejpb.2017.09.006
Received 14 June 2017; Received in revised form 18 August 2017; Accepted 11 September 2017
Available online 12 September 2017

been widely investigated for improving the topical skin therapy. Their phospholipid nature contributes to low toxicity and high compatibility with physiological skin lipids, especially in the SC [10]. These lipid-based nanocarriers have shown to enhance the penetration through the skin by overcoming the intact skin barrier and allowing dermal delivery of associated drugs [11]. One of the first proposed vesicular nanosystems were the conventional liposomes (CLs). Their structure permits the incorporation of lipophilic, hydrophilic and amphiphilic compounds [12]. The similarities between CLs and skin lipids allow their accumulation on the SC surface and fusion with skin lipids. This induces changes in the SC intercellular lipids, thus increasing the skin permeability and drug penetration [10]. However, most of the literature proves that CLs remain mainly confined to the SC thus building a reservoir to release slowly the associated drug. To improve drug penetration deeper into the skin layers, deformable liposomes (DLs) were proposed by Cevc and Blume [13]. These liposomes are composed of lipids and an edge activator, which provides elasticity and deformability to the liposomes. Consequently, DLs could potentially squeeze through the SC thus increasing the transport of the drug deeper into the skin layers [14].

Alternative to liposomes are particulate lipid-based nanosystems, such as solid lipid nanoparticles (SLNs). SNLs are composed of one or more solid lipids dispersed in an aqueous medium with an addition, if necessary, of a surfactant as a stabiliser [15]. These nanocarriers lack the bilayer structure of the liposomes, thus being more stable in both hydrophilic and lipophilic environment [16]. SLNs allow controlled release of the drug and penetration enhancement exerted by their occlusive properties [17]. Furthermore, they exhibit good skin tolerability, and are considered to be safe and biocompatible [18].

The lipid composition of the lipid-based nanocarriers is strongly influencing their physicochemical characteristics, such as particle size, surface charge, bilayer elasticity and thermodynamic phase. By optimizing the lipid composition, it is possible to influence/optimize vesicle deposition onto/within the skin and modulate the depth to which the drug will be delivered [19].

For the first time, we directly compared the skin penetration enhancement of three different lipid-based nanocarriers on the isolated human skin flap (IPHSF) model, a recently developed human skin perfusion model [20]. To follow the drug penetration from different lipid-based nanocarriers, two fluorescent markers with different lipophilicities, calcein and rhodamine, were employed and their penetration from the CLs, DLs and SLNs followed. The IPHSF model offers the advantage of working with the skin in the presence of dermal circulation, thus mimicking the *in vivo* human conditions to a higher extent. The confocal laser scanner microscopy (CLSM) technique was used to follow the penetration profiles. Moreover, a comparison of the marker penetration on IPHSF model with some of the established skin penetration models such as cellophane membrane and full thickness pig/human skin in the Franz diffusion cells system was performed.

2. Materials and methods

2.1. Materials

Lipoid S 100 (phosphatidylcholine from soybean, > 94% pure; PC) was a gift from Lipoid GmbH (Ludwigshafen, Germany). Calcein, rhodamine B, methanol CHROMASOLV®, magnesium sulfate heptahydrate, potassium chloride, sodium bicarbonate, sodium chloride, trichloroacetic acid (≥99.0%), Fiske-Subbarow reducer reagent, ammonium molybdate, phosphorus standard solution, sodium deoxycholate (SDCh) and Triton™ X-100 were purchased from Sigma-Aldrich Chemie (Steinheim, Germany). Potassium dihydrogen phosphate, glucose, hydrogen peroxide (30%) and calcium chloride were obtained from Merck KGaA (Darmstadt, Germany). Propylene glycol (PG) was purchased from NMD – Norwegian Medical Depot AS (Oslo, Norway), Albunorm® (human serum albumin, 200 mg/mL) from Octapharma AG (Lachen, Switzerland) and sucrose from VWR International bvba/sprl (Leuven, Belgium). Sulfuric acid was purchased from May and Baker LTD (Dagenham, UK). Cellophane membrane was obtained from Max Bringmann KG (Wendelstein, Germany) and pig ears from Nortura AS (Bardufoss, Norway).

2.2. Preparation of liposomes

CLs and DLs with calcein or rhodamine were prepared by the film hydration method [21].

PC (300 mg) for CLs or PC/SDCh (total 300 mg; 85/15% as weight ratio) for DLs were dissolved in approximately 20 mL of methanol in a round bottomed flask. When applicable, rhodamine (47.9 mg) was dissolved together with the lipid in organic solvent resulting in 10 mM rhodamine solution. The organic solvent was completely removed under a vacuum (50 mbar) using a rotary vacuum evaporator (Büchi Rotavapor R-124 with Büchi Vacuum Pump V-700, Büchi Labortechnik AG, Flawil, Switzerland) for 1 h at 45 °C. The resulting lipid film was then rehydrated in 10 mL of modified Krebs-Henseleit buffer (KHb) (pH 7.40; 280 mOsm; 110 mM NaCl, 3.8 mM KCl, 1.4 mM KH_2PO_4, 1.2 mM $MgSO_4$, 31 mM $NaHCO_3$, 2.5 mM $CaCl_2$, 11 mM glucose and 10 mM sucrose) by hand shaking at room temperature (23–24 °C) for 20 min. For calcein-containing liposomes, calcein (62.2 mg) was dissolved in the KHb to form 10 mM calcein solution used to rehydrate the film. All liposomal suspensions were stored overnight in the fridge (+4 °C) prior to the characterisation.

2.3. Preparation of solid lipid nanoparticles

SLNs with calcein or rhodamine were prepared by the solvent injection method [22] with some modifications. PC (1.20 g) was dissolved in methanol. The obtained lipid solution (120 mg/mL; 2 mL) was then rapidly injected via an injection needle (Sterican® 0.30 × 12 mm, Braun Melsungen AG, Melsungen, Malaysia) into KHb solution (6 mL) under the stirring (300 rpm). For SLNs containing calcein, the marker was dissolved in the KHb solution used to prepare nanoparticles, whereas for SLNs containing rhodamine, the lipophilic marker was dissolved in the lipid solution. Both markers were applied in the same concentrations as used for CLs and DLs preparation. The suspension was stirred for 2 h at room temperature (23–24 °C) and kept overnight in the fridge (+4 °C) prior to the characterisation.

2.4. Size reduction

The original size of CLs, DLs and SLNs containing either calcein or rhodamine was reduced by the hand extrusion through the polycarbonate membrane (Nuclepore® Track-Etched Membranes, Whatman House, Maidstone, UK). The pore size of the membranes and the number of extrusion cycles were adjusted for each formulation to obtain vesicles within the size range of 200–300 nm. CLs, DLs and SLNs containing calcein were extruded stepwise through the 0.8, 0.4 and 0.2 μm pore size membranes, three times for each pore size. The same was done for CLs containing rhodamine, while DLs containing rhodamine were extruded two times through the 1.2 μm pore size membrane. SLNs containing rhodamine were extruded stepwise through 0.8 and 0.4 μm pore size membranes (three times each) and two times through 0.2 μm pore size membranes. All extruded CLs, DLs and SLNs were then kept in the fridge (+4 °C) for a minimum of 3 h prior to characterisation and usage.

2.5. Size measurements

The particle size distributions of all CL, DL and SLN suspensions were determined by the dynamic light scattering [23] (NICOMP Submicron Particle Sizer Model 370; NICOMP Particle Sizing system, Santa Barbara, California, USA). The sample preparation was performed in a

laminar flow bench. Firstly, the test tubes were flushed once with KHb previously filtrated through 0.2 μm syringe filter (Bulk Acrodisc® 25 mm Syringe Filter, Pall Life Sciences, East Hills, New York, USA). The samples were diluted with the KHb to obtain a particle intensity between 250 and 350 kHz. The analyses were run in a vesicle mode for CLs and DLs, and solid particle mode for SLNs, respectively. Each measurement was done in triplicates (runtime of 10 min; 23–24 °C). The size distributions of all nanocarriers, expressed as the mean diameter and polydispersity index (PI), were determined using the intensity-weighted distribution.

2.6. Zeta potential measurements

The zeta potential of liposomal and solid lipid nanoparticles suspensions was determined on Malvern Zetasizer Nano – ZS (Malvern, Oxford, UK) [24]. The instrument was calibrated with Malvern Zeta potential transfer standard (-42 ± 4.2 mV). A folded capillary cell (DTS1060) was used for the measurements. The cell was rinsed with ethanol and then with filtered water (0.2 μm syringe filter) prior to the sample. Each sample was diluted in a filtrated water (1:10 and 1:20 vol ratio for calcein- and rhodamine-containing nanocarriers, respectively) to achieve a suitable count rate. The diluted sample was injected into the folded capillary cell, assuring that no air bubbles formed during the injection. All measurements were performed at 25 °C with an equilibration time of 180 s. Three measurement runs were performed for each sample, assuring an attenuator of 6–7.

2.7. Entrapment efficiency determination

The unentrapped calcein was separated from the extruded CLs, DLs and SLNs by dialysis. Typically, 5 mL of suspension were placed in a dialysis bag (Mw cut off 12,000–14,000 Da, Medicell International Ltd, London, UK) and dialysed against 500 mL of KHb for 6 h at room temperature. The dialysis bag was immersed in fresh KHb (500 mL) and dialysis continued for additional 3 h. The volume of the receptor medium was chosen to assure the sink conditions. After the dialysis, CLs, DLs and SLNs were mixed with a Triton solution (5%, v/v) to dissolve the lipids before quantification of calcein by measuring fluorescence on a Polarstar fluorimeter (Fluostar; BMG Technologies, Offenburg, Germany) with excitation and emission wavelengths at 485 and 520 nm, respectively. Standard curves of calcein in KHb solution and calcein in Triton solution (5%, v/v) were used to determine the unentrapped and entrapped calcein, respectively. A concentration range between 0.12 and 1.37 μg/mL was used for both the standard curves (R^2 of minimum 0.9990). A blank consisting of KHb or Triton solution (5%, v/v) was subtracted from the fluorescence values.

Ultracentrifugation was performed to separate unentrapped rhodamine from CLs and SLNs, while gentle centrifugation was used for DLs. Extruded CLs and SLNs were centrifuged (Beckam model L8-70M ultracentrifuge with an SW 60 Ti rotor, Beckam Instruments, Palo Alto, California, USA) at 110,000*g* for 1 h at 10 °C. Extruded DLs were centrifuged (Biofuge stratos centrifuge with a swinging bucket rotor 4 × 180 mL; Heraeus instruments GmbH, Hanau, Germany), at 3,000*g* for 25 min at 10 °C. The supernatants were separated from the pellets, which were resuspended in KHb. Lipids in both supernatants and pellets were dissolved in methanol and the rhodamine content was determined fluorometrically on a Polarstar fluorimeter (Fluostar; BMG Technologies, Offenburg, Germany) with excitation and emission wavelengths at 544 and 590 nm, respectively. To avoid evaporation of methanol during the fluorescence measurements, all samples were diluted in KHb to obtain a methanol concentration of 50% (v/v). The standard curve of rhodamine in methanol/KHb solution (1:1, v/v) was prepared using the concentrations ranging from 0.10 to 1.20 μg/mL (R^2 of minimum 0.9980). A blank consisting of methanol/KHb solution was subtracted from the fluorescence values.

The recovery of calcein and rhodamine was determined and found to be between 100.3 and 107.7%, respectively.

2.8. Phospholipid content

The phospholipid content in CLs, DLs and SLNs was determined to enable calculation of entrapment efficiency expressed as the marker/lipid ratio. A modification of Bartlett method was used [25]. In brief, all samples were diluted in distilled water (typically 1:200, v/v). An aliquot of diluted sample (1 mL) was mixed with sulfuric acid (5 M; 0.5 mL) and then incubated at 160 °C for a minimum of 3 h. After the cooling, two drops of hydrogen peroxide 30% were added and the solutions incubated at 160 °C for 1.5 h. After the cooling, ammonium molybdate (0.22%, w/v; 4.6 mL) and Fiske-Subbarow reducer (0.2 mL) were added, vortexed and incubated at 100 °C for 7 min. The samples were then cooled down and analysed by UV–VIS spectrophotometry at 830 nm using a SpectraMax 190 Microplate Reader (Molecular Devices, California, USA). The standard curve was prepared using a phosphorus standard solution in a concentration range of 1–8 μg/mL (R^2 of minimum 0.9990).

2.9. Skin penetration experiments on IPHSF model

The skin penetration of calcein and rhodamine from CLs, DLs and SLNs was evaluated on the recently established IPHSF model [20]. The human skin flaps (the mean age of 49.3 years, range 26–72 years) were obtained from the abdominoplasty operations of female patients, after receiving their written consent prior to the surgery. The excess of skin and subcutaneous fatty tissue as residue after the surgery are normally disposed, therefore no ethical approval by the Norwegian Ethical Committee was required. However, all experiments were performed in accordance with the Declaration of Helsinki Principles. Each formulation (CLs, DLs and SLNs containing either calcein or rhodamine) was tested in triplicates on three independent human skin flaps, obtained from different female donors. Human serum albumin (final concentration of 30 mg/mL) was included in the KHb to prepare the perfusate solution. The human skin flaps were cannulated and perfused with the perfusate within 90 min after their excision. The temperature of the perfusate entering the flap (inlet temperature) was maintained at approximately 32 °C using a heating circulator set at 38 °C. The use of an infrared (IR) camera (FLIR ONE, Thermal Imaging Camera for iOS; FLIR Systems) allowed the selection of the best perfused skin diffusion area (49 cm^2) having a skin temperature of *ca.* 32 °C. The formulation (7 mL) was applied onto the selected perfused skin diffusion area using an adhesive patch as described by Ternullo and colleagues [20]. The experiments were carried out for 6 h and sampling was performed by collecting the perfusate every hour, assuring the sink conditions throughout the experiment. The physiological parameters, namely the perfusion inlet pressure, perfusion flow rate and inlet temperature, were recorded throughout the experiments [20]. To exclude oedema formation, the weight and thickness of each flap were measured before and at the end of the experiment. A weight and thickness variations of less than 10% was found acceptable. Blood cells were removed from the collected perfusate by the centrifugation (1914*g*, 20 min), while plasma proteins were precipitated using trichloroacetic acid (58.82%, w/v) [20]. The obtained samples were then analysed fluorometrically, as described above, to quantify the penetrated markers through the full thickness IPHSF. Moreover, the amount of the markers retained onto the skin flap surface was determined fluorometrically.

2.9.1. Confocal laser scanning microscopy on IPHSF model

To localise the two markers in the IPHSF model after the skin penetration experiments, CLSM technique was employed [20] (Leica TCS SP5 microscope equipped with an Argon laser; Leica Microsystems CMS GmbH, Mannheim, Germany). Briefly, the imprint technique was used to prepare the samples. At the end of the skin penetration experiments, the treated perfused skin flap area was cut cross-sectionally and

Table 1
Characteristics of phospholipid-based nanocarriers containing calcein or rhodamine (n = 3 ± SD).

Marker	*Nanocarrier*	*Diameter (nm)*[a]	*PI*[b]	*Zeta potential (mV)*	*Marker/lipid ratio (μg/mg)*
calcein	CL	265 ± 3 (100%)	0.16 ± 0.02	−1.2 ± 0.2	72.3 ± 7.6
	DL	201 ± 1[c] (100%)	0.06 ± 0.00	−32.8 ± 0.5	79.6 ± 14.2
	SLN	220 ± 12 (100%)	0.16 ± 0.03	−2.9 ± 1.2	82.3 ± 2.1
rhodamine	CL	244 ± 16 (100%)	0.17 ± 0.06	−1.4 ± 0.1	92.9 ± 2.2
	DL[d]	294 ± 34 (87.4%) 76 ± 18 (12.6%)	0.27 ± 0.03	−31.5 ± 0.5	63.3 ± 4.1
	SLN[d]	227 ± 26 (93.5%) 24 ± 42 (6.5%)	0.18 ± 0.01	+1.6 ± 0.1	53.0 ± 3.4

[a] The diameter is expressed as peaks in size distributions (nm) and weight intensity of each peak (%), which is indicated in parentheses.
[b] Polydispersity index.
[c] $p < 0.05$.
[d] Bimodal size distribution.

attached onto a microscope slide. Formalin (SPRAYFIX®, Histolab Products AB, Gothenburg, Sweden) was sprayed to fix the cells that remained on the slide. Laser lines of 488 and 568 nm were used to excite calcein and rhodamine, respectively. A spectral range of 500–550 nm and 570–610 nm were used to detect the calcein and rhodamine fluorescence, respectively.

2.10. In vitro skin penetration experiments

Franz diffusion cells (PermeGear, Bethlehem, USA) were used to perform *in vitro* skin penetration experiments following the method reported earlier [20]. Cells of 1.77 cm^2 diffusion area with a receptor volume of 12 mL were used. Cellophane membrane was pre-soaked in KHb for 30 min prior to the experiment. KHb constituted the receptor phase, which was maintained at 37 °C throughout the experiment to assure the physiological skin temperature of 32 °C. CLs, DLs and SLNs containing either calcein or rhodamine were added to the donor chamber (sample volume of 600 μL). As controls, calcein in KHb and rhodamine in KHb/PG (0.5%, v/v) were used. The content of the two markers in the tested samples was determined fluorometrically prior to the penetration study and the concentration of markers in the donor chamber was equalised in all samples to assure the same concentration gradient. Sampling from the receptor chamber was done every hour for a period of 8 h. The withdrawn samples (500 μL) were replaced by an equal volume of fresh KHb to assure the sink conditions. All experiments were performed in triplicates. The markers penetrated through the cellophane membrane and non-penetrated markers were quantified fluorometrically as described in Section 2.7.

2.11. Ex vivo skin penetration experiments

Full thickness pig and human skin were used for *ex vivo* skin penetration studies [20]. Frozen pig ear skin slices were thawed, rinsed with water and cleared from the subcutaneous fat. Human skin was obtained from the resected skin during abdominoplasty of female patients, after their written consent was received. No ethical approval for the use of human skin was required by the Norwegian Ethical Committee, since the excess of skin panni is normally disposed after the surgery. The experiments were conducted in accordance with the Declaration of Helsinki Principles. The excised portion of human skin was rinsed with water and, after a removal of the subcutaneous fat, stored at −20 °C and thawed 30 min before the start of the experiment. Each formulation and controls were tested in triplicates on human skin that was obtained from the same patient. Pig and human skin thicknesses were measured prior to the experiment and skin with thickness of approximately 1.50 mm was used. The skin was mounted into the same Franz diffusion cells used for the *in vitro* experiments; the SC side was facing the donor chamber. The tested formulations, receptor medium and sampling time were the same as in the *in vitro* skin penetration experiments (Section 2.10). The markers penetrated through the full thickness pig/human skin and non-penetrated markers were quantified as described in Section 2.7.

2.12. Statistical analyses

The student's *t*-test (paired) was used to determine a statistical significance. A *p* value of less than 0.05 was considered statistically significant.

3. Results and discussion

Improved drug delivery to deeper skin layers could enable improved drug outcome in many topical therapies reducing the need for systemic treatment. However, the complex barrier of the skin, particularly the SC, which is the barrier responsible for rate-limiting step in skin drug penetration, should be addressed when designing/developing the dermal formulations [26]. Phospholipid-based nanocarriers have shown ability to enhance drug penetration through the SC and allow the sustained and controlled release of associated drugs [27–29]. The changes in the composition of phospholipid-based nanocarriers affect their interaction with the skin [14]. Therefore, a direct comparison of the skin penetration enhancement by the different phospholipid-based nanocarriers is helpful in the optimization of efficient nanopharmaceuticals destined for localized skin therapy. The right choice of the nanocarrier would lead to the optimal therapeutic drug levels in the specific skin layers, and could be tailored for the specific skin disease.

3.1. Characteristics of the phospholipid-based nanosystems

Table 1 presents the characteristics of phospholipid-based nanosystems used in this study. The optimal size of nanocarriers for dermal drug delivery was proposed to be 200–300 nm [30]. The size of liposomes and solid lipid nanoparticles containing either calcein or rhodamine was between 200 and 300 nm, as targeted. The extrusion as a method for a vesicle/particle size reduction has shown to be a suitable method to obtain the desired vesicle/particle size and rather homogenous systems. The PI was found to be lower than 0.3 for all vesicles/particles (between 0.06 and 0.27) indicating relative homogeneity in size. Among the nanocarriers containing calcein, a significant difference ($p < 0.05$) in the size was observed for DLs, which were smaller (201 nm) as compared to both CLs (265 nm) and SLNs (220 nm), respectively. Our finding is in accordance with literature [31–33]. The presence of SDCh in the phospholipid bilayers of DLs provides elasticity and flexibility to the liposomes, and reduces their surface tension. Rather homogenous size (PI < 0.3) was also obtained for rhodamine-containing nanocarriers. CLs and SLNs were of similar mean size (244 and 227 nm, respectively); a bimodal size distribution (Nicomp distribution) was observed for SLNs where a small percentage (6.5%) of

smaller particles (24 nm) was found. DLs containing rhodamine were characterised by a bimodal size distribution (Table 1) as observed for SLNs. The main peak within the size distribution of DLs was higher (294 nm) compared to both CLs and SLNs; the PI (0.27) was also the highest as compared to the other formulations. This size was obtained after only two cycles of extrusion through the polycarbonate membrane with 1.2 μm pore size membranes. Considering a potential pilot scale manufacturing, this could be considered an advantage regarding the manufacturing.

The surface charge of nanocarriers is also a factor that can play an important role in the skin penetration of associated drugs [34]. Our phospholipid-based nanosystems exhibited zeta potential in accordance with the nature of the material used for their preparation. CLs and SLNs containing either calcein or rhodamine had a zeta potential close to neutral, due to the main presence of neutral PC. DLs containing either calcein or rhodamine beard a strong negative surface charge, providing them with additional stability [21]. Although the skin has a net negative charge, negatively charged liposomes have shown to enhance skin drug penetration [34].

To assure improved skin deposition of nanocarrier-associated drugs, it is crucial to assure high drug load. In this study, we have used two different markers as model substances for hydrophilic and lipophilic drugs, respectively. The entrapment efficiencies for nanocarriers containing calcein, expressed as a marker/lipid ratio, were not significantly different. Unexpectedly, DLs entrapped more calcein compared to CLs, although DLs were smaller. The presence of SDCh may increase the incorporation of this marker in DLs [35]. We expected a lower entrapment efficiency for SLNs, since they are known to possess low loading capacity for hydrophilic compounds [36]. However, Suter and collaborators [37] have recently demonstrated that SLNs might also incorporate high load of hydrophilic compounds, such as peptides, which is in agreement with our results. CLs containing rhodamine incorporated the highest amount of the marker compared to both DLs and SLNs (Table 1). The presence of SDCh in DLs decreased the entrapment efficiency, possibly due to a competition between rhodamine and SDCh both accommodated in the phospholipid bilayer of liposomes [31]. It is known that the lipids in SLN can re-crystallize into a highly ordered crystalline structure. This process can cause drug expulsion, reducing the entrapment efficiency [38]. Our results are in accordance with literature [39].

3.2. Penetration enhancing effect of the phospholipid-based nanocarriers in the IPHSF model

Optimization of effective nanosystems for skin therapy requires validated skin penetration models. The recently established drug penetration (IPHSF) model was used for this purpose. The model offers the possibility of working with the presence of dermal circulation in the conditions similar to the *in vivo*, important parameter in the penetration studies [40]. The use of an IR camera allowed visualisation of the perfused skin flap area destined for the topical application of the tested formulations on the IPHSF model and served as a validation module of the model. IR images of the representative flaps taken during the experiments are shown in Fig. S1. The skin area, where the formulations were applied, was perfused throughout the whole penetration experiment. The physiological parameters were monitored during the experiment. The perfusion inlet pressure, flow and inlet temperature were adjusted to maintain the perfusion of the human skin flaps (skin surface temperature of *ca.* 32 °C). Physiological parameters recorded during the skin penetration experiments in the IPHSF model are shown in Fig. S2. Although the perfusion inlet pressures varied, the flap perfusion was assured throughout the experiments and the variation of weight and thickness of flaps was found to be less than 10% (data not included). The lower perfusion inlet pressures did not affect the perfusion and the higher pressures did not cause oedema formation, which was found acceptable. The temperature remained constant throughout the experiments.

No markers were found in the perfusate, indicating that our nanocarriers were not able to deliver the two markers deeper into the dermis layer allowing them to become absorbed in the systemic circulation. Therefore, all the investigated nanocarriers can be used as drug delivery systems for dermal, rather than transdermal drug therapy. This was expected considering their size. However, the limited time (6 h) of the experiment should be considered. Whether a longer time would permit some of the nanocarriers to penetrate deep enough into the dermis to enable marker absorption remain to be addressed in *in vivo* experiments. Our results are in accordance with Chen and colleagues [19], although their studies were performed using human skin in the Franz diffusion cells. No permeation of the tested markers through the full thickness human skin was observed in finite dose application for all tested nanocarriers and only low percentages (0.001%) of the hydrophilic marker were detected in the receptor fluid when the formulations were applied in infinite dose [19]. The perfusion of the IPHSF could not be assured over a longer time (more than 6 h), and we assumed that the perfused skin should permit penetration through the full thickness skin barrier at faster rate than the non-living skin. Assessment of the penetration potential of three types of nanocarriers containing either calcein or rhodamine was also evaluated by the amount of the marker retained on the top of the skin at the end of skin penetration experiments. Fig. 1 presents the percentages of the non-penetrated markers, indicating the markers retained on the top of skin surface of the IPHSF. The rank order of the tested nanocarriers according to their capability to enhance the penetration of the two markers through the SC was CLs $<$ DLs $\approx$ SLNs. DLs are expected to be more effective than CLs in drug transport across

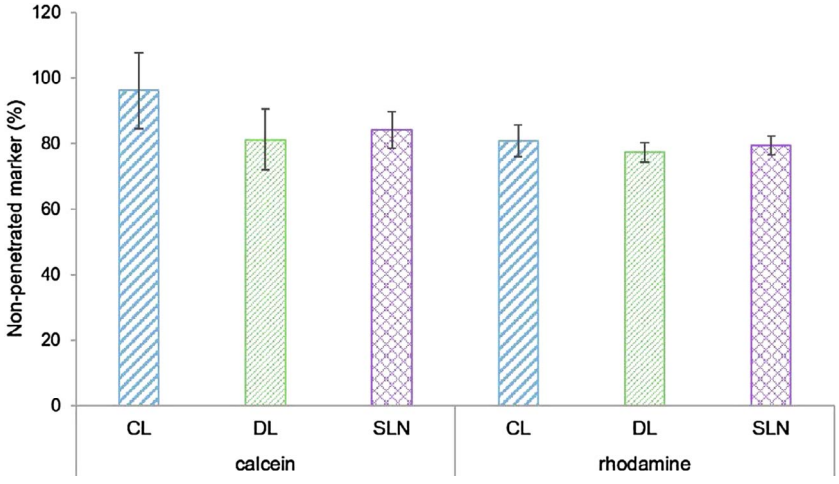

Fig. 1. Skin penetration of calcein and rhodamine from phospholipid-based nanocarriers (CL, DL, SLN) through the IPHSF model. The penetrated amount (marker in perfusate) was below detectable level in all skin penetration experiments (6 h). The non-penetrated markers were quantified after 6 h experiments. Results are presented as mean ± SD (n = 3).

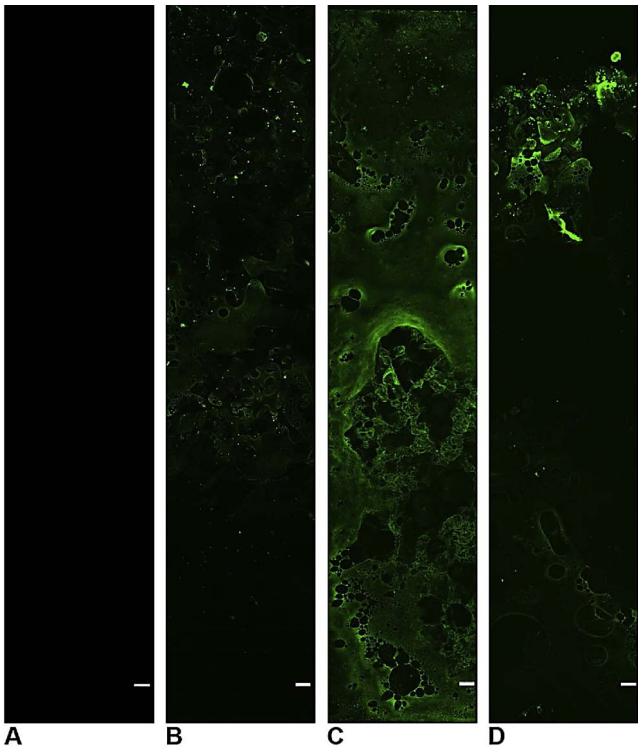

Fig. 2. Representative CLSM images of calcein-in-nanocarriers in IPHSF after 6 h of skin penetration experiments. The IPHSF was cross-sectionally cut, starting from the skin surface (upper side) to the subcutaneous fatty tissue (lower side). (A) Control, untreated IPHSF. (B), (C) and (D) IPHSF treated with calcein-containing CLs, DLs and SLNs, respectively.

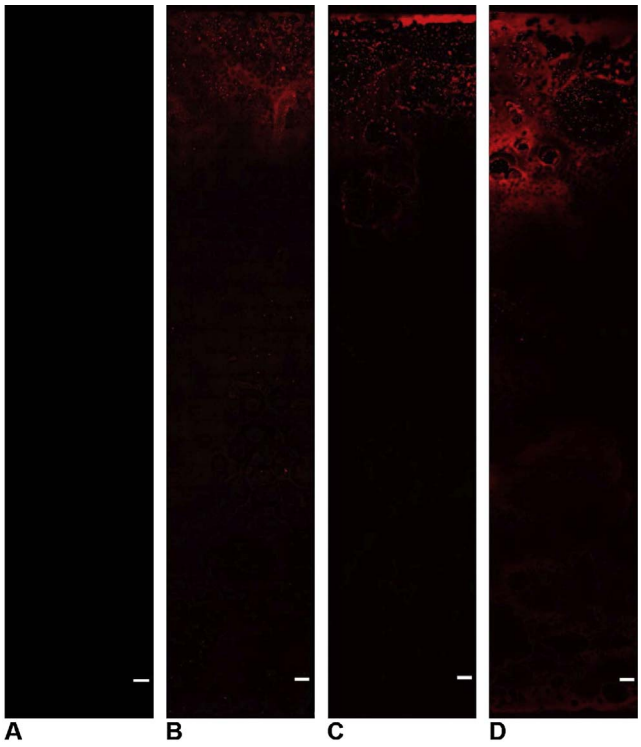

Fig. 3. Representative CLSM images of rhodamine-in-nanocarriers in IPHSF after 6 h of skin penetration experiments. The IPHSF was cross-sectionally cut, starting from the skin surface (upper side) to the subcutaneous fatty tissue (lower side). (A) Control, untreated IPHSF. (B), (C) and (D) IPHSF treated with rhodamine-containing CLs, DLs and SLNs, respectively.

the skin [41]. Regarding SLNs, our results are in accordance with literature [27]. Clares and colleagues [27] did not find a significant difference in the permeation of retinyl palmitate from CLs and SLNs (4.36 and 3.64 μg, respectively) through human skin. However, SLNs were found to be more effective in enhancing the penetration into the upper SC, similar to our findings.

To assure that our assumption on the penetration within the SC was correct and visualise the differences between the investigated nanocarriers, a CLSM study was performed. The obtained confocal images (Figs. 2 and 3) supported our findings on the skin penetration profiles through the IPHSF model. Compared to the control (untreated human skin flap), fluorescence was detected in all skin samples, indicating a presence of marker. The delivery of the two markers into/through the skin layers was, however, dependent on the investigated nanocarriers. Calcein distribution through the IPHSF was found more uniform throughout the whole skin flaps treated with DLs (Fig. 2C) compared to CLs (Fig. 2B). This confirmed the better ability of DLs to enhance the skin penetration of the marker deeper through/into the skin layers. Earlier CLSM studies comparing skin-penetration depth of the hydrophilic marker fluorescein sodium from CLs and DLs showed stronger fluorescence and deeper penetration in the skin samples treated with DLs compared to CLs [42]. Although the authors performed the penetration study using the pig skin, the same results as obtained in our model were reported. Calcein from SLNs was found in the deeper skin layers (Fig. 2D) as compared to CLs-associated calcein. This indicates and confirms the ability of SLNs to enhance the penetration of calcein as a hydrophilic model substance through the SC. For rhodamine, the strongest fluorescence was found in SC and was not depend on the type of vesicles, in agreement with literature [19]. The weakest fluorescence was detected in the IPHSF treated with the rhodamine-containing CLs (Fig. 3B), while the strongest was detected in the flaps treated with SLNs (Fig. 3D). DLs and SLNs assured higher penetration of rhodamine through/into the skin layers (Fig. 3C and D) compared to CLs. These results might be explained in part by the negatively charged surface of DLs; accumulation within the skin has shown to be more pronounced for negatively charged liposomes [14]. The enhanced penetration of lipophilic compounds from SLNs through the SC is also in agreement with literature [43,44].

The depth of the skin penetration of the two markers was clearly affected by the type of lipid-based nanocarriers the markers were associated with. The different composition of the nanocarriers plays a crucial role in determining their mechanism of action. CLs made of PC possess certain similarities with the SC lipids, which allow the fusion of the vesicles with the SC lipids, causing changes in the structure of the intercellular SC lipids. Therefore, CLs can act as penetration enhancers by loosening the lipid structure of the SC and lowering the permeability barrier of the skin. CLs can collapse onto the skin due to their fusion/mixing with the SC lipids, leading to the formation of an additional barrier and limiting the penetration of the incorporated drug to a higher extent [11].

When SDCh is incorporated in liposomes to form DLs, the skin penetration enhancing effect appears to be stronger. The presence of an edge activator in the lipid bilayer determines flexibility of the DLs and allows them to potentially squeeze into the corneocytes in the SC, thus delivering the drug deeper into the skin layers. Therefore, DLs appear to enhance drug penetration due to a synergistic effect between their deformability and their action as penetration enhancers. The deformability of DLs is also composition dependent. El Zaafarany and collaborators [28] have shown that the optimal deformability of DLs is reached when the ratio of phosphatidylcholine:edge activator is 85:15%, the same as used in our study. This further explains the capability of DLs in enhancing drug penetration into the skin compared to CLs [28]. As discussed earlier, the surface charge of nanocarriers plays a role in the skin penetration of drugs. Our DLs were negatively charged and it has been shown that a negative vesicle surface charge increases drug skin penetration [14].

Regarding SLNs, two mechanisms of skin penetration enhancement are proposed; SLNs can adhere and fuse with the SC lipid [43] or they can form an occlusive film onto the skin surface preventing transepidermal water loss [29,45]. The penetration enhancement of SLNs is dependent on the physicochemical properties of the encapsulated drug and the lipids. A stronger fluorescence observed for rhodamine as compared to calcein indicates that SLNs assured higher penetration of rhodamine through/into the skin layers (Fig. 3). This might be explained by the lipophilicity of the drugs, which affects the drug-particle interactions, the distribution of the drug within the SLNs and consequently the drug delivery by SLNs [46]. Küchler and collaborators performed electron spin resonance spectroscopy studies on SLNs using the spin probes with different lipophilicities. The authors showed that lipophilic probes were attached to the particles lipid surface, while hydrophilic probe was located in the layer of the surfactant. These distributions in the SLNs affected the skin penetration: the lipophilic probe penetrated faster and in a higher extent compared to the hydrophilic one [46], in agreement with our results. Similar studies have been performed by Saeidpour and collaborators [47], regarding the distribution of a lipophilic drug, dexamethasone, in SLNs. The authors found that the drug is located in the outer shell of the SLNs when immersed in aqueous solution but it can be easily released from the nanoparticles, which is in accordance to our results on rhodamine-containing SLNs (Fig.3D).

When describing the skin penetration process of drugs, the interaction between the nanocarrier and the skin is not the only factor that has to be taken into account. The partitioning of the drug from the nanocarrier to the skin also plays a role in the skin penetration [19]. Comparing the penetration of calcein and rhodamine in the IPHSF model, calcein was found to be more uniformly distributed throughout the skin layers (Fig. 2) compared to rhodamine (Fig. 3), which was mainly accumulated in the SC. The percentage of non-penetrated calcein, a hydrophilic marker with a low log*P* (−5.02), was higher compared to rhodamine that has lipophilic properties and higher log*P* (1.95). The same behaviour was observed for all investigated nanosystems. The lipophilic rhodamine is mainly released from nanocarriers in the lipophilic environment provided by the SC [48], while the hydrophilic calcein is able to reach deeper into the hydrophilic dermal layer that is maintained perfused by KHb (hydrophilic medium) [20]. Therefore, dermal perfusion affected the skin penetration of the hydrophilic marker. Moreover, DLs and SLNs enhanced skin penetration of calcein to a higher extent compared to CLs, whereas the difference between DLs/SLNs and CLs was not observed for rhodamine (Fig. 1). This might be explained by the difference in lipophilicity of the two markers. For highly lipophilic compounds, such as rhodamine, the penetration enhancement by the nanocarriers is less evident because they possess the intrinsic capacity to move with relative ease through the SC. In the case of hydrophilic substances such as calcein, the nanocarriers have the opportunity to act as penetration enhancer due to the low partition coefficient of hydrophilic compounds [19].

3.3. In vitro and ex vivo skin penetration

All nanocarriers exhibited a sustained permeation of calcein through the cellophane membrane compared to the control (calcein in KHb solution) (Fig. 4A). Among the investigated nanocarriers, the highest calcein permeation was observed from CLs. DLs are known to increase the penetration of incorporated drugs due to their elasticity [31]. We did not observe this typical mechanism of action for DLs in our *in vitro* studies. A possible explanation might be due to their net negative surface charge (−32 mV), which is similar to the charge of cellophane membranes [49]. Since both surfaces have negative zeta potentials, the energy barrier might prevent DLs deposition on the cellophane membrane, interfering with calcein penetration through the barrier. SLNs permitted the lowest calcein penetration through the barrier, in agreement with reported studies on SLNs incorporating hydrophilic compounds [38,50].

Rhodamine permeation profiles from all nanocarriers through the cellophane membrane are presented in Fig. 4B. Both CLs and SLNs were able to sustain the permeation of rhodamine, as expected for lipophilic compounds [27,29]. However, SLNs sustained rhodamine release to a higher extent compared to CLs. The presence of a solid lipid matrix in SLNs, in contrast with the fluid core of liposomes, reduces the mobility of the incorporated drugs. This might assure a more controlled release of the drug from the SLNs compare to CLs [51]. The highly ordered crystalline structure of the SLNs strongly accommodates the drug and slows the drug release [38]. DLs containing rhodamine exhibited the highest marker penetration through the barrier. Although a charge repulsion between the DLs and cellophane membrane might be relevant for the calcein penetration (Fig. 4A), for rhodamine the observed higher higher release, compared to the other nanocarriers, might be contributed to the lipophilicity of the marker. Rhodamine is accommodated in the bilayer of DLs, while calcein is incorporated in the inner aqueous core. Therefore, rhodamine is more likely to be released from DLs even with a possible charge repulsion of DLs with the cellophane membrane.

Skin permeation of calcein from nanocarriers through the full thickness pig skin is shown in Fig. 4C. The amount of penetrated calcein through the full thickness pig skin from all nanocarriers was lower compared to *in vitro* studies (cellophane membrane). A sustained release of calcein from all nanocarriers was obtained compared to the control. DLs assured higher calcein penetration through the full thickness pig skin compared to CLs and SLNs, as expected [42]. These results also confirmed that the lower calcein permeation from DLs observed in *in vitro* studies (Fig. 4A) might be due to charge repulsion between DLs and cellophane membrane. Skin penetration of rhodamine from nanocarriers through the full thickness pig skin (Fig. 4D) showed similar trend as in *in vitro* studies as well as in literature [52]. However, no significant difference was observed among the nanocarriers and the penetration of rhodamine through the full thickness pig skin was lower from all nanocarriers compared to *in vitro* studies. Both markers, regardless of the nanocarrier type, were not found to permeate the full thickness human skin in the Franz diffusion cells system (data not shown). Therefore, the skin penetration through the full thickness human skin in the Franz diffusion system appears to closely resemble the penetration observed in our IPHSF model. This highlights the importance of using the human skin in the skin penetration studies.

The amount of non-penetrated markers (retained on the top of the different skin membrane models) was quantified at the end of *in vitro* and *ex vivo* skin penetration experiments to compare the penetration determined on the IPHSF model with the established skin models. Fig. 5 represents a summary of the two markers penetration through the *in vitro* and *ex vivo* full thickness skin models. As discussed earlier, all nanocarriers exhibited lower penetration of calcein compared to the control both through the cellophane membrane and full thickness pig skin; while no calcein was detected in the receptor medium when full thickness human skin was tested in Franz diffusion cells system. Moreover, all nanocarriers were able to retain higher amount of calcein on the top of the skin in all tested skin models as compared to the control (Fig. 5A). Retention of calcein on the top of the human skin in the Franz diffusion cells system and IPHSF model were comparable, except for SLNs. SLNs mediated a lower retention of associated calcein on the IPHSF model compared to *ex vivo* human skin. This might be explained by the fact that the perfusion of human skin flap is performed with an aqueous medium (KHb), which can influence skin penetration of hydrophilic compounds [20].

Retention of rhodamine on the top of all skin models is shown in Fig. 5B. The non-penetrated amount of rhodamine was found to be lower compared to calcein, in agreement with data obtained from the IPHSF model. Our results indicate that rhodamine remained accumulated within the SC, due to its lipophilic nature. Among the investigated nanocarriers, CLs and SLNs assured higher retention of rhodamine on all the skin models, while DLs were able to enhance rhodamine

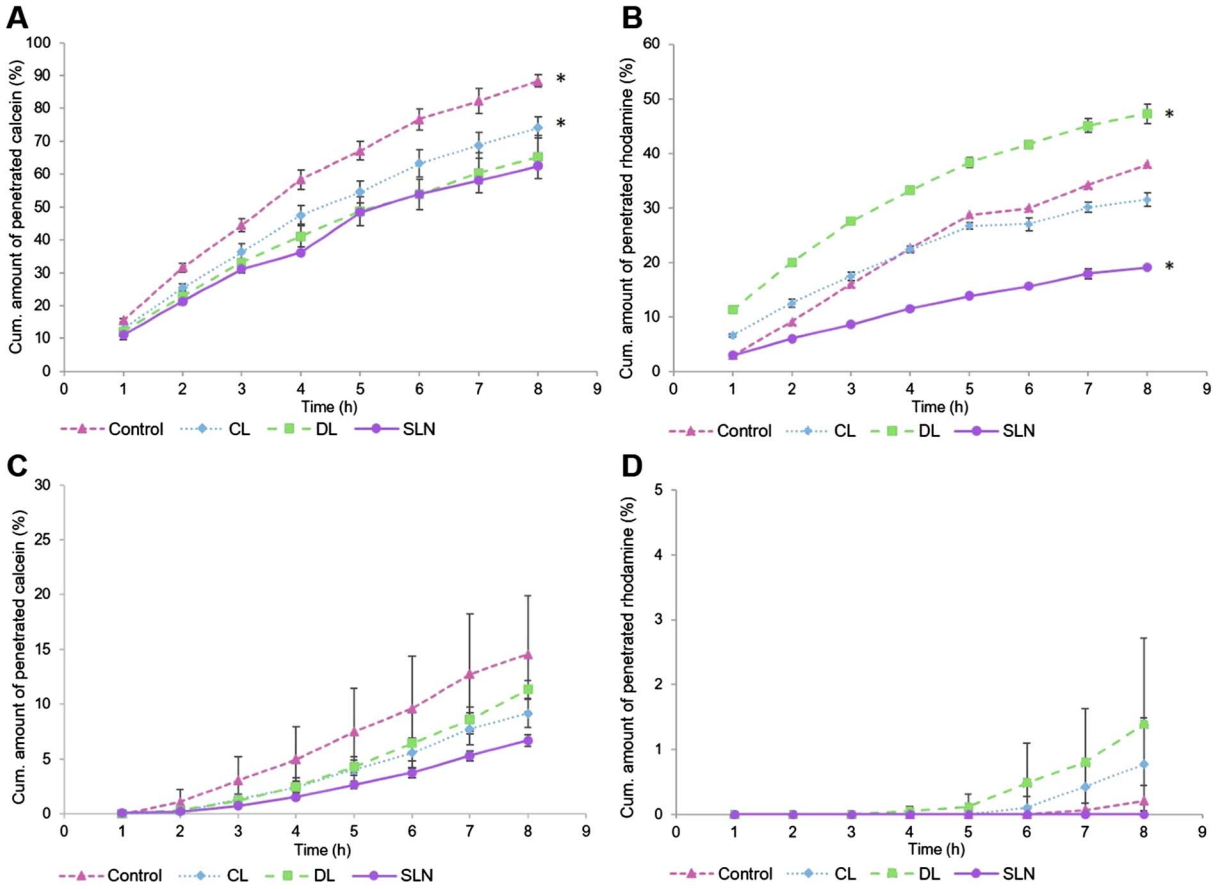

Fig. 4. Penetration profiles of calcein (left column) and rhodamine (right column) from CLs, DLs and SLNs through the cellophane membrane (A, B) and full thickness pig skin (C, D) using the Franz diffusion cells. As control, calcein in KHb and rhodamine in KHb/PG (0.5%, v/v) were used. The concentration of markers was equalised in all tested formulations to assure the same concentration gradient. The skin penetration experiments were carried out for a period of 8 h and results are presented as the mean ± SD (n = 3). $^{*}p < 0.05$.

penetration through the full thickness skin barriers. DLs containing rhodamine were earlier tested in the pig skin by Carrer and co-authors [53]. The authors found that negatively charged DLs, as our DLs, were able to increase a marker penetration through the pig skin to a greater extent. CLs and SLNs did create a drug reservoir in the skin [53]. Jensen and collaborators [29] tested the penetration properties of SLNs containing corticosteroids, lipophilic drugs, in the pig skin and compared SLNs with an ointment. The penetration of the drug through the intact skin was reduced when the drug was formulated in SLNs and a higher amount of drug remained in the upper layers of the skin [29], in agreement with our findings. DLs exhibited the lowest retention of rhodamine on the human skin in Franz diffusion cells compared to the other nanocarriers. This suggests that DLs improved the penetration of the marker through the human SC. Skin penetration studies and two-photon microscopy analysis from Simonsson and collaborators [54] support our findings. Although they tested rhodamine-containing ethosomes, they found an increased penetration of rhodamine from ethosomes compared to the hydroethanolic solution. Moreover, as we observed in the CLSM studies on the IPHSF model, they also observed a strong fluorescence from rhodamine in the SC when incorporated in ethosomes. Penetration of rhodamine from all nanocarriers through the IPHSF model was found to be more similar to the *ex vivo* human skin than through cellophane membrane and pig skin; the same trend as observed for calcein.

Although the penetration profile observed for all nanocarriers incorporating either calcein or rhodamine through all the full thickness skin barrier models was the same, the retention of the two markers on the top of cellophane membrane and pig skin differed significantly ($p < 0.03$) from the human skin and IPHSF model. The artificial membranes have already shown their limited ability to reflect the complex interactions between the human skin and the applied formulations, often resulting in non-comparable findings [55]. Although pig ear skin is more able to represent *in vivo* human skin than artificial membranes [56], recent studies have shown that frozen/thawed pig skin is more permeable than freshly excised skin. It has been postulated that the high ceramide and low cholesterol levels in pig skin might cause an easy disruption of the SC due to ice crystalline formation. This leads to impaired SC barrier and thus higher permeability of drugs [57]. Moreover, especially for pig skin, the total recovery of both markers was reported to be lower than the stated ideal value (100 ± 15%) [58]. Although we only quantified the markers penetrated through the full thickness skin barriers and non-penetrated markers and did not extract any markers retained in the barriers, it might be hypothesised that the impaired SC barrier of frozen/thawed pig skin favours the retention of the markers, especially the lipophilic rhodamine, within the skin. Therefore, the low recovery might be explained by the non-considered amount of markers retained in the skin. Moreover, the markers penetrated through the full thickness skin barriers and non-penetrated amounts of both markers were calculated from the content of the two markers in the formulations determined fluorometrically prior to the penetration study. Therefore, another possible explanation for the low recovery might be an underestimation of the marker content, determined prior to the experiment, from the theoretical amount.

The results indicate that it is crucial to test the nanocarriers on the reliable skin models able to mimic *in vivo* studies as close as possible and that the direct comparison of various nanocarriers can serve as an important step in development of the optimal dermal formulation targeting a specific dermal condition. It is necessary to note that the described nanocarriers will require a suitable vehicle to assure their retention on the skin.

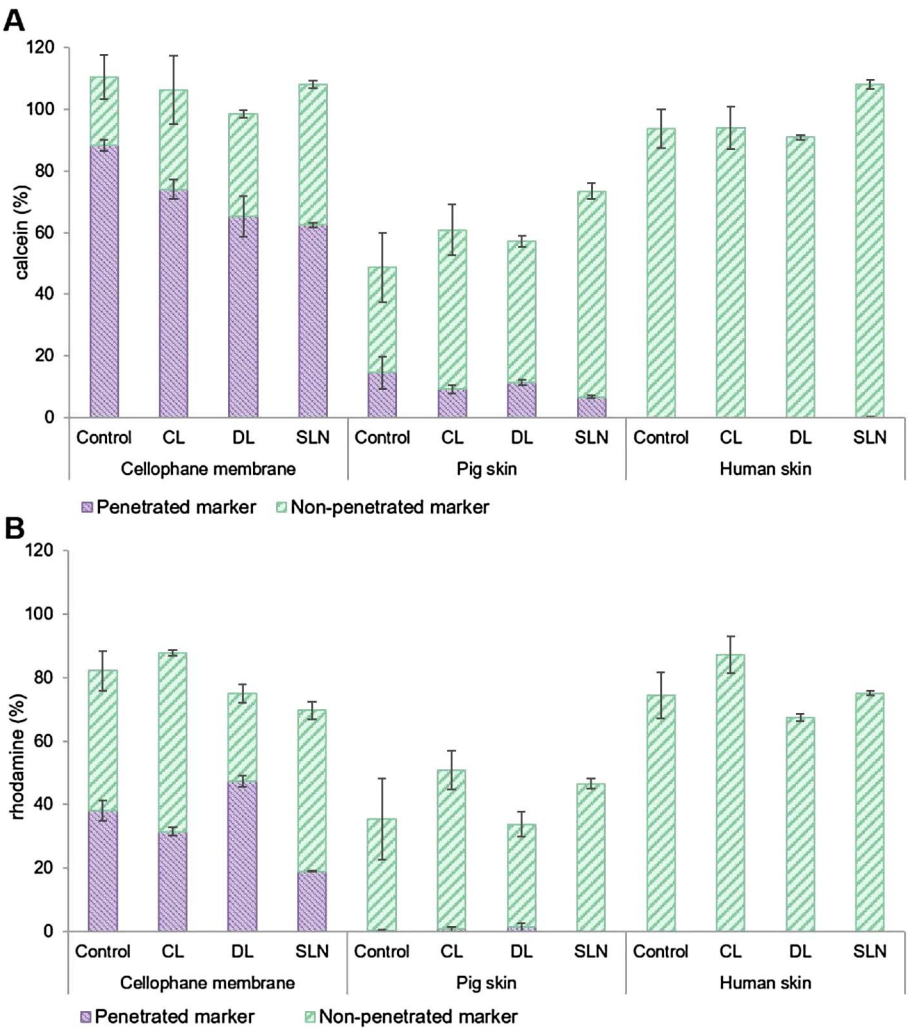

Fig. 5. *In vitro* and skin penetration studies (8 h) of calcein (A) and rhodamine (B) from CLs, DLs and SLNs through the cellophane membrane, full thickness pig and human skin using the Franz diffusion cells (n = 3). As control, calcein in KHb and rhodamine in KHb/PG (0.5%, v/v) were used. Calcein and rhodamine concentrations were equalised in all tested formulations to assure the same concentration gradient.

4. Conclusions

This study confirmed the different skin penetration potential of three phospholipid-based nanocarriers using the IPHSF model, a model closely resembling the human studies. The differences in their lipid nanocarriers composition and surface charge determined their mechanism of action and a different skin penetration depth of the two markers. DLs and SLNs exhibited higher penetration of the two markers compared to CLs through the isolated perfused human skin flap model. Moreover, DLs and SLNs delivered both markers deeper into the skin layers compared to CLs. This comparative study could serve in the optimization of phospholipid-based nanosystems for localized skin therapy and assist in the right selection of the nanocarrier for targeted drug delivery into the specific skin layers, depending on the targeted skin condition/disease.

Acknowledgements

The authors thank Knut Steinnes for the technical support and the Department of Medical Biology at the Faculty of Health Sciences, University of Tromsø The Arctic University of Norway, for the use of their laboratory facility. The authors are grateful to Lipoid GmbH (Ludwigshafen, Germany) for generously providing the phospholipids.

Conflict of interest

The authors declare no conflict of interest.

Appendix A. Supplementary material

Supplementary data associated with this article can be found, in the online version, at http://dx.doi.org/10.1016/j.ejpb.2017.09.006.

References

[1] R.J. Hay, N.E. Johns, H.C. Williams, I.W. Bolliger, R.P. Dellavalle, D.J. Margolis, R. Marks, L. Naldi, M.A. Weinstock, S.K. Wulf, C. Michaud, C.J.L. Murray, M. Naghavi, The global burden of skin disease in, an analysis of the prevalence and impact of skin conditions, J. Invest. Dermatol. 134 (2014) (2010) 1527–1534.
[2] M. Gupta, U. Agrawal, S.P. Vyas, Nanocarrier-based topical drug delivery for the treatment of skin diseases, Expert Opin. Drug Deliv. 9 (2012) 783–804.
[3] R. Goyal, L.K. Macri, H.M. Kaplan, J. Kohn, Nanoparticles and nanofibers for topical drug delivery, J. Control. Release 240 (2016) 77–92.
[4] S.G. Ingebrigtsen, A. Didriksen, M. Johannessen, N. Škalko-Basnet, A. Mari, Holsæter, Old drug, new wrapping – a possible comeback for chloramphenicol? Int. J. Pharm. 526 (2017) 538–546.
[5] R. Banerjee, Overcoming the stratum corneum barrier: a nano approach, Drug Deliv. Transl. Res. 3 (2013) 205–208.
[6] H.C. Korting, M. Schäfer-Korting, Carriers in the topical treatment of skin disease, in: M. Schäfer-Korting (Ed.), Drug Delivery, Handbook of Experimental Pharmacology, Springer-Verlag, Berlin Heidelberg, Berlin, 2010, pp. 435–468.
[7] L.A. DeLoiuse, Applications of nanotechnology in dermatology, J. Invest. Dermatol. 132 (2012) 964–975.
[8] R. Saraceno, A. Chiricozzi, M. Gabellini, S. Chimenti, Emerging applications of nanomedicine in dermatology, Skin Res. Technol. 19 (2013) 13–19.
[9] A. Patzelt, W.C. Mak, S. Jung, F. Knorr, M.C. Meinke, H. Richter, E. Rühl, K.Y. Cheung, N.B.N.N. Tran, J. Lademann, Do nanoparticles have a future in dermal drug delivery? J. Control. Release 246 (2017) 174–182.
[10] B. Geusens, T. Strobbe, S. Bracke, P. Dynoodt, N. Sanders, M. Van Gele, J. Lambert, Lipid-mediated gene delivery to the skin, Eur. J. Pharm. Sci. 43 (2011) 199–211.
[11] S. Fireman, O. Toledano, K. Neinmann, N. Loboda, N. Dayan, A look at emerging

delivery systems for topical drug products, Dermatol. Ther. 24 (2011) 477–488.
[12] J. de Leeuw, H.C. de Vijlder, P. Bjerring, H.A.M. Neumann, Liposomes in dermatology today, J. Eur. Acad. Dermatol. Venereol. 23 (2009) 505–516.
[13] G. Cevc, G. Blume, Lipid vesicles penetrate into intact skin owing to the transdermal osmotic gradients and hydration force, Biochim. Biophys. Acta 1104 (1992) 226–232.
[14] M.L. González-Rodríguez, A.M. Rabasco, Charged liposomes as carrier to enhance the permeation through the skin, Expert Opin. Drug Deliv. 8 (2011) 857–871.
[15] J. Kristl, K. Teskač, P.A. Grabnar, Current view on nanosized solid lipid carriers for drug delivery to the skin, J. Biomed. Nanotechnol. 6 (2010) 529–542.
[16] D. Papakostas, F. Rancan, W. Sterry, U. Blume-Peytavi, A. Vogt, Nanoparticles in dermatology, Arch. Dermatol. Res. 303 (2011) 533–550.
[17] A. Lauterbach, C.C. Müller-Goymann, Applications and limitations of lipid nanoparticles in dermal and transdermal drug delivery via the follicular route, Eur. J. Pharm. Biopharm. 97 (2015) 152–163.
[18] S. Doktorovová, A.B. Kovačević, M.L. Garcia, E.B. Souto, Preclinical safety of solid lipid nanoparticles and nanostructured lipid carriers: current evidence from *in vitro* and *in vivo* evaluation, Eur. J. Pharm. Biopharm. 108 (2016) 235–252.
[19] M. Chen, X. Liu, A. Fahr, Skin penetration and deposition of carboxyfluorescein and temoporfin from different lipid vesicular systems: in vitro study with finite and infinite dosage application, Int. J. Pharm. 408 (2011) 223–234.
[20] S. Ternullo, L. de Weerd, G.E. Flaten, A.M. Holsæter, N. Škalko-Basnet, The isolated perfused human skin flap model: a missing link in skin penetration studies? Eur. J. Pharm. Sci. 96 (2017) 334–341.
[21] Z. Palac, J. Hurler, N. Škalko-Basnet, J. Filipović-Grčić, Ž. Vanić, Elastic liposomes-in-vehicle formulations destined for skin therapy: the synergy between type of liposomes and vehicle, Drug Dev. Ind. Pharm. 41 (2015) 1247–1253.
[22] M.A. Schubert, C.C. Müller-Goymann, Solvent injection as a new approach for manufacturing lipid nanoparticles – evaluation of the method and process parameters, Eur. J. Pharm. Biopharm. 55 (2003) 125–131.
[23] M.W. Jøraholmen, Ž. Vanić, I. Tho, N. Škalko-Basnet, Chitosan-coated liposomes for topical vaginal therapy: assuring localized drug effect, Int. J. Pharm. 472 (2014) 94–101.
[24] S.G. Ingebrigtsen, N. Škalko-Basnet, C. de Albuquerque Cavalcanti Jacobsen, A.M. Holsæter, Successful co-encapsulation of benzoyl peroxide and chloramphenicol in liposomes by a novel manufacturing method - dual asymmetric centrifugation, Eur. J. Pharm. Sci. 97 (2017) 192–199.
[25] G.R. Bartlett, Phosphorus assay in column chromatography, J. Biol. Chem. 234 (1959) 466–468.
[26] G.K. Menon, G.W. Cleary, M.E. Lane, The structure and function of the stratum corneum, Int. J. Pharm. 435 (2012) 3–9.
[27] B. Clares, A.C. Calpena, A. Parra, G. Abrego, H. Alvarado, J.F. Fangueiro, E.B. Souto, Nanoemulsions (NEs), liposomes (LPs) and solid lipid nanoparticles (SLNs) for retinyl palmitate: effect on skin permeation, Int. J. Pharm. 473 (2014) 591–598.
[28] G.M. El Zaafarany, G.A.S. Awad, S.M. Holayel, N.D. Mortada, Role of edge activators and surface charge in developing ultradeformable vesicles with enhanced skin delivery, Int. J. Pharm. 397 (2010) 164–172.
[29] L.B. Jensen, K. Petersson, H.M. Nielsen, *In vitro* penetration properties of solid lipid nanoparticles in intact and barrier-impaired skin, Eur. J. Pharm. Biopharm. 79 (2011) 68–75.
[30] J. du Plessis, C. Ramachandran, N. Weiner, D.G. Müller, The influence of particle size of liposomes on the deposition of drug into the skin, Int. J. Pharm. 103 (1994) 277–282.
[31] A. Gillet, F. Lecomte, P. Hubert, E. Ducat, B. Evrard, G. Piel, Skin penetration behaviour of liposomes as a function of their composition, Eur. J. Pharm. Biopharm. 79 (2011) 43–53.
[32] Z. Palac, A. Engesland, G.E. Flaten, N. Škalko-Basnet, J. Filipović-Grčić, Ž. Vanić, Liposomes for (trans)dermal drug delivery: the skin-PVPA as a novel *in vitro stratum corneum* model in formulation development, J. Liposome Res. 24 (2014) 313–322.
[33] Ž. Vanić, A. Hafner, M. Bego, N. Škalko-Basnet, Characterization of various deformable liposomes with metronidazole, Drug Dev. Ind. Pharm. 39 (2013) 481–488.
[34] A. Gillet, P. Compère, F. Lecomte, P. Hubert, E. Ducat, B. Evrard, G. Piel, Liposome surface charge influence on skin penetration behaviour, Int. J. Pharm. 411 (2011) 223–231.
[35] A.P.C.O. Bahia, E.G. Azevedo, L.A.M. Ferreira, F. Frézard, New insights into the mode of action of ultradeformable vesicles using calcein as hydrophilic fluorescent marker, Eur. J. Pharm. Sci. 39 (2010) 90–96.
[36] J. Pardeike, A. Hommoss, R.H. Müller, Lipid nanoparticles (SLN, NLC) in cosmetic and pharmaceutical dermal products, Int. J. Pharm. 366 (2009) 170–184.
[37] F. Suter, D. Schmid, F. Wandrey, F. Zülli, Heptapeptide-loaded solid lipid nanoparticles for cosmetic anti-aging applications, Eur. J. Pharm. Biopharm. 108 (2016) 304–309.
[38] G. Zoubari, S. Staufenbiel, P. Volz, U. Alexiev, R. Bodmeier, Effect of drug solubility and lipid carrier on drug release from lipid nanoparticles for dermal delivery, Eur. J. Pharm. Biopharm. 110 (2017) 39–46.
[39] K. Ferderber, S. Hook, T. Rades, Phosphatidyl choline-based colloidal systems for dermal and transdermal drug delivery, J. Liposome Res. 19 (2009) 267–277.
[40] U.F. Schaefer, S. Hansen, M. Schneider, J. Luengo Contreras, C.M. Lehr, Models for skin absorption and skin toxicity testing, in: K. Kim, K.J. Ehrhardt (Eds.), Drug Absorption Studies: In Situ, In Vitro and in Silico Models, Springer, New York, 2008, pp. 3–33.
[41] T. Uchino, F. Lefeber, G. Gooris, J. Bouwstra, Characterization and skin permeation of ketoprofen-loaded vesicular systems, Eur. J. Pharm. Biopharm. 86 (2014) 156–166.
[42] T. Subongkot, S. Duangjit, T. Rojanarata, P. Opanasopit, T. Ngawhirunpat, Ultradeformable liposomes with terpenes for delivery of hydrophilic compound, J. Liposome Res. 22 (2012) 254–262.
[43] L. Vidlářová, J. Hanuš, M. Veselý, P. Ulbrich, F. Štěpánek, J. Zbytovská, Effect of lipid nanoparticle formulations on skin delivery of a lipophilic substance, Eur. J. Pharm. Biopharm. 108 (2016) 289–296.
[44] J. Chen, N. Wei, M. Lopez-Garcia, D. Ambrose, J. Lee, C. Annelin, T. Peterson, Development and evaluation of resveratrol, Vitamin E, and epigallocatechin gallate loaded lipid nanoparticles for skin care applications, Eur. J. Pharm. Biopharm. 117 (2017) 286–291.
[45] L.M. Andrade, C. de Fátima Reis, L. Maione-Silva, J.L.V. Anjos, A. Alonso, R. Caixeta Serpa, R. Neves Marreto, E. Martins Lima, S. Fleury Taveira, Impact of lipid dynamic behavior on physical stability, *in vitro* release and skin permeation of genistein-loaded lipid nanoparticles, Eur. J. Pharm. Biopharm. 88 (2014) 40–47.
[46] S. Küchler, W. Herrmann, G. Panek-Minkin, T. Blaschke, C. Zoschke, K.D. Kramer, R. Bittl, M. Schäfer-Korting, SLN for topical application in skin diseases-Characterization of drug-carrier and carrier-target interactions, Int. J. Pharm. 390 (2010) 225–233.
[47] S. Saeidpour, S.B. Lohan, A. Solik, V. Paul, R. Bodmeier, G. Zoubari, M. Unbehauen, R. Haag, R. Bittl, M.C. Meinke, C. Teutloff, Drug distribution in nanosctructured lipid particles, Eur. J. Pharm. Biopharm. 110 (2017) 19–23.
[48] G. Bastiat, C.O. Pritz, C. Roider, F. Fouchet, E. Lignières, A. Jesacher, R. Glueckert, M. Ritsch-Marte, A. Schrott-Fischer, P. Saulnier, J.P. Benoit, A new tool to ensure the fluorescent dye labeling stability of nanocarriers: a real challenge for fluorescence imaging, J. Control. Release 170 (2013) 334–342.
[49] M.Y. Boluk, T.G.M. van de Ven, Effects of polyelectrolytes on flow-induced deposition of titanium dioxide particles onto a cellophane surface, Colloids Surf. 46 (1990) 157–176.
[50] L.G. Souza, E.J. Silva, A.L.L. Martins, M.F. Mota, R.C. Braga, E.M. Lima, M.C. Valadares, S.F. Taveira, R.N. Marreto, Development of topotecan loaded lipid nanoparticles for chemical stabilization and prolonged release, Eur. J. Pharm. Biopharm. 79 (2011) 189–196.
[51] H.S. Jeon, J.E. Seo, M.S. Kim, M.H. Kang, D.H. Oh, S.O. Jeon, S.H. Jeong, Y.W. Choi, S. Lee, A retinyl palmitate-loaded solid lipid nanoparticle system: effect of surface modification with dicetyl phosphate on skin permeation *in vitro* and anti-wrinkle effect *in vivo*, Int. J. Pharm. 452 (2013) 311–320.
[52] C.M.S. Cereda, M. Franz-Montan, C.M.G. da Silva, B.R. Casadei, C. Crepaldi Domingues, G. Radomille Tofoli, D. Ribeiro de Araujo, E. de Paula, Transdermal delivery of butamben using elastic and conventional liposomes, J. Liposome Res. 23 (2013) 228–234.
[53] D.C. Carrer, C. Vermehren, L.A. Bagatolli, Pig skin structure and transdermal delivery of liposomes: a two photon microscopy study, J. Control. Release 132 (2008) 12–20.
[54] C. Simonsson, J.T. Madsen, A. Graneli, K.E. Andersen, A.-T. Karlberg, C.A. Jonsson, M.B. Ericson, A study of the enhanced sensitizing capacity of a contact allergen in lipid vesicle formulations, Toxicol. Appl. Pharmacol. 252 (2011) 221–227.
[55] C. Herkenne, A. Naik, Y.N. Kalia, J. Hadgraft, R.H. Guy, Ibuprofen transport into and through skin from topical formulations: *in vitro-in vivo* comparison, J. Invest. Dermatol. 127 (2007) 135–142.
[56] P.W. Wertz, Current understanding of skin biology pertinent to skin penetration: skin biochemistry, Skin Pharmacol. Physiol. 26 (2013) 217–226.
[57] A.C. Sintov, Cumulative evidence of the low reliability of frozen/thawed pig skin as a model for *in vitro* percutaneous permeation testing, Eur. J. Pharm. Sci. 102 (2017) 261–263.
[58] T. Haque, K.M. Rahman, D.E. Thurston, J. Hadgraft, M.E. Lane, Topical delivery of anthramycin I. Influence of neat solvents, Eur. J. Pharm. Sci. 104 (2017) 188–195.

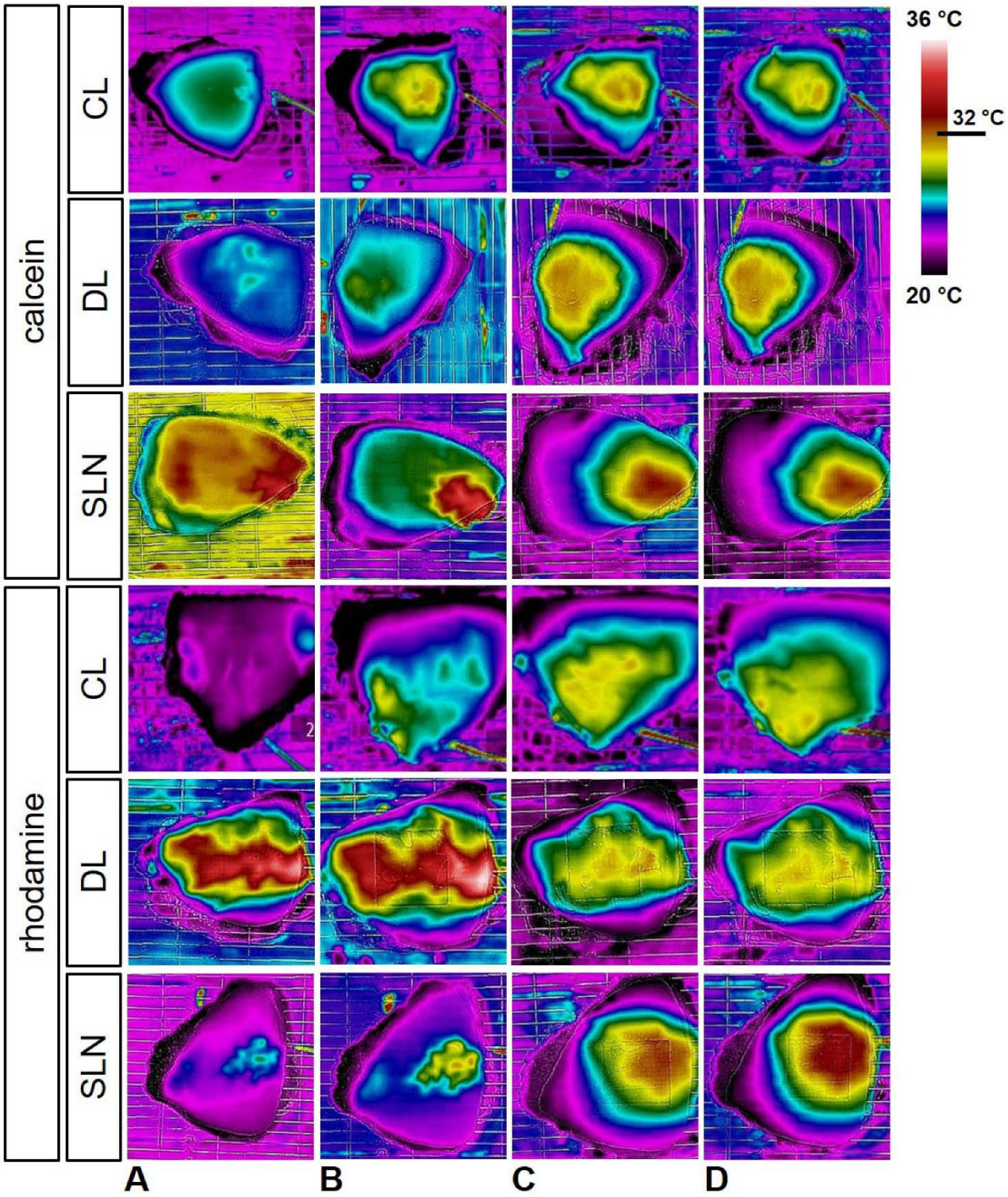

Fig. S1. IR images of the representative human skin flaps taken during 6 h of skin penetration experiments. (A) IR images recorded before application of the formulations. (B), (C) and (D) IR images recorded at time 0, 3 and 6 h after the application of the formulations, respectively. A perfused skin area (skin temperature at *ca*. 32 ºC) was assured throughout the experiment.

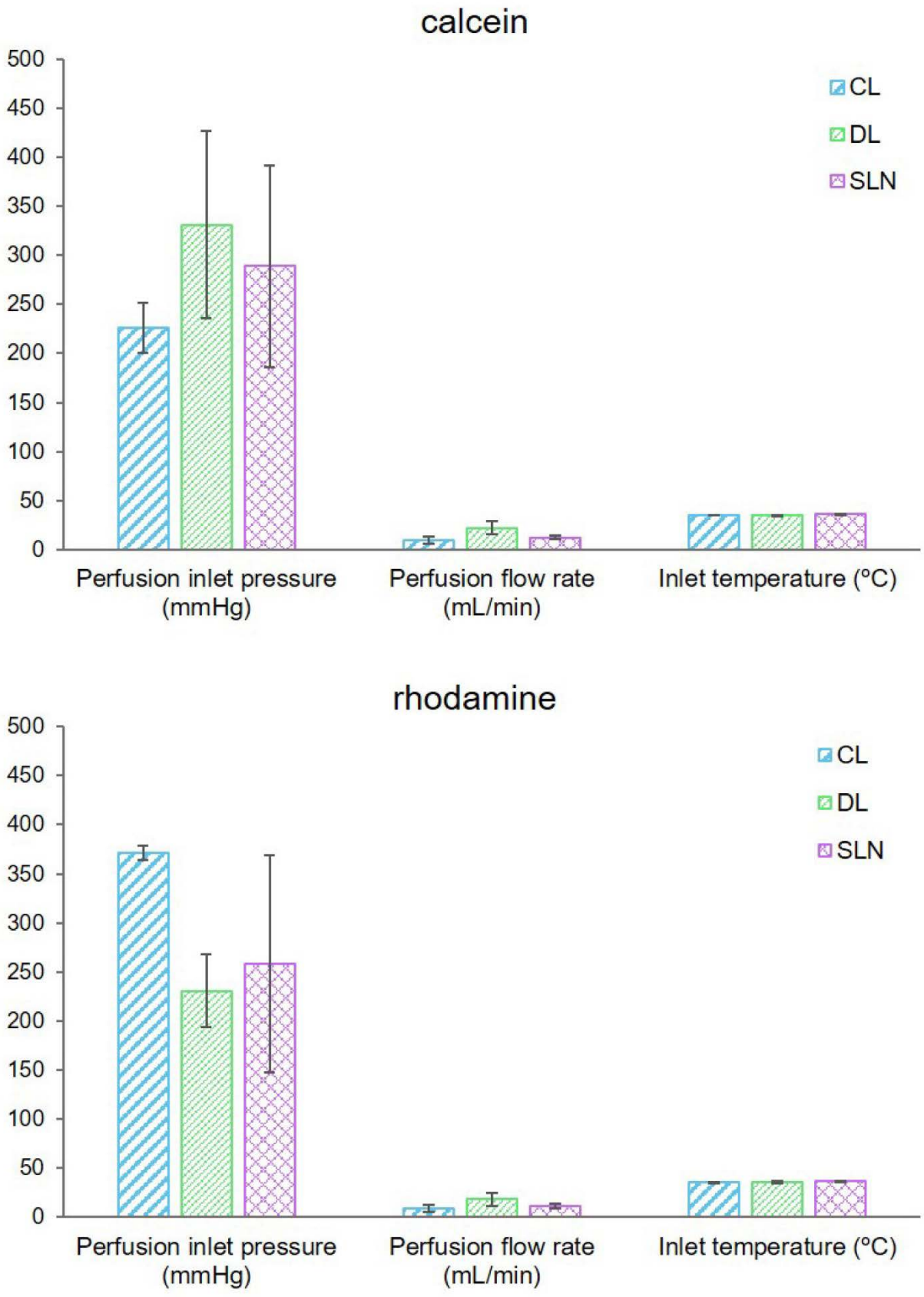

Fig. S2. Physiological parameters recorded throughout the skin penetration experiments (6 h).

Values are presented as the mean ± SD (n = 3).

Paper III

Deformable liposomes for dermal delivery of human epidermal growth factor: The effect of liposomal surface charge

Selenia Ternullo[a], Purusotam Basnet[b,c], Ann Mari Holsæter[a], Gøril Eide Flaten[a], Louis de Weerd[d,e], Nataša Škalko-Basnet[a,*]

[a]Drug Transport and Delivery Research Group, Department of Pharmacy, University of Tromsø The Arctic University of Norway, Universitetsveien 57, 9037 Tromsø, Norway

[b]IVF Clinic, Department of Obstetrics and Gynecology, University Hospital of North Norway, Sykehusvegen 38, 9019 Tromsø, Norway

[c]Women's Health and Perinatology Research Group, Department of Clinical Medicine, University of Tromsø The Arctic University of Norway, Universitetsveien 57, 9037 Tromsø, Norway

[d]Department of Plastic and Reconstructive Surgery, University Hospital of North Norway, Sykehusvegen 38, 9019 Tromsø, Norway

[e]Research Group for Medical Imaging, Department of Clinical Medicine, University of Tromsø The Arctic University of Norway, Universitetsveien 57, 9037 Tromsø, Norway

[*]Corresponding author: Nataša Škalko-Basnet, Drug Transport and Delivery Research Group, Department of Pharmacy, University of Tromsø The Arctic University of Norway, Universitetsveien 57, 9037 Tromsø, Norway; Tel: +47-776-46640; Fax: +47-776-46151; Email: natasa.skalko-basnet@uit.no

Abstract

Improving chronic wound therapy is becoming essential considering the increasing healthcare burden related to treatment of increasingly prevalent non-healed chronic wounds. The topical administration of exogenous human epidermal growth factor (hEGF) is an improved and a promising approach for chronic wound treatment. Deformable liposomes (DLs) are an attractive nanocarrier formulations since they can provide sustained drug release and prolonged drug retention within the skin layers, thus minimizing both systemic absorption and administration frequency. To develop therapeutically superior hEGF formulation, we prepared hEGF-containing neutral (NDLs), cationic (CDLs) and anionic (ADLs) DLs, respectively, since it is known that the liposomal surface charge can affect both the liposomal physicochemical properties and their skin penetration potential. All prepared liposomes were of similar size (300-350 nm) with high hEGF load (~80 % entrapment efficacy). Among the studied DLs, ADLs were found to be most promising for sustained release of hEGF, as assessed *in vitro* using the polyamide membrane. *Ex vivo* studies revealed that all DLs were excellent carriers for dermal delivery and no penetration of hEGF through the full thickness human skin was detected. ADLs provided a depot exhibiting the highest hEGF retention onto the human skin surface. ADLs also revealed enhanced mitogenic activities in human fibroblasts compared to both NDLs and CDLs after 48 hrs treatment. Moreover, hEGF-containing ADLs significantly enhanced mitogenic activity in fibroblast as comparing to activity of hEGF solution (positive control). Similar trends were observed in human keratinocytes after 24 hrs of treatment. We proved that the liposomal surface charge affects the therapeutic potential of hEGF-containing liposomes. hEGF-containing ADLs are thus a promising nanocarrier-based formulation for localized therapy of chronic wounds.

Key words: hEGF (human epidermal growth factor); deformable liposomes; liposome surface charge; human skin; chronic wound healing

Abbreviations: ADLs, anionic deformable liposomes; CDLs, cationic deformable liposomes; DLs, deformable liposomes; ELISA, enzyme-linked immunosorbent assay; HaCaT, human immortalised keratinocytes; hEGF, human epidermal growth factor; HF, human foreskin fibroblasts; HLB, hydrophilic-lipophilic balance; IMDM, Iscove's modified Dulbecco's medium; NDLs, neutral deformable liposomes; PI, polydispersity index; PBS, phosphate buffer saline; SC, *stratum corneum*; SPC, soybean phosphatidylcholine.

1. Introduction

The high prevalence of chronic wounds, their impact on patients' quality of life and the high healthcare costs call for an urgent need for improved chronic wound therapies (Hamdan et al., 2017). Moreover, the increasing proportion of high-risk population, such as diabetic, obese, and elderly people, further rises chronic wounds' incidence; it is estimated that up to 2 % of the today's population will experience chronic wounds in their lifetime (Garcia-Orue, et al., 2017b; Ashtikar and Wacker, 2018). To enhance wound healing, novel strategies comprising agents to prevent/reduce wound infection, moisturize the wound, stimulate the healing mechanism and accelerate wound closing as well as scarring control are proposed (Kalashnikova et al., 2015). In the normal wound healing process, growth factors play a central role since they are involved in different phases of wound healing by promoting angiogenesis, stimulating the formation of granulation tissue and remodelling the re-epithelisation (Jahromi et al., 2018). Chronic wounds fail to achieve the anatomic and functional integrity of the wounded area due to persistent inflammation, impaired angiogenesis, poor and delayed cellular proliferation and re-epithelialisation (Xue et al., 2018). The high levels of inflammatory cells are responsible for massive secretion of proteases in the wound bed. These enzymes degrade the growth factors, whose deficiency further delays the chronic wound healing (Saghazadeh et al., 2018). Human epidermal growth factor (hEGF) represents one of the main growth factors involved in the wound healing phases. Therefore, topical application of exogenous hEGF represents a promising approach for improving chronic wound therapy assuring faster and more effective wound healing (Garcia-Orue, et al., 2017b). However, there are several challenges related to the employment of hEGF in dermal therapy for treatment of chronic wounds. Major limitations related to local administration of hEGF are its low *in vivo* stability and rapid degradation by proteases present in the wound (Zeng and Harris, 2014). Those limitations would require frequent hEGF

administrations to assure sufficiently high local concentrations for exerting its therapeutic effect (Gainza et al., 2015b). Subsequently, a systemic absorption and undesired side effects can occur.

Phospholipid-based nanocarriers have shown to be promising dermal drug delivery systems for improved chronic wound therapy. Liposomes were employed as superior alternative to traditional drug delivery systems due to their excellent biocompatibility and biodegradability (Boateng and Catanzano, 2015). Their peculiar structure of the phospholipid bilayer closely resembles human cell membranes thus allowing high tolerance for liposomes applied on the skin. Moreover, they can offer i) protection of the incorporated drug, ii) sustained and controlled drug release, and iii) drug accumulation onto/into the skin due to their structure resembling the skin composition (Sala et al., 2018). All these functions exerted by liposomes might synergistically assure reduction in the frequencies of administration, high drug concentration at the skin site and avoidance of rapid absorption into the systemic circulation (Xue et al., 2018). However, conventional liposomes commonly bear an unstable membrane, which negatively affects the entrapment efficiency and causes relatively uncontrolled drug release (Garcia-Orue, et al., 2017b). Deformable liposomes (DLs), on the other hand, are designed as superior system to conventional liposomes overcoming the limitations of the latter in assuring effective dermal delivery of drugs (Sala et al., 2018). The surface charge has shown to contribute to the efficacy of liposomes as dermal delivery systems. The liposomal surface charge assures the interactions between liposomes and membrane of keratinocytes, which can contribute to the successful delivery of the associated drug (Mota et al., 2017). It has been postulated that this interaction might be better promoted when liposomes are positively charged thus triggering electrostatic interactions with the negatively charged skin membrane (Jain et al., 2017). However, negatively charged liposomes have also proven their ability in promoting drug delivery through skin (Mota et al., 2017).

So far, different phospholipid-based nanocarriers have been employed for dermal delivery of hEGF, such as conventional liposomes, solid lipid nanoparticles, nanostructured lipid carriers and nanofibers (Alemdaroğlu et al., 2008; Gainza et al., 2014; Garcia-Orue et al., 2017a; Jeon et al., 2012; Kaminski et al., 2016). To the best of our knowledge, deformable liposomes containing hEGF have only been investigated as positively charged nanocarriers (Choi et al., 2017).

To further explore the effect of liposomal charge on the dermal delivery of hEGF, we prepared hEGF-containing neutral (NDLs), cationic (CDLs) and anionic (ADLs) deformable liposomes, respectively. All liposomes were characterised for *in vitro* hEGF release through polyamide membrane and *ex vivo* hEGF penetration through full thickness human skin. The toxicity of liposomes was evaluated *in vitro* by MTT assay. Finally, the mitogenic activity of hEGF-containing DLs was evaluated *in vitro* in human foreskin fibroblasts (HF) and human immortalised keratinocytes (HaCaT).

2. Material and methods

2.1 Material

Soybean phosphatidylcholine (Lipoid S100, SPC) was a generous gift from Lipoid GmbH (Ludwigshafen, Germany). hEGF, methanol CHROMASOLV®, acetic acid, sodium phosphate dibasic dihydrate, potassium phosphate monobasic, sodium chloride, polysorbate 20, stearylamine and sodium deoxycholate were obtained from Sigma-Aldrich Chemie (Steinheim, Germany).

2.2 Preparation of liposomes

Stock solution of hEGF (1 mg/mL) was prepared by dissolving hEGF (500 µg) in 0.5 mL of 10 mM acetic acid solution in MilliQ water, previously filtered through 0.20 µm syringe filter (Bulk Acrodisc® 25 mm Syringe Filter, Pall Life Sciences, East Hills, New York, USA). The stock solution was then diluted to the final concentration of 20 µg/mL with phosphate buffer saline (PBS) (pH 7.4, 2.98 g/L Na_2HPO_4 x $2H_2O$, 0.19 g/L KH_2PO_4 and 8 g/L NaCl). PBS was employed to assure optimal binding of hEGF to receptors (Nunez et al., 1993).

NDLs were composed of SPC and polysorbate 20 in a ratio of 85:15 (w/w), respectively. CDLs were made of SPC and stearylamine (weight ratio of 9:1, respectively), and polysorbate 20. The ratio between SPC and polysorbate 20 was the same as employed for NDLs (85:15, w/w). ADLs were composed of SPC and sodium deoxycholate (85:15, w/w). Table 1 provides an overview of different liposomal compositions. hEGF-containing deformable liposomes were prepared by the dry film method (Ternullo et al., 2017b). SPC and different surfactants, depending on the type of deformable liposomes (Table 1), were dissolved in methanol. The solvent was evaporated on a Büchi Rotavapor R-124 with Büchi Vacuum Pump V-700 (Büchi Labortechnik AG, Flawil, Switzerland) for 1 hr at 55 mbar and 45 °C. The obtained lipid film was then resuspended in 5 mL of hEGF solution (20 µg/mL) in PBS (pH 7.4), previously prepared as described above. Liposomal formulations were stored at 4 °C for 24 hrs prior further processing.

For the cell toxicity and proliferation studies, empty DLs of different surface charges were prepared using the same lipid and surfactant compositions as for hEGF-containing DLs (Table 1).

Table 1. Composition of hEGF-containing deformable liposomes bearing different surface charge.

2.3 Size reduction of DLs

Extrusion through polycarbonate membrane (Nuclepore® Track-Etched Membranes, Whatman House, Maidstone, UK) was employed to reduce liposomal size (Ternullo et al., 2017b). The pore size of the polycarbonate membrane and the number of extrusion cycles employed for each liposomal formulation were adjusted to obtain a vesicle ranging between 300-350 nm in size. Therefore, NDLs were extruded 10 times through 800 nm pore size membrane and 15 times through 400 nm. CDLs were extruded 10 times through 800 nm pore size membrane. ADLs were extruded 5 times through 800 nm pore size membrane. All extruded liposomal formulations were stored at 4 °C for a minimum of 2 hrs before further usage.

2.4 Liposomal characterization

Size distribution and zeta potential analyses of hEGF-containing deformable liposomes were performed using a Malvern Zetasizer Nano – ZS (Malvern, Oxford, UK) (Ingebrigtsen et al., 2017; Ternullo et al., 2017b). For size measurements, all liposomes were diluted 1:50 with filtered PBS (0.20 μm syringe filter) to achieve an attenuator of 6-7. The zeta potential of all liposomes was determined by diluting each liposomal formulation with filtered (0.20 μm syringe filter) water (1:20 volume ratio). Prior to the actual measurement, an attenuator of 6-7 was assured for each formulation. Both the size and zeta potential measurements were performed in triplicates, at 25 °C and with an equilibration time of 180 seconds.

2.5 hEGF entrapment

Free (non-encapsulated) hEGF was removed from liposomal dispersions by dialysis (MW cutoff 12,000-14,000 Da, Medicell International Ltd, London, UK). Liposomal dispersion (2 mL) was dialysed against 200 mL of PBS under the sink conditions. Dialysis was carried out for 6 hrs. Both the original and dialysed liposomes were diluted in methanol to dissolve liposomes and hEGF was subsequently quantified using the Enzyme-Linked Immunosorbent Assay (ELISA) as explained in Section 2.6. The entrapment efficiency (%) was determined by the following relationship ($\mu g\ hEGF_{retenate}/\ \mu g\ hEGF_{total}$) x 100, which compares the amount of hEGF in dialysed liposomes and the total amount of hEGF in the original liposomes.

2.6 Quantification of hEGF

The quantification of hEGF was performed using ELISA kit for hEGF (Human EGF ELISA kit, Sigma-Aldrich, Saint Louis, USA), according to the manufacturer's instructions. Aliquots of samples were diluted with ELISA Diluent Buffer B, the solutions added onto an antibody-coated ELISA plate together with standards, and finally incubated for 2.5 hrs at room temperature (23 °C). Diluted biotinylated antibody solution, horseradish peroxidase-conjugated streptavidin solution and tetramethyl benzidine reagent were stepwise added and incubated according to the incubation times recommended in the kit instructions. The final colorimetric reaction was stopped by addition of Stop Solution and absorbance was read immediately at 450 nm with a SpectraMax 190 Microplate Reader (Molecular Devices, California, USA). A standard curve was obtained using standard hEGF provided in the ELISA kit within the concentration range of 1 and 200 pg/mL. Data was fitted with a four-parameter logistic regression equation using SigmaPlot version 13.0 (Systat Software, Inc., San Jose California, USA).

2.7 In vitro hEGF release

The *in vitro* hEGF release from all deformable liposomes was conducted using polyamide membrane (Sartorius polyamide membrane, 0.2 µm pore size, Sartorius AG, Gröttingen, Germany) in the Franz diffusion cells (1.77 cm^2 diffusion area, 12 mL acceptor volume; PermeGear, Bethlehem, USA) (Jøraholmen et al., 2017). The acceptor chamber was filled with PBS (pH 7.4) and kept at 32 °C during the whole experiment using a heating circulator. hEGF-NDLs, hEGF-CDLs and hEGF-ADLs were added in the donor chamber (600 µL) and hEGF release from liposomes was investigated for 6 hrs. Sampling (500 µL) of the acceptor medium was performed after 1, 4 and 6 hrs. Equal volume of fresh PBS was used to replace the withdrawn samples to maintain the sink conditions. hEGF in withdrawn samples was quantified by ELISA as described in Section 2.6. The experiments were performed in duplicates.

2.8 Preparation of human skin tissue

The human skin used in this study was obtained from the abdomen of female patients who underwent abdominoplasty and gave their written consent prior the surgery and patient identity was protected. The excess of skin panni from plastic surgery is generally disposed, thus no ethical approval by the Norwegian Ethical Committee was required. The experiments were conducted in accordance with the Declaration of Helsinki Principles. The skin panni obtained from plastic surgery was cleared from the subcutaneous fat and the remaining full thickness skin rinsed and moisten with PBS (pH 7.4) and stored at -20 °C. Prior use, skin slices were thawed in PBS at room temperature (23 °C). The thickness of full thickness human skin samples ranged between 1.50 and 1.70 mm.

2.9 Ex vivo skin penetration studies

The effect of the different surface charge of deformable liposomes on the skin penetration of hEGF was evaluated using the full thickness human skin, prepared as described above (Section 2.8) (Ternullo et al., 2017b). After thawing, the human skin was cut to slices to closely fit between the donor and acceptor chambers of the same Franz diffusion cells system used for the *in vitro* drug release experiments (Section 2.7). All liposomal formulations (hEGF-NDLs, hEGF-CDLs and hEGF-ADLs) and control (hEGF in PBS solution) (600 µL), respectively were added in the donor chamber and the experiments carried out for 6 hrs. Samples (500 µL) from the acceptor medium (PBS at 32 °C) were withdrawn after 1, 4 and 6 hrs and replaced with equal volume of fresh PBS, assuring sink conditions. Penetrated (found in the acceptor medium) and non-penetrated (retained in the donor chamber) hEGF were quantified by ELISA following the protocol described in Section 2.6. The experiments were done in triplicates.

2.10 In vitro cell toxicity and proliferation study

2.10.1 Cell culture

Human foreskin fibroblasts (HF) (CCD-1112Sk, ATCC® CRL-2429™, ATCC, Manassas, USA) were cultured in a 75 cm^2 flask with Iscove's modified Dulbecco's medium (IMDM) (Sigma-Aldrich Chemie, Steinheim, Germany), supplemented with 10 % (v/v) fetal bovine serum and penicillin-streptomycin at 37 °C in 5 % CO_2.

Human immortalised keratinocytes (HaCaT) (ATCC, Manassas, USA) were cultured on RPMI-1640 medium (Sigma-Aldrich Chemie, Steinheim, Germany) supplemented with 10 % (v/v) fetal bovine serum and penicillin-streptomycin and incubated at 37 °C in 5 % CO_2.

2.10.2 Cell toxicity and proliferation study

All liposomal formulations containing hEGF were tested for their toxicity and capability to stimulate cell proliferation in HF and HaCaT cells, respectively. To perform the experiment, all liposomes (hEGF-NDLs, hEGF-CDLs and hEGF-ADLs) were prepared to be of a smaller size (ca. 150 nm) to avoid sedimentation of liposomal dispersions during the experiments. The amount of entrapped hEGF in the 150 nm-deformable liposomes was quantified as described in Sections 2.5 and 2.6. Moreover, the amount of lipid in all extruded liposomal formulations was determined to confirm that no loss of SPC during the extrusion and separation of unentrapped hEGF from liposomes occurred (data not shown). The cells, previously grown as described in Section 2.10.1, were seeded (100 µL) on a 96-wells plate with a density of 25.000 cells/mL, using the same medium as for cell culture (IMDM and RPMI-1640 for HF and HaCaT, respectively) (Section 2.10.1). The plates were then incubated for 24 hrs at 37 °C in 5 % CO_2 to allow the cells to stabilise and adhere. After 24 hrs, 10 µL of each formulation (hEGF-NDLs, hEGF-CDLs, hEGF-ADLs) were added to the cells and the cells subsequently incubated for 24 and 48 hrs, respectively. Three different lipid concentrations of each liposomal formulation were tested, namely 1, 10 and 50 µg/mL, which were prepared by diluting each liposomal formulation in the growth medium used for cell culturing. The corresponding concentrations of hEGF in the diluted liposomal dispersions were 0.08, 0.8 and 4 µg/mL, respectively. Additionally, the following formulations were tested: 1) PBS, 2) empty NDLs, CDLs and ADLs, at the same lipid concentrations as for hEGF-containing liposomes, 3) free hEGF, in PBS in similar concentration as in liposomes. Untreated cells were used as a negative control. After the incubation times, the HF living cells were quantified using CCK-8 kit (Sigma-Aldrich Chemie, Steinheim, Germany). Briefly, 10 µL of CCK-8 were added to each well and incubated for 4 hrs. The absorbance was read at 450 nm using an Epoch Microplate Spectrophotometer (BioTek Instruments, Vermont, USA). HaCaT

living cells were quantified using Cell Proliferation Kit I (MTT) (Roche Diagnostics GmbH, Mannheim, Germany). MTT labeling reagent (10 μL, final concentration of 0.5 mg/mL) was added to each well and cells were incubated for 4 hrs under the same conditions. After the incubation period, the formed formazan crystals were dissolved with solubilization buffer (100 μL). Absorbance was then measured at 600 nm (Epoch Microplate Spectrophotometer, BioTek Instruments, Vermont, USA). All experiments were performed in triplicates.

2.11 Statistical analysis

All results are expressed as mean ± standard deviation. To determine statistical significance, Student's *t*-test or one-way ANOVA followed by Bonferroni's multiple comparisons test were performed using GraphPad Prism version 7.00 for Windows (GraphPad Software, La Jolla CA, USA). A p value < 0.05 was considered significant.

3. Results and discussion

The chronic wounds are, in addition to a decreased quality of patient's life, causing a serious financial burden on healthcare systems (Xue et al., 2018). This burden is destined to rise due to the increase of risk factors, such as age, obesity, diabetes, all responsible of delayed chronic wound healing (Gainza et al., 2015b). The urgent need for improved chronic wound therapies is essential to improve the life quality of patients and reduce healthcare costs (Frykberg and Banks, 2015). Nanopharmaceuticals offer potential to improve the healing of chronic wounds by acting on infection control, wound closure, quality of skin regeneration, both functionally and aesthetically (Ashtikar and Wacker, 2018). Since all chronic wounds are characterised by the impaired perfusion, oxygenation and limited angiogenesis, the growth factors have been

proposed as an emerging strategy to improve wound healing of chronic wounds by increasing the oxygenation in the wound tissue (Desmet et al., 2018). This led to the increased interest in developing effective topical formulations for exogenous growth factors such as hEGF. Although hEGF represents one of the main growth factor involved in the wound healing phases, its clinical application is restricted due to its low *in vivo* stability and rapid degradation by proteases (Zeng and Harris, 2014). Future chronic wound treatments that can assure a sustained release of the active ingredients might reduce the frequencies of administration, pain and stress to the patients, as well as increase the effectiveness of the incorporated drug (Boateng and Catanzano, 2015). Phospholipid-based nanocarriers have shown to be promising for improved chronic wound therapy. We focused on deformable liposomes, which have shown to possess better capability in enhancing drug penetration through the skin and delivering the incorporated drug deeper into the skin layers than conventional liposomes (Brewer, et al., 2013; Zhai et al., 2014). One of the factors responsible for the efficiency of liposomes as dermal delivery systems is their surface charge (González-Rodríguez and Rabasco, 2011). The incorporation of hEGF in deformable liposomes might lead to the development of an effective liposomal formulation destined for the treatment of chronic wounds.

3.1 Characteristics of deformable liposomes

In the optimisation process of effective liposomal formulations destined for dermal drug delivery, it is important to screen liposomal physicochemical properties, not only their vesicle size distribution but also their surface charge (Roberts et al., 2017). Moreover, it is also interesting to investigate how the type of surfactants used to obtain deformable liposomes influences their physicochemical properties.

The optimal size of liposomes destined for dermal therapies, in terms of offering the highest drug concentration in the reservoir provided by liposomes, has been shown to be around 300 nm (du Plessis et al., 1994). Furthermore, our previous study on different types of phospholipid-based nanosystems has shown that the incorporation of a model hydrophilic compound, calcein, in 200 nm deformable liposomes was effective in terms of both high entrapment efficiency and successful dermal delivery of the hydrophilic compound even in the deeper human skin layers (Ternullo et al., 2017b). In contrast, smaller liposomes (30-40 nm) have shown to be appropriate for transdermal drug delivery by passing through the SC and enabling the incorporated drug access to systemic absorption (Hood et al., 2014). We therefore aimed at obtaining deformable liposomes of 300-350 nm, considering also that hEGF is a rather large molecule (6 kDa) and that smaller liposome may provide limited aqueous space for its entrapment. We selected the extrusion as method for liposome size reduction since we reported earlier that the extrusion results in vesicles of homogenous size distributions (low polydispersity index, PI) (Ternullo et al., 2017b). All our hEGF-containing liposomes exhibited vesicle size within the targeted size range with a PI below 0.30 (Table 2). The hEGF-containing CDLs exhibited a slightly larger vesicle size (361.7 nm) and PI (0.30) than NDLs and ADLs (Table 2). The most homogenous vesicle population was observed for NDLs (PI = 0.22). Therefore, the incorporation of ionic surfactants in the lipid bilayer resulted in a slight increase in polydispersity as compared to neutral deformable liposomes. Similar findings were reported by Dragicevic-Curic and collaborators (Dragicevic-Curic et al., 2010). A possible explanation might rely on the number of the hydrophobic carbon chains in the surfactants incorporated in the deformable liposomes. It has been previously stated that surfactants with more than one hydrophobic chain are responsible for a more homogeneous size distribution due to their better capability to anchor within the lipid bilayer (Bnyan et al., 2018). In our case, NDLs contained only polysorbate 20 that possesses more than one

hydrophobic chain, thus explaining the lower PI compared to CDLs and ADLs. CDLs and ADLs were prepared using stearylamine and sodium deoxycholate, respectively; two ionic surfactants with only one hydrophobic chain in the structure thus resulting in the increased polydispersity.

The surface charge has been proven to contribute to the liposomes' capability as dermal delivery systems. Promising outcomes in terms of skin penetration enhancing effect mediated by deformable liposomes have been observed for both positively and negatively charged liposomes (Mota et al., 2017). To the best of our knowledge, only cationic hEGF-containing deformable liposomes have been previously studied (Choi et al., 2017). The cationic liposomes developed by Choi and co-workers showed to enhance skin penetration of hEGF and to improve its therapeutic effect in diabetic wounds. The effect of the negative surface charge in improving wound healing with hEGF-containing nanoformulations was only revealed with other types of nanocarriers, namely solid lipid nanoparticles and nanostructured lipid nanocarriers. As observed for cationic nanocarriers, the anionic nanoparticles exhibited good potentials for treatment of chronic wounds (Gainza et al., 2014). We therefore aimed to prepare neutral, cationic and anionic deformable liposomes to investigate the role of the surface charge in the optimization of an effective liposomal formulation for dermal delivery of hEGF and treatment of chronic wounds. The surfactants were selected to prepare liposomes with neutral, cationic and anionic surface charge (Table 2). NDLs exhibited a slightly negative zeta potential (-0.5 mV), which can be considered as neutral. CDLs and ADLs possessed highly positive and negative surface charges (45.8 mV and - 35.7 mV, respectively) due to the presence of stearylamine, known to provide positive zeta potential and sodium deoxycholate, which exerts negative surface charge (Al Shuwaili et al., 2016; Dragicevic-Curic et al., 2010). The absolute values of the zeta potential of CDLs and ADLs were very similar, thus allowing comparison of the two charged deformable liposomal formulations.

One important factor to consider when developing effective nanosystems is drug entrapment efficiency since a high drug concentration on the site of action is a prerequisite to exert the targeted therapeutic effect. All our liposomes exhibited a high entrapment efficiency (Table 2). Moreover, the entrapment efficiency appeared not to be affected by liposomal surface charge. A hydrophilic drug 5-aminolevulinic acid was successfully entrapped in deformable liposomes bearing different surface charges (Oh et al., 2011). We have used two surfactants with high hydrophilic-lipophilic balance (HLB) value (~ 16 for both polysorbate 20 and sodium deoxycholate), which are considered to provide better encapsulation of hydrophilic drugs (Bnyan et al., 2018). Al Shuwaili et al. (2016) reported similar results by loading a hydrophilic drug, pentoxifylline, in deformable liposomes both containing amphiphilic surfactant (sodium cholate) and non-ionic surfactant (polysorbate 20). The authors compared these surfactants with other type of surfactants, stating that the higher drug entrapment was obtained when sodium cholate and polysorbate 20 were used. The explanation might be related to their chemical structures; the presence of OH groups assures good hydrophilic binding sites for the incorporated hydrophilic drugs (Al Shuwaili et al., 2016). This further supports the hypothesis that by using surfactants with high HLB values, a high incorporation of hydrophilic drugs is promoted. Zhang and co-workers, who incorporated a protein, ovalbumin, in deformable liposomes made of sodium cholate and stearylamine also reported the same findings for ionic surfactants. Therefore, the interaction between the two ionic surfactants and lipids in the deformable liposomes can provide a high protein entrapment (Zhang et al., 2017). Moreover, the hEGF entrapment in all our liposomes was corresponding to the published data on other phospholipid-based nanocarriers, such as solid lipid nanoparticles and nanostructured lipid carriers. Gainza and collaborators (2014) prepared vesicles of similar size as our liposomes (300 nm) and reported a high hEGF entrapment in both solid lipid and nanostructured lipid carriers (Gainza et al., 2014). Although the difference

was not significant, our hEGF-ADLs exhibited slightly higher hEGF entrapment (84.1 %) compared to both NDLs and CDLs (80.5 and 80.8 %, respectively). The good entrapment efficiency exhibited by ADLs was already observed in our previous work, where anionic deformable liposomes with sodium deoxycholate revealed high entrapment of a hydrophilic marker, calcein (Ternullo et al., 2017b). Considering the higher hEGF entrapment observed for ADLs, ADLs might be the most suitable nanocarriers for dermal delivery of hEGF compared to NDLs and CDLs.

Table 2. Characteristics of the deformable liposomes containing hEGF (n = 3 ± SD).

3.2 In vitro hEGF release

To explore the effect of liposomal charge on the dermal delivery of hEGF, we firstly performed a pilot study on hEGF release from DLs using polyamide membrane in the Franz diffusion cells (Fig.1). Polyamide membrane has earlier been employed for testing *in vitro* release of high molecular weight and hydrophilic drugs, such as interferon α-2β; the pore size of the membrane should be sufficiently large to allow the diffusion of the hEGF (Jøraholmen et al., 2017). We could also exclude the possible passage of liposomes through the polyamide membrane. No presence of lipids in the acceptor chamber in the Franz cell systems was detected when liposomes, smaller (200-300 nm) than our deformable liposomes (ca. 350 nm), were tested (Hurler et al., 2012). Therefore, the release of hEGF mediated by all deformable liposomes was mainly attributed to their intrinsic properties of nanocarriers. Considering the liposome surface charge, no significant differences in mediating the *in vitro* hEGF release from liposomes were observed. However, CDLs exhibited a slightly higher hEGF release after 6 hrs than both NDLs and ADLs. Therefore, it might be postulated that the positive surface charge of cationic liposomes exerts a positive effect on the hEGF release through the

artificial membrane. Choi and collaborators have recently found an enhancement in the release of EGF mediated by cationic elastic liposomes as compared to neutral elastic liposomes (Choi et al., 2017). On the other hand, liposomes coated with a negatively charged polymer (xanthan) exhibited a more sustained EGF release (Kaminski et al., 2016); results similar to ADLs. The *in vitro* release of hEGF from ADLs was also in agreement with findings reported by Gainza and collaborators. Although the authors investigated the *in vitro* hEGF release from different phospholipid-based nanocarriers, namely solid lipid nanoparticles and nanostructured lipid carriers, the amount of hEGF released in 6 hrs was similar (ca. 50 % in 5 hrs) in agreement to our findings for ADLs (Gainza et al., 2014).

Fig. 1. *In vitro* hEGF release over 6 hrs from different liposomal formulations through polyamide membrane (n = 2 ± SD).

3.3 Ex vivo hEGF penetration through human skin

The development of effective topical formulations destined to exert local effect onto/into the skin requires testing the drug penetration into/through the skin under the conditions that closely mimic the *in vivo* conditions (Flaten et al., 2015). Therefore, in addition to the *in vitro* hEGF release from the liposomal formulations, we tested hEGF-containing deformable liposomes under *ex vivo* conditions using the full thickness human skin and the Franz diffusion cells system. No hEGF was found to penetrate the human skin. These results differ from the *in vitro* drug release findings, where hEGF was found to permeate through polyamide membrane from all liposomes and could be detected in the acceptor phase of the Franz cells system (Fig. 1). Similarly, for a lipophilic drug (tretinoin), the same difference between *in vitro* and *ex vivo* studies was observed when testing deformable liposomes

(Ascenso et al., 2014). Polyamide membrane, and other artificial membranes, do not possess the lipid composition and arrangement of the human skin, thus leading to discrepancy between *in vitro* and *ex vivo* results (Flaten et al., 2015; Ternullo et al., 2017a), indicating the limitations of *in vitro* release studies. Moreover, this finding shows that our liposomes are suitable for dermal delivery of hEGF by reducing any possible systemic absorption of the drug and consequently minimizing undesired side effects. However, one can argue that in the conditions of wounded skin with reduced barrier properties, the findings may differ. We, therefore, decided to quantify the amount of hEGF retained onto the human skin surface at the end of the *ex vivo* skin penetration studies to possibly detect any differences among the surface charged liposomes and their effect regarding skin penetration of hEGF. The charged deformable liposomes exhibited higher retention of hEGF onto the skin surface compared to both hEGF in solution (control) and NDLs (Fig. 2). NDLs showed minimal improvement in skin penetration enhancement of hEGF (0.55 % more compared to control). On the other hand, both CDLs and ADLs exhibited higher hEGF retention onto the skin surface, retaining 3.72 and 7.94 % more hEGF onto the skin surface than control, respectively. This enhancement in the depot effect mediated by charged DLs was more evident in comparison to NDLs; the CDLs and ADLs retained 4.26 and 8.48 % more hEGF than NDLs, respectively. This indicates that the liposomal surface charge affects the dermal delivery of hEGF mediated by DLs. Deformable liposomes have been reported to provide protection of the drug against rapid clearance into the dermis blood circulation, assuring depot system of the drug on, in and below the skin barrier (Ascenso et al., 2014). Moreover, hEGF reservoir onto the skin, due to the drug incorporation in micro- and nanosystems, has been previously reported (Al Haushey et al., 2010; Gainza et al., 2015a; Jin et al., 2013). In our case, the comparison of DLs bearing different surface charge allowed us to hypothesise that a better retention of hEGF onto the skin surface is achieved when DLs are negatively charged. The ability of anionic nanocarriers

in allowing high retention of hEGF onto the skin surface was also observed for solid lipid nanoparticles and nanostructured lipid carriers (Gainza et al., 2015a). This further confirms the ability of anionic nanocarriers in assuring a sustained hEGF release over time, as observed in the *in vitro* study (Fig. 1). Regarding effective chronic wound therapy, the hEGF depot and its sustained release mediated by ADLs can reduce the frequency of administration thus improving patient compliance, as well as reducing the pain related to dressing change. Pleguezuelos-Villa and co-workers reported similar skin penetration profiles mediated by ADLs. They incorporated naringin, a high molecular weight compound with hydrophilic properties as hEGF, in deformable liposomes and tested the *ex vivo* penetration through pig skin. Similarly to what we observed for hEGF-ADLs, more than 90 % of detected compound was found in the donor compartment after the *ex vivo* penetration study (Pleguezuelos-Villa et al., 2018),

CDLs were slightly superior to ADLs in terms of their ability to enhance hEGF penetration through the skin, which is in accordance with published data (Oh et al., 2011). Although the authors incorporated a different hydrophilic drug, anionic deformable liposomes retained higher amount of the drug onto the mouse skin surface, while cationic deformable liposomes exhibited better ability in enhancing drug penetration through the skin (Oh et al., 2011). The same behaviour was also observed for lipophilic compounds, such as imperatorin. When the compound was incorporated in different surface charged deformable liposomes, cationic deformable liposomes exhibited the best penetration enhancing effect through rat skin (Lin et al., 2018). The possible explanation might rely on the electrostatic interaction between the positive surface charge of CDLs and the negative charge of the skin surface thus resulting in an increased drug penetration when incorporated in CDLs (Oh et al., 2011; Choi et al., 2017).

Fig. 2. Retention of hEGF onto the full thickness human skin surface from different liposomal formulations after *ex vivo* skin penetration studies over 6 hrs (n = 3 ± SD).

3.4 Mitogenic effect of hEGF-containing deformable liposomes

hEGF is one of the growth factors involved in the cell growth, differentiation and proliferation processes. These properties of hEGF are responsible for its positive contribution in many phases of wound healing (Desmet et al., 2018). Due to its low concentrations within chronic wounds, the external administration of hEGF is a promising approach for successful treatment of chronic wounds. However, hEGF bears several drawbacks that make its topical administration challenging. hEGF possesses a short half-life and is undergoing to rapid enzymatic degradation in the wound bed (Zeng and Harris, 2014). The incorporation of hEGF in nanosystems has already shown to assure its protection against degradation, a sustained drug release in the administration site and an increase in its therapeutic effect. We therefore tested our hEGF-containing deformable liposomes for mitogenic activity in human cells. We chose two dermal cell lines, namely human fibroblasts (HF) and human keratinocytes (HaCaT), whose proliferation in the wound bed would contribute to wound healing (Stunova and Vistejnova, 2018; Werner et al., 2007).

To perform the *in vitro* cell proliferation assay, we firstly reduced the liposome size to ca. 150 nm to avoid possible liposome precipitation during the experiment. Therefore, we performed more cycles of extrusion through polycarbonate membrane to obtain the desired liposome size (172.80±2.80, 191.53±7.44 and 168.23±2.73 nm for NDLs, CDLs and ADLs, respectively). We also determined the entrapment efficiency, which was found to be of 82.03, 79.33 and 82.52 % for NDLs, CDLs and ADLs, respectively. The additional size reduction did not affect the entrapment efficiency in all liposomes compared to liposomes having a size of 350 nm (Table 2). The amount of SPC in all liposomes was also determined in order to assure any

SPC loss during the extrusion and separation of unentrapped hEGF by dialysis. A SPC loss below 3.5 % was found for all liposomal formulations (data not shown).

Regarding hEGF-NDLs, a mitogenic effect in HF was observed only at the highest lipid concentration (50 µg/mL) (Fig. 3a). This effect was already evident after 24 hrs treatment, when a significant increase ($p < 0.03$) was observed compared to the untreated HF cells (control) and became even more evident after 48 hrs treatment ($p < 0.0001$). The mitogenic activity of hEGF-NDLs was, at the highest lipid concentration, stronger than activity of free hEGF (hEGF in PBS; $p < 0.03$) (Fig. 3a, d) after 48 hrs treatment.

hEGF-CDLs at both 1 and 10 µg/mL lipid concentrations showed no significant improvement on HF proliferation after 24 hrs treatment compared to control (Fig. 3b). However, the highest concentration of hEGF-CDLs exhibited a lower cell proliferation rate compared to the other tested formulations (Fig. 3b, d). This dose-dependent cytotoxic effect might be related to the presence of stearylamine, which can interact with the cell membrane thus damaging membranes' integrity and function (Tahara et al., 2018). However, empty CDLs at the same (highest) lipid concentration were not toxic to HF, therefore, the low cell proliferation observed for the highest concentration of hEGF-CDLs might be contributed to the high dose of hEGF (4 µg/mL), rather than the lipid. Interestingly, after 48 hrs treatment, hEGF-CDLs at lipid concentration of 10 µg/mL increased the HF proliferation by 40 % as compared to control ($p < 0.0001$) (Fig. 3b). This indicates that up to 10 µg/mL lipid concentration and 0.8 µg/mL hEGF concentration, hEGF-CDLs are not toxic to cells and can be employed for wound healing treatment. This positive effect was not detectable after 24 hrs treatment indicating that the cell response is dependent on the incubation time, as previously reported (Bertoncelj et al., 2014). The highest tested concentration of hEGF-CDLs showed lower mitogenic effect after 48 hrs treatment thus confirming the dose-dependency of cellular response.

hEGF-ADLs did not exhibit any significant enhancement in terms of HF proliferation after 24 hrs treatment compared to control and the other tested formulations (Fig. 3c, d). However, after 48 hrs, hEGF-ADLs at both lipid concentrations (10 and 50 μg/mL) exhibited a greater mitogenic effect than untreated cells ($p < 0.002$), allowing 48 and 77 % HF more proliferation than control, respectively. Moreover, the highest lipid and hEGF concentrations in hEGF-ADLs enhanced HF proliferation to a greater extent than both empty ADLs and free hEGF, by 33 and 45 % respectively (Fig. 3c, d). This further confirms the findings for hEGF-NDLs and hEGF-CDLs, indicating that the keratinocytes response depends both on the incubation time and hEGF/lipid concentrations. This is in accordance with previously published data on the keratinocytes response when exposed to growth factors-containing nanosystems (Bertoncelj et al., 2014). Comparing the three hEGF-containing liposomal formulations, the hEGF-ADLs assured the greatest mitogenic effect when tested at the highest lipid and hEGF concentrations (Fig. 3). *Ex vivo* skin penetration studies revealed the depot effect of hEGF-ADLs (Fig. 2), thus enabling its sustained release into human skin. This can assure a continuous binding of hEGF to its receptor, thus constantly activating the signalling pathway and prolonging the proliferation effect in cells. The similar trend was observed for hEGF incorporated in other nanosystems, such as nanofibers, solid lipid nanoparticles and nanostructured lipid carriers (Gainza et al., 2014; Garcia-Orue et al., 2017a; Jin et al., 2013).

The mitogenic effect of the hEGF liposomal formulations on HaCaT cells is shown in Fig. 4. The 24 hrs treatment showed that only the highest tested hEGF concentration (4 μg/mL), in both NDLs and ADLs was more effective in enhancing cell proliferation compared to both untreated cells and free hEGF (Fig.4a, c, d). hEGF-NDLs assured 26 and 32 % more cell proliferation more than control and free hEGF, respectively. On the other hand, hEGF-ADLs increased the percentage of living cells by respectively 36 and 41 % more compared to control and free hEGF. Therefore, between the two liposomal formulations, anionic deformable

liposomes (hEGF-ADLs) exhibited stronger mitogenic activity compared to hEGF-NDLs. This confirms the findings from the cell proliferation studies in HF, which, taken together, highlights the superiority of ADLs in improving the mitogenic effect of hEGF as compared to NDLs and CDLs. Regarding CDLs, 24 hrs treatment revealed the same trend as observed for the HF cell line (Fig. 3b). Up to a lipid concentration of 10 µg/mL, hEGF-containing CDLs showed to be not toxic also in HaCaT cell line, while a lower cell proliferation rate was observed for hEGF-CDLs at the highest lipid concentration (Fig. 4b). HaCaT cells treated for 48 hrs with all liposomal formulations proliferated to a lower extent compared to control (Fig. 4a, b, c). These findings differ from the results obtained with the HF cell line (Fig. 3a, b, c), showing that the growth rate is also dependent on the cell line employed for the *in vitro* cell proliferation assay in agreement with Gainza et al. (2014). In the case of hEGF-CDLs at the highest lipid and hEGF concentrations, lower mitogenic effect was also observed for both empty CDLs and free hEGF (Fig. 4b, d). Considering NDLs and CDLs, the lower proliferation activity might be related to the presence of polysorbate 20. Contri and co-workers observed the same decrease in cellular viability when nanocapsules containing similar surfactant, polysorbate 80, were tested on keratinocytes (Contri et al., 2016). The stronger cytotoxic effect observed for hEGF-CDLs compared to hEGF-NDLs might be due to a synergistic effect between polysorbate 20 and stearylamine. The stronger toxicity observed for hEGF-CDLs compared to empty CDLs highlights the dose-dependency response of HaCaT to hEGF, as found for HF cell line (Fig. 3b).

In addition to the influence of the surfactants, the reduced mitogenic effect observed at the highest concentration of hEGF-CDLs in both cell lines might be explained by the results from *in vitro* drug release and *ex vivo* skin penetration studies (Fig. 1, 2). CDLs were able to enhance both *in vitro* hEGF release and its skin penetration through the SC, resulting in a faster hEGF release from the cationic vesicles compared to neutral and anionic ones. This

might cause a faster uptake of hEGF followed by a rapid clearance from the site of action, thus reducing its therapeutic effect. ADLs enabled a more sustained hEGF release and depot onto the skin surface, which could explain the prolonged and stronger mitogenic activity of hEGF when incorporated in ADLs. This might be considered a further advantage in terms of reduction of administration frequency (Gainza et al., 2015a). Moreover, the enhanced long-term mitogenic effect of hEGF when incorporated in ADLs compared to the free hEGF suggests that ADLs offer protection of the drug, assuring longer stability and thus contributing to an enhanced therapeutic effect.

Fig. 3. Mitogenic effect of hEGF-containing deformable liposomes on human skin fibroblasts (HF) (n = 3 ± SD).

Fig. 4. Mitogenic effect of hEGF-containing deformable liposomes on human immortalized keratinocytes (HaCaT) (n = 3 ± SD).

We confirmed the potential of anionic deformable liposomes in *in vitro* conditions; however, their real clinical potential will have to be confirmed in animal and clinical studies.

4. Conclusions

Neutral, cationic and anionic deformable liposomes containing hEGF were prepared to improve dermal delivery of growth factors. The formulations were evaluated in terms of their physicochemical characteristics, *in vitro* drug release, *ex vivo* drug penetration through human skin, as well as the *in vitro* mitogenic activity in human fibroblasts and keratinocytes. All

deformable liposomes exhibited high hEGF entrapment, with a slightly higher entrapment efficiency for anionic deformable liposomes. hEGF-containing anionic deformable liposomes exhibited the most sustained *in vitro* release of hEGF and assured a depot system on the *ex vivo* human skin compared to neutral and cationic deformable liposomes. In addition, anionic deformable liposomes revealed to be the most effective in enhancing the mitogenic effect of hEGF in HF and HaCaT cell lines compared to the neutral and cationic deformable liposomes as well as hEGF in solution. Anionic deformable liposomes have shown to be a promising system for improved chronic wound therapy. Their clinical potential will have to be further explored.

Conflict of interest

The authors declare no conflicts of interest.

Acknowledgements

The authors thank Lipoid GmbH for kindly providing the lipids used in the experiments.

REFERENCES

Al Haushey, L., Bolzinger, M.A., Fessi, H., Briançon, S., 2010. rhEGF microsphere formulation and in vitro skin evaluation. J. Microencaps. 27, 14-24.

Al Shuwaili, A.H., Rasool, B.K.A., Abdulrasool, A.A., 2016. Optimization of elastic transfersomes formulations for transdermal delivery of pentoxifylline. Eur. J. Pharm. Biopharm. 102, 101-114.

Alemdaroğlu, C., Degim, Z., Celebi, N., Şengezer, M., Alömeroglu, M., Nacar, A., 2008. Investigation of epidermal growth factor containing liposome formulation effects on burn wound healing. J. Biomed. Mater. Res. A 85, 271-283.

Ascenso, A., Salgado, A., Euletério, C., Garcia Praça, F., Lopes Badra Bentley, M.V., Marques, H.C., Oliveira, H., Santos, C., Simões, S., 2014. *In vitro* and *in vivo* topical delivery studies of tretinoin-loaded ultradeformable vesicles. Eur. J. Pharm. Biopharm. 88, 48-55.

Ashtikar, M., Wacker, M.G., 2018. Nanopharmaceuticals for wound healing – Lost in translation? Adv. Drug Deliv. Rev. https://doi.org/10.1016/j.addr.2018.03.005

Bertoncelj, V., Pelipenko, J., Kristl, J., Jeras, M., Cukjati, M., Kocbek, P., 2014. Development and bioevaluation of nanofibers with blood-derived growth factors for dermal wound healing. Eur. J. Pharm. Biopham. 88, 64-74.

Bnyan, R., Khan, I., Ehtezazi, T., Saleem, I., Gordon, S., O'Neill, F., Roberts, M., 2018. Surfactant effects on lipid-based vesicles properties. J. Pharm. Sci. 107, 1237-1246.

Boateng, J., Catanzano, O., 2015. Advanced therapeutic dressings for effective wound healing - A review. J. Pharm. Sci. 104, 3653-3680.

Brewer, J., Bloksgaard, M., Kubiak, J., Ahm Sørensen, J., Bagatolli, L.A., 2013. Spatially resolved two-color diffusion measurements in human skin applied to transdermal liposome penetration. J. Investig. Dermatol. 133, 1260-1268.

Choi, J.U., Lee, S.W., Pangeni, R., Byun, Y., Yoon, I-S., Park, J.W., 2017. Preparation and *in vivo* evaluation of cationic elastic liposomes comprising highly skin-permeable growth factors combined with hyaluronic acid for enhanced diabetic wound-healing therapy. Acta Biomater. 57, 197-215.

Contri, R.V., Fiel, L.A., Alnasif, N., Pohlmann, A.R., Guterres, S.S., Schäfer-Korting, M., 2016. Skin penetration and dermal tolerability of acrylic nanocapsules: Influence of the surface charge and a chitosan gel used as vehicle. Int. J. Pharm. 507, 12-20.

Desmet, C.M., Préat, V., Gallez, B., 2018. Nanomedicine and gene therapy for the delivery of growth factors to improve perfusion and oxygenation in wound healing. Ad. Drug Deliv. Rev. Doi: 10.1016/j.addr.2018.02.001.

Dragicevic-Curic, N., Gräfe, S., Gitter, B., Winter, S., Fahr, A., 2010. Surface charged temoporfin-loaded flexible vesicles: *In vitro* skin penetration studies and stability. Int. J. Pharm. 384, 100-108.

du Plessis, J., Ramachandran, C., Weiner, N., Müller, D.G., 1994. The influence of particle size of liposomes on the deposition of drug into the skin. Int. J. Pharm. 103, 277-282.

Flaten, G.E., Palac, Z., Engesland, A., Filipović-Grčić, J., Vanić, Ž., Škalko-Basnet, N., 2015. *In vitro* skin models as a tool in optimization of drug formulation. Eur. J. Pharm. Sci. 75, 10-24.

Frykberg, R.G., Banks, J., 2015. Challenges in the treatment of chronic wounds. Adv. Wound Care 4, 560-582.

Gainza, G., Pastor, M., Aguirre, J.J., Villullas, S., Pedraz, J.L., Hernandez, R.M., Igartua, M., 2014. A novel strategy for the treatment of chronic wounds based on the topical administration of rhEGF-loaded lipid nanoparticles: *In vitro* bioactivity and *in vivo* effectiveness in healing-impaired *db/db* mice. J. Control. Release 185, 51-61.

Gainza, G., Chu, W.S., Guy, R.H., Pedraz, J.L., Hernandez, R.M., Delgado-Charro, B., Igartua, M., 2015a. Development and *in vitro* evaluation of lipid nanoparticle-based dressings for topical treatment of chronic wounds. Int. J. Pharm. 490, 404-411.

Gainza, G., Villullas, S., Pedraz, J.L., Hernandez, R.M., Igartua, M., 2015b. Advances in drug delivery systems (DDSs) to release growth factors for wound healing and skin regeneration. Nanomedicine: NBM 11, 1551-1573.

Garcia-Orue, I., Gainza, G., Gutierrez, F.B., Aguirre, J.J., Evora, C., Pedraz, J.L., Hernandez, R.M., Delgado, A., Igartua, M., 2017a. Novel nanofibrous dressings containing rhEGF and *Aloe vera* for wound healing applications. Int. J. Pharm. 523, 556–566.

Garcia-Orue, I., Pedraz, J.L., Hernandez, R.M., Igartua, M., 2017b. Nanotechnology-based delivery systems to release growth factors and other endogenous molecules for chronic wound healing. J. Drug Deliv. Sci. Technol. 42, 2-17.

González-Rodríguez, M.L., Rabasco, A.M., 2011. Charged liposomes as carrier to enhance the permeation through the skin. Expert Opin. Drug Deliv. 8, 857-871.

Hamdan, S., Pastar, I., Drakulich, S., Dikici, E., Tomic-Canic, M., Deo, S., Daunert, S., 2017. Nanotechnology-driven therapeutic interventions in wound healing: potential uses and applications. ACS Cent. Sci. 3, 163-175.

Hood, R.R., Kendall, E.L., Junqueira, M., Vreeland, W.N., Quezado, Z., Finkel, J.C., DeVoe, D.L., 2014. Microfluidic-enabled liposomes elucidate size-dependent transdermal transport. PLoS ONE 9(3): e92978.

Hurler, J., Berg, O.A., Skar, M., Conradi, A.H., Johnsen, P.J., Škalko-Basnet, N., 2012. Improved burns therapy: Liposomes-in-hydrogel delivery system for mupirocin. J. Pharm. Sci. 101, 3906-3915.

Ingebrigtsen, S.G., Škalko-Basnet, N., de Albuquerque Cavalcanti Jacobsen, C., Holsæter, A.M., 2017. Successful co-encapsulation of benzoyl peroxide and chloramphenicol in liposomes by a novel manufacturing method – dual asymmetric centrifugation. Eur. J. Pharm. Sci. 97, 192-199.

Jahromi, M.A.M., Zangabad, P.S., Basri, S.M.M., Zangabad, K.S., Ghamarypour, A., Aref, A.R., Karimi, M., Hamblin, M.R., 2018. Nanomedicine and advanced technologies for burns: preventing infection and facilitating wound healing. Adv. Drug Deliv. Rev. 123, 33-64.

Jain, S., Patel, N., Shah, M.K., Khatri, P., Vora, N., 2017. Recent advances in lipid-based vesicles and particulate carriers for topical and transdermal application. J. Pharm. Sci. 106, 423-445.

Jeon, S.O., Hwang, H.J., Oh, D.H., Seo, J.E., Chun, K.H., Hong, S.M., Kim, M.J., Kim, W.C., Park, M.S., Yoon, C.H., Min, K.H., Suh, C.W., Lee, S., 2012. Enhanced percutaneous delivery of recombinant human epidermal growth factor employing nano-liposome system. J. Microencapsul. 29, 234-241.

Jin, G., Prabhakaran, M.P., Kai, D., Ramakrishna, S., 2013. Controlled release of multiple epidermal induction factors through core-shell nanofibers for skin regeneration. Eur. J. Pharm. Biopharm. 85, 689-698.

Jøraholmen, M.W., Basnet, P., Acharya, G., Škalko-Basnet, N., 2017. PEGylated liposomes for topical vaginal therapy improve delivery of interferon alpha. Eur. J. Pharm. Biopharm. 113, 132-139.

Kalashnikova, I., Das, S., Seal, S., 2015. Nanomaterials for wound healing: scope and advancement. Nanomedicine (Lond.) 10, 2593-2612.

Kaminski, G.A.T., Sierakowski, M.R., Pontarolo, R., dos Santos, L.A., de Freitas, R.A., 2016. Layer-by-layer polysaccharide-coated liposomes for sustained delivery of epidermal growth factor. Carbohydr. Polym. 140, 129–135.

Lin, H., Xie, Q., Huang, X., Ban, J., Wang, B., Wei, X., Chen, Y., Lu, Z., 2018. Increased skin permeation efficiency of imperatorin via charged ultradeformable lipid vesicles for transdermal delivery. Int. J. Nanomed. 13, 831-842.

Mota, A.H., Rijo, P., Molpeceres, J., Pinto Reis, C., 2017. Broad overview of engineering of functional nanosystems for skin delivery. Int. J. Pharm. 532, 710-728.

Nunez, M., Mayo, K.H., Starbuck, C., Lauffenburger, D., 1993. pH sensitivity of epidermal growth factor receptor complexes. J. Cell. Biochem. 51, 312-321.

Oh, E.K., Jin, S.E., Kim, J.K., Park, J.S., Park, Y., Kim, C.K., 2011. Retained topical delivery of 5-aminolevulinic acid using cationic ultradeformable liposomes for photodynamic therapy. Eur. J. Pharm. Sci. 44, 149–157.

Pleguezuelos-Villa, M., Mir-Palomo, S., Díez-Sales, O., Vila Buso, M.A.O., Ruiz Sauri, A., Nácher, A., 2018. A novel ultradeformable liposomes of Naringin for anti-inflammatory therapy. Colloids Surf. B. Biointerfaces 162, 265-270.

Roberts, M.S., Mohammed, Y., Pastore, M.N., Namjoshi, S., Yousef, S., Alinaghi, A., Haridass, I.N., Abd, E., Leite-Silva, V.R., Benson, H.A.E., Grice, J.E., 2017. Topical and cutaneous delivery using nanosystems. J. Control. Release 247, 86-105.

Saghazadeh, S., Rinoldi, C., Schot, M., Kashaf, S.S., Sharifi, F., Jalilian, E., Nuutila, K., Giatsidis, G., Mostafalu, P., Derakhshandeh, H., Yue, K., Swieszkowski, W., Memic, A.,

Tamayol, A., Khademhosseini, A., 2018. Drug delivery systems and materials for wound healing applications. Adv. Drug Deliv. Rev. https://doi.org/10.1016/j.addr.2018.04.008

Sala, M., Diab, R., Elaissari, A., Fessi, H., 2018. Lipid nanocarriers as skin drug delivery systems: Properties, mechanisms of skin interactions and medical applications. Int. J. Pharm. 535, 1-17.

Stunova, A., Vistejnova, L., 2018. Dermal fibroblasts – A heterogenous population with regulatory function in wound healing. Cytokine Growth Factor Rev. 39, 137-150.

Tahara, K., Kobayashi, M., Yoshida, S., Onodera, R., Inoue, N., Takeuchi, H., 2018. Effects of cationic liposomes with stearylamine against virus infection. Int. J. Pharm. 543, 311-317.

Ternullo, S., de Weerd, L., Flaten, G.E., Holsæter, A.M., Škalko-Basnet, N., 2017a. The isolated perfused human skin flap model: A missing link in skin penetration studies? Eur. J. Pharm. Sci. 96, 334-341.

Ternullo, S., de Weerd, L., Holsæter, A.M., Flaten, G.E., Škalko-Basnet, N., 2017b. Going skin deep: A direct comparison of penetration potential of lipid-based nanovesicles on the isolated perfused human skin flap model. Eur. J. Pharm. Biopharm. 121, 14-23.

Werner, S., Krieg, T., Smola, H., 2007. Keratinocyte–fibroblast interactions in wound healing. J. Investig. Dermatol. 127, 998-1008.

Xue, M., Zhao, R., Lin, H., Jackson, C., 2018. Delivery systems of current biologicals for the treatment of chronic cutaneous wounds and severe burns. Adv. Drug Deliv. Rev. https://doi.org/10.1016/j.addr.2018.03.002

Zeng, F., Harris, R.C., 2014. Epidermal growth factor, from gene organization to bedside. Semin. Cell. Dev. Biol. 28, 2-11.

Zhai, Y., Zhai, G., 2014. Advances in lipid-based colloid systems as drug carrier for topic delivery. J. Control. Release 193, 90-99.

Zhang, Y., Ng, W., Feng, X., Cao, F., Xu, H., 2017. Lipid vesicular nanocarrier: Quick encapsulation efficiency determination and transcutaneous application. Int. J. Pharm. 516, 225-230.

Figures:

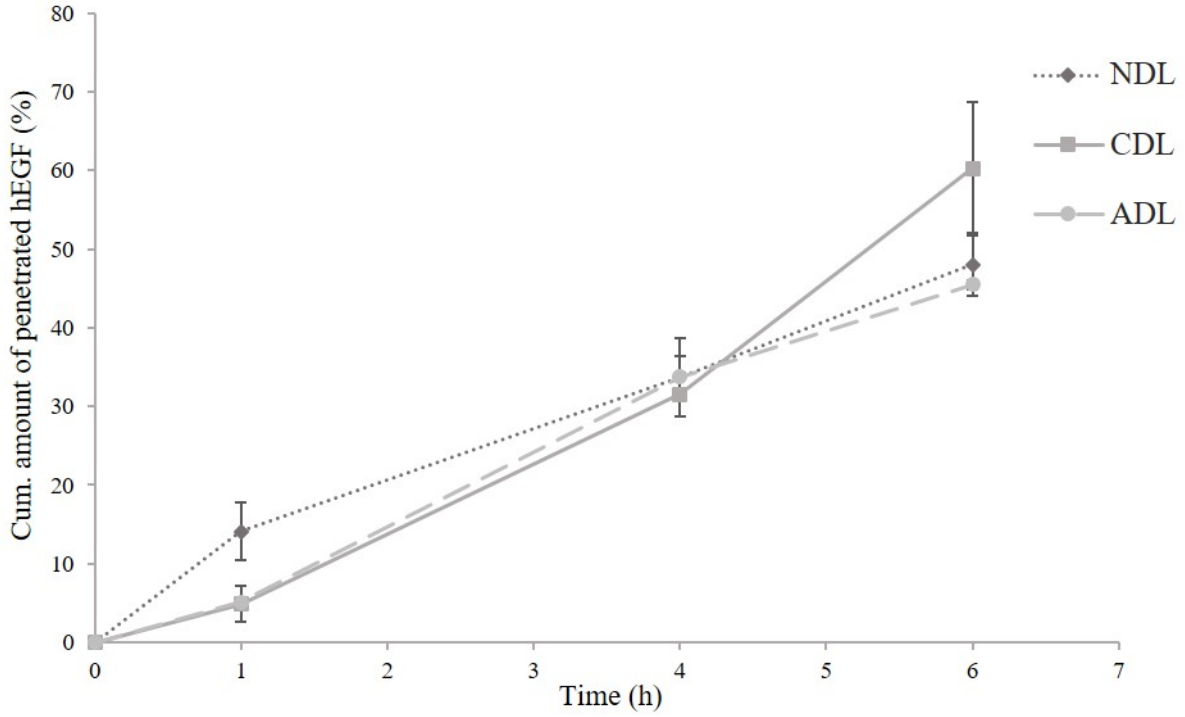

Fig. 1. *In vitro* hEGF release over 6 hrs from different liposomal formulations through polyamide membrane (n = 2 ± SD).

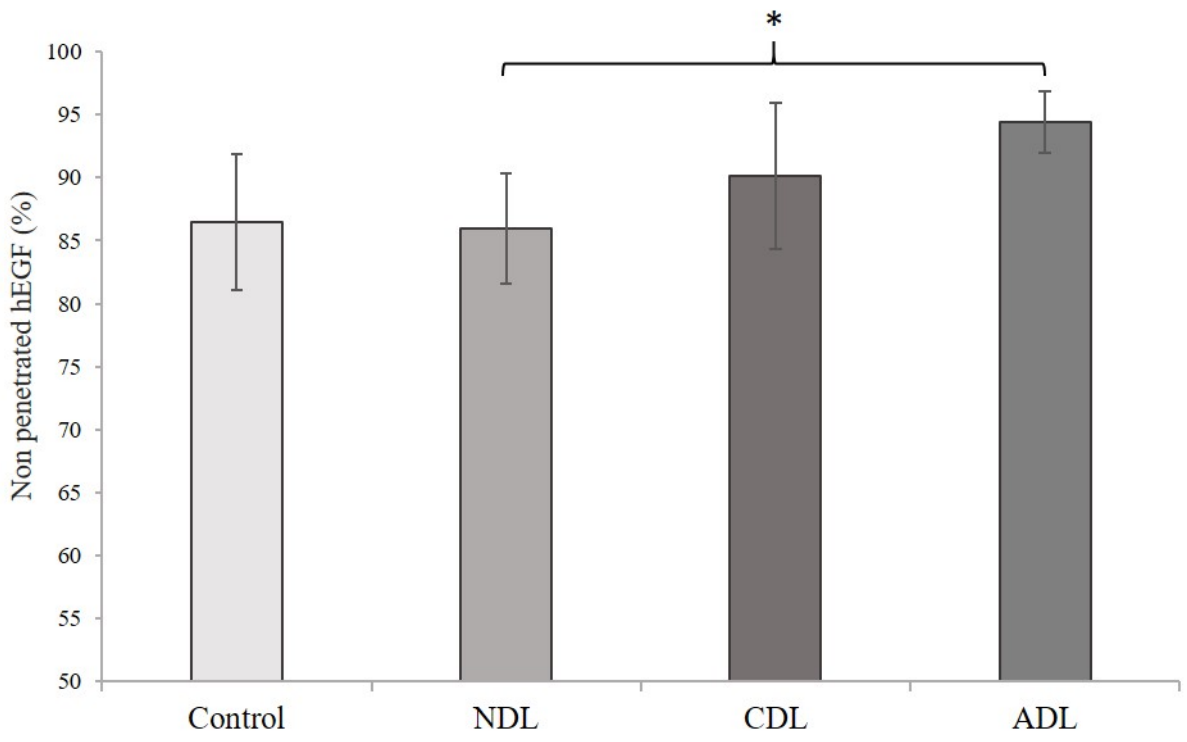

Fig. 2. Retention of hEGF onto the full thickness human skin surface from different liposomal formulations after *ex vivo* skin penetration studies over 6 hrs (n = 3 ± SD).

As a control, hEGF in PBS at similar concentration as hEGF in liposomes was used.

$^{*}p = 0.04$

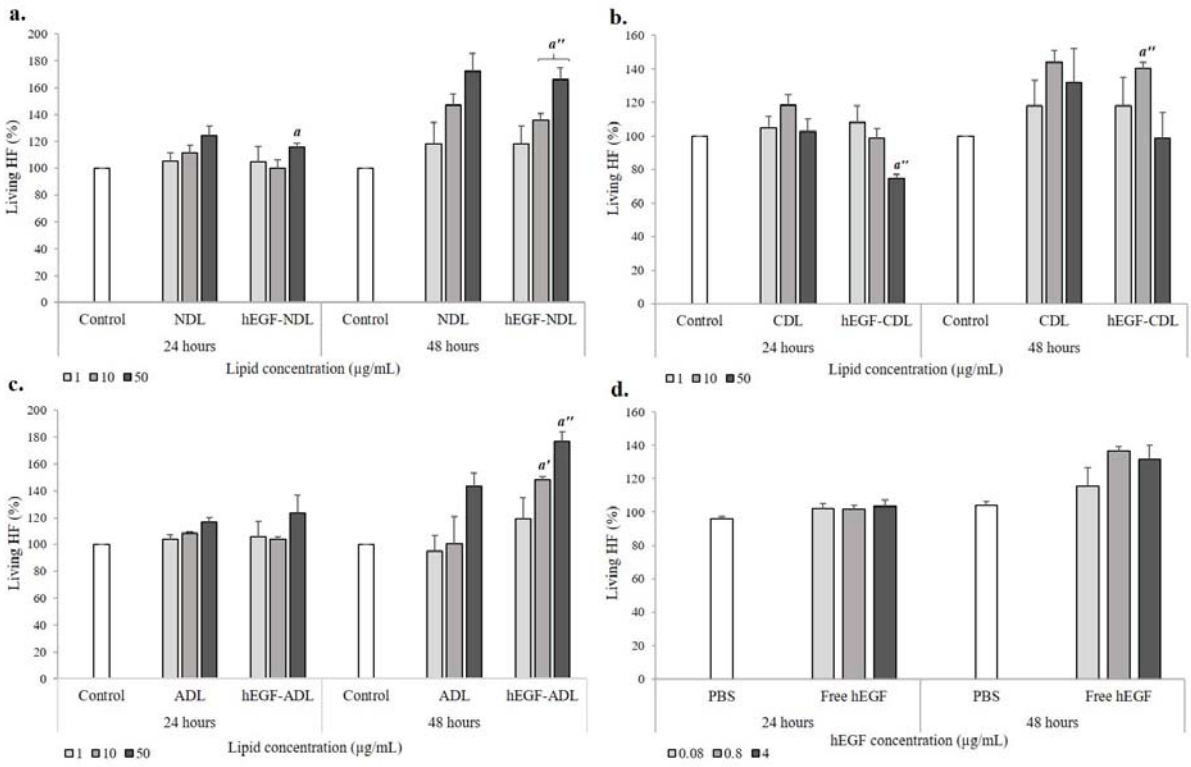

Fig. 3. Mitogenic effect of hEGF-containing deformable liposomes on human skin fibroblasts (HF) (n = 3 ± SD).

The mitogenic effect of hEGF-NDLs (a), hEGF-CDLs (b) and hEGF-ADLs (c) on HF cells was investigated for 24 and 48 hours, respectively. NDLs, CDLs and ADLs represent empty neutral, cationic and anionic deformable liposomes, respectively. Untreated cells are referred as control. The d represents the mitogenic effect of hEGF in PBS (free hEGF) at same tested concentrations as for hEGF entrapped in liposomes.

[a]Significantly higher than control ([a]$p < 0.03$, [a']$p < 0.002$, [a'']$p < 0.0001$)

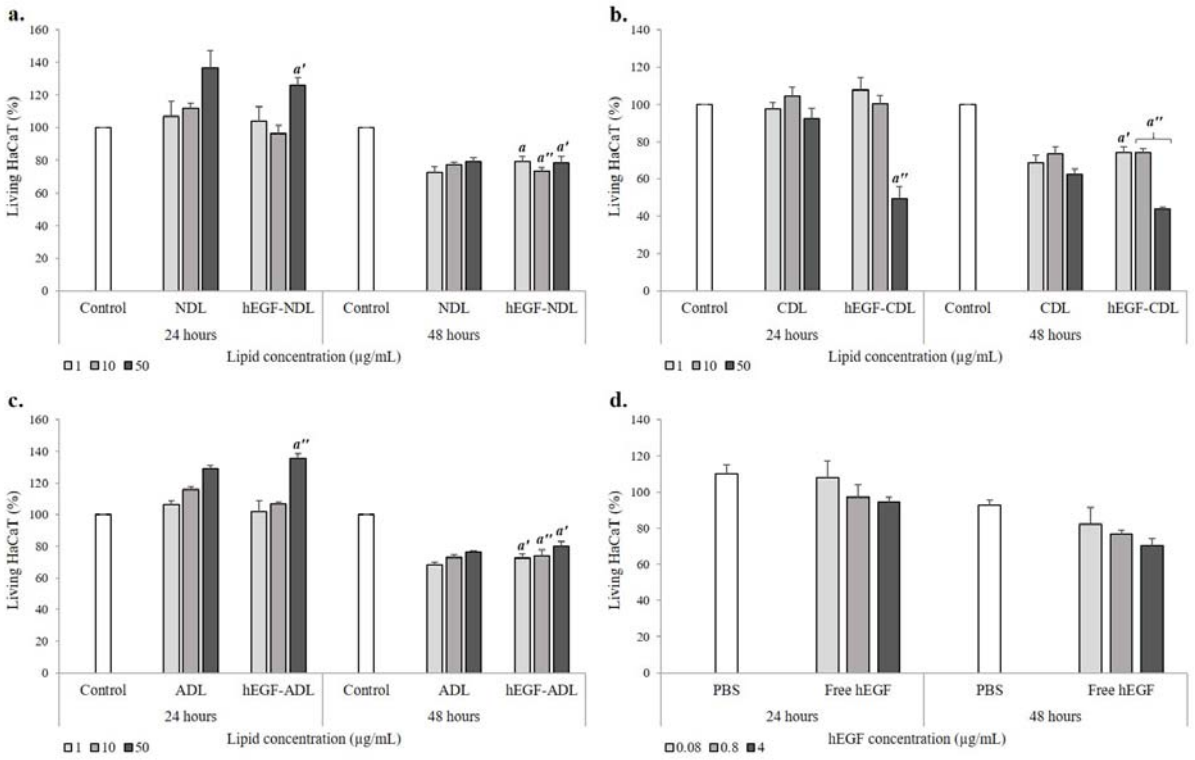

Fig. 4. Mitogenic effect of hEGF-containing deformable liposomes on human immortalized keratinocytes (HaCaT) (n = 3 ± SD).

The mitogenic effect of hEGF-NDLs (a), hEGF-CDLs (b) and hEGF-ADLs (c) on HaCaT cells was investigated for 24 and 48 hours, respectively. NDLs, CDLs and ADLs represent empty neutral, cationic and anionic deformable liposomes, respectively. Untreated cells are referred as control. The d represents the mitogenic effect of drug in PBS (free hEGF) at same tested concentrations as for hEGF entrapped in liposomes.

[a]Significantly higher than control ([a]$p < 0.03$, [a']$p < 0.002$, [a'']$p < 0.0001$)

Tables:

Table 1. Composition of hEGF-containing deformable liposomes bearing different surface charge.

Liposomes[a, b]	hEGF (μg)	SPC (mg)	Polysorbate 20 (mg)	Stearylamine (mg)	Sodium deoxycholate (mg)
hEGF-NDLs	100	170	30	-	-
hEGF-CDLs	100	153	30	17	-
hEGF-ADLs	100	170	-	-	30

[a]All liposomal formulations were prepared to a final volume of 5 mL.

[b]Empty NDLs, CDLs and ADLs (without hEGF) were prepared using the same composition as for hEGF-NDLs, hEGF-CDLs and hEGF-ADLs, respectively.

Table 2. Characteristics of the deformable liposomes containing hEGF (n = 3 ± SD).

Formulation	Size (nm)	PI[a]	Zeta potential (mV)	Entrapment efficiency (%)
hEGF-NDLs	350.0 ± 8.2	0.22 ± 0.01	-0.5 ± 0.6	80.5 ± 1.5
hEGF-CDLs	361.7 ± 32.5	0.30 ± 0.02	45.8 ± 1.8	80.8 ± 0.7
hEGF-ADLs	322.7 ± 12.5	0.26 ± 0.00	-35.7 ± 1.2	84.1 ± 6.1

[a]Polydispersity index

Paper IV

Nanocarriers for dermal delivery: The carrier surface charge affects biological activities of curcumin

Running title: *dermal curcumin therapy*

Selenia Ternullo[a], Eivind Gagnat[a], Kjersti Julin[b], Mona Johannessen[b], Purusotam Basnet[c,d], Željka Vanić[e], Nataša Škalko-Basnet[a,*]

[a]Drug Transport and Delivery Research Group, Department of Pharmacy, University of Tromsø The Arctic University of Norway, Universitetsveien 57, 9037 Tromsø, Norway

[b]Research Group of Host Microbe Interactions, Department of Medical Biology, University of Tromsø The Arctic University of Norway, Universitetsveien 57, 9037 Tromsø, Norway

[c]IVF Clinic, Department of Obstetrics and Gynecology, University Hospital of North Norway, Sykehusvegen 38, 9019 Tromsø, Norway

[d]Women's Health and Perinatology Research Group, Department of Clinical Medicine, University of Tromsø The Arctic University of Norway, Universitetsveien 57, 9037 Tromsø, Norway

[e]Department of Pharmaceutical Technology, Faculty of Pharmacy and Biochemistry, University of Zagreb, A. Kovačića 1, 10 000 Zagreb, Croatia

[*]Corresponding author: Nataša Škalko-Basnet, Drug Transport and Delivery Research Group, Department of Pharmacy, University of Tromsø The Arctic University of Norway,

Universitetsveien 57, 9037 Tromsø, Norway; Tel: +47-776-46640; Fax: +47-776-46151; Email: natasa.skalko-basnet@uit.no

Abstract

Curcumin, a multi-targeting pharmacologically active compound, is a promising molecule for the treatment of skin inflammation and infections. However, its hydrophobic nature is a challenge for the development of its pharmaceutical products, including dermatopharmaceuticals. Here we propose deformable liposomes (DLs) as a mean to overcome the curcumin limitations related to skin treatment. We explored the properties and biological effects of curcumin containing DLs with varying surface charge by preparing the neutral (NDLs), cationic (CDLs) and anionic (ADLs) nanocarriers. With a vesicle size range of 200-300 nm, DLs exhibited entrapment efficiencies mirroring the type of employed surfactant. Curcumin-CDLs provided the most sustained *ex vivo* penetration of curcumin through the full thickness human skin. When tested against *Staphylococcus aureus* and *Streptococcus pyogenes*, all DLs inhibited *in vitro* bacterial growth significantly. CDLs showed the most potent anti-bacterial activity. All curcumin-DLs showed better *in vitro* anti-inflammatory activity compared to curcumin in solution (control); curcumin-CDLs were found to be the most potent. Curcumin-DLs did not show toxic effects *in vitro* on human skin fibroblasts. The incorporation of curcumin in DLs enabled both its sustained skin penetration and enhancement of its therapeutic properties. Cationic nanocarriers enhanced the activities of curcumin to a greatest extent.

Keywords: curcumin; deformable liposomes; liposome surface charge; skin penetration; anti-bacterial; anti-inflammatory.

Abbreviations: ADLs, anionic deformable liposomes; CCK-8, Cell Counting Kit-8; CDLs, cationic deformable liposomes; DLs, deformable liposomes; DOTAP, 1,2-dioleoyl-3-

trimethylammonium propane; HFF, human foreskin fibroblasts; HLB, hydrophilic/lipophilic balance; IMDM, Iscove's modified Dulbecco's medium; LPS, lipopolysaccharide; NDLs, neutral deformable liposomes; NO, nitric oxide; NFκB, nuclear transcription factor kappa B; PBS, phosphate buffer saline; PCS, photon correlation spectroscopy; PI, polydispersity index; P20, polysorbate 20; PG, propylene glycol; SDC, sodium deoxycholate; SPC, soybean phosphatidylcholine; SA, stearylamine; SC, *stratum corneum*.

1. Introduction

Curcumin is a polyphenol found in the rhizome of the turmeric plant *Curcuma longa L*. This natural compound is nowadays considered a "gold" molecule due to its anti-oxidant, anti-bacterial and anti-inflammatory properties, among other therapeutic activities [1]. Research over the past 30 years confirmed its therapeutic potential against several inflammatory-related diseases, such as the cancer, autoimmune diseases, neurological diseases, lung and liver diseases [2]. The anti-inflammatory properties of curcumin are the result of its interaction with several molecules involved in inflammation pathways. Curcumin is able to decrease the expression of various pro-inflammatory cytokines by downregulating the nuclear transcription factor kappa B (NFκB) pathway thus contributing to reduced inflammation [3]. Additionally, the suppression of cyclooxygenases, lipoxygenase and inducible nitric oxide (NO) synthase enzymes mediated by curcumin has shown to be beneficial to decrease the inflammation degree in several inflammatory diseases [4,5,6]. In spite of the evidently high potential of this pleiotropic active compound in the treatment of inflammatory diseases, its limitations such as low solubility and poor bioavailability limit its oral administration. Research has therefore moved towards topical administration of curcumin, which has shown to be equally promising; for example, in vaginal administration for treatment of chronic vaginal inflammation [4]. Topical administration onto skin appears equally encouraging and curcumin has shown to be a good candidate for the treatment of hyper-inflammatory wounds, such as chronic wounds and burns [7]. Moreover, curcumin is highly promising in controlling the scar formation and treatment of hypertrophic post burn scarring [8]. In addition to the well-established anti-inflammatory property of curcumin, its anti-bacterial activity become equally important as alternative antimicrobial considering the ongoing evolvement of bacterial resistance to antibiotics [9]. Moreover, curcumin as a topical anti-bacterial agent might be a promising alternative to the overuse of antibiotics, both locally and systemically. The wounded/impaired

skin is highly prone to bacterial colonization due to the nutrient-rich environment provided by high levels of wound exudate [10]. Curcumin might therefore synergistically act in the treatment of chronic wounds and burns. Similarly to its anti-inflammatory activity, the anti-bacterial potential of curcumin is related to its action at molecular level, including suppression of one of the essential protein, FtsZ, which initiates bacterial cell division [11].

However, the hydrophobic nature of curcumin limits its formulation in pharmaceutical products for localized skin therapy, such as hydrophilic wound dressings such as hydrogels. Moreover, it is chemically unstable, especially at the physiological pH, if not protected by a carrier. Its direct applications locally onto the skin, in a vehicle without a carrier, might cause erythema, peeling and hot phenomenon, due to its photosensitivity [12]. Therefore, the main focus is on finding novel approaches to enable curcumin solubilization and increase its stability to achieve optimal therapeutic outcome while minimizing the side effects. Nanotechnology-based delivery systems are one of the novel strategies employed to overcome limited pharmaceutical and therapeutic potential of curcumin for topical administration. Up to now, several phospholipid-based nanocarriers have been employed to overcome its limitations in dermal delivery [1,7]. Deformable liposomes (DLs) were proposed a superior carrier for dermal delivery of molecules, including poorly soluble ones. DLs can incorporate lipophilic drugs in their phospholipid bilayer thus improving their solubility and assuring protection from chemical instability [13,14]. Moreover, DLs can prolong drug retention time onto/in the skin and assure sustained/controlled drug release [15]. An additional advantage of DLs is the possibility to modify their composition to obtain tailored physicochemical properties, directly affecting their fate as dermal nanocarriers. The liposomal surface charge plays an important role in the interaction between liposomes and *stratum corneum* (SC) corneocytes, thus influencing the skin penetration of incorporated drug mediated by the liposomes [16]. Curcumin, as described earlier, is active at cellular level exerting both anti-bacterial and anti-inflammatory activities

[17]. Therefore, it is expected that DLs enable a targeted delivery of curcumin to the cellular level, thus enhancing its cellular uptake and improving its therapeutic effect. This mechanism has shown to be related to the liposomal surface charge [18]. As for the nanocarrier/corneocytes interaction, electrostatic interactions might occur between charged DLs and cell membranes. Positively charged DLs are expected to exhibit higher affinity for the negatively charged domains of the cell membranes thus enhancing a cellular uptake of curcumin [19].

The aim of the present study was to develop an efficient liposomal formulation for dermal delivery of curcumin focusing on its potential for treatment of skin infection and inflammation. Therefore, neutral, cationic and anionic deformable liposomes (NDLs, CDLs and ADLs, respectively) containing curcumin were prepared. The role of the liposomal surface charge was evaluated in *ex vivo* skin penetration studies using the full thickness human skin. The *in vitro* anti-bacterial and anti-inflammatory activities of curcumin-DLs were evaluated. *In vitro* cell viability study using human foreskin fibroblasts (HFF) was performed to assess the safety of the liposomal formulations in healthy human skin cells.

2. Materials and methods

2.1. Materials

Curcumin (≥ 94 % curcuminoid content; ≥ 80 % curcumin) was purchased from Sigma-Aldrich (St. Louis, USA). Lipoid S 100 (> 94 % soybean phosphatidylcholine, SPC) was a generous gift from Lipoid GmbH (Ludwigshafen, Germany). Polysorbate 20 (P20), stearylamine (SA), sodium deoxycholate (SDC), propylene glycol (PG), methanol, disodium hydrogen phosphate dihydrate, monobasic potassium phosphate, sodium chloride, ammonium molybdate, Fiske-Subbarow reducer agent, phosphorus standard solution, RPMI 1640 medium, lipopolysaccharide (LPS) and Iscove's modified Dulbecco's medium (IMDM) were obtained

from Sigma-Aldrich (St. Louis, USA). Hydrogen peroxide 30 % was purchased from Merck KGaA (Darmstadt, Germany), sulphuric acid from May & Baker LTD (Dagenham, UK), sulfanilamide, naphthylethylenediamine dihydrochloride and phosphoric acid from Sigma Life Science (Sigma-Aldrich Norway AS, Oslo) and Albunorm® (human serum albumin, 200 mg/mL) from Octapharma AG (Lachen, Switzerland). HFF (CCD-1112Sk, ATCC® CRL-2429™) and murine macrophage RAW 264.7 cell lines were purchased from ATCC (Manassas, USA).

2.2. Preparation of deformable liposomes

NDLs were made of SPC and P20 (total 200 mg) in a weight ratio of 85:15, respectively. CDLs were prepared by addition of SA in the same lipid mixture as used for NDLs. The ratio of SA to SPC was 1:9 (w/w). ADLs were made of SPC and SDC, maintaining the same weight ratio between lipid and surfactant (85:15, respectively) as for NDLs and CDLs. A complete overview of the liposomal composition is given in Table 1.

All DLs were prepared by the conventional film method [20]. Briefly, curcumin (20 mg) and lipid (200 mg: SPC and, when applicable, P20, SA and SDC), were dissolved in methanol. A thin lipid film was obtained after evaporation of the solvent in a rotary vacuum evaporator (Büchi Rotavapor R-124 with Büchi Vacuum Pump V-700, Büchi Labortechnik AG, Flawil, Switzerland). The lipid film was kept under vacuum (55 mbar) for 1 hr at 55 ºC and subsequently resuspended in 10 mL of phosphate buffer saline (PBS) (pH 7.4; 2.98 g/L Na_2HPO_4 $2H_2O$, 0.19 g/L KH_2PO_4, 8 g/L NaCl). The liposomal formulations were stored at 4 °C overnight. For assessment of liposomes' elasticity, anti-bacterial and anti-inflammatory activities of curcumin-DLs and *in vitro* cell viability study, empty (curcumin-free) NDLs, CDLs and ADLs were prepared using the same liposomal composition as for curcumin-DLs (Table 1).

The size of all DLs was reduced by hand extrusion through the polycarbonate membrane (Nuclepore® Track-Etched Membranes, Whatman House, Maidstone, UK). The pore size of the membranes and the number of extrusion cycles were optimized for each liposomal formulation to obtain liposomes between 200 and 300 nm in size (Table 1). Five cycles of extrusion through 800 nm pore size membrane were performed for all DLs. Subsequently, NDLs were extruded four times through 400 nm pore size membrane, while CDLs and ADLs were extruded through the same pore size membrane two and seven times, respectively. Prior to extrusion, CDLs (empty and curcumin containing) were thermostated for 10 min at 55 °C.

Table 1. Composition of curcumin-DLs.

Liposomes[a]	Curcumin (mg)	SPC (mg)	P20 (mg)	SA (mg)	SDC (mg)	Extrusion through polycarbonate membrane[b]
NDLs	20	170	30	-	-	5 x 800 nm 4 x 400 nm
CDLs	20	153	30	17	-	5 x 800 nm 2 x 400 nm
ADLs	20	170	-	-	30	5 x 800 nm 7 x 400 nm

[a]Each liposomal formulation was prepared in triplicates. The final volume was 10 mL. For empty liposomes (without curcumin), the same lipid/surfactant composition was used.

[b]The extrusion is described as the number of extrusion cycles through the corresponding pore size membrane (nm).

2.3. Liposomal size and zeta potential measurements

The vesicle size of all DLs was determined by photon correlation spectroscopy (PCS) using a NICOMP Submicron Particle Sizer Model 370 (NICOMP Particle Sizing system, Santa

Barbara, California, USA) [20]. The liposomes were diluted with PBS to obtain a suitable particle intensity (250-350 kHz). All measurements were run in triplicates (run time of 10 min for each measurement) at room temperature (23-24 °C) and using the intensity-weighted distribution mode.

Zeta potential determination was performed using Malvern Zetasizer Nano – ZS (Malvern, Oxford, UK) [20]. Samples were diluted 1:20 (v/v) with filtered water (0.2 µm syringe filter, Bulk Acrodisc® 25 mm Syringe Filter, Pall Life Sciences, East Hills, New York, USA) or filtered water containing SDC for ADLs. An attenuator of 6-7 was used for all measurement runs (equilibration time of 180 s, 25 °C). The measurements were performed in triplicates.

2.4. Entrapment efficiency of curcumin in DLs

DLs were centrifuged (Biofuge stratos centrifuge with a swinging bucket rotor 4 x 180 mL; Heraeus instruments GmbH, Hanau, Germany) at 3,000 *g* for 10 min (10 °C) to remove the free (unentrapped) curcumin. After dissolving the lipids with methanol, the entrapped curcumin in all DLs (supernatant) was quantified by UV–VIS spectrophotometry at 425 nm (SpectraMax 190 Microplate Reader, Molecular Devices, California, USA). Prior to the absorbance measurement, all samples were further diluted 1:1 (v/v) with PBS to avoid evaporation of methanol. A standard curve of curcumin in methanol/PBS (1:1, v/v) was used in the concentration range of 1-20 µg/mL ($R^2 = 0.9996$).

2.5. Phospholipid content measurement

To express the entrapment efficiency as the curcumin/lipid ratio and follow to possible loss of lipids during the extrusion, the amount of SPC in all liposomal dispersions was quantified by phosphorous assay [21]. Aliquots of liposomes (50 µL) were diluted to a final volume of 10

mL with distilled water and then incubated at 160 °C for 3 hrs after the addition of sulfuric acid (5 M). Hydrogen peroxide 30 % was added and the samples incubated at 160 °C for additional 1.5 hrs. After the heating, ammonium molybdate (0.22 %, w/v) and Fiske-Subbarow reducer were added and the solution incubated at 100 °C for 7 min. The samples were then analyzed spectrophotometrically on a SpectraMax 190 Microplate Reader (Molecular Devices, California, USA) at 830 nm using a standard curve of phosphorous standard solution.

2.6. Liposome elasticity measurements

The bilayer elasticity of all DLs was determined as reported earlier [22]. The liposomal dispersions were extruded through the polycarbonate membrane with a pore size of 100 nm at a constant external pressure of 2.5 bar. The amount of liposomal dispersion after 5 min of extrusion was determined (J). The vesicle mean diameter and polydispersity index were monitored by PCS measurements before and after the extrusion, respectively. The degree of membrane elasticity (E) of all curcumin-DLs was calculated using the following equation:

$$E = J \cdot \left(r_v / r_p\right)^2,$$

where J is the amount of liposomal dispersion (g) extruded in 5 min, r_v is the mean diameter (nm) of liposomes after the extrusion and r_p is the pore size membrane (nm).

Empty NDLs, CDLs and ADLs (without curcumin) were used as control, respectively.

Empty and curcumin containing CDLs were thermostated at 55°C prior to measurements.

2.7. Ex vivo skin penetration studies

Curcumin penetration through the full thickness human skin was investigated in the Franz diffusion cells of 1.77 cm^2 diffusion area (PermeGear, Bethlehem, USA) [20]. Human skin,

derived from the excess of skin panni, was obtained from the abdomen of female patients after plastic surgery. The patients were informed on the use of the skin residue for this study and signed a written consent prior the surgery. The excess of skin panni is normally discarded after surgery, therefore no ethical approval by the Norwegian Ethical Committee was required. The experiments were carried out in accordance with the Declaration of Helsinki Principles. The full thickness human skin was separated from the subcutaneous fat and rinsed with PBS (pH 7.4). The human skin samples were stored at -20 °C and thawed prior the use. The human skin, with a thickness of 1.10-1.30 mm, was mounted with SC facing the donor chamber. The receptor chamber (volume of 12 mL) was filled with Albunorm® (5 %, v/v) in PBS (pH 7.4) solution and the receptor medium was maintained at 32 °C during the experiment. All curcumin-DLs were tested. To explore the effect of the liposomal surface charge on the skin penetration of curcumin, deformable liposomes with neutral surface (NDLs) were used as a control. Each formulation (600 µL) was pipetted in the donor chamber; the experiments were performed for 24 hrs and samples (500 µL) withdrawn from receptor medium at certain time intervals (1, 2, 3, 4, 5, 6, 7, 8 and 24 hrs, respectively). After each sampling, the receptor chamber was refilled with equal volume of fresh receptor medium to assure the sink conditions. At the end of the experiment, curcumin in the receptor medium (penetrated) was quantified as described in Section 2.4. The quantification of penetrated curcumin was performed using a standard curve in Albunorm® (5 %, v/v) in PBS (pH 7.4). The experiments were run in triplicates.

2.8. Anti-bacterial susceptibility testing

All curcumin-DLs were assessed in terms for their *in vitro* anti-bacterial activity against two clinical strains of Gram-positive bacteria, namely *Staphylococcus aureus subsp. aureus* Rosenbach MSSA476 (ATCC- BAA-1721, LGC standard AB, Sweden) and *Streptococcus*

pyogenes (ATCC 19615), using the modified broth dilution method [23]. To perform the experiment, a bacterial suspension with a turbidity of 0.5 McFarland was prepared in sterile saline solution (0.85 %, w/v), corresponding to $1\text{-}2\cdot10^8$ CFU/mL. The bacterial suspension containing *S. aureus* and *S. pyogenes* was further diluted in Mueller Hinton broth or Mueller Hinton broth with 5 % horse blood, respectively, to obtain the concentration of approx. 10^6 CFU/mL. Subsequently, two-fold serial dilutions of the test formulations were prepared in growth medium using a 96-well plate. All tested DLs were reduced in size to approx. 100 nm average diameter to avoid possible liposome precipitation during the experiment. Curcumin and lipid contents in the liposomal formulations were determined as described in Sections 2.4 and 2.5, respectively. Two lipid concentrations of curcumin-DLs were tested, namely 2 and 4 mg/mL, corresponding to the curcumin concentrations of 100 and 200 μg/mL, respectively. Moreover, as the controls, the following samples (in growth medium) were tested: i) PG (20 %, w/v) solution in PBS, ii) empty NDLs, CDLs, ADLs, at similar lipid concentration as in curcumin-DLs, iii) curcumin in PG solution (20 %, w/v) in similar concentrations as curcumin in DLs. As a negative control, one row of the 96-well plate was filled only with the growth medium. The bacterial suspension, previously prepared as described above, was then added to each well to a final concentration of $5x10^5$ CFU/mL and incubated at 37 °C for 4 hrs. The bacterial survival after treatment with the tested formulations was evaluated by serial dilution of the bacterial suspension from each well with subsequent plating on blood agar plates following overnight incubation at 37 °C. The percentage of bacterial survival was determined by comparing surviving bacteria to the negative control (100%).

2.9. Inhibition of NO production measurements

The *in vitro* anti-inflammatory activity of curcumin-DLs was assessed in terms of their effect on the inhibition of NO production in LPS-induced murine macrophage RAW 264.7 cells [4].

The cells (1×10^5 cells/mL) were cultured in a 24-wells plate with RPMI 1640 medium supplemented containing 10 % fetal bovine serum and glutamine. The cells were then incubated for 24 hrs at 37 °C/5 % CO_2. RPMI medium was replaced with LPS solution (1 µg/mL) in RPMI to induce NO production. Additionally, the test formulations (curcumin-DLs) were added (10 µL) at various lipid concentrations, namely 1, 10 and 50 µg/mL, corresponding to curcumin concentrations of 0.05, 0.5 and 2.5 µg/mL. The controls for curcumin and curcumin liposomes were the same as the ones used for anti-bacterial susceptibility testing (Section 2.8). As a negative control, the cells treated with LPS were used. After 24 hrs incubation, the NO production was measured in terms of nitrite formation in the media by the addition of Griess reagent (1 % sulfanilamide, 0.1 % naphthylethylenediamine dihydrochloride, 2.5 % phosphoric acid) (1:1 as volume ratio with RPMI). The absorbance was read at 540 nm using an Epoch Microplate Spectrophotometer (BioTek Instruments, Vermont, USA). The effect of the curcumin in liposomal formulations on the inhibition of NO production was expressed as percentage of produced NO, in comparison to 100 % NO detected in the control (cells treated with 1 µg/mL LPS).

2.10. In vitro cell viability testing

The cell viability of HFF cells exposed to curcumin-DLs was tested to evaluate possible cytotoxic effect of curcumin-DLs on healthy skin cells. The HFF cells (50,000 cells/mL) were cultured in a 96-wells plate with IMDM together with 10 % (v/v) fetal bovine serum at 37 °C in 5 % CO_2. After 24 hrs, 10 µL of test formulations were added and incubated for 12 and 24 hrs, respectively. All test formulations were the same as the ones tested in NO production measurements (Section 2.9). Living cells were quantified using the Cell Counting Kit-8 (CCK-8) (Sigma-Aldrich Chemie, Steinheim, Germany) after 12 and 24 hrs exposure, respectively. CCK-8 (10 µL) was added to the cells and the absorbance was read at 450 nm using an Epoch

Microplate Spectrophotometer (BioTek Instruments, Vermont, USA) after 4 hrs incubation following the instruction provided by the kit supplier.

2.11. Statistical analysis

Statistical analyses were performed using one-way ANOVA test followed by Bonferroni's multiple comparisons test performed on GraphPad Prism version 7.00 for Windows (GraphPad Software, La Jolla CA, USA). Results were expressed as mean ± SD. A p value < 0.05 was considered significant.

3. Results and discussion

Curcumin is one of the "hot" molecules with potential in treatment of various diseases, especially chronic, ranging from cancer to skin diseases [24]. However, its poor solubility, low chemical stability and short half-life following systemic absorption make curcumin a pharmaceutical challenge [1,5]. Numerous delivery systems have been proposed as means to tailor its biological properties [25,26]. We were particularly interested in a potential of curcumin as active ingredient in wound dressings. Various topical formulations have been evaluated for their potential to enhance curcumin's therapeutic activities relevant for wound healing [6]. The conventional liposomes can incorporate lipophilic compounds, such as curcumin, in their phospholipid bilayer thus enhancing their solubilization and providing their stability and protection [5]. Their phospholipid structure resembles the skin lipid composition thus enabling accumulation of the incorporated drug into the skin [14]. However, conventional liposomes act by forming a depot on the skin surface and our aim was to act on the bacterial infections in wound bed, which are often not reachable and require drug/carrier penetration to achieve total eradication [27]. Deformable liposomes have been shown superior to conventional

liposomes in improving dermal drug delivery, assuring prolonged retention time of the drug within the skin and sustained/controlled drug release [15]. Incorporation of curcumin in DLs should provide solubilization of curcumin, increase its stability and assure sustained release over the desired time. This can subsequently provide a high curcumin concentration within the skin, including wound bed, minimizing systemic absorption and undesired side effects. Moreover, the liposomal surface charge contributes to the liposomes' behavior as dermal nanocarriers [16]. Considering that curcumin acts at cellular level, the liposomal surface charge might facilitate the interaction between curcumin carrier and targeted cell membrane [18]. Consequently, the targeted delivery of curcumin at the cellular level mediated by DLs is expected to improve its therapeutic effects.

3.1. Liposomal characteristics

The characterization of liposomes in terms of their physicochemical properties is fundamental to develop effective liposomal formulations destined for dermal therapy. The vesicle size has shown to play an important role in the dermal delivery mediated by nanocarriers. The liposome size will determine the depth in skin layers where the entrapped drug is delivered [28]. Considering that our aim was to assure local effects of curcumin, we chose to develop curcumin-DLs within a size range of 200-300 nm; the size range has shown to provide the highest reservoir in the deeper skin layers [29]. Based on our previous findings [20], the hand extrusion through polycarbonate membrane was found to be optimal for manufacturing the DLs of desired size. Table 2 shows the vesicle size of all curcumin-DLs. A bimodal size distribution (Nicomp distribution) was observed for both NDLs and CDLs, presenting a minor particle size peak out of the targeted size range. However, the main peaks in size distribution were in the range of 200-300 nm, as targeted. The polydispersity index (PI) below 0.25 confirmed a satisfactory size distribution for all curcumin-DLs regardless of the liposomal surface charge.

The surface charge of all DLs mirrored the type of surfactants/lipids used in the liposome preparation (Table 2). The slightly negative zeta potential observed for NDLs was still considered to be neutral, due to the presence of a neutral lipid (SPC) and a non-ionic surfactant (P20). CDLs bear a strong positive surface charge, whereas ADLs a strong negative charge; both can be attributed to the incorporation of a positively surface charged lipid (SA) and negatively surface charged ionic surfactant (SDC), respectively.

In the development of effective nanocarriers for dermal drug delivery, it is important to obtain high drug loading capacity to assure a high drug concentration in/within the skin. It is known that for DLs, the incorporation of surfactants in the phospholipid bilayer can affect the entrapment efficiency [16]. This mainly affects incorporation of lipophilic/amphiphilic drugs in DLs. Their lipophilic nature permits their accommodation in the phospholipid bilayer of liposomes. Therefore, a competition might occur between the lipophilic drug and surfactant thus affecting the amount of incorporated drug in the DLs. This also applies to curcumin, a lipophilic compound with high log P (3.29) [30]. Therefore, curcumin is expected to accommodate itself in the phospholipid bilayer of the liposomes, similarly as other polyphenolic compounds, such as resveratrol [31]. As reported in Table 2, the amount of incorporated curcumin varied among the DLs. ADLs exhibited the highest entrapment of curcumin, whereas the lowest was found for CDLs. The presence of SA in CDLs has previously been shown to cause low entrapment efficiency for celecoxib, drug with similar lipophilicity as curcumin [32]. SA might be responsible for causing the repulsions within the lipid bilayers, thus triggering alterations in bilayers packing [33]. Therefore, curcumin might encounter impediments when accommodating itself in the lipid bilayer of CDLs. Moreover, CDLs were made of P20 and SA, both confined in the lipid bilayer together with curcumin. In ADLs, curcumin has only to compete with SDC, thus allowing incorporation of higher amount of curcumin. Although NDLs include only P20 as a surfactant in the lipid bilayers, the entrapment

of curcumin in NDLs was still lower than in ADLs. The reason behind could be the different carbon chain length of the two surfactants, which determines their lipophilicity. The longer the carbon chain length, in our case SDC, the higher lipophilicity is expected, thus increasing the entrapment efficiency of lipophilic compounds [34,35].

The SPC recovery after the extrusion was found to be more than 80 % for all liposomal formulations (Table 2). This confirmed that the incorporated curcumin was associated with the phospholipid bilayer. This was in accordance with previously published data on conventional liposomes [4].

Table 2. Characteristics of curcumin-DLs.

Liposomes	Diameter (nm)[a]	PI[b]	Zeta potential (mV)	Curcumin per lipid (mg/mg)	SPC recovery (%)
NDLs	286.1±60.8 (87 %) 130.8±14.5 (13 %)	0.17±0.02	-2.3±0.2	0.07±0.00	80.2±0.6
CDLs	231.5±68.1 (90 %) 392.3±61.8 (10 %)	0.22±0.04	33.7±1.1	0.04±0.01	97.1±3.3
ADLs	299.3±22.8 (100 %)	0.20±0.03	-54.3±4.3	0.11±0.01	89.1±0.9

[a]The diameter is indicated as peaks in size distributions (nm). The weight intensity of each peak (%) is indicated in parentheses.

[b]Polydispersity index.

Results are expressed as mean ± SD (n = 3).

The membrane elasticity is the distinctive characteristic of DLs enabling them to squeeze through the skin pores much smaller than their size and consequently enhance the transport of incorporated drug into the deeper skin layers [16]. The DLs elasticity is determined by the presence of surfactant in the lipid bilayer. Surfactants possess high radius curvature thus destabilizing the lipid bilayer and improving liposome membrane elasticity by influencing the interfacial tension of DLs. The membrane elasticity can therefore be affected by the type of employed surfactant [33]. In this study, we employed different surfactants to prepare DLs bearing different surface charges. We incorporated P20 in both NDLs and CDLs, whereas SDC was employed to prepare ADLs. CDLs additionally contained SA to confer the positive surface charge to the vesicles. To determine the DLs elasticity and liposomal deformability, the liposomal dispersions were passed through the polycarbonate membrane (100 nm as pore size) using a constant external pressure of 2.5 bar. The DLs elasticity was determined considering both the vesicle size (r_v) after the extrusion and the amount of liposomal dispersions (J) extruded in 5 min. Table 3 shows the degree of membrane elasticity (E) of all DLs, together with the determined parameters after the extrusion used to calculate the E. Regarding empty DLs (without curcumin), E was mostly dependent on the J. The highest E was obtained with empty ADLs, whereas empty CDLs exhibited the lowest E value. CDLs were composed of both P20 and SA. Although P20 showed to provide elasticity to NDLs, the same effect was not observed when incorporated in CDLs. As discussed above, the presence of SA in CDLs might cause repulsions when accommodating itself in the lipid bilayers consequently causing alterations in the lipid packing. This might reduce the CDLs elasticity. The presence of curcumin in all DLs influenced their degree of membrane elasticity (Table 3). The incorporation of curcumin in both NDLs and ADLs reduced their E values by more than five- and three-fold, respectively, as compared to empty vesicles. Interestingly, the entrapment of curcumin in CDLs enabled an increase in membrane elasticity by more than 30-fold in comparison to empty CDLs. A possible

explanation might be that the presence of curcumin in CDLs can change the surfactant arrangement in the lipid bilayer and limit the lipid packing alterations caused by SA. The degree of membrane elasticity of all curcumin-DLs was in agreement with E values typical for elastic vesicles reported in literature [22]. Moreover, all curcumin-DLs exhibited similar E values. In this study, our focus was on the role of liposome surface charge in the dermal delivery of curcumin. Therefore, the similar membrane elasticity observed for all curcumin-DLs allowed us to compare the different DLs only exploring the effect of their surface charge and excluding any possible effects related to their membrane elasticity.

Table 3. The membrane elasticity of curcumin-DLs.

Liposomes	Surface charge	r_v/r_p	J (g)	E
Empty DLs	Neutral	1.76 ± 0.04	4.73 ± 0.11	14.59 ± 0.30
	Cationic	1.75 ± 0.02	0.05 ± 0.00	0.16 ± 0.01
	Anionic[a]	1.44	12.70	26.41
Curcumin-DLs	Neutral[a]	1.71	1.61	4.72
	Cationic	1.64 ± 0.07	2.36 ± 0.14	6.38 ± 0.90
	Anionic[a]	1.39	2.83	5.46

The degree of membrane elasticity (E) was calculated considering both the r_v/r_p and J. r_v is the vesicle diameter (nm) after extrusion, r_p is the pore size membrane (nm) and J is the amount (g) of liposomal dispersion extruded in 5 min (constant pressure of 2.5 bar). Empty DLs bearing different surface charge were used as control.

Results are expressed as mean ± SD (n = 2). [a]n=1.

3.2. Ex vivo human skin penetration of curcumin mediated by DLs

The skin penetration potential of liposomally-associated substance/drug is fundamental to assure targeted drug delivery and, consequently, effectiveness of the nanoformulation. The use of human skin in the Franz diffusion cells is one of the most appropriate skin model to obtain diffusion kinetics closer to the *in vivo* conditions [36]. Although diseased skin often exhibits compromised SC barrier and the drug/substance penetration might be therefore enhanced, the assessment of the skin penetration potential of nanocarriers using the full thickness human skin can serve as a pilot study assisting in the selection of the appropriate nanocarrier. This is mainly applicable during the screening of nanocarriers with different properties, as, in our case, with different liposomal surface charge. Curcumin, a lipophilic compound, is not expected to partition from the skin into the aqueous receptor fluid. We therefore incorporated 5 % (v/v) of Albunorm® in receptor medium, corresponding to 10 mg/L of albumin, to overcome the scarce solubility of curcumin in an aqueous media and avoid negligible diffusion kinetics. Moreover, it is known that the *in vitro* testing tends to underestimate *in vivo* skin penetration of lipophilic compounds. It was therefore suggested that the addition of solubilizing agents in the receptor medium could overcome the poor *in vitro/in vivo* correlation [37]. Commonly used are solubilizing agents such as alcohol derivatives [37,38], however their presence does not mimic the physiological composition of receptor media. We therefore used Albunorm® as a source of albumin, which is physiologically present in the receptor fluid; thus mimicking the *in vivo* conditions to a higher extent while avoiding impairment of the membrane barrier function [39]. The cumulative amount of penetrated curcumin from the different DLs through the full thickness human skin is presented in Fig. 1.

After 24 hrs, the amount of penetrated curcumin through the full thickness human skin was low for all DLs. These results are in accordance with previous reports on human skin penetration profiles of curcumin when incorporated in lipid-core nanocapsules [40]. Although the

penetration of curcumin through the full thickness human skin mediated by our DLs was limited, these findings confirm the ability of DLs to deliver the incorporated active compound in the deeper skin layers reaching the dermis layer [41]. We have proven that our curcumin-DLs possess elastic membrane contributing to the curcumin delivery into the deeper skin layers mediated by DLs [22,42]. However, the low amount of curcumin that reached the receptor medium indicates also a retention of curcumin within the skin thus showing good suitability of these nanocarriers for dermal therapy of curcumin. The comparison of the different DLs indicates different behavior of nanocarriers as dermal delivery systems. CDLs enabled the most sustained skin penetration of curcumin, whereas ADLs exhibited the highest skin penetration enhancement of curcumin (Fig.1). The similar degree of membrane elasticity observed for all curcumin-DLs (Table 3) indicates that the differences in the skin penetration profiles of curcumin were mainly determined by the liposomal surface charge, which has shown to influence skin penetration of drugs mediated by liposomes [43]. Considering the negative charge of the corneocytes membrane, electrostatic interactions between liposome and SC cells might be favorable when the liposomal surface charge is positive [16]. This stronger interaction might cause a long-term retention of curcumin on the skin thus sustaining its penetration through/into the skin layers. Cationic deformable liposomes containing curcumin have been recently studied by Jose and co-workers [44]. The authors prepared cationic deformable liposomes made of 1,2-dioleoyl-3-trimethylammonium propane (DOTAP) and sodium cholate with a vesicle size of 100 nm, whereas our curcumin-CDLs differed in lipid/surfactant composition and were bigger in vesicle size (231 nm). Although dissimilarities in liposomes' composition and size, the sustained skin penetration of curcumin observed for our CDLs in human skin was in accordance with their findings using pig skin [44]. The skin penetration enhancement effect of negatively charged DLs for incorporated lipophilic compounds has been previously observed using pig skin [45,46]. Paolino and collaborators [41] found an

enhancement in human skin penetration of lipophilic compounds for DLs comprising SDC, in accordance with our findings. More recently, we have also shown the capability of ADLs to deliver lipophilic compounds into the deeper skin layers through *ex vivo* human skin in Franz diffusion cells [20].

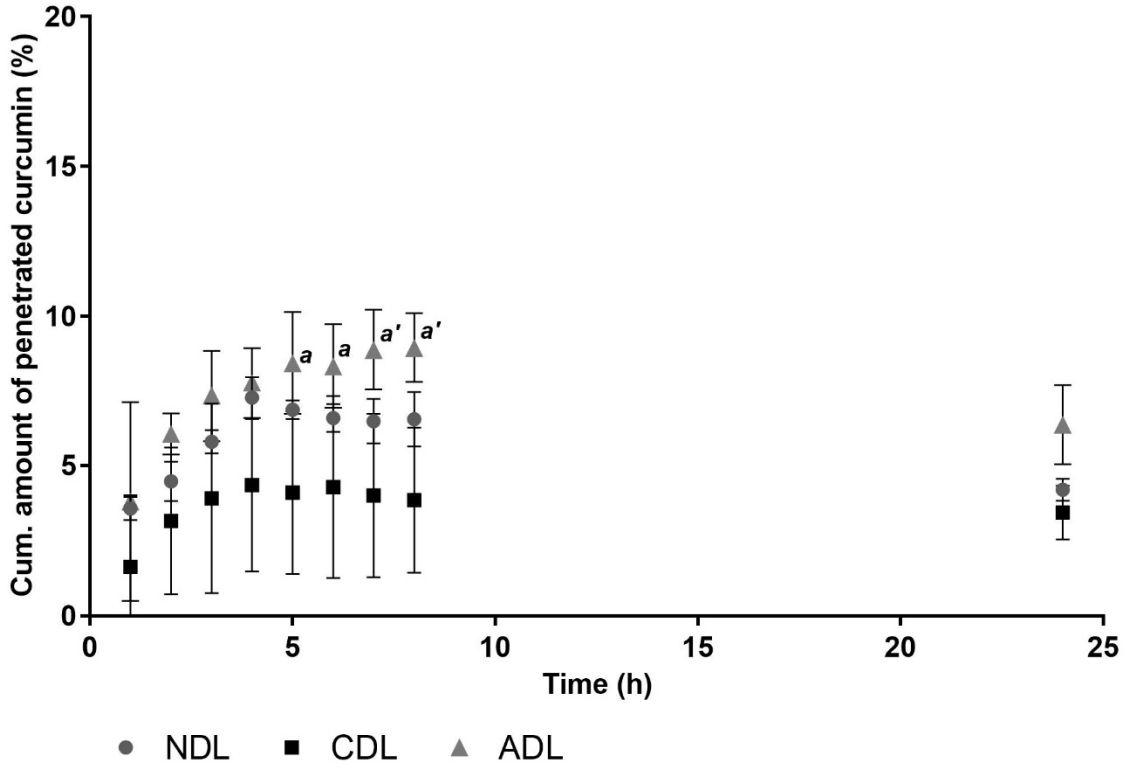

Fig. 1. Curcumin penetration from different deformable liposomes through the full thickness human skin over 24 hrs. Results are expressed as mean ± SD (n = 3).

[a:] $p < 0.05$, [a':] $p < 0.005$ *vs*. CDL.

3.3. Anti-bacterial activity of curcumin-DLs

Skin, especially skin with compromised barrier and chronic wounds, are prone to colonization by bacteria. Bacterial infections contribute to delayed healing thereof increasing the incidence of morbidity and mortality in patients [47]. Gram-positive bacteria, specifically *S. aureus* and *S. pyogenes* are responsible for skin infections in general [10,48,49]. Therefore, curcumin liposomal formulations that prevent/treat microbial contamination can contribute to improved skin therapy and prevention of bacterial biofilms in chronic wounds [50]. Additionally, dermal (localized) therapy for chronic wound treatment might limit the high incidence of bacterial resistance related to the overuse of antibiotics orally and systemically [51]. Curcumin can therefore be a promising alternative to common antibiotics with evolved resistance against broad spectrum of bacteria, including *S. aureus* [9]. All liposomal formulations with curcumin were tested against two clinical strains, *S. aureus* and *S. pyogenes*. Curcumin as antimicrobial is not fully utilized and the potential of nanocarriers in modulating its antimicrobial effects are currently, although very promising, not fully explored [11]. Therefore, broader use of curcumin as antimicrobials can contribute to limiting the use of antibiotics. We aimed firstly to evaluate the anti-bacterial effect of curcumin when incorporated in DLs and secondly, to explore the effect of the liposomal surface charge on curcumin-DLs anti-bacterial activity. Since we developed a system which would serve as an alternative to antibiotics, and as a mean to recue antibiotic use, we did not include antibiotics as positive control in the anti-bacterial activity testing.

All curcumin-DLs inhibited both *S. aureus* and *S. pyogenes* growth compared to control (untreated bacteria) (Fig. 2a, c). No differences in anti-bacterial activity were observed between the two tested concentrations of curcumin (100 and 200 μg/mL, respectively), indicating that lower curcumin concentration was already sufficient to exert the anti-bacterial effect. This might also be beneficial considering the possibility of side effects related to high curcumin

concentration at the site of administration [12]. Curcumin-NDLs exhibited the weakest inhibition of *S. aureus* growth compared to both CDLs and ADLs (Fig. 2a). The same trend was observed with *S. pyogenes* (Fig. 2c). These findings suggest that the liposomal surface charge influences the liposomal interaction with the bacterial cell membrane. The neutral liposomal membrane of NDLs might limit this interaction thus reducing curcumin availability at the targeted bacterial membrane resulting in a weak anti-bacterial activity. The strongest activity was observed for curcumin-CDLs against both *S. aureus* and *S. pyogenes*. Moreover, CDLs inhibited bacterial growth to a higher extent than free curcumin (curcumin in PG solution) (Fig. 2b, d). Therefore, the positive surface charge of CDLs may facilitates their interactions with the negatively charged bacterial cell membrane thus increasing the anti-bacterial activity of the incorporated curcumin. The effect could have been even more pronounced if the incubation time was prolonged. However, we were very encouraged by the promising findings achieved after 4 hrs incubation time allowing detection of differences between the DLs bearing different surface charges. Moreover, all curcumin-DLs inhibited bacteria growth by more than 50 %, therefore longer incubation time may result in stronger effect making the differences among the DLs less evident. Free curcumin would require more time to initially interact with the pathogen surface membrane and then to exert the therapeutic effect [49].

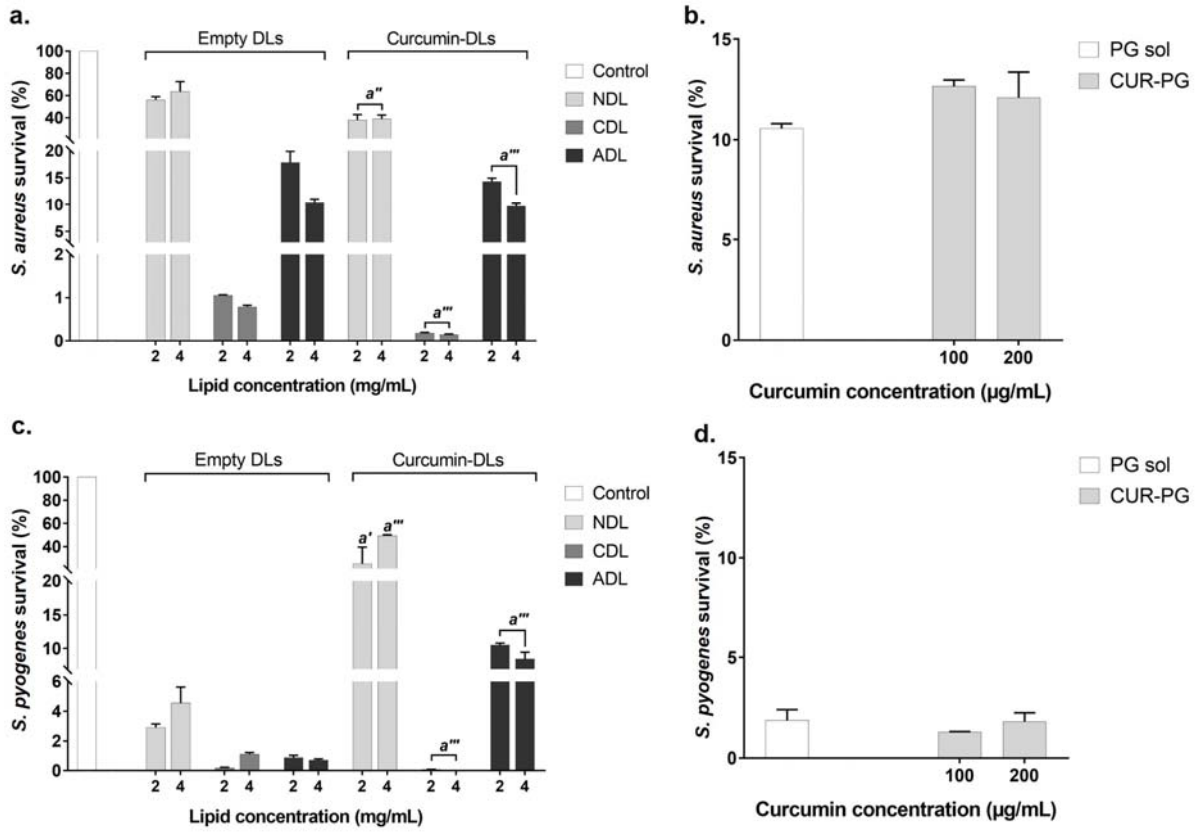

Fig. 2. Effect of different curcumin-DLs on *S. aureus* (upper part) and *S. pyogenes* (lower part) growth after 4 hrs incubation.

(a) and (c) show the effect of curcumin-DLs on *S. aureus* and *S. pyogenes*, respectively. Control refers to untreated bacteria. Empty DLs are curcumin-free NDLs, CDLs and ADLs, respectively, with similar lipid concentrations as curcumin-DLs. (b) and (d) represent the effect of free curcumin (CUR-PG), meaning curcumin in PG solution (20 % w/v) with same concentrations as in deformable liposomes. PG sol is PG (20 % w/v) solution in PBS.

Bar graphs showing mean ± SD (n = 2). $^{a:}$ $p < 0.03$, $^{a':}$ $p < 0.002$, $^{a'':}$ $p < 0.0002$, $^{a''':}$ $p < 0.0001$.

Additionally, we also tested all liposomal formulations against a clinical strain of Gram-negative bacteria, namely *Pseudomonas aeruginosa* (ATCC 27853), using the agar diffusion method to determine eventual zones of inhibition, as described earlier [52]. However, none of

the curcumin-DLs exhibited stronger inhibition of *P. aeruginosa* growth than the free curcumin (curcumin in PG solution) (data not shown). Krausz and collaborators [50] also observed that Gram-negative bacteria, particularly *P. aeruginosa*, were less susceptible than Gram-positive bacteria to curcumin-containing nanoparticles. The properties of Gram-negative bacteria cell membrane, both in terms of the surface charge and composition, compared to Gram-positive bacteria might result in a limited nanoparticle interaction with the Gram-negative cells [50].

3.4. Effect of curcumin-DLs on NO production in LPS-induced macrophages

Skin inflammatory diseases, especially chronic wounds and burns, are often delayed in the healing process due to persistent inflammation. NO is known to play a central role in the inflammation pathways thus worsening healing of chronic wounds [6]. During the inflammation process, NO is secreted in large quantities by LPS-induced macrophages. NO production can help as cytotoxic mediator thus preventing microorganism invasion. However, an excessive NO production can interact with oxygen radicals forming an extremely reactive radical (peroxinitrite), which induces inflammatory cellular cytokines thus causing cell death and impaired healing [53]. Moreover, in chronic wounds, an excessive production of NO also causes an impairment of collagen synthesis [54], further delaying the wound healing process. Therefore, a local therapy based on a formulation that inhibits NO production will possibly reduce the persistent inflammation distinctive in chronic wounds and burns. Fig. 3 shows the effect of curcumin-DLs on NO production in LPS-induced macrophages. Regardless of the liposomal surface charge, a concentration-dependent inhibition of NO production was observed for all curcumin-DLs (Fig. 3a-c). At the lowest lipid concentration (1 μg/mL), no inhibitory effect on NO production was observed for all DLs. In contrast, they exhibited an inhibitory effect at 10 μg/mL, which was stronger than the effect of free curcumin (curcumin in PG solution) (Fig. 3d). This effect was more evident at the highest tested lipid concentration (50

μg/mL). Free curcumin (curcumin in solution) has widely confirmed to possess anti-inflammatory activity, exhibiting even stronger effect compared to other well-known anti-inflammatory compounds, such as vitamin C, lipoid acid and L-nitro-arginine methyl ester [4]. In this study we could observe that DLs enhanced curcumin's anti-inflammatory activity, as previously shown for conventional neutral liposomes [4]. The increased inhibitory effect of NO production when curcumin is incorporated in DLs might be a consequence of i) increased curcumin stability due to the liposomes' ability to protect it from UV- and pH-induced degradation, ii) enhanced curcumin uptake in macrophages, and iii) improvement of curcumin aqueous solubility thus maximizing its bioavailability and tissue distribution [1]. Recent studies on liposomes containing glucocorticoid by Gauthier and collaborators [55] have showed the ability of phosphatidylserine-modified liposomes to enable faster uptake in macrophages, thus promoting targeted delivery of the incorporated drug and enhancing its anti-inflammatory effect.

Comparing the liposomal surface charge, the strongest inhibitory effect was obtained with CDLs (Fig. 3b). At the highest lipid concentration, CDLs inhibited NO production by almost 10 % more than both NDLs and ADLs (Fig. 3a, c). The stronger effect of CDLs might be explained by the higher affinity of positively charged DLs towards the negative cell membrane, facilitating their interactions. Moreover, the more sustained skin penetration of curcumin observed with CDLs (Fig. 1) might prolong the retention time of curcumin at the targeted site of action. This would facilitate and prolong CDLs interaction with macrophages, thus allowing continuous curcumin cellular uptake and enhancing its effect at cellular level, as observed for the anti-bacterial effect (Fig. 2a, c). Studies regarding possible curcumin uptake by macrophages would be necessary to confirm our hypothesis, however this correlation between sustained release and enhanced anti-inflammatory activity has been previously observed with other nanocarriers, such as propylene glycol liposomes [12].

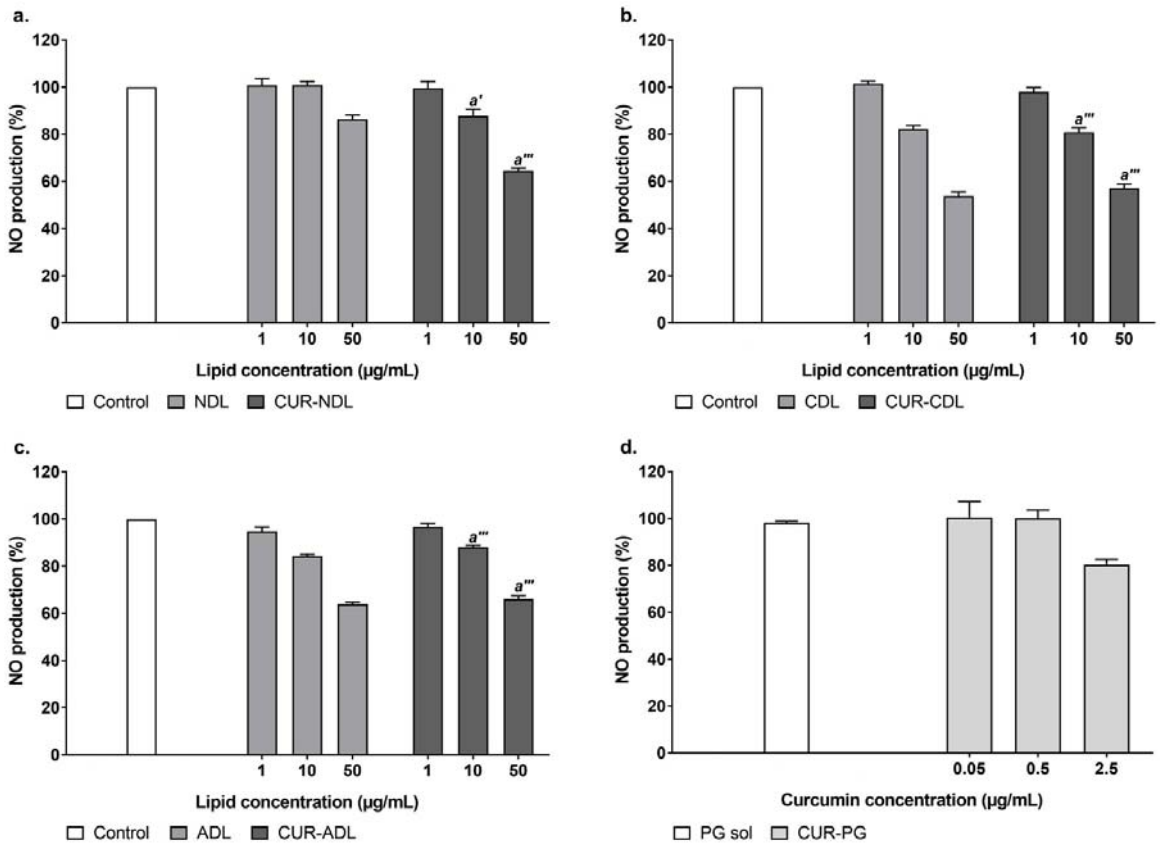

Fig. 3. Effect of different curcumin-DLs on NO production in LPS-induced macrophages. LPS-induced macrophages were treated with: (a) curcumin neutral deformable liposomes (CUR-NDLs), (b) curcumin cationic deformable liposomes (CUR-CDLs) and (c) curcumin anionic deformable liposomes (CUR-ADLs), incubated for 24 hrs. Untreated LPS-induced macrophages were used as a control. NDLs, CDLs and ADLs are empty deformable liposomes, tested at the same lipid concentrations as curcumin-DLs. (d) curcumin in PG solution (CUR-PG) at the same curcumin concentration as in deformable liposomes. PG sol is PG (20 % w/v) solution in PBS.

Results are expressed as mean ± SD (n = 3). $^{a:}$ $p < 0.03$, $^{a':}$ $p < 0.002$, $^{a'':}$ $p < 0.0002$, $^{a''':}$ $p < 0.0001$.

3.5. Effect of curcumin-DLs on healthy human skin cells

The incorporation of cationic lipid and surfactants, especially ionic, in DLs destined for dermal therapy might rise toxicity concerns [19]. Moreover, curcumin as polyphenolic compound might exhibit side effects on skin cells when administered at high concentrations [6]. To explore possible cytotoxic effect of curcumin-DLs to skin fibroblasts, different surface charged DLs were incubated with HFF cells for 12 and 24 hrs, respectively. As shown in Fig. 4, all DLs were found to be safe for HFF cells, in agreement with previous findings on other type of nanocarriers containing curcumin [40]. Moreover, a proliferation effect of curcumin-DLs was observed (Fig. 4a, b, c). Similar findings have been reported by Gopinath and co-workers [56], who observed fibroblast proliferation mediated by curcumin in collagen films. More recently, Manca and co-workers [57] studied the effect of curcumin-in-hyalurosomes on human keratinocytes and found an increase in cell viability, as observed for our liposomal formulations. Curcumin-NDLs (Fig. 4a) and curcumin-ADLs (Fig. 4c) showed a concentration dependent cell proliferation enhancement. After 12 hrs exposure, both curcumin-NDLs and curcumin-ADLs exhibited greater proliferation effect than the control (untreated HFF cells) at lipid concentrations of 10 and 50 μg/mL. NDLs, at 10 and 50 μg/mL, enhanced the number of living cells by 24 and 32 % compared to control, respectively. ADLs exhibited weaker cell proliferation ability compared to NDLs, however they still enabled 12 and 14 % more proliferation than control at 10 and 50 μg/mL, respectively. The same trend was observed when comparing curcumin-DLs with free curcumin (curcumin in PG solution) (Fig. 4d). At the highest lipid concentration (50 μg/mL), NDLs enhanced cell proliferation by 32 %, whereas ADLs enhanced by 14 %. This cell proliferation activity was more evident after 24 hrs exposure. For both NDLs and ADLs, an enhancement in cell proliferation by 50 % compared to free curcumin was observed (Fig. 4a, c, d). Our results are in agreement with published data on other type of nanocarriers, showing that curcumin incorporation in phospholipid-based nanosystems is beneficial to diminish its toxicity

concerns [26]. Regarding CDLs (Fig. 4b), the tested lipid concentrations of 1 and 10 μg/mL exhibited similar proliferation effect as observed for NDLs and ADLs. The enhanced *in vitro* proliferation effect in HFF observed for curcumin-DLs may be additionally beneficial in treatment of chronic wounds and burns, but also in atopic dermatitis, ichthyosis vulgaris, all characterized by a conspicuous human skin cells death. In these conditions, a cell proliferation effect helps and accelerate the normal reconstitution of the skin layers. Interestingly, the CDLs at the highest lipid concentration (50 μg/mL) showed lower proliferation effect than at concentration of 10 μg/mL. By increasing the surfactant concentration, the interaction between the amphiphilic ionic surfactant and the cellular lipid bilayer is more likely to occur, resulting in disruption of the plasma membrane [58]. This lower proliferation effect of CDLs at higher concentrations (50 μg/mL) was not observed for NDLs and ADLs, indicating that the liposomal surface charge influences the extent of the interaction between nanocarrier and cell membrane. Due to the negative charge of the cellular membrane, electrostatic interactions are more likely to occur with positively charged liposomes thus facilitating the possible cytotoxic effect exerted by CDLs. However, CDLs at the highest lipid concentration assured equal or higher cell viability than control after both 12 and 24 hrs exposure. This excludes any cytotoxic effect of CDLs. To the best of our knowledge, the cytotoxicity of stearylamine liposomes, as our CDLs, has only been tested in human lung epithelial cells by Tahara and collaborators, who found no negative effect of stearylamine liposomes on cell viability after 4 hrs exposure [59].

Regarding the anti-inflammatory activity of curcumin-CDLs (Fig. 3b), it can be postulated that the strong inhibitory effect on NO production observed for CDLs is due to their potential cell toxicity and that the reduction of NO production is only a consequence of apoptosis/necrosis of macrophages caused by CDLs. However, the findings from the cell viability study showed a clear lack of cytotoxicity of CDLs (Fig. 4b) and even more, demonstrated a proliferative effect, which further supports our hypothesis.

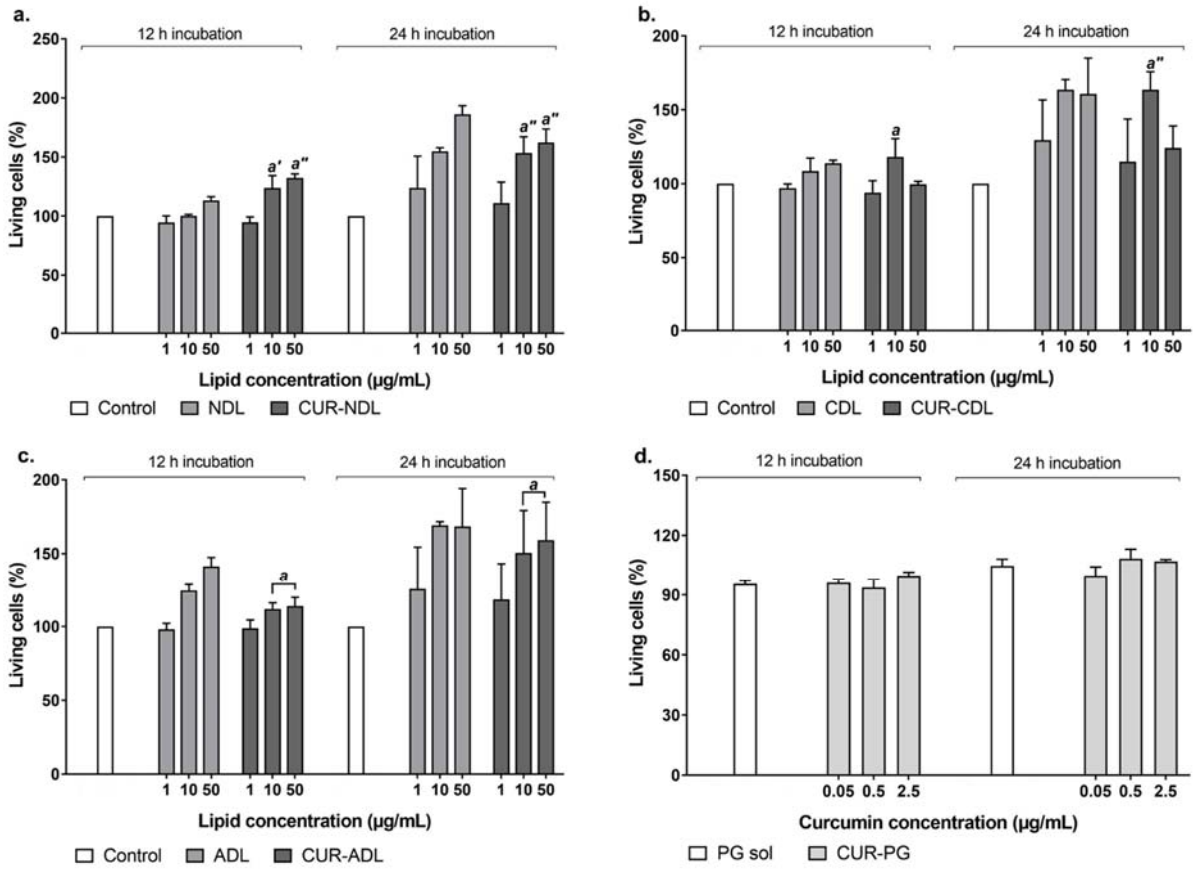

Fig. 4. **Effect of different curcumin-DLs on viability of human foreskin fibroblast (HFF) cells after 12 and 24 hrs exposure.**

HFF cells were exposed to: (a) curcumin neutral deformable liposomes (CUR-NDLs), (b) curcumin cationic deformable liposomes (CUR-CDLs) and (c) curcumin anionic deformable liposomes (CUR-ADLs), respectively. Untreated HFF cells were used as control. NDLs, CDLs and ADLs represent empty deformable liposomes, tested at the same lipid concentrations as curcumin-DLs. (d) represents the percentage of living cells after exposure to PG (20 % w/v) solution (PG sol) in PBS and curcumin in PG solution (CUR-PG) at the same curcumin concentration as in deformable liposomes.

Results are expressed as mean ± SD (n = 3). $^{a:}$ $p < 0.03$, $^{a':}$ $p < 0.002$, $^{a'':}$ $p < 0.0002$.

Considering that DLs suspensions are liquid in nature, their topical administration onto the skin surface can be improved by their incorporation into a vehicle, such as hydrogel, to develop final skin formulations. The selection of the best final formulation, according to the liposomal surface charge, would be a consequent step for further studies on the effectiveness of curcumin-DLs in hydrogel systems destined for localized skin therapy. Using the same approach as applied in this study, the future investigations would possibly be performed avoiding *in vivo* animal testing due to the rising ethical restrictions that limit their use further leading to find other alternatives.

4. Conclusion

We achieved a successful employment of nanotechnology by optimizing deformable vesicles to improve dermal delivery of curcumin. All prepared deformable liposomes enabled relatively high curcumin entrapment, thus assuring high curcumin concentration at the skin site and limiting the systemic absorption, as observed in the *ex vivo* skin penetration studies. Moreover, we were able to discriminate between the different skin penetration potentials of the nanocarriers. Cationic deformable liposomes exhibited the most sustained curcumin penetration through the full thickness human skin, assuring high retention of curcumin within the skin. All liposomal formulations exerted concentration-dependent anti-bacterial and anti-inflammatory activities, superior to activities of non-liposomal curcumin. Additionally, all liposomal formulations were found non-toxic in the tested human skin fibroblast cells and even more, exhibited a cell proliferation effect. We propose that successful incorporation of curcumin in cationic deformable liposomes enhances its multi-targeting properties. Moreover, the curcumin-containing novel liposomes can be utilized in treatment of various skin diseases which pathologies involve infection and inflammation.

Conflict of interests

The authors declare no conflict of interest.

Author Contributions

S.T., K.J., M.J., P.B., Z.V. and N.S.-B. designed and planned the experiments. S.T. and E.G. conducted all experiments, with exception of microbiological testing (K.J.) and vesicle deformability testing (Z.V.). All authors contributed to the manuscript preparation. N.S.-B. is the senior author and project leader.

Acknowledgements

PhD student S. Ternullo is supported by the University of Tromsø The Arctic University of Norway. The authors are grateful to Lipoid GmbH for providing the lipids.

References

[1] M. Mehanny, R.M. Hathout, A.S. Geneidi, S. Mansour, Exploring the use of nanocarrier systems to deliver the magical molecule; Curcumin and its derivatives, J. Control. Release 225 (2016) 1-30.

[2] B. Kocaadam, N. Şanlier, Curcumin, an active component of turmeric (*Curcuma longa*), and its effects on health, Crit. Rev. Food Sci. Nutr. 57 (2017) 2889–2895.

[3] S. Prasad, S.C. Gupta, A.K. Tyagi, B.B. Aggarwal, Curcumin, a component of golden spice: From bedside to bench and back, Biotechnol. Adv. 32 (2014) 1053-1064.

[4] P. Basnet, H. Hussain, I. Tho, N. Škalko-Basnet, Liposomal delivery system enhances anti-inflammatory properties of curcumin, J. Pharm. Sci. 101 (2012) 598-609.

[5] P. Basnet, N. Škalko-Basnet, Curcumin: An anti-inflammatory molecule from a curry spice on the path to cancer treatment, Molecules 16 (2011) 4567-4598.

[6] C. Mohanty, S.K. Sahoo, Curcumin and its topical formulations for wound healing applications, Drug Discov. Today 22 (2017) 1582-1592.

[7] Z. Hussain, H.E. Thu, S-F. Ng, S. Khan, H. Katas, Nanoencapsulation, an efficient and promising approach to maximize wound healing efficacy of curcumin: A review of new trends and state-of-the-art, Colloids Surf. B Biointerfaces 150 (2017b) 223-241.

[8] S. Amini-Nik, Y. Yousuf, M.G. Jeschke, Scar management in burn injuries using drug delivery and molecular signaling: Current treatments and future directions, Adv. Drug Deliv. Rev. 123 (2018) 135-154.

[9] J. Zhou, D. Yao, Z. Qian, S. Hou, L. Li, A.T.A. Jenkins, Y. Fan, Bacteria-responsive intelligent wound dressing: Simultaneous *In situ* detection and inhibition of bacterial infection for accelerated wound healing, Biomaterials 161 (2018) 11-23

[10]. A.L. Byrd, Y. Belkaid, J.A. Segre, The human skin microbiome, Nat. Rev. Microbiol. 16 (2018) 143-155

[11] A.C. da Silva, P.D. de Freitas Santos, J.T. do Prado Silva, F.V. Leimann, L. Bracht, O. Hess Gonçalves, Impact of curcumin nanoformulation on its antimicrobial activity, Trends Food Sci. Technol. 72 (2018) 74-82.

[12] Y-Z. Zhao, C-T. Lu, Y. Zhang, J. Xiao, Y-P. Zhao, J-L. Tian, Y-Y. Xu, Z-G. Feng, C-Y. Xu, Selection of high efficient transdermal lipid vesicle for curcumin skin delivery, Int. J. Pharm. 454 (2013) 302-309.

[13] K. Kaplani, S. Koutsi, V. Armenis, F.G. Skondra, N. Karantzelis, S. Champeris Tsaniras, S. Taraviras, Wound healing related agents: Ongoing research and perspectives, Adv. Drug Deliv. Rev. 129 (2018) 242-253.

[14] M. Sala, R. Diab, A. Elaissari, H. Fessi, Lipid nanocarriers as skin drug delivery systems: Properties, mechanisms of skin interactions and medical applications, Int. J. Pharm. 535 (2018) 1-17.

[15] M.S. Roberts, Y. Mohammed, M.N. Pastore, S. Namjoshi, S. Yousef, A. Alinaghi, I.N. Haridass, E. Abd, V.R. Leite-Silva, H.A.E. Benson, J.E. Grice, Topical and cutaneous delivery using nanosystem, J. Control. Release 247 (2017) 86-105.

[16] S. Jain, N. Patel, M.K. Shah, P. Khatri, N. Vora, Recent advances in lipid-based vesicles and particulate carriers for topical and transdermal application, J. Pharm. Sci. 106 (2017) 423-445.

[17] S.C. Gupta, S. Prasad, J. Hye Kim, S. Patchva, L.J. Webb, I.K. Priyadarsini, B.B. Aggarwal, Multitargeting by curcumin as revealed by molecular interaction studies, Nat. Prod. Rep. 28 (2011) 1937-1955.

[18] H. Meng, W. Leong, K.W. Leong, C. Chen, Y. Zhao, Walking the line: The fate of nanomaterials at biological barriers, Biomaterials 174 (2018) 41-53.

[19] V.V. Dhawan, M.S. Nagarsenker, Catanionic systems in nanotherapeutics – Biophysical aspects and novel trends in drug delivery applications, J. Control. Release 266 (2017) 331-345.

[20] S. Ternullo, L. de Weerd, A.M. Holsæter, G.E. Flaten, N. Škalko-Basnet, Going skin deep: A direct comparison of penetration potential of lipid-based nanovesicles on the isolated perfused human skin flap model, Eur. J. Pharm. Biopharm. 121 (2017) 14-23.

[21] G.R. Bartlett, Phosphorus assay in column chromatography, J. Biol. Chem. 234 (1959) 466-468.

[22] Z. Palac, A. Engesland, G.E. Flaten, N. Škalko-Basnet, J. Filipović-Grčić, Ž. Vanić, Liposomes for (trans)dermal drug delivery: the skin-PVPA as a novel *in vitro stratum corneum* model in formulation development, J. Liposome Res. 24 (2014) 313–322.

[23] M. Balouiri, M. Sadiki, S. Koraichi Ibnsouda, Methods for *in vitro* evaluating antimicrobial activity: A review, J. Pharm. Anal. 6 (2016) 71-79.

[24] Z. Hussain, H.E. Thu, M.W. Amjad, F. Hussain, T.A. Ahmed, S. Khan, Exploring recent developments to improve antioxidant, anti-inflammatory and antimicrobial efficacy of curcumin: A review of new trends and future perspectives, Mat. Sci. Eng. C 77 (2017a) 1316-1326.

[25] V.V. Karri, G, Kuppusamy, S.V. Talluri, S.S. Mannemala, R. Kollipara, A.D. Wadhwani, S. Mulukutla, K.R. Raju, R. Malayandi, Curcumin loaded chitosan nanoparticles impregnated into collagen-alginate scaffolds for diabetic wound healing, Int. J. Biol. Macromol. 93 (2016) 1519-1529.

[26] N. Kianvash, A. Bahador, M. Pourhajibagher, H. Ghafari, V. Nikoui, S.M. Rezayat, A.R. Dehpour, A. Partoazar, Evaluation of propylene glycol nanoliposomes containing curcumin on burn wound model in rat: biocompatibility, wound healing, and anti-bacterial effects, Drug Deliv. Transl. Res. 7 (2017) 654-663.

[27] L.A. DeLouise, Applications of nanotechnology in dermatology, J. Invest. Dermatol. 132 (2012) 964-975.

[28] B. Baroli, Penetration of nanoparticles and nanomaterials in the skin: fiction or reality? J. Pharm. Sci. 99 (2010) 21-50.

[29] S. Hua, Lipid-based nano-delivery systems for skin delivery of drugs and bioactives, Front. Pharmacol. 6 (2015) 219.

[30] A. Araiza-Calahorra, M. Akhtar, A. Sarkar, Recent advances in emulsion-based delivery approaches for curcumin: From encapsulation to bioaccessibility, Trends Food Sci. Technol. 71 (2018) 155-169.

[31] C. Caddeo, M. Manconi, M.C. Cardia, O. Díez-Sales, A.M. Fadda, C. Sinico, Investigating the interactions of resveratrol with phospholipid vesicle bilayer and the skin: NMR studies and confocal imaging, Int. J. Pharm. 484 (2015) 138-145.

[32] M. Bragagni, N. Mennini, F. Maestrelli, M. Cirri, P. Mura, Comparative study of liposomes, transfersomes and ethosomes as carriers for improving topical delivery of celecoxib, Drug Deliv. 19 (2012) 354-361.

[33] G.M. El Zaafarany, G.A.S. Awad, S.M. Holayel, N.D. Mortada, Role of edge activators and surface charge in developing ultradeformable vesicles with enhanced skin delivery, Int. J. Pharm. 397 (2010) 164-172.

[34] H. Chaudhary, K. Kohli, V. Kumar, Nano-transfersomes as a novel carrier for transdermal delivery, Int. J. Pharm. 454 (2013) 367-380.

[35] R. Bnyan, I. Khan, T. Ehtezazi, I. Saleem, S. Gordon, F. O'Neill, M. Roberts, Surfactant effects on lipid-based vesicles properties, J. Pharm. Sci. 107 (2018) 1237-1246.

[36] V. Planz, C-M. Lehr, M. Windbergs, *In vitro* models for evaluating safety and efficacy of novel technologies for skin drug delivery, J. Control. Release 242 (2016) 89-104.

[37] R. Agrawal, S.K. Sandhu, I. Sharma, I.P. Kaur, Development and evaluation of curcumin-loaded elastic vesicles as an effective topical anti-inflammatory formulation, AAPS PharmSciTech. 16 (2015) 364-374.

[38] E. Esposito, L. Ravani, P. Mariani, N. Huang, P. Boldrini, M. Drechsler, G. Valacchi, R. Cortesi, C. Puglia, Effect of nanostructured lipid vehicles on percutaneous absorption of curcumin, Eur. J. Pharm. Biopharm. 86 (2014) 121-132.

[39] K. Moser, K. Kriwet, A. Naik, Y.N. Kalia, R.H. Guy, Passive penetration enhancement and its quantification *in vitro*, Eur. J. Pharm. Biopharm. 52 (2001) 103-112.

[40] R.B. Friedrich, B. Kann, K. Coradini, H.L. Offerhaus, R.C.R. Beck, M. Windbergs, Skin penetration behavior of lipid-core nanocapsules for simultaneous delivery of resveratrol and curcumin, Eur. J. Pharm. Sci. 78 (2015) 204-213.

[41] D. Paolino, D. Cosco, F. Cilurzo, E. Trapasso, V.M. Morittu, C. Celia, M. Fresta, Improved *in vitro* and *in vivo* collagen biosynthesis by asiaticoside-loaded ultradeformable vesicles, J. Control. Release 162 (2012) 143-151.

[42] Ž. Vanić, J. Hurler, K. Ferderber, P. Golja Gašparović, N. Škalko-Basnet, J. Filipović-Grčic, Novel vaginal drug delivery system: deformable propylene glycol liposomes-in-hydrogel, J. Liposome Res. 24 (2014) 27-36.

[43] M.L. González-Rodríguez, A.M. Rabasco, Charged liposomes as carrier to enhance the permeation through the skin, Expert Opin. Drug Deliv. 8 (2011) 857–871.

[44] A. Jose, S. Labala, V.V.K. Venuganti, Co-delivery of curcumin and STAT3 siRNA using deformable cationic liposomes to treat skin cancer, J. Drug Target. 25 (2017) 330-341.

[45] A. Ascenso, A. Salgado, C. Euletério, F. Garcia Praça, M.V. Lopes Badra Bentley, H.C. Marques, H. Oliveira, C. Santos, S. Simões, *In vitro* and *in vivo* topical delivery studies of tretinoin-loaded ultradeformable vesicles, Eur. J. Pharm. Biopharm. 88 (2014) 48-55.

[46] M. Manconi, C. Caddeo, C. Sinico, D. Valenti, M.C. Mostallino, G. Biggio, A.M. Fadda, *Ex vivo* skin delivery of diclofenac by transcutol containing liposomes and suggested mechanism of vesicle-skin interaction, Eur. J. Pharm. Biopharm. 78 (2011) 27-35.

[47] A.R. Siddiqui, J.M. Bernstein, Chronic wound infection: facts and controversies, Clin. Dermatol. 28 (2010) 519-526.

[48] A.F. Cardona, S.E. Wilson, Skin and soft-tissue infections: A critical review and the role of telavancin in their treatment, Clin. Infect. Dis. 61 (2015) 69-78.

[49] D. Simões, S.P. Miguel, M.P. Ribeiro, P. Coutinho, A.G. Mendonça, I.J. Correia, Recent advances on antimicrobial wound dressing: a review, Eur. J. Pharm. Biopharm. 127 (2018) 130-141.

[50] A.E. Krausz, B.L. Adler, V. Cabral, M. Navati, J. Doerner, R.A. Charafeddine, D. Chandra, H. Liang, L. Gunther, A. Clendaniel, S. Harper, J.M. Friedman, J.D. Nosanchuk, A.J. Friedman, Curcumin-encapsulated nanoparticles as innovative antimicrobial and wound healing agent, Nanomedicine: NBM 11 (2015) 195-206.

[51] J. Hurler, O.A. Berg, M. Skar, A.H. Conradi, P.J. Johnsen, N. Škalko-Basnet, Improved burns therapy: Liposomes-in-hydrogel delivery system for mupirocin, J. Pharm. Sci. 101 (2012) 3906-3915.

[52] S.G. Ingebrigtsen, A. Didriksen, M. Johannessen, N. Škalko-Basnet, A.M. Holsæter, Old drug, new wrapping – A possible comeback for chloramphenicol? Int. J. Pharm. 526 (2017) 538-546.

[53] Y. Deldar, Y. Pilehvar-Soltanahmadi, M. Dadashpour, S. Montazer Saheb, M. Rahmati-Yamchi, N. Zarghami, An *in vitro* examination of the antioxidant, cytoprotective and anti-

inflammatory properties of chrysin-loaded nanofibrous mats for potential wound healing applications, Artif. Cells Nanomed. Biotechnol. 46 (2018) 706-716.

[54] J.E. Park, M.J. Abrams, P.A. Efron, A. Barbul, Excessive nitric oxide impairs wound collagen accumulation, J Surg. Res. 183 (2013) 487–492.

[55] A. Gauthier, A. Fisch, K. Seuwen, B. Baumgarten, H. Ruffner, A. Aebi, M. Rausch, F. Kiessling, M. Bartneck, R. Weiskirchen, F. Tacke, G. Storm, T. Lammers, M-G. Ludwig, Glucocorticoid-loaded liposomes induce a pro-resolution phenotype in human primary macrophages to support chronic wound healing, Biomaterials (2018), https://doi.org/10.1016/j.biomaterials.2018.04.006

[56] D. Gopinath, M. R. Ahmed, K. Gomathi, K. Chitra, P.K. Sehgal, R. Jayakumar, Dermal wound healing processes with curcumin incorporated collagen films, Biomaterials 25 (2004) 1911-1917.

[57] M.L. Manca, I. Castangia, M. Zaru, A. Nácher, D. Valenti, X. Fernàndez-Busquets, A.M. Fadda, M. Manconi, Development of curcumin loaded sodium hyaluronate immobilized vesicles (hyalurosomes) and their potential on skin inflammation and wound restoring, Biomaterials 71 (2015) 100-109.

[58] C. Maupas, B. Moulari, A. Béduneau, A. Lamprecht, Y. Pellequer, Surfactant dependent toxicity of lipid nanocapsules in HaCaT cells, Int. J. Pharm. 411 (2011) 136-141.

[59] K. Tahara, M. Kobayashi, S. Yoshida, R. Onodera, N. Inoue, H. Takeuchi, Effects of cationic liposomes with stearylamine against virus infection, Int. J. Pharm. 543 (2018) 311-317.

FIGURE LEGENDS

Fig. 1. Curcumin penetration from different deformable liposomes through the full thickness human skin over 24 hrs. Results are expressed as mean ± SD (n = 3).

[a:] $p < 0.05$, [a':] $p < 0.005$ *vs*. CDL.

Fig. 2. Effect of different curcumin-DLs on *S. aureus* (upper part) and *S. pyogenes* (lower part) growth after 4 hrs incubation.

(a) and (c) show the effect of curcumin-DLs on *S. aureus* and *S. pyogenes*, respectively. Control refers to untreated bacteria. Empty DLs are curcumin-free NDLs, CDLs and ADLs, respectively, with similar lipid concentrations as curcumin-DLs. (b) and (d) represent the effect of free curcumin (CUR-PG), meaning curcumin in PG solution (20 % w/v) with same concentrations as in deformable liposomes. PG sol is PG (20 % w/v) solution in PBS.

Bar graphs showing mean ± SD (n = 2). [a:] $p < 0.03$, [a':] $p < 0.002$, [a'':] $p < 0.0002$, [a''':] $p < 0.0001$.

Fig. 3. Effect of different curcumin-DLs on NO production in LPS-induced macrophages.

LPS-induced macrophages were treated with neutral deformable liposomes (CUR-NDLs) (a), cationic deformable liposomes (CUR-CDLs) (b) and anionic deformable liposomes (CUR-ADLs) (c) containing curcumin and incubated for 24 hrs. Untreated LPS-induced macrophages were used as a control. NDLs, CDLs and ADLs are empty deformable liposomes, tested at the same lipid concentrations as curcumin-DLs. (d) is curcumin in PG solution (CUR-PG) at the same curcumin concentration as in deformable liposomes. PG sol is PG (20 % w/v) solution in PBS.

Results are expressed as mean ± SD (n = 3). [a:] $p < 0.03$, [a':] $p < 0.002$, [a'':] $p < 0.0002$, [a''':] $p < 0.0001$.

Fig. 4. **Effect of different curcumin-DLs on viability of human foreskin fibroblast (HFF) cells after 12 and 24 hrs exposure.**

HFF cells were exposed to neutral deformable liposomes (CUR-NDLs) (a), cationic deformable liposomes (CUR-CDLs) (b) and anionic deformable liposomes (CUR-ADLs) (c) containing curcumin, respectively. Untreated HFF cells were used as control. NDLs, CDLs and ADLs represent empty deformable liposomes, tested at the same lipid concentrations as curcumin-DLs. The (d) represents the percentage of living cells after exposure to PG (20 % w/v) solution (PG sol) in PBS and curcumin in PG solution (CUR-PG) at the same curcumin concentration as in deformable liposomes.

Results are expressed as mean ± SD (n = 3). $^{a:}$ $p < 0.03$, $^{a':}$ $p < 0.002$, $^{a'':}$ $p < 0.0002$.

TABLE LEGENDS

Table 1. Composition of curcumin-DLs.

[a]Each liposomal formulation was prepared in triplicates. The final volume was 10 mL. For empty liposomes (without curcumin), the same lipid/surfactant composition was used.

[b]The extrusion is described as the number of extrusion cycles through the corresponding pore size membrane (nm).

Table 2. Characteristics of curcumin-DLs.

[a]The diameter is indicated as peaks in size distributions (nm). The weight intensity of each peak (%) is indicated in parentheses.

[b]Polydispersity index.

Results are expressed as mean ± SD (n = 3).

Table 3. The membrane elasticity of curcumin-DLs.

The degree of membrane elasticity (E) was calculated considering both the r_v/r_p and J. r_v is the vesicle diameter after extrusion, r_p is the pore size membrane and J is the amount of liposomal dispersion extruded in 5 min. Empty DLs bearing different surface charge were used as control. Results are expressed as mean ± SD (n = 2). [a]n=1.

Paper V

Curcumin-in-deformable liposomes-in-hydrogel: The effect of liposomal surface charge on dermal delivery of curcumin

Selenia Ternullo, Laura Schulte-Werning, Nataša Škalko-Basnet*

Drug Transport and Delivery Research Group, Department of Pharmacy, University of Tromsø The Arctic University of Norway, Universitetsveien 57, 9037 Tromsø, Norway

*Corresponding author: Nataša Škalko-Basnet, Drug Transport and Delivery Research Group, Department of Pharmacy, University of Tromsø The Arctic University of Norway, Universitetsveien 57, 9037 Tromsø, Norway; Tel: +47-776-46640; Fax: +47-776-46151; Email: natasa.skalko-basnet@uit.no

Abstract

Liposomes-in-hydrogel systems as advanced wound dressings are promising for improved chronic wound therapy, including dermal delivery of curcumin. The combined delivery systems, comprising the nanocarriers able to enhance solubility of poorly soluble drugs/active substance and hydrogels with superior dressing properties, can assure controlled and sustained skin penetration of the incorporated drug/active substance, increase drug/active substance retention at the skin site, improving the therapy outcome. With the aim to optimize the properties of the two advanced delivery systems, we incorporated curcumin-containing deformable liposomes (DLs) in chitosan hydrogel and explored the effect of the liposomal surface charge on the properties of the advanced delivery system and curcumin delivery. Curcumin, a multitargeting poorly soluble active substance with known beneficial properties for improved wound healing, was incorporated in neutral (NDLs), cationic (CDLs) and anionic (ADLs) DLs, respectively, which were further incorporated in chitosan hydrogel. The charged DLs exhibited a positive effect on the hydrogel's hardness, whereas negatively affected both the hydrogel´s cohesiveness and adhesiveness. Interestingly, the incorporation of DLs, regardless of their charge, in chitosan hydrogel, did not decrease system´s bioadhesion to

human skin. Moreover, NDLs-in-hydrogel exhibited the strongest bioadhesion. Stability testing showed that the incorporation of CDLs in hydrogel preserved hydrogel´s bioadhesiveness to a higher degree as compared to both NDLs and ADLs. *Ex vivo* skin penetration studies revealed that CDLs-in-hydrogel system enabled the most sustained skin penetration of curcumin. Cationic deformable liposomes and chitosan hydrogel as a vehicle for DLs assured a superior longer-term bioadhesion to human skin and sustained skin penetration of curcumin. The combined delivery system has a good potential to be further evaluated for its therapeutic effects on chronic wounds.

Key words: curcumin; deformable liposomes; liposome surface charge; hydrogel; chitosan; skin therapy.

1. Introduction

The need for improved chronic wound therapy calls for the development of advanced wound dressings that, in contrast to traditional dressings, can guarantee controlled and sustained release of the incorporated drug thus resulting in enhanced therapeutic outcome and reduction of pain accompanied with wound dressing changes (Boateng and Catanzano, 2015). Natural polymer-based wound dressings, such as hydrogels, have potential to fulfil these criteria and represent promising advanced delivery systems with low risk of toxicity and side effects due to their biodegradability and biocompatibility (Bhattarai et al., 2010). Hydrogels additionally possess good bioadhesiveness that can contribute to prolonged retention time of the incorporated drug/active substance at the wounded skin site. This, together with the sustained drug release via hydrogel, can result in higher drug/active substances concentrations at the skin site while reducing possible systemic absorption and consequent adverse effects (Pitorre et al., 2017). Chitosan represents one of the most studied natural polymer for development of effective hydrogel-based wound dressings due to its numerous intrinsic biological properties (Billard et al., 2015). Chitosan biocompatibility and bioadhesiveness together with its intrinsic bacteriostatic effect make this biopolymer effective in promoting wound healing while also preventing biofilm formation (Ng et al., 2014; Pérez-Díaz et al., 2016). In spite of the numerous advantages of chitosan hydrogels as dermal

delivery systems, the hydrophilic environment provided by chitosan hydrogel limits the incorporation of lipophilic drugs/active compounds and remains a pharmaceutical challenge. The use of liposomes as a mean to overcome this hydrogel limitation has been proposed and the combination of these two advanced delivery systems revealed to be a promising approach to achieve controlled dermal drug delivery and effective localized skin therapy (Grijalvo et al., 2016, Hurler et al., 2013a). The liposomal phospholipid bilayers allow incorporation of lipophilic substances improving their solubilisation and enabling their incorporation into the hydrophilic chitosan hydrogel. Moreover, the ability of liposomes to assure controlled drug/substance release might improve targeted drug delivery to the specific skin layer(s) (Banerjee, 2013). The sustained drug release from both advanced delivery systems might be increased and the retention time at skin site improved, resulting in an enhanced efficacy of the advanced wound dressing (Billard et al., 2015). Liposomes also benefit from their incorporation in hydrogel vehicle. The hydrogel can prevent rapid liposomes clearance from the skin site and additionally protect from rapid degradation by preserving their membrane integrity (Gao et al., 2014). Moreover, incorporation of liposomes in hydrogel will confer to the liposomal dispersions adequate viscosity to be topically administered (Pavelić et al., 2001), including onto the skin.

The development of effective liposomes-in-hydrogel systems with controlled drug/active substance release requires optimization of several parameters related to both hydrogel and liposomes' properties (Hurler et al., 2013b). The drug/substance release from liposomes-in-hydrogel system is determined by the hydrogel properties, such as the polymer composition, mesh size and porosity, combined with the liposomal physicochemical characteristics, namely liposomal composition, size and surface charge. In addition, the lipophilicity of the incorporated drug needs to be considered. Lipophilic drugs will have to partition from the liposomal membrane into the hydrophilic hydrogel matrix and their release will be therefore mainly affected by the lipid concentration of liposomes embedded in the hydrogel (Mourtas et al., 2007; Hurler et al., 2013b). To the best of our knowledge, relatively little has been published on incorporation of deformable liposomes (DLs) in chitosan hydrogel. DLs have shown superior ability in promoting drug penetration into the deeper skin layers in comparison to conventional liposomes (Jain et al., 2017). In this study we designed the DLs-in-chitosan hydrogel as combined advanced delivery system, wound dressing for improved skin therapy, particularly targeting treatment of chronic wounds. Considering that chitosan

has lateral amino groups conferring positive charge to its chains, the incorporation of charged liposomes could trigger interactions between the two delivery systems affecting hydrogel's texture properties, liposomes' integrity and drug release (Hurler et al., 2013b). We therefore focused on the effect of liposomal surface charge on hydrogel's properties, such as the texture properties and bioadhesiveness; the neutral (NDLs), cationic (CDLs) and anionic (ADLs) DLs were individually incorporated in chitosan hydrogel.

To further explore the combined dermal delivery systems, we selected curcumin as lipophilic model compound to be incorporated in the DLs bearing different surface charge. The selection of curcumin was also motivated by its several beneficial effects, such as anti-oxidant, anti-inflammatory and anti-bacterial, making this pleiotropic molecule highly promising for treatment of chronic wounds and management of scars (Mehanny et al., 2016; Amini-Nik et al., 2018). The effect of liposomal surface charge on curcumin penetration from DLs-in-hydrogel systems through the *ex vivo* full thickness human skin was also evaluated.

2. Materials and methods

2.1 Materials

Curcumin (≥ 94% curcuminoid content; ≥ 80% curcumin) was purchased from Sigma-Aldrich (St. Louis, USA). Lipoid S 100 (> 94% soybean phosphatidylcholine, PC) was a generous gift from Lipoid GmbH (Ludwigshafen, Germany). High molecular weight (MW) chitosan (Brookfield viscosity 800.000 cps and degree of deacetylation of 77%), polysorbate 20, stearylamine (SA), sodium deoxycholate (SDCh), methanol, disodium hydrogen phosphate dihydrate, monobasic potassium phosphate, sodium chloride, propylene glycol (PG), glycerol and acetic acid were obtained from Sigma-Aldrich (St. Louis, USA). Albunorm® (human serum albumin, 200 mg/mL) was purchased from Octapharma AG (Lachen, Switzerland).

2.2 Preparation and characterization of deformable liposomes

Curcumin-containing DLs bearing different surface charge were prepared by the film hydration method as previously described (Ternullo et al., 2017). NDLs were composed of PC and polysorbate 20 (total 200 mg), in a weight ratio of 85:15. CDLs were made of the same lipid and surfactant composition as NDLs, with the addition of SA in a weight ratio 1:9 with PC. ADLs

were composed of PC and SDCh (total 200 mg) in a ratio 85:15 (w/w), respectively. All DLs were prepared by dissolving curcumin (20 mg), PC and, when applicable, the different surfactants, in methanol. The organic solvent was evaporated under vacuum (55 mbar) at 55 °C (Büchi Rotavapor R-124 with Büchi Vacuum Pump V-700, Büchi Labortechnik AG, Flawil, Switzerland) and the obtained lipid film hydrated with 10 mL of phosphate buffer saline (PBS). PBS (pH 7.4) was previously prepared with the following salts composition: 2.98 g/L Na2HPO4.2H2O, 0.19 g/L KH2PO4, 8 g/L NaCl. The liposomal dispersions were kept at 4 °C for 24 hrs prior to size reduction.

All DLs were reduced to a vesicle size of 200-300 nm by the hand extrusion through the polycarbonate membrane (Nuclepore® Track-Etched Membranes, Whatman House, Maidstone, UK). In brief, all DLs were extruded five times through 800 nm pore size membrane. NDLs were further extruded four times through 400 nm pore size membrane, whereas CDLs and ADLs were extruded through the same pore size membrane two and seven times, respectively. All liposomal dispersions were characterized in terms of vesicle size by photon correlation spectroscopy using a NICOMP Submicron Particle Sizer Model 370 (NICOMP Particle Sizing system, Santa Barbara, California, USA) and zeta potential using Malvern Zetasizer Nano – ZS (Malvern, Oxford, UK) (Ternullo et al., 2017).

The entrapment efficiency of curcumin in all DLs was determined after the centrifugation of the liposomal dispersion at 3,000 *g* for 10 min using a Biofuge stratos centrifuge (Heraeus instruments GmbH, Hanau, Germany) to remove unentrapped curcumin. PC was subsequently dissolved in methanol and the entrapped curcumin determined spectophotometrically at 425 nm (SpectraMax 190 Microplate Reader, Molecular Devices, California, USA). The entrapment efficiency was expressed as curcumin/lipid ratio (μg/mg), after quantification of PC content in all DLs formulations (data not shown).

2.3 Preparation of chitosan hydrogels

Chitosan hydrogels were prepared according to a method described earlier (Hurler et al., 2012). In short, glycerol (10%, w/w) was mixed with an aqueous solution of acetic acid (2.5%, w/w). High MW chitosan (2.5%, w/w) was consequently added and the mixture hand shaken. To remove entrapped air, the mixture was bath-sonicated for 30 min. The prepared hydrogels were stored in a sealed container at room temperature for 48 hrs to allow them to swell.

2.4 Preparation of DLs-in-hydrogels

To prepare 10 g of liposomal hydrogel formulation, 1.5 g of the different DLs (15%, w/w) were individually incorporated in the freshly prepared chitosan hydrogel (Section 2.3) by hand-stirring (Hurler et al., 2012). The final concentration of curcumin in the liposomal hydrogel was 135 μg/g. As a control, free curcumin was incorporated in the hydrogel in the same concentration. For that purpose, curcumin was dissolved in PG in the same concentration as in DLs and then incorporated in chitosan hydrogel by hand-stirring. The DLs-in-hydrogel formulations were kept at room temperature for 2 hrs prior to further use and characterization.

2.5 Texture analysis

All liposomal hydrogel formulations were characterised in terms of the hardness, cohesiveness and adhesiveness using a Texture Analyzer TA.XT Plus (Stable Micro Systems Ltd., Surrey, UK) (Hurler et al., 2012). Each hydrogel (25 g) was placed in a beaker and a disc of 35 mm diameter was pushed down into the gel (distance of 10 mm) and redrawn at a speed of 4 mm/s. The starting position of the disc was below the hydrogel surface. The hardness was calculated as the maximal force achieved when the disc was pushed down into the gel. The cohesiveness was expressed as the work necessary to push down the disc into the hydrogel, while the adhesiveness as the work required during the upwards movement of the disc. Each formulation was tested five time and the measurements performed in triplicates.

2.6 Bioadhesion test

The bioadhesion of all hydrogel formulations to human skin was tested as described earlier (Hurler and Škalko-Basnet, 2012). The full thickness human skin derived from the abdomen of female patients after plastic surgery. A written consent was obtained from the patients prior the surgery. No ethical approval was required by the Norwegian Ethical Committee due to normal disposal of the abdomen skin panni after the surgery; the experiments were conducted according to the Declaration of Helsinki Principles. The human skin was cleared from the subcutaneous fatty tissue and rinsed with PBS prior the storage at -20 °C. The human skin was thawed ca. 30 min prior the experiment and subsequently fixed on a mucoadhesion rig for

Texture Analyzer TA.XT Plus (Stable micro systems, Surrey, UK). The bioadhesion test was performed by applying the hydrogel formulation (150 µL) onto the dye that was part of the rig. The die was consequently pinched onto the human skin for 10 s with a force of 25 g. The bioadhesion was determined by measuring the force required to detach the dye from the skin (detachment speed of 0.1 mm/s). Moreover, the dye was weighed before and after each bioadhesion test to determine the amount of formulation retained onto the skin surface at the end of the test. Each formulation was tested five times and the human skin rinsed with ethanol between each measurement. Tests were conducted in triplicates.

2.7 Hydrogel stability testing

To evaluate chitosan hydrogel stability and the influences of the liposomal surface charge on the stability of DLs-in-hydrogel, the stability testing was performed after the storage of the DLs-in-chitosan hydrogels for one month at room temperature (23-24 °C). Texture properties (Section 2.5) and bioadhesiveness (Section 2.6) of chitosan hydrogel were determined before (one day after the formulation was prepared) and after the storage (day 30).

2.8 Ex vivo skin penetration studies

Ex vivo curcumin penetration from the different DLs-in-chitosan hydrogels was evaluated using the full thickness human skin in Franz diffusion cells (diffusion area of 1.77 cm^2, PermeGear, Bethlehem, USA) (Ternullo et al., 2017). The human skin derived from the excised skin panni of female patients who underwent abdominoplasty, after they gave a written consent (see section 2.6). The experiments were conducted in agreement with the Declaration of Helsinki Principles. The human skin for the *ex vivo* penetration studies was prepared as described in Section 2.6. The slices of human skin used in the skin penetration studies had a thickness of 1.10-1.30 mm. All DLs-in-chitosan hydrogel formulations (1.2 mL) were added in the donor chamber, whereas the receptor chamber was filled with 12.0 mL of Albunorm (5%, v/v) solution in PBS. The experiments were conducted for 8 hrs and sampling of the receptor medium (500 µL) was performed every hr. To maintain the sink conditions, the withdrawn receptor medium was replaced by an equal volume of fresh Albunorm® (5%, v/v) solution in PBS. The penetrated curcumin was quantified as described in Section 2.2 using a standard

curve of curcumin in Albunorm® (5%, v/v) solution in PBS. Experiments were performed in three replicates.

2.9 Statistical analysis

To determine level of significance ($p < 0.05$), statistical analyses were performed using one-way ANOVA test followed by Bonferroni's multiple comparisons test performed on GraphPad Prism version 7.00 for Windows (GraphPad Software, La Jolla CA, USA).

3. Results and discussion

3.1 Liposomal characteristics

The liposomal size has shown to have an influence on both hydrogel properties and release of lipophilic compounds from liposomes-in-hydrogel systems (Hurler et al., 2013b). Therefore, aiming at exploring only the effect of the liposomal surface charge on both hydrogel properties and curcumin penetration through human skin, all DLs were prepared to be of similar vesicle size. The chosen vesicle size range was 200-300 nm, which has been found to be appropriate in assuring dermal delivery via liposomes by offering the reservoir of the liposome-associated drug in the skin (du Plessis et al., 1994). The extrusion as method to reduce the vesicle size allows manufacture of rather homogeneously distributed vesicles in the desired size range, as we reported earlier (Ternullo et al., 2017). For each liposomal dispersion, we adjusted both the number of cycles of the extrusion and pore size membrane, obtaining curcumin-containing DLs within 200 and 300 nm (Table 1), as targeted. Moreover, the vesicle size distribution was rather homogeneous for all DLs, considering the rather low polydispersity index.

DLs bearing different surface charge (Table 1) were obtained by including the appropriate surfactant in the liposomal phospholipid bilayers. NDLs contained polysorbate 20 as a non-ionic surfactant, which conferred neutral surface to DLs together with the presence of the neutral lipid, namely PC. Ionic surfactants were employed to obtain CDLs and ADLs, respectively. SA was responsible for the positive charge of CDLs, whereas SDCh conferred the negative charge to ADLs surface, both in agreement with literature (Al Shuwaili et al., 2016; Dragicevic-Curic et al., 2010).

The entrapment efficiency of curcumin in the different DLs varied according to their composition (Table 1). The presence of surfactant might contribute to a lower entrapment efficiency of lipophilic compounds, such as curcumin, both competing for accommodation in the liposomal phospholipid bilayer. The level of influence on the drug loading capacity is additionally dependent on the type of employed surfactant (Bnyan et al., 2018). In our case, ADLs exhibited the highest entrapment efficiency of curcumin. A possible explanation might rely on the higher lipophilicity of SDCh compared to polysorbate 20 thus improving curcumin solubility and therefore enhancing the curcumin loading capacity of ADLs (Bnyan et al., 2018). The presence of SA in CDLs has shown to alter the lipid packing of liposomes by causing charge repulsion (El Zaafarany et al., 2010). This can therefore affect curcumin accommodation in the CDLs bilayer, as previously observed for the drugs bearing similar lipophilicity as curcumin, such as celecoxib (Bragagni et al., 2012).

3.2 Effect of liposomal surface charge on the hydrogel texture properties

The development of effective hydrogel-based wound dressings requires their characterization in terms of hydrogel texture properties. Hydrogel's hardness can determine the ease of hydrogel application onto the skin, whereas adhesiveness influences the hydrogel contact time with the skin. These factors consequently contribute to the efficacy of the treatment and assure patient compliance by reducing the frequencies of administration and the related pain caused by wound dressing changes (Koehler et al., 2018). When optimizing liposomal hydrogel formulations, evaluation of the texture properties of the hydrogel are required considering that the incorporation of DLs bearing different surface charge can affect the hydrogel texture properties (Hurler et al., 2013b). Possible interactions between charged DLs and positive chitosan chains might change/affect the chitosan network thus modifying its texture characteristics. The effect of the liposomal surface charge on curcumin-containing DLs in chitosan hydrogel's properties is shown in Table 2.

The incorporation of all DLs negatively affected the original hydrogel texture properties (plain hydrogel). All DLs-in-hydrogel also weakened the hydrogel properties to a higher extent than incorporation of free curcumin (CUR-in-hydrogel, Table 2). Due to the hydrophobic nature of curcumin, its incorporation in chitosan hydrogel as free curcumin (not incorporated in DLs) was achieved by prior dispersion of curcumin in PG. The presence of PG has shown to exert a

positive effect on the viscoelastic properties of hydrogels by triggering hydrogen bonding between chitosan, water and the solvent (Islam et al., 2004). This might explain the positive effect of free curcumin on the hydrogel properties compared to DLs. Vanić and co-workers (2014) observed reduced hydrogel texture properties when deformable propylene glycol liposomes were incorporated in Carbopol hydrogel, in agreement with the effect observed with our DLs. The incorporation of DLs in Carbopol hydrogel has also shown to change the hydrogel texture when compared to a marketed gel product, although the authors did not focus on the liposomal surface charge (Garg et al., 2017). Weakened chitosan hydrogel texture properties after the incorporation of conventional liposomes bearing different surface charge have been observed by Hurler and collaborators (2013b), in agreement with our findings. Considering the liposomal surface charge, the charged DLs enhanced the hydrogel hardness while weakening both cohesiveness and adhesiveness, as compared to NDLs. Possible electrostatic interactions between charged DLs and chitosan might destabilize the chitosan network to a higher extent compared to the neutral DLs. NDLs are not expected to interact with the polymer and this might explain their rather positive influence on the texture properties compared to the charged DLs.

3.3 Effect of liposomal surface charge on hydrogel bioadhesion to human skin

Bioadhesiveness represents an important feature responsible for the effectiveness of hydrogel-based wound dressings. Good hydrogel bioadhesion to human skin can prolong the retention time of the incorporated drug/active substance at the skin site thus resulting in enhanced therapeutic effect. Considering the presence of the exudate in chronic wounds/burns, the contact time of the hydrogel to the skin might be reduced by a loss of hydrogel texture characteristics due to the presence of high water content in the wounded area (Boateng and Catanzano, 2015). Satisfactory hydrogel bioadhesion to human skin might overcome this limitation. We therefore evaluated any possible effect of liposomal surface charge on the chitosan hydrogel's bioadhesiveness. Based on the method developed earlier in our laboratory (Hurler and Škalko-Basnet, 2012), we determined the hydrogel bioadhesion to human skin by determining the force required to break bonds between the hydrogel formulations and human skin (Figure 1a) and the amount of hydrogel formulations retained onto the skin surface at the end of the bioadhesion test (Figure 1b).

The bioadhesiveness expressed as the detachment force was not affected by the incorporation of curcumin-containing DLs, regardless of the liposomal surface charge. Both CDLs- and ADLs-in-hydrogel exhibited similar bioadhesiveness as plain hydrogel, whereas NDLs-in-hydrogel showed strongest bioadhesion to human skin. As observed for the texture properties, NDLs with neutral surface seemed to stabilize the chitosan network to a higher extent compared to the charged DLs. Their neutral surface might enable minimal interactions with the polymer thus leaving unaltered the intrinsic bioadhesiveness properties of chitosan hydrogel.

The amount of the hydrogel retained onto the skin was similar for all tested DLs-in-hydrogel systems. Moreover, the high amount of hydrogel retained onto the skin (approx. 70%) observed for all DLs-in-hydrogel is promising to potentially overcome the challenge of exposure to wound exudate and reduced retention time when hydrogel is applied on exudate-rich wounded area. The high water content of those wound types is responsible for the limited adhesion of the wound dressing at the skin site. Therefore, the good bioadhesive properties of DLs-in-hydrogel systems confirmed herewith are promising in prolonging the retention time of curcumin at the wounded area rich in exudate, potentially enhancing its therapeutic outcome. Further studies involving the exposure to wound exudate are required to confirm these preliminary findings.

3.4 Stability of hydrogel

The incorporation of charged DLs in chitosan hydrogel has shown to influence both hydrogel's texture properties (Table 2) and bioadhesiveness (Figure 1), possibly related to triggered interactions between charged DLs and chitosan. We therefore further explored the effect of liposomal surface charge on the stability of chitosan hydrogel. Wound dressings that can maintain their original properties when stored for certain period of time at room temperature rather than in the refrigerated conditions, contribute to the efficacy of the formulation and enable easiness of administration. The liposomal hydrogel formulations were stored at room temperature (23-24 °C) for one month and both the texture properties and bioadhesiveness were determined and compared with the properties of the original formulations. The original texture properties were preserved to a higher extent when NDLs were incorporated in the hydrogel compared to both CDLs and ADLs (Figure 2). The weaker interaction of neutral DLs

seems to alter the original hydrogel texture properties to a lower extent compared to the charged DLs, which can electrostatically interact with the polymer chains weakening its texture properties.

Interestingly, the evaluation of hydrogel's stability in terms of bioadhesiveness showed that the original bioadhesion to human skin was better preserved when CDLs were incorporated in the hydrogel (Figure 3). Both detachment force (Figure 3a) and the amount of formulation retained onto the skin surface (Figure 3b) for CDLs-in-hydrogel slightly increased compared to both NDLs- and ADLs-in-chitosan hydrogel.

The original bioadhesiveness was enhanced by the presence of NDLs suggesting that the neutral surface of NDLs might exert a positive effect on hydrogel bioadhesiveness (Figure 1). However, results from hydrogel stability testing indicate that the positively charged DLs can better preserve hydrogel bioadhesiveness for a longer period of time than NDLs. The repulsion between positive CDLs and chitosan chains might stabilize the liposomes in the hydrogel matrix to a greater extent thus preserving chitosan bioadhesion to human skin.

The bioadhesiveness is one of the main factors determining the prolonged retention time of curcumin at the skin administration time. Despite the rather negative effect of charged liposomes on the texture properties of DLs-in-hydrogel, the incorporation of CDLs in hydrogel might result in increased hydrogel stability over a longer period of time regarding the bioadhesiveness thus assuring prolonged retention time of curcumin at the skin site. Visual evaluation of the different formulations after one-month storage showed that curcumin-in-hydrogel (non-entrapped curcumin) exhibited curcumin precipitation phenomenon (data not shown). This was an additional advantage of enhancement of curcumin stability in hydrogel formulations mediated by DLs as nanocarriers for curcumin.

3.5 Curcumin penetration from DLs-in-hydrogel through ex vivo human skin

As dermal delivery systems, both DLs and chitosan hydrogel have shown to assure controlled and sustained skin penetration of the associated drug. When used in combination, this action can be increased and, together with the prolonged retention time at the targeted skin site, might result in improved localized wound therapy (Billard et al., 2015; Hurler at al., 2013a). Moreover, this can lead to a reduction of frequencies of wound dressings' changes, improving the patient compliance and easiness of dressing administration. The incorporation of DLs in

hydrogel introduces additional barriers that curcumin has to face and cross before reaching the targeted skin site. Therefore, curcumin release from the DLs-in-hydrogel followed by its skin penetration is a complex process and depends on several factors. Curcumin has initially to partition from the liposomal bilayer into the hydrogel and then diffuse into the hydrophilic environment provided by the chitosan network to finally penetrate into/through the skin. The lipophilicity of curcumin will influence this process, especially its partitioning into the hydrogel, whereas its aqueous solubility will determine the diffusion rate through the hydrophilic hydrogel matrix, as observed for other lipophilic compounds (Mourtas et al., 2007). The liposomal surface charge represents an additional factor that can affect curcumin penetration through/into the skin (Jain et al., 2017). Moreover, due to the positively charged chitosan chains, the liposomal surface charge can determine possible interaction between DLs and chitosan (Hurler et al., 2013b). This can affect the integrity of the liposomal bilayer when embedded into the hydrogel thus influencing the release of curcumin. By exploring this above mentioned, the development of liposomal hydrogel formulations with controlled dermal delivery of curcumin can be achieved and effective therapies assured.

Figure 4 shows the skin penetration profiles of curcumin from the different DLs-in-hydrogel systems. A minimal amount of penetrated curcumin was observed, regardless of the liposomal surface charge. This might be explained by the possible slow diffusion of curcumin when released into the hydrophilic hydrogel due to its poor water solubility. Slow *in vitro* release of curcumin from lipospheres embedded in hydroxyl propyl methyl cellulose-based gel has been recently reported by Jain and collaborators (2016), in agreement with our findings.

NDLs-in-hydrogel exhibited the highest amount of penetrated curcumin, also in comparison to curcumin-in-hydrogel (control) (Figure 4). As discussed earlier, NDLs with their neutral surface are not expected to interact with the chitosan chains. This might result in a minor impact on the curcumin release and further penetration into the skin thus explaining the highest skin penetration of curcumin via NDLs-in-hydrogel. The minimal interaction between NDLs and chitosan chains might also marginally interfere with NDLs' mobility within the polymer matrix allowing faster curcumin delivery into/through the skin via NDLs. The enhancement of skin penetration of curcumin from nanosystems-in-chitosan hydrogel compared to free curcumin-in-hydrogel has been also observed by Thomas and collaborators (2017). They incorporated curcumin in nanoemulsions further loaded in chitosan hydrogel and observed a higher rat skin penetration of curcumin when compared to free curcumin-in-

hydrogel. Sun and co-workers (2017) observed higher penetration of curcumin from PLGA nanoparticles-loaded in Carbopol gel compared to free curcumin-in-gel, although they tested the formulations in mouse skin.

The charged DLs-in-hydrogel exhibited the most sustained skin penetration of curcumin compared to NDLs-in-hydrogel and control (curcumin-in-hydrogel). Considering the possible electrostatic interactions that can be triggered when charged DLs are embedded into the chitosan network, the liposomal membrane might be more preserved thus limiting curcumin partitioning into the hydrogel. The electrostatic interactions between negative DLs and positive chitosan chains can cause immobilization of ADLs within the hydrogel matrix thus limiting curcumin diffusion initially and then into the hydrogel in order to reach the skin. Low mobility of liposomes bearing opposite charge compared to the hydrogel chains has been recently reported by El Kechai and collaborators (2017), who observed that positive liposomes were highly immobilized in the negative hyaluronic acid hydrogel. On the other hand, the higher repulsion occurring between CDLs and chitosan, both positively charged, might leave the CDLs membrane more intact and limit curcumin partitioning into the chitosan hydrogel, thus explaining the most sustained skin penetration of curcumin via CDLs. Hurler and collaborators (2013b) observed the same findings when testing the *in vitro* release of a lipophilic compound from positively charged liposomes embedded in chitosan hydrogel. This can result in a more prolonged retention time of curcumin at the skin site to exert its therapeutic effect. The findings should be further explored to confirm the potential of a proposed system as an advanced wound dressing.

4. Conclusions

In this work, deformable liposomes enabled incorporation of curcumin into a hydrogel-based wound dressing. Both texture properties and bioadhesiveness of DLs-in-chitosan hydrogel were found to be affected by the liposomal surface charge. Although the texture properties were weakened to a certain degree, the incorporation of deformable liposomes in the chitosan hydrogel did not negatively affect its bioadhesiveness. Neutral deformable liposomes-in-hydrogel exhibited the strongest bioadhesiveness, however their neutral surface did not preserve the hydrogels´s bioadhesion to human skin over longer periods of time. The positively charged deformable liposomes exhibited the best ability in stabilizing chitosan

bioadhesiveness and additionally assured the most sustained penetration of curcumin through the *ex vivo* full human skin. By exploring the effect of liposomal surface charge on both the chitosan properties and skin penetration of curcumin, cationic deformable liposomes in chitosan hydrogel showed to be the most appropriate combination of the two delivery systems assuring good and stable hydrogel´s bioadhesiveness and sustained skin penetration of curcumin. The developed advanced dermal delivery system is therefore promising as a wound dressing.

Conflicts of interest

The authors declare no conflicts of interest.

Acknowledgements

The authors thank Lipoid GmbH for generously providing the phospholipids.

References

Al Shuwaili, A.H., Rasool, B.K.A., Abdulrasool, A.A., 2016. Optimization of elastic transfersomes formulations for transdermal delivery of pentoxifylline. Eur. J. Pharm. Biopharm. 102, 101-114.

Amini-Nik, S., Yousuf, Y., Jeschke, M.G., 2018. Scar management in burn injuries using drug delivery and molecular signalling: Current treatments and future directions. Adv. Drug Deliv. Rev. 123, 135-154.

Banerjee, R., 2013. Overcoming the stratum corneum barrier: a nano approach. Drug Deliv. Transl. Res. 3, 205-208.

Bhattarai, N., Gunn, J., Zhang, M., 2010. Chitosan-based hydrogels for controlled, localized drug delivery. Adv. Drug Deliv. Rev. 62, 83-99.

Billard, A., Pourchet, L., Malaise, S., Alcouffe, P., Montembault, A., Ladavière, C., 2015. Liposome-loaded chitosan physical hydrogel: toward a promising delayed-release biosystem. Carbohydr. Polym. 115, 651-657.

Bnyan, R., Khan, I., Ehtezazi, T., Saleem, I., Gordon, S., O'Neill, F., Roberts, M., 2018. Surfactant effects on lipid-based vesicles properties. J. Pharm. Sci. 107, 1237-1246.

Boateng, J., Catanzano, O., 2015. Advanced therapeutic dressings for effective wound healing - A review. J. Pharm. Sci. 104, 3653-3680.

Bragagni, M., Mennini, N., Maestrelli, F., Cirri, M., Mura, P., 2012. Comparative study of liposomes, transfersomes and ethosomes as carriers for improving topical delivery of celecoxib. Drug Deliv. 19, 354-361.

Dragicevic-Curic, N., Gräfe, S., Gitter, B., Winter, S., Fahr, A., 2010. Surface charged temoporfin-loaded flexible vesicles: *In vitro* skin penetration studies and stability. Int. J. Pharm. 384, 100-108.

du Plessis, J., Ramachandran, C., Weiner, N., Müller, D.G., 1994. The influence of particle size of liposomes on the deposition of drug into the skin. Int. J. Pharm. 103, 277-282.

El Kechai, N., Geiger, S., Fallacara, A., Cañero Infante, I., Nicolas, V., Ferrary, E., Huang, N., Bochot, A., Agnely, F., 2017. Mixtures of hyaluronic acid and liposomes for drug delivery: Phase behavior, microstructure and mobility of liposomes. Int. J. Pharm. 523, 246-259.

El Zaafarany, G.M., Awad, G.A.S., Holayel, S.M., Mortada, N.D., 2010. Role of edge activators and surface charge in developing ultradeformable vesicles with enhanced skin delivery. Int. J. Pharm. 397, 164-172.

Gao, W., Vecchio, D., Li, J., Zhu, J., Zhang, Q., Fu, V., Li, J., Thamphiwatana, S., Lu, D., Zhang, L., 2014. Hydrogel containing nanoparticle-stabilized liposomes for topical antimicrobial delivery. ACS Nano. 8, 2900-2907.

Garg, V., Singh, H., Bhatia, A., Raza, K., Singh, S.K., Singh, B., Beg, S., 2017. Systematic development of transethosomal gel system of piroxicam: Formulation optimization, *in vitro* evaluation, and *ex vivo* assessment. AAPS PharmSciTech. 18, 58-71.

Grijalvo, S., Mayr, J., Eritja, R., Díaz Díaz, D., 2016. Biodegradable liposome-encapsulated hydrogels for biomedical applications: a marriage of convenience. Biomater. Sci. 4, 555-574.

Hurler, J., Engesland, A., Poorahmary Kermany, B., Škalko-Basnet, N., 2012. Improved texture analysis for hydrogel characterization: Gel cohesiveness, adhesiveness, and hardness. J. Appl. Polym. Sci. 125, 180-188.

Hurler, J., Škalko-Basnet, N., 2012. Potentials of chitosan-based delivery systems in wound theapy: bioadhesion study. J. Funct. Biomater. 3, 37-48.

Hurler, J., Sørensen, K.K., Fallarero, A., Vuorela, P., Škalko-Basnet, N., 2013a. Liposomes-in-hydrogel delivery system with mupirocin: *In vitro* antibiofilm studies and *in vivo* evaluation in mice burn model. Biomed. Res. Int. 498485.

Hurler, J., Žakelj, S., Mravljak, J., Pajk, S., Kristl, A., Schubert, R., Škalko-Basnet, N., 2013b. The effect of lipid composition and liposome size on the release properties of liposomes-in-hydrogel. Int. J. Pharm. 456, 49-57.

Islam, M.T., Rodríguez-Hornedo, N., Ciotti, S., Ackermann, C., 2004. Rheological characterization of topical carbomer gels neutralized to different pH. Pharm. Res. 21, 1192-1199.

Jain, A., Doppalapudi, S., Domb, A.J., Khan, W., 2016. Tacrolimus and curcumin co-loaded liposphere gel: Synergistic combination towards management of psoriasis. J. Control. Release 243, 132-145.

Jain, S., Patel, N., Shah, M.K., Khatri, P., Vora, N., 2017. Recent advances in lipid-based vesicles and particulate carriers for topical and transdermal application. J. Pharm. Sci. 106, 423-445.

Koehler, J., Brandl, F.P., Goepferich, A.M., 2018. Hydrogel wound dressings for bioactive treatment of acute and chronic wounds. Eur. Polym. J. 100, 1-11.

Mehanny, M., Hathout, R.M., Geneidi, A.S., Mansour, S., 2016. Exploring the use of nanocarrier systems to deliver the magical molecule; Curcumin and its derivatives. J. Control. Release 225, 1-30.

Mourtas, S., Fotopoulou, S., Duraj, S., Sfika, V., Tsakiroglou, C., Antimisiaris, S.G., 2007. Liposomal drugs dispersed in hydrogels. Effect of liposome, drug and gel properties on drug release kinetics. Colloids Surf. B. Biointerfaces. 55, 212-221.

Ng, V.W., Chan, J.M., Sardon, H., Ono, R.J., García, J.M., Yang, Y.Y., Hedrick, J.L., 2014. Antimicrobial hydrogels: a new weapon in the arsenal against multidrug-resistant infections. Adv. Drug Deliv. Rev. 78, 46-62.

Pavelić, Ž., Škalko-Basnet, N., Schubert, R., 2001. Liposomal gels for vaginal drug delivery. Int. J. Pharm. 219, 139-149.

Pérez-Díaz, M., Alvarado-Gomez, E., Magaña-Aquino, M., Sánchez-Sánchez, R., Velasquillo, C., Gonzalez, C., Ganem-Rondero, A., Martínez-Castañon, G., Zavala-Alonso, N., Martinez-Gutierrez, F., 2016. Anti-biofilm activity of chitosan gels formulated with silver nanoparticles and their cytotoxic effect on human fibroblasts. Mater. Sci. Eng. C. 60, 317-323.

Pitorre, M., Gondé, H., Haury, C., Messous, M., Poilane, J., Boudaud, D., Kanber, E., Rossemond Ndombina, G.A., Benoit, J-P., Bastiat, G., 2017. Recent advances in nanocarrier-loaded gels: Which drug delivery technologies against which diseases? J. Control Release. 266, 140-155.

Sun, L., Liu, Z., Wang, L., Cun, D., Tong, H.H.Y., Yan, R., Chen, X., Wang, R., Zheng, Y., 2017. Enhanced topical penetration, system exposure and anti-psoriasis activity of two particle-sized, curcumin-loaded PLGA nanoparticles in hydrogel. J. Control. Release 254, 44-54.

Ternullo, S., de Weerd, L., Holsæter, A.M., Flaten, G.E., Škalko-Basnet, N., 2017. Going skin deep: A direct comparison of penetration potential of lipid-based nanovesicles on the isolated perfused human skin flap model. Eur. J. Pharm. Biopharm. 121, 14-23.

Thomas, L., Zakir, F., Mirza, M.A., Anwer, M.K., Ahmad, F.J., Iqbal, Z., 2017. Development of Curcumin loaded chitosan polymer based nanoemulsion gel: *In vitro*, *ex vivo* evaluation and in vivo wound healing studies. Int. J. Biol. Macromol. 101, 569-579.

Vanić, Ž., Hurler, J., Ferderber, K., Golja Gašparović, P., Škalko-Basnet, N., Filipović-Grčić, J., 2014. Novel vaginal drug delivery system: deformable propylene glycol liposomes-in-hydrogel. J. Liposome Res. 24, 27-36.

Figures:

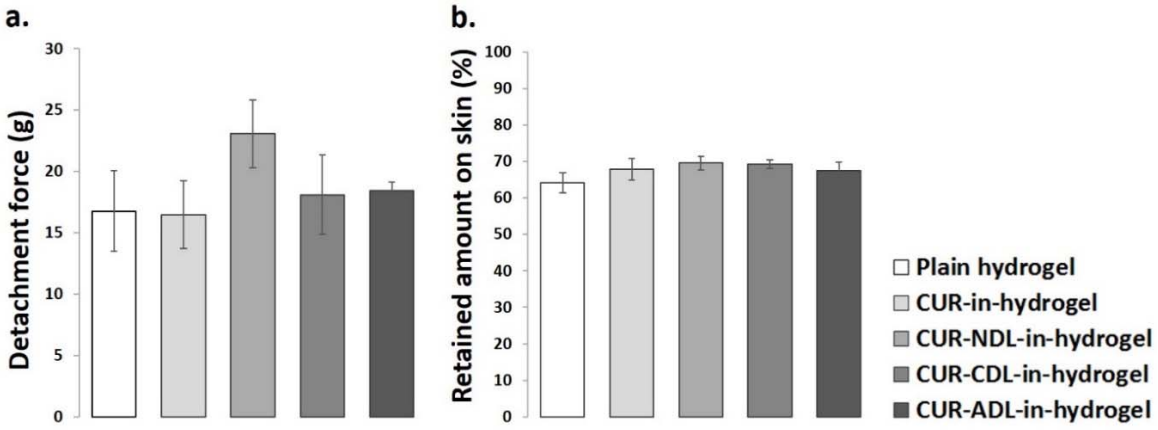

Figure 1. Effect of liposomal surface charge on hydrogel bioadhesiveness, expressed as (a) detachment force and (b) amount of formulation retained onto the human skin surface.

Results expressed as mean (n =3) ± SD.

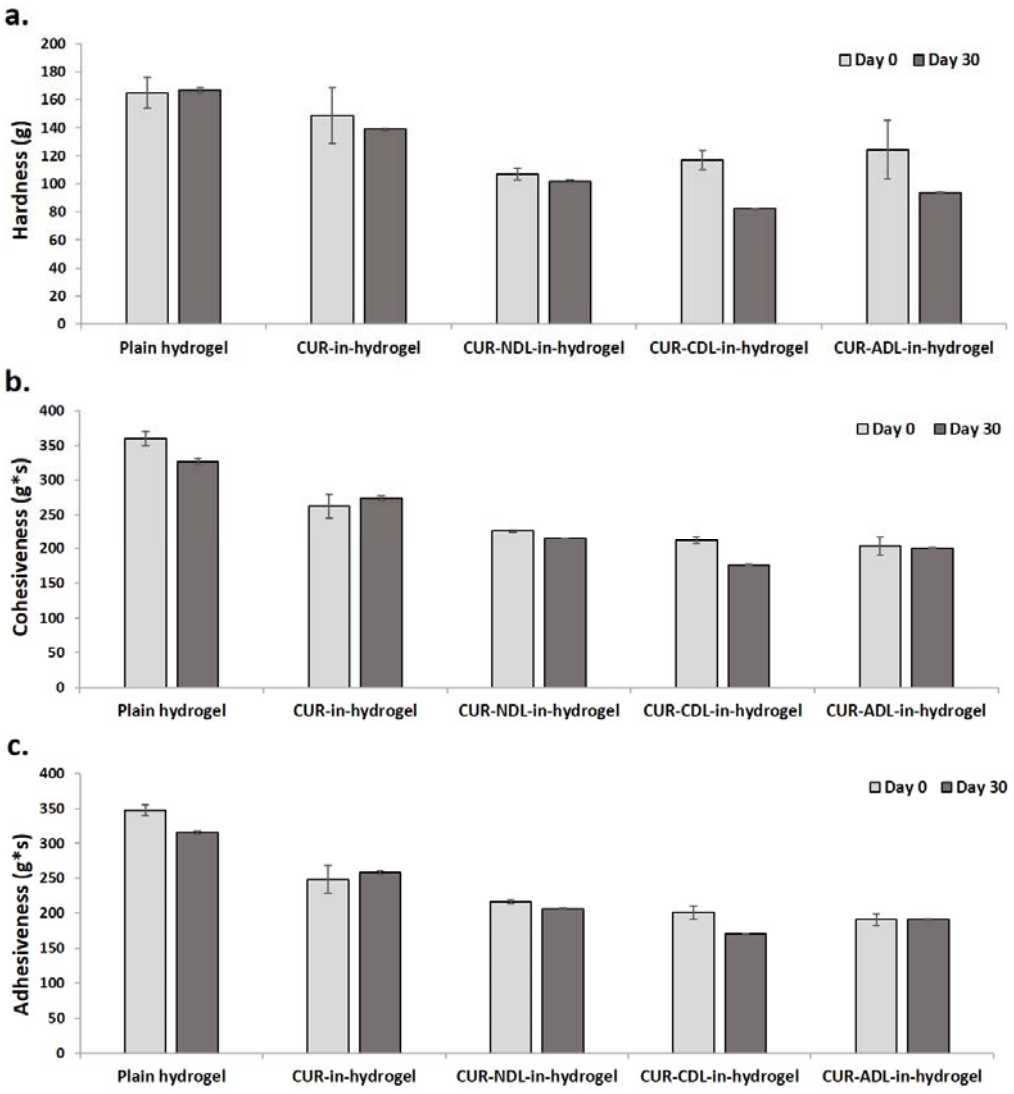

Figure 2. The effect of liposomal surface charge on hydrogel texture properties: stability testing. (a) hardness, (b) cohesiveness and (c) adhesiveness, determined for original hydrogel formulations (day 0) and after the storage at 23-24 °C for 30 days (day 30).

Results are expressed as mean (n = 3) ± SD.

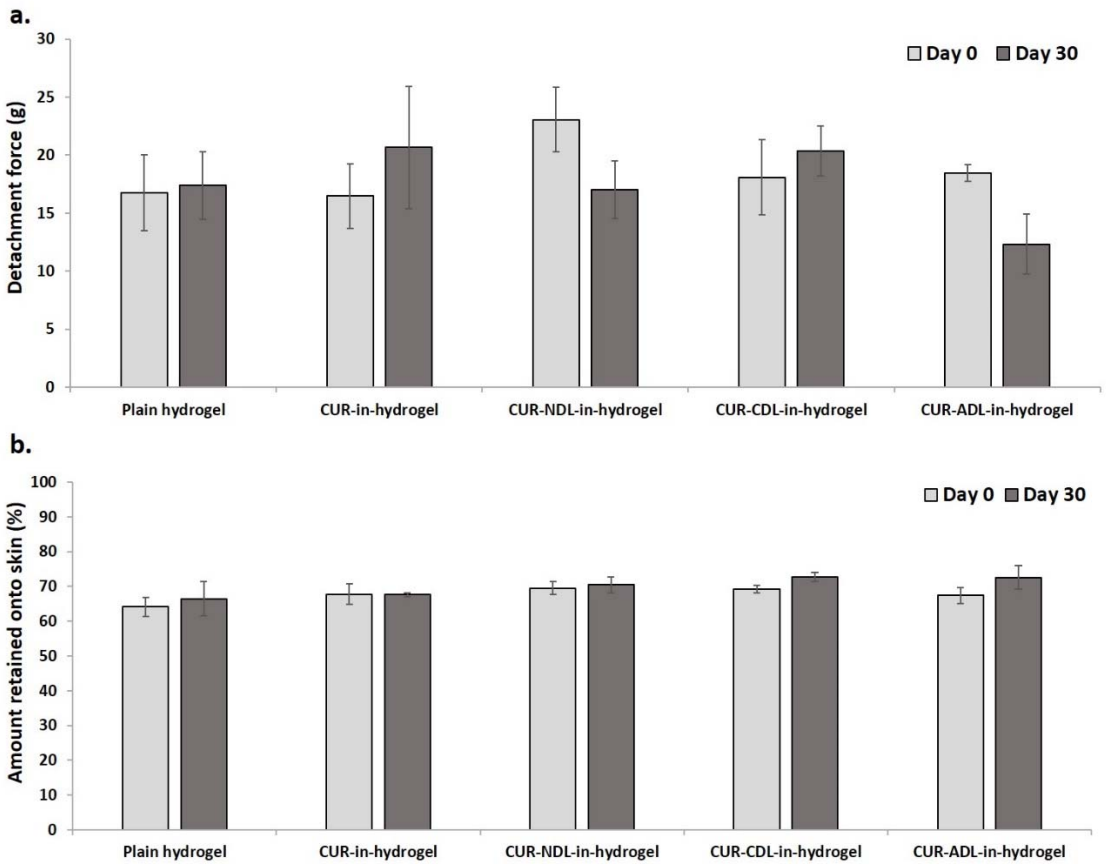

Figure 3. The effect of liposomal surface charge on hydrogel bioadhesiveness: stability testing. (a) detachment force and (b) amount of formulation retained onto the skin surface, measured for original hydrogel formulations (day 0) and after the storage at 23-24 °C for 30 days (day 30). Results are expressed as mean (n = 3) ± SD.

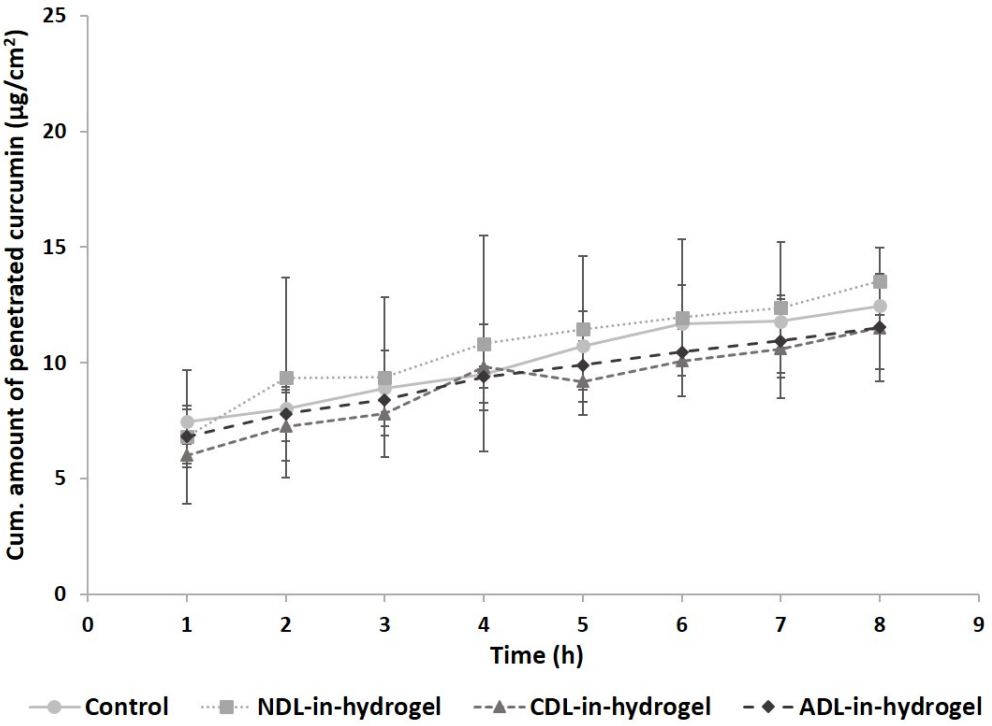

Figure 4. Curcumin penetration from different DLs-in-hydrogel through *ex vivo* full thickness human skin (n = 3 ± SD).

As a control, curcumin-in-hydrogel was used where curcumin was incorporated as solution in PG in same concentration as in DLs.

Tables:

Table 1. Liposomal characteristics.

Liposomes	Diameter (nm)	Polydispersity index	Zeta potential (mV)	Curcumin/lipid ratio (µg/mg)
NDLs	288.73 ± 2.46	0.17 ± 0.02	-3.03 ± 0.24	51.54[a] ± 0.99
CDLs	252.24 ± 51.63	0.17 ± 0.01	34.01 ± 0.56	71.94 ± 2.32
ADLs	291.54 ± 26.48	0.17 ± 0.01	-34.83 ± 0.64	89.67 ± 14.03

Results are presented as mean (n = 3) ± SD. [a]Significantly lower *vs*. ADLs ($p < 0.05$).

Table 2. The effect of liposomal surface charge on hydrogel texture properties.

Chitosan hydrogel composition	Hardness (g)	Cohesiveness (g*s)	Adhesiveness (g*s)
Plain hydrogel	164.8 ± 11.1	359.6 ± 10.6	346.8 ± 8.0
CUR-in-hydrogel	148.7 ± 20.1	262.2 ± 17.0	248.5 ± 20.1
CUR-NDL-in-hydrogel	107.0[a] ± 4.2	226.5[a, b] ± 1.7	216.5[a] ± 2.8
CUR-CDL-in-hydrogel	116.8[a] ± 6.7	212.3[a, b] ± 5.5	200.9[a, b] ± 9.4
CUR-ADL-in-hydrogel	124.6 ± 21.0	204.0[a, b] ± 13.5	190.7[a, b] ± 8.6

Results are presented as mean (n = 3) ± SD. CUR: curcumin. [a]Significantly lower *vs*. plain hydrogel ($p < 0.05$), [b]significantly lower *vs*. CUR-in-hydrogel ($p < 0.05$).